Duane C Wallace

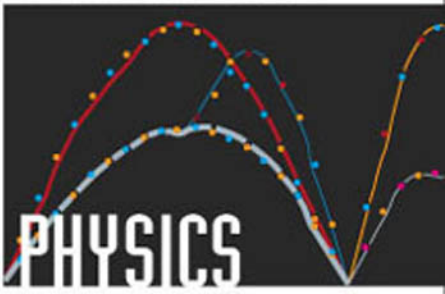

# STATISTICAL PHYSICS OF CRYSTALS AND LIQUIDS

*A Guide to Highly Accurate Equations of State*

World Scientific

# STATISTICAL PHYSICS OF CRYSTALS AND LIQUIDS

*This page intentionally left blank*

**Duane C Wallace**
*Los Alamos National Laboratory, USA*

# STATISTICAL PHYSICS OF CRYSTALS AND LIQUIDS

*A Guide to Highly Accurate Equations of State*

World Scientific

NEW JERSEY • LONDON • SINGAPORE • BEIJING • SHANGHAI • HONG KONG • TAIPEI • CHENNAI

*Published by*

World Scientific Publishing Co. Pte. Ltd.

5 Toh Tuck Link, Singapore 596224

*USA office:* Suite 202, 1060 Main Street, River Edge, NJ 07661

*UK office:* 57 Shelton Street, Covent Garden, London WC2H 9HE

**British Library Cataloguing-in-Publication Data**
A catalogue record for this book is available from the British Library.

**STATISTICAL PHYSICS OF CRYSTALS AND LIQUIDS**
**A Guide to Highly Accurate Equations of State**



ISBN 981-238-112-0
ISBN 981-238-113-9 (pbk)

Printed in Singapore by Mainland Press

# Preface

This monograph presents three main topics, only fragments of which are otherwise covered in textbooks and research treatises: (a) construction of the complete Hamiltonian for crystals, amorphous solids, and liquids, (b) presentation of liquid dynamics theory based on this Hamiltonian, and (c) comparison of theory and experiment over a broad range of properties for crystals and liquids. The work is limited primarily to the elements, but the same principles apply to alloys and compounds. Our presentation is aimed at addressing questions along the lines of: What is our "best" theory for a given property? How accurate is a good theory? What information is gained by a comparison of theory and experiment? How accurate is a good experiment? What small effects need to be accounted for in order to extract the most accurate data from an experiment? The techniques discussed are those which the author has found useful in forty-three years of condensed matter research, and which might be useful to other researchers as well, both theorists and experimentalists.

The condensed matter Hamiltonian consists of four contributions which represent, in order of strongly decreasing overall importance, the groundstate energy with static nuclei, the motion of nuclei, excitation of electrons from their groundstate, and interaction between nuclear motion and electronic excitation. The last two contributions are significant only for metals. All the parameters of the Hamiltonian, the various potentials and interactions, are defined in principle through electronic structure theory, and can be obtained in practice from density functional calculations. Hence the groundstate, and all the excited states, and all the equilibrium statistical mechanical properties, are encoded into a single Hamiltonian function

(operator), all whose terms we know in principle how to calculate.

For a crystal, the Hamiltonian is transformed to a set of phonons, plus phonon-phonon interactions (anharmonicity), excited electronic states, and electron-phonon interactions. Once the phonons and electrons are defined, their interactions are completely prescribed, by the unique total Hamiltonian. This internal consistency condition is sometimes of essential importance, but is hardly ever recognized. For elemental crystals, theory and experiment are compared at the highest possible level of accuracy for many properties, with special emphasis on phonon frequencies and thermodynamic entropy. Quantum and classical regimes are identified, temperature and volume effects are separated, anharmonic contributions are assessed, and electronic-excitation and electron-phonon contributions are analyzed.

For a liquid, the underlying picture of the monatomic liquid state is presented. This picture is derived from three properties deduced from experimental data: (a) the melting of an element falls into one of two classes, normal melting in which there is no significant change in the electronic structure, and anomalous melting which is otherwise; (b) the entropy of melting at constant volume is very nearly a universal constant for normal melting; and (c) the specific heat of the liquid at melt corresponds to nearly harmonic motion of the nuclei. From these properties we infer that the potential energy surface seen by the nuclei is composed of a very large number of intersecting nearly-harmonic many-particle valleys, and the nuclear motion consists of oscillations within these valleys, and nearly-instantaneous transits between valleys. The picture is confirmed by computer simulation studies. Theory and experiment are compared for equilibrium statistical mechanical properties of monatomic liquids, and liquid dynamics theory is shown to be reliable and of respectable accuracy in zeroth order, with well-defined higher order corrections remaining to be studied.

We live with an apparently never-ending debate over the interpretation of statistical mechanics. The author has survived discussions of such questions as, "What is the temperature of an atom?" and, "How does the reservoir interact with the systems of an ensemble?" But statistical mechanics is not a mystery whose meaning we must divine, it is rather a tool we make to do useful work. Here we present statistical mechanics in a way that is direct, practical, and as rigorous as any other. We consider a many-atom mechanical system with prescribed Hamiltonian and boundary conditions, intended to represent a real laboratory system, and we calculate

macroscopic properties by averaging over the system's phase space, with a weight function. The purpose of the weight function is to enforce constraints. We recover the standard partition-function formulation, in a way that makes it easy to discuss the effects of boundary conditions, and to see what is involved in comparing theory and experiment. We also derive classical statistics as a well-defined regime within quantum statistics, and we discuss statistical averages for a molecular dynamics system. An approximate extension of equilibrium statistical mechanics to metastable states is presented. Equilibrium crystal-crystal and crystal-liquid phase transitions are discussed, and an application to the glass transition is made, to illustrate a nonequilibrium process.

Pseudopotential perturbation theory was developed in the early 1960s, as an approximate electronic structure theory for nearly-free-electron metals. This theory taught the physics community that a quantitative understanding of every equilibrium property of a metal can be achieved through its electronic structure. Though the modern electronic structure paradigm is density functional theory, pseudopotential perturbation theory is still extremely useful. First, this theory is an excellent learning device, since it presents a simple analytic description of all the essential metallic properties, namely Fermi statistics, electron response, exchange-correlation corrections, the electron-ion interaction, the effective ion-ion interaction, and excited electronic states. Second, when calibrated to density functional calculations, or directly to experimental data, pseudopotential perturbation theory gives a highly accurate overall description of a metal. The one-parameter fit to the phonon dispersion curves of Al, done in 1969 and shown in Fig. 5.1, is still a very good model. Fewer parameters means better physics. Our 1968 model for Na is compared with experiment throughout this monograph, to demonstrate what is achievable with a highly accurate Hamiltonian. A detailed formulation of pseudopotential perturbation theory is presented, and is used to illustrate various theoretical topics throughout this work.

This book carries the subtitle *A Guide to Highly Accurate Equations of State*. By equations of state, we mean the complete set of thermodynamic functions for a given material, over a wide range of temperature and pressure. From the analysis presented here, it is clear that we know in principle how to calculate *ab initio* the equation of state of an elemental solid or liquid, to an accuracy on the same order as the accuracy of experimental data. We also know a great deal about the errors associated with vari-

ous approximations, such as the neglect of anharmonicity, or the neglect of electron-phonon interactions. This level of understanding will allow us to construct condensed matter equations of state of the highest possible accuracy, not only in regions where experimental data are available for calibration, but also in regions where such data are not available.

This monograph is not an "update" of my previous book *Thermodynamics of Crystals* (Wiley, New York, 1972; reprinted by Dover, New York, 1998), since a much broader scope of condensed matter theory is presented here. On the other hand, *Thermodynamics of Crystals* contains much useful information not included here, for example, lattice dynamics of nonprimitive lattices. Here we shall often mention relevant information which can be found in that book, citing only the title and location.

The experimental data tabulated in this monograph are of the highest accuracy available today. Data from unreliable experimental techniques are omitted from consideration. By way of notation, a number in parentheses is a value which *might* be in error, not by a lot, but by a little more than the other numbers in the same column. The parentheses appear because there is a discrepancy in the experimental data base, or because we have resorted to a slight extrapolation somewhere within the data analysis. References to experimental data are generally not given here, but they can be found in the publications cited here, where the data analysis was originally done.

Some comments on notation will be useful. We use the word *structure* with two different meanings, namely (a) as in *electronic structure*, meaning the wave functions and energy levels of the system electrons, and (b) as in *crystal structure*, meaning any stable-equilibrium configuration of the nuclei. To indicate atmospheric pressure we sometimes write $P = 1$ bar, but usually write $P = 0$. *On the order*, or the symbol $\sim$, means within a factor of two or so, while *approximately equal*, or $\approx$, means much closer, and usually indicates an approximation based on a small parameter. The symbol $\doteq$ is used here to denote a relation which we believe to be highly accurate, almost exact.

It is amazing to realize how many people, whose names and faces I remember, have had a positive influence on my work. Perhaps a meaningful expression of appreciation can be achieved by acknowledging the places where this work was carried on: the physics department at Iowa State University, the research groups at Sandia National Laboratories, the theoretical physics department at Ecole Polytechnique Federale de Lausanne, the Commonwealth Scientific and Industrial Research Organization

in Sydney, the physics department at the University of Antwerp, and the theoretical division at Los Alamos National Laboratory. Los Alamos has supported this work for many years on the grounds that it leads to a better understanding of the motion of particles in condensed matter systems, and hence leads to improved equations of state for real materials. During the preparation of this monograph, I have had the benefit of encouragement and valuable insights from James N. Johnson, Brad Clements, John Wills, and Eric Chisolm. Collaboration with Nicolas Bock and Dermot Coffey on electron-phonon interactions has been very helpful. The work of transforming my handwritten pages into book format was done with extraordinary skill by Kay Grady. And always cheerfully, Jo Ann Brown has provided me with communications services.

Duane C. Wallace
Los Alamos
September 2002

*This page intentionally left blank*

# Contents

*This page intentionally left blank*

# Chapter 1

# Condensed Matter Hamiltonian

## 1 NATURE OF CONDENSED MATTER

### *Structure of the Theory*

Ultimately our goal is to understand, at the highest level of accuracy possible, the binding and the excitations of condensed matter systems. Condensed matter means solids and liquids, where solids can be crystalline or amorphous. The excitations consist of two classes, (a) motion of the nuclei, resolved into harmonic vibrational motion (phonons), plus corrections which are characteristic of solids, or of liquids, and (b) excitation of the electrons, modified through interaction with the nuclear motion. From the outset the complete theory is developed, to include metals and insulators, solids and liquids, within a single formulation. The accuracy and generality of theory is determined by comparisons with experimental data for real materials, and also by comparisons with computer simulations for model Hamiltonians. Only highly accurate experimental data are used, and those measurements which provide the most useful information in the present study are the phonon dispersion curves and elastic constants, and the thermodynamic entropy as function of temperature for solid and liquid phases.

Our study is limited to the elements, where the most extensive and reliable experimental data are available, and where the theory is as simple as possible. The nature of binding and excitations, and of the equilibrium statistical mechanical properties, is the same for alloys and compounds.

Our procedure is classic many-body physics. For a given material, all our information is coded into its Hamiltonian. All the equilibrium prop-

erties which can be compared with experiment follow in principle from the Hamiltonian. Indeed, nonequilibrium properties follow from the same Hamiltonian, but practical application of nonequilibrium statistical mechanics is not sufficiently developed to be helpful in our present study. On the other hand, precise information gained here, about the Hamiltonian and its equilibrium statistical properties, will help in developing the nonequilibrium theory. As we shall see in the following sections, the Hamiltonian for a condensed system of nuclei and electrons can be written

$$\mathcal{H} = \sum_K \frac{\mathbf{p}_K^2}{2M} + \Phi(\{\mathbf{r}_K\}) + \mathcal{H}_{EX}, \tag{1.1}$$

where the nuclei are labeled by the index $K$ and have momenta and positions $\mathbf{p}_K$ and $\mathbf{r}_K$ respectively, and where $M$ is the nuclear mass, $\Phi(\{\mathbf{r}_K\})$ is the potential for the nuclear motion, and $\mathcal{H}_{EX}$ expresses electronic excited states. This form of $\mathcal{H}$ covers our entire program, but its appearance is deceptively simple. It is necessary to use our deepest understanding of condensed matter to express (1.1) in a form which is tractable even in leading order. This is illustrated by the example of a crystal, where we know that the nuclei move only in the near vicinity of the lattice sites, so in leading approximation the potential $\Phi$ can be expanded to quadratic order in displacements from equilibrium, and the electronic states can be evaluated for the perfect crystal. In a similar way, a newly developed picture of the motion of nuclei in a monatomic liquid transforms the Hamiltonian of Eq. (1.1) into a tractable approximation for equilibrium liquid dynamics (Chapter 5).

A condensed matter system is composed of nuclei and electrons, point particles with only mutual Coulomb interactions. Fermi statistics is always important for the electrons, just as in free atoms, while the nuclear exchange statistics is almost always unimportant because, in most solids and liquids, the nuclei remain sufficiently well separated that exchange is virtually zero. Condensed matter systems where nuclear exchange is important, such as helium isotopes, are not covered by our presentation. It is also justified to treat condensed matter as a collection of rigid ions plus valence electrons, where each ion is a nucleus with a closed-shell core of electrons, and the valence electrons are those which participate in the binding and the excitations of the system. The core electrons remain nearly the same as the inner shells of a free atom, but the valence electrons occupy col-

lective states of the whole system, whose energies are spread into bands. Qualitatively, the binding of a condensed matter system is composed of an attractive term and a repulsive term, expressing the same physics as the binding of a molecule. The attractive term arises because, when a number of free atoms are brought together, so that their electrons begin to overlap, the electron density can move preferentially into spaces directly between nearest-neighbor nuclei, thus lowering the Coulomb energy of the system. The repulsion arises because, as a result of spin statistics, electron wavefunctions must be mutually orthogonal in real space, and this is achieved by wavefunction oscillations, producing (positive) kinetic energy. This term is also called Pauli repulsion. We shall now discuss how the various binding types of solid and liquid elements result from different ways in which the valence electrons can maximize the total binding energy.

### *Metals*

For a metal, the valence band is broad and continuous in energy, and the groundstate energy is lowered with respect to free atoms by putting the valence electrons into the lower levels of the valence band (or bands). This means there are empty electronic states immediately above the highest occupied states, hence the electrons can move around easily, and this gives rise to the high conductivity of metals. For this reason the valence electrons, or sometimes the most mobile of them, are called conduction electrons. The high mobility of conduction electrons gives metals their strong screening capability, so that the effective internuclear forces, or interionic forces, are screened Coulomb forces. The presence of empty electronic states immediately above the Fermi energy also allows significant thermal excitation of electrons, at all temperatures of interest in condensed matter physics, and this gives rise to a free energy contribution present only in metals. These properties hold for all metallic systems, elements and alloys in solid and liquid phases.

An important subgroup of metals is the nearly-free-electron (NFE) metals, also called the simple metals. Their importance derives from two factors: (a) experimentally, these are the most thoroughly studied of all the elements in solid and liquid form, and accurate experimental data are available for many properties under widely varying conditions, and (b) we have a simple approximate electronic structure theory, and a corresponding Hamiltonian of the form of Eq. (1.1), which give good theoretical accounts

of the microscopic and macroscopic properties of the NFE metals. This theory, pseudopotential perturbation theory, is presented in Sec. 5. The corresponding interionic potential has the form

$$\Phi(\{\mathbf{r}_K\}) = \Omega(V) + \frac{1}{2}\sum_{KL}\phi(|\mathbf{r}_K - \mathbf{r}_L|; V) + \frac{1}{6}\sum_{KLM}\phi_{KLM} + \cdots \quad . \quad (1.2)$$

Here $\Omega(V)$ is large and negative, is the main contribution to the binding energy, and depends on only the volume $V$, or more precisely on the volume per atom $V_A$. The pair potential $\phi(r; V)$ depends on the ion positions, hence controls the motion of the ions, and $\phi(r; V)$ also depends explicitly on $V$, because it works through the screening electrons. Three-ion interactions $\phi_{KLM}$, and higher order interactions represented by $+\cdots$ in Eq. (1.2), are present in the theory, but are formally small and usually neglected. Qualitatively for NFE metals at normal density, the magnitude $|\Sigma_{KL}\phi_{KL}|$ is small compared to $|\Omega(V)|$, and the depth of the attractive well in $\phi(r; V)$ is on the order of the melting temperature.

The theoretical pair potential for metallic Na is shown in Fig. 1.1. In pseudopotential perturbation theory, $\phi(r; V)$ has long range Friedel oscillations, but their magnitude is small compared to the accuracy of the theory. Hence it is justified to damp out the oscillations, to achieve a short range potential convenient for molecular dynamics simulations, as shown in the figure.

Among the well-studied elements in the periodic table, there are 22 NFE metals, 22 transition metals, 14 lanthanides, and a few actinides. Density functional theory does well for the electronic structure of all metals, except for the problem of localized f electrons (see the discussion at the end of Sec. 2). For non-NFE metals, there are no general theoretical forms for $\Phi(\{\mathbf{r}_K\})$, such as the NFE form given by Eq. (1.2), but much work is being done in this area. We are aware of no exceptions to the two rules, that solid metals melt to liquid metals, and that metals remain metals under compression. Whenever we study the physical properties of an elemental solid or liquid, we tend to compare them with the corresponding properties of a representative metal, that is to say, metals are our reference condensed-matter system.

The elements As, Sb, and Bi are metals with extremely small Fermi surfaces, corresponding to almost filled and almost empty bands, hence these elements have very small conductivities, and are called semimetals. These

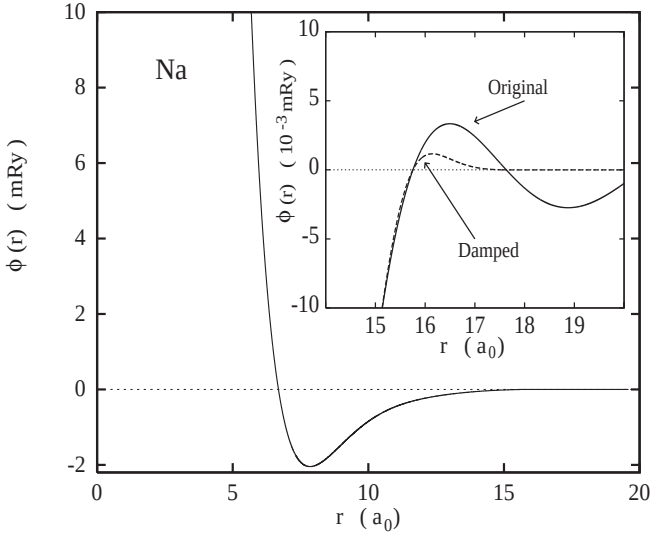


Figure 1.1. The ion-ion potential for pseudopotential sodium at $V_A = 278a_0^3$, the atomic volume of liquid sodium at melt. The original potential is from Wallace (1968), and the damped potential is from Wallace and Clements (1999).

elements melt to ordinary liquid metals, which in reasonable approximation are NFE metals, and as solids they are expected to become metallic upon sufficient compression.

### *Van der Waals Forces*

In a free rare-gas atom, the electrons fill a closed shell. The atomic charge density, nucleus plus electrons, undergoes quantum fluctuations, all multipoles appear, but on average the charge density is spherically symmetric. When two such atoms are present, the fluctuating electrostatic multipole-multipole interaction can be treated in perturbation theory, and in second order, where the interactions are squared before they are averaged, a nonzero energy appears. The leading electrostatic energy is an attractive dipole-dipole interaction, proportional to $r^{-6}$, where $r$ is the nuclear separation. This is the van der Waals interaction, and is responsible for most of the binding of a condensed system of rare-gas atoms. When two rare-gas atoms are far apart, such that the transit time of a photon between them is greater than the nominal charge-fluctuation time, then the electrostatic

potential becomes retarded, and the interatomic potential goes over to an $r^{-7}$ dependence, and is a Casimir interaction (see Milonni, 1994, Chaps. 7 and 8; also Spruch, 1986).

When two rare-gas atoms are close enough that their electron densities overlap, the Pauli repulsion appears, and is especially strong because the electrons fill closed atomic shells. The *ab initio* theory of the forces between rare gas atoms, called dispersion forces, is under development still today. Density functional theory, in the form currently applied to condensed matter, is unable to account for dispersion forces. An empirical potential representing the interaction between two rare-gas atoms is the Lennard-Jones (LJ) potential,

$$\phi(r) = 4\epsilon \left[ \left(\frac{\sigma}{r}\right)^{12} - \left(\frac{\sigma}{r}\right)^{6} \right] \quad , \tag{1.3}$$

where $\phi(r)$ passes through zero at $r = \sigma$, and has a minimum of $-\epsilon$ at slightly larger $r$. Parameters in the LJ potential are determined by fitting to experimental data (see Hirschfelder, Curtiss, and Bird, 1954; Guyer, 1969; Nardone *et al.*, 1996; and Suni, 1997). Parameters determined by fitting theoretical virial coefficients to experimental gas data are, from Hirschfelder *et al.* (1954),

$$\text{LJAr}: \quad \epsilon/k = 119.8K, \quad \sigma = 3.405 \overset{o}{A} \quad . \tag{1.4}$$

We have used this potential in computer simulations, and it gives agreement at the few percent level with thermodynamic data for crystal and liquid Ar.

For a rare-gas solid or liquid, with the LJ potential, or with any central potential $\phi(r)$, the total nuclear-motion potential is

$$\Phi(\{\mathbf{r}_K\}) = \frac{1}{2} \sum_{KL} \phi\left(|\mathbf{r}_K - \mathbf{r}_L|\right) \quad . \tag{1.5}$$

The system is weakly bound, hence has large compressibility and large thermal expansion. These properties are revealed in the scaled quantities listed in Table 1.1, where the volumes $V_0$, $V_{cm}$, and $V_{lm}$ are respectively the volume of the crystal at $T = 0$, the crystal at melt, and the liquid at melt. The relative expansion of the crystal from $T = 0$ to melt is larger for van der Waals than metallic forces, and the relative expansion from crystal

to liquid at melt is *much larger* for van der Waals than metallic forces. $T_m$ and $T_v$ are respectively the melting and vaporization temperature, and the last column shows that the van der Waals liquid at melt is *barely bound*. As a consequence, rare-gas liquids at melt are in fact halfway between a liquid and a gas (see Sec. 23 for a more precise characterization). On the other hand, the strong binding of metallic liquids, shown in the last column of Table 1.1, is due to the large contribution $\Omega(V)$, present in Eq. (1.2) but not in (1.5).

Table 1.1. Scaled quantities showing weakness of binding in van der Waals elements compared to metals, and showing the rigidity of covalent bonds relative to metals. There are no covalent liquids among the elements we have studied.

| Bonding type | $\frac{V_{cm}-V_0}{V_0}$ | $\frac{V_{lm}-V_{cm}}{V_{cm}}$ | $\frac{T_v-T_m}{T_m}$ |
|---|---|---|---|
| van der Waals | 0.10 | 0.15 | 0.04 |
| metal | 0.07 | 0.04 | 1.5 |
| covalent | 0.02 | — | — |

The LJ model for Ar has been a paradigm for liquid theory for many years. The gaslike nature of this system was not recognized, and this inhibited development of a physically realistic theory of liquid dynamics. Fortunately, this problem does not appear when one studies liquid metals, which possess thoroughly liquid properties. Meanwhile it was found that modestly compressed Ar exhibits ordinary liquid behavior (see Fig. 23.1, and the compression dependence of melting in Sec. 26). We expect that all rare gases will be ordinary monatomic liquids when slightly compressed, and that all will become metals under sufficient compression.

### *Covalent Bonding and Other Types*

Covalent electron wavefunctions consist (approximately) of linear combinations of atomic wavefunctions, split into bonding and antibonding orbitals. Covalent bonds are strongest when the bonding orbitals are completely filled, and the antibonding orbitals are completely empty. The hydrogen

molecule bond, formed with two electrons having antiparallel spins, is the prototype covalent bond. The diamond structure elements C, Si, Ge, and $\alpha$-Sn are covalent. We shall omit C from our study, since dia-C at low pressure is metastable with respect to graphite, and graphite, also covalent, is strongly two-dimensional in character. Very little data are available for B, so the only covalent elements we can study are Si, Ge, and $\alpha$-Sn.

Density functional theory does well for the electronic structure of the diamond crystals. A first approximation for the electronic structure is obtained from tight binding theory, with Bloch functions based on atomic $sp^3$ orbitals. There is a gap between bonding and antibonding valence bands, the lower band is filled, and the crystal is an insulator. The bonds are oriented toward the corners of a tetrahedron, and are quite rigid, i.e., are hard to stretch and hard to bend. The rigidity gives rise to very low compressibility and thermal expansion, and to high phonon frequencies. The extremely low relative expansion of the crystal from $T = 0$ to melt is shown in Table 1.1.

Aside from C, column IVA of the periodic table consists of Si, Ge, Sn, and Pb. Si and Ge are covalent to melt, $\alpha$-Sn is covalent and transforms at around 0.6 $T_m$ to metallic $\beta$-Sn, and Pb is metallic to melt. Liquid Si, Ge, Sn, and Pb are all NFE metals. Upon compression, $\alpha$-Sn, Si, and Ge transform to the metallic phase with tetragonal ($\beta$-Sn) structure, and are expected to remain metals with further compression.

The elements H, N, O, and the halogens condense to diatomic molecular liquids and solids at low pressure. Also, P, S, Se, and Te have complicated bonding and very little experimental data. These systems are omitted from consideration in our study. All these elements are expected to become metallic under compression, and as metals, our present analysis will apply.

### *Condensed Matter Regime*

We need to specify a criterion for condensed matter, consistent with the theoretical framework to be developed, and consistent with the conclusions to be drawn on the nature of solids and liquids. In all the work presented here, indeed in all our experience with solids and liquids, the essential character of condensed matter is that of collective nuclear motion within nearly-harmonic many-particle potential energy valleys. Correspondingly, the dominant term in the nuclear motion Hamiltonian is $\mathcal{H}_{ph}$, expressing resolution of this motion into a set of independent quasiharmonic phonons,

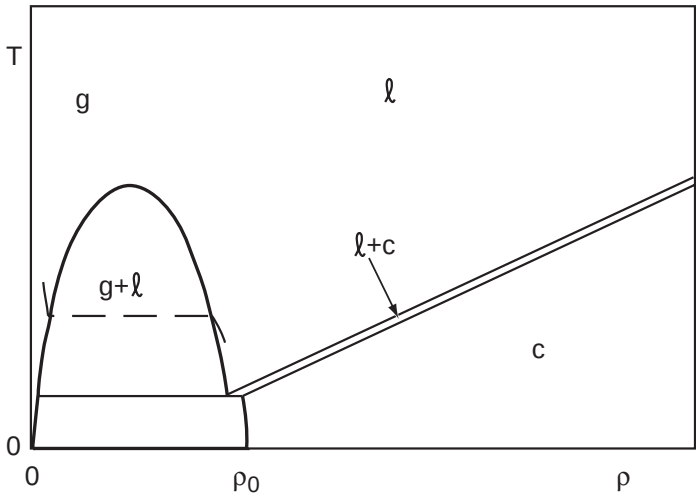


Figure 1.2. Generic phase diagram for an element in $T - \rho$ space, where g = gas, $\ell$ = liquid, and c = crystal. The dashed line through the gas + liquid region indicates vaporization (or condensation) at constant $T$ and $P$.

and the nuclear motion entropy or specific heat is approximately that due to quasiharmonic phonons in quantum statistical mechanics. This property of the nuclear motion entropy or specific heat will be our criterion for condensed matter. When the nuclear motion is classical, which is usually the case at temperatures above a few tenths of $T_m$, the quasiharmonic specific heat is $3k$ per nucleus. In contrast, the nuclear motion specific heat for an ideal gas is $\frac{3}{2}k$ per nucleus.

Figure 1.2 shows a generic phase diagram for an element in temperature-density space. Several crystal phases are usually present, but only one is indicated. Density of the crystal at $T = 0$ and $P = 1$ bar is denoted $\rho_0$, and the term *normal density* means any density in the vicinity of $\rho_0$. At any temperature, if density is decreased from normal density, the system properties become more like a gas. When density is increased from normal density, the system should remain ordinary condensed matter, as indicated in the figure. At very high densities, our description will fail because the system will ultimately become relativistic, where particles are created out of the vacuum. This effect should be negligible to at least $10^3$ or $10^4$ g/cm$^3$.

When the liquid is heated at 1 bar, thermal expansion carries it to lower densities, and eventually it arrives at the gas-liquid phase boundary,

where vaporization begins (see Fig. 1.2). The liquid might pass out of the condensed matter regime before it reaches the gas-liquid boundary. On the other hand, if the liquid is heated at constant density, it never vaporizes, and it changes only continuously and slowly to a gas. We estimate in Sec. 23 that the condensed matter criterion holds at temperatures up to around $5T_m$ at a given density. At higher temperatures, higher nuclear kinetic energy enables more gaslike motion. This effect, and other processes in condensed matter at very high temperatures, is discussed in Sec. 25.

This monograph carries the subtitle *A guide to accurate equations of state*. By equation of state, we mean the complete set of thermodynamic functions for a given material, which can be obtained from the Helmholtz free energy, which in turn is obtained from the canonical partition function. Through extensive comparison of theory and experiment, we shall demonstrate that the condensed matter Hamiltonian is sufficiently well understood, and the statistical mechanical procedures are sufficiently well tested, that we know in principle how to calculate *ab initio* the equation of state of an elemental solid or liquid, throughout the condensed matter regime, to an accuracy on the same order as the accuracy of experimental equation-of-state data. In addition, much has been learned about the errors associated with various simplifying approximations. Because it is physically based, our equation-of-state formulation provides functions of the correct form for fitting to experimental data, and provides the most reliable prediction of thermodynamic properties whenever experimental data are not available. Detailed discussions of the equation of state may be found in Secs. 20 and 25.

## 2 DENSITY FUNCTIONAL THEORY

### *Many-Electron Problem*

The condensed matter system is composed of a large number of atoms, or in more detail, a collection of nuclei and electrons. The system is electrically neutral. The first step in solving for the motion is to fix the positions of the nuclei, and solve for the energy levels of the electronic system in the presence of the nuclear potential. There are $\mathcal{Z}$ electrons, labeled $\alpha = 1, \cdots, \mathcal{Z}$, and the position of electron $\alpha$ is $\mathbf{r}_\alpha$. The total electronic kinetic energy

is $\mathcal{T}_E$,

$$\mathcal{T}_E = -\sum_\alpha \frac{\hbar^2 \nabla_\alpha^2}{2m} \quad , \tag{2.1}$$

and the total electron-electron Coulomb interaction is $\Omega_{EE}$,

$$\Omega_{EE} = \frac{1}{2}{\sum_{\alpha\beta}}' \frac{e^2}{|\mathbf{r}_\alpha - \mathbf{r}_\beta|} \quad . \tag{2.2}$$

Each electron sees a potential $\mathcal{V}(\mathbf{r})$ due to the fixed set of nuclei, so that the total electronic Hamiltonian is

$$\mathcal{H}_E = \mathcal{T}_E + \Omega_{EE} + \sum_\alpha \mathcal{V}(\mathbf{r}_\alpha) \quad . \tag{2.3}$$

Equation (2.3) is the customary Hamiltonian for the electronic structure problem. But notice there is a potential contribution that has not been mentioned, namely the Coulomb interaction among the nuclei. Common practice, followed here, is to include this interaction in $\Sigma_\alpha \mathcal{V}_\alpha$, though it does not actually depend on the electron positions. In this way, the Coulomb divergences present in $\Omega_{EE}$ and $\Sigma_\alpha \mathcal{V}_\alpha$ sum to zero. Exact composition of the total potential will be made explicit in the total Hamiltonian, Sec. 4. Since there is no spin dependence in $\mathcal{H}_E$, its eigenstates are spin degenerate. Spin dependent density functional theory describes magnetic states, and will not be treated in this monograph.

Let us briefly discuss the many-electron wavefunctions, for the purpose of defining electron correlation effects. It will be necessary to include spin, so that the spin states can be counted. An electron has position $\mathbf{r}$ and spin $\sigma$, where $\sigma = 1, 2$. A normalized wavefunction is $\Phi(\mathbf{r}_1\sigma_1, \cdots, \mathbf{r}_\mathcal{Z}\sigma_\mathcal{Z})$ and satisfies

$$\sum_{\{\sigma\}} \int \cdots \int \Phi^*(\mathbf{r}_1\sigma_1, \cdots, \mathbf{r}_\mathcal{Z}\sigma_\mathcal{Z}) \Phi(\mathbf{r}_1\sigma_1, \cdots, \mathbf{r}_\mathcal{Z}\sigma_\mathcal{Z}) d\mathbf{r}_1 \cdots d\mathbf{r}_\mathcal{Z} = 1 \tag{2.4}$$

where the specified sum is over both spin states for every electron. The one-electron density is $\rho(\mathbf{r})$, the probability per unit volume of having an electron at $\mathbf{r}$,

$$\rho(\mathbf{r}_1) = \mathcal{Z} \sum_{\{\sigma\}} \int \cdots \int \Phi^* \Phi \; d\mathbf{r}_2 \cdots d\mathbf{r}_\mathcal{Z} \quad . \tag{2.5}$$

The normalization is

$$\int \rho(\mathbf{r})d\mathbf{r} = \mathcal{Z} \quad . \tag{2.6}$$

The two-electron density is $\rho(\mathbf{r}_1, \mathbf{r}_2)$ ,

$$\rho(\mathbf{r}_1, \mathbf{r}_2) = \mathcal{Z}(\mathcal{Z}-1) \sum_{\{\sigma\}} \int \cdots \int \Phi^* \Phi \; d\mathbf{r}_3 \cdots d\mathbf{r}_{\mathcal{Z}} \quad . \tag{2.7}$$

The normalization is

$$\int \rho(\mathbf{r}_1, \mathbf{r}_2)d\mathbf{r}_2 = (\mathcal{Z}-1)\rho(\mathbf{r}_1) \quad . \tag{2.8}$$

This normalization is consistent with liquid theory (Hansen and McDonald, 1986, Sec. 2.5). Parr and Yang (1989, Eq. (2.4.3)) insert a factor of $\frac{1}{2}$ in $\rho(\mathbf{r}_1, \mathbf{r}_2)$. Positional correlations of the electrons are contained in $\rho(\mathbf{r}_1, \mathbf{r}_2)$. These correlations are isolated in the pair correlation function $g(\mathbf{r}_1, \mathbf{r}_2)$, defined by

$$\rho(\mathbf{r}_1, \mathbf{r}_2) = \rho(\mathbf{r}_1)\rho(\mathbf{r}_2)g(\mathbf{r}_1, \mathbf{r}_2) \quad . \tag{2.9}$$

The pair correlation function is a conditional probability: given an electron at $\mathbf{r}_1$, the probability per unit volume of an electron at $\mathbf{r}_2$ is $\rho(\mathbf{r}_2)g(\mathbf{r}_1, \mathbf{r}_2)$. At large separations, there is no correlation, so $g(\mathbf{r}_1, \mathbf{r}_2) \to 1$ at large separations, and the *local* correlation is contained in the function $h(\mathbf{r}_1, \mathbf{r}_2) = g(\mathbf{r}_1, \mathbf{r}_2) - 1$. The density $\rho(\mathbf{r}_2)h(\mathbf{r}_1, \mathbf{r}_2)$ is the exchange-correlation hole around an electron at $\mathbf{r}_1$, and from the above equations it follows

$$\int \rho(\mathbf{r}_2)h(\mathbf{r}_1, \mathbf{r}_2)d\mathbf{r}_2 = -1 \quad . \tag{2.10}$$

In words, if an electron is located at $\mathbf{r}_1$, then in the vicinity of $\mathbf{r}_1$ the density of the *remaining* electrons is deficient by one.

When the electronic system is in the state with wavefunction $\Phi$, the total Coulomb energy (2.2) can be written with the aid of (2.7),

$$\Omega_{EE} = \frac{e^2}{2} \iint \frac{\rho(\mathbf{r}_1, \mathbf{r}_2)}{|\mathbf{r}_1 - \mathbf{r}_2|} d\mathbf{r}_1 d\mathbf{r}_2 \quad . \tag{2.11}$$

This can be separated into the uncorrelated and correlated parts respectively, as

$$\frac{e^2}{2}\iint \frac{\rho(\mathbf{r}_1)\rho(\mathbf{r}_2)}{|\mathbf{r}_1-\mathbf{r}_2|}d\mathbf{r}_1 d\mathbf{r}_2 + \frac{e^2}{2}\iint \frac{\rho(\mathbf{r}_1)\rho(\mathbf{r}_2)h(\mathbf{r}_1,\mathbf{r}_2)}{|\mathbf{r}_1-\mathbf{r}_2|}d\mathbf{r}_1 d\mathbf{r}_2 \quad . \tag{2.12}$$

The second term contains the positional correlations, and is the exchange-correlation energy. This term *reduces* the total Coulomb energy, since the electrons are always able to avoid one another to some degree, as indicated by the minus sign in (2.10).

### *Many-Electron Groundstate*

This monograph is written primarily for individuals who are interested in the elementary excitations in condensed matter, the phonons and electrons, and the statistical mechanics of those excitations. The electronic structure community is currently able to calculate the parameters of the elementary excitations, through density functional theory. Here we shall give a brief but rigorous outline of density functional theory of the many-electron groundstate. Our intention is to assist communication between the electronic structure community, and those who need to use the calculated results of electronic structure theory. Thorough presentations of density functional theory are provided by Parr and Yang (1989), and Dreizler and Gross (1990).

The Rayleigh-Ritz variational principle tells us that the groundstate energy $\mathcal{E}_g$ is given by the minimum value of $\langle\Psi|\mathcal{H}_E|\Psi\rangle$, where the minimization is over the space of normalized antisymmetric $\mathcal{Z}$-electron functions. The minimizing function is the groundstate wavefunction $\Psi_g$, and this wavefunction gives the groundstate multielectron densities, among them the one-electron density $\rho_g(\mathbf{r})$. To convert this variational principle into density functional theory, it is only necessary to organize the variational process into the constrained search described by Levy (1979), and discussed further by Lieb (1982). Let $\Psi_\rho$ be a normalized many-electron function which integrates to a specified one-electron density $\rho(\mathbf{r})$. Then $\mathcal{E}[\rho]$ is a functional of $\rho(\mathbf{r})$, defined by

$$\mathcal{E}[\rho] = \min\langle\Psi_\rho|\mathcal{H}_E|\Psi_\rho\rangle \quad , \tag{2.13}$$

where the minimization is over all $\Psi_\rho$ for the given $\rho(\mathbf{r})$. Then from the

Rayleigh-Ritz principle,

$$\mathcal{E}_g = \min \mathcal{E}[\rho] \quad , \tag{2.14}$$

where the minimization is over all $\rho(\mathbf{r})$. The minimizing one-electron density is the groundstate density $\rho_g(\mathbf{r})$. For applications in the present monograph, the electronic system will have a nondegenerate groundstate. In this case, (2.14) establishes a one-to-one correspondence between $\mathcal{E}_g$ and $\rho_g(\mathbf{r})$. In the derivation leading to (2.14), the only restriction on the one-electron density is that it be obtained from a normalized antisymmetric $\mathcal{Z}$-electron function. Such a density is called *$\mathcal{Z}$-representable* (Levy 1979).

In Eq. (2.3), $\mathcal{H}_E$ is written as the sum of three terms. Each term contributes to the right side of (2.13), hence each term corresponds to a functional contributing to $\mathcal{E}[\rho]$. Let $\Psi_\rho(\min)$ be the function which minimizes $\langle\Psi_\rho|\mathcal{H}_E|\Psi_\rho\rangle$. We then have the functionals

$$\mathcal{T}_E[\rho] = \langle\Psi_\rho(\min)|\mathcal{T}_E|\Psi_\rho(\min)\rangle \quad , \tag{2.15}$$

$$\Omega_{EE}[\rho] = \langle\Psi_\rho(\min)|\Omega_{EE}|\Psi_\rho(\min)\rangle \quad , \tag{2.16}$$

and the total energy functional is

$$\mathcal{E}[\rho] = \mathcal{T}_E[\rho] + \Omega_{EE}[\rho] + \int \rho(\mathbf{r})\mathcal{V}(\mathbf{r})d\mathbf{r} \quad . \tag{2.17}$$

Now in the minimization of $\langle\Psi_\rho|\mathcal{H}_E|\Psi_\rho\rangle$, Eq. (2.13), $\rho(\mathbf{r})$ is held constant, hence the contribution $\int\rho(\mathbf{r})\mathcal{V}(\mathbf{r})d\mathbf{r}$ is also constant, so that the minimizing function $\Psi_\rho(\min)$ is independent of the potential $\mathcal{V}(\mathbf{r})$. Hence $\mathcal{T}_E[\rho]$ and $\Omega_{EE}[\rho]$ are universal functionals, independent of $\mathcal{V}(\mathbf{r})$. An important early step in the development of density functional theory was the proof of the existence of the universal functional $F[\rho] = \mathcal{T}_E[\rho] + \Omega_{EE}[\rho]$, by Hohenberg and Kohn (1964). Through the Levy constrained search outlined above, we now have equations for the universal functionals, albeit complicated equations, namely Eqs. (2.15) and (2.16).

### *Kohn-Sham Formulation*

Kohn and Sham (1965) presented a formulation for the groundstate energy of an interacting many-electron system, where the only restriction in principle is that $\rho(\mathbf{r})$ be *noninteracting V-representable* (explained below). They

first consider a noninteracting $\mathcal{Z}$-electron system with Hamiltonian $\Sigma_\alpha \mathcal{H}^s_\alpha$, where $\mathcal{H}^s_\alpha$ is the single-electron Hamiltonian

$$\mathcal{H}^s_\alpha = -\frac{\hbar^2 \nabla^2_\alpha}{2m} + V^s(\mathbf{r}_\alpha) \quad , \tag{2.18}$$

and where $V^s(\mathbf{r})$ is a fixed potential acting on an electron at $\mathbf{r}$, with $V^s(\mathbf{r})$ to be determined so as to facilitate the many-electron solution. The single-electron Hamiltonian has a complete set of eigenfunctions $\psi_\lambda(\mathbf{r})$, with eigenvalues $E_\lambda$, $\lambda = 1, 2, \cdots$, which satisfy

$$\mathcal{H}^s \psi_\lambda(\mathbf{r}) = E_\lambda \psi_\lambda(\mathbf{r}) \quad , \tag{2.19}$$

$$\int \psi^*_\lambda(\mathbf{r}) \psi_{\lambda'}(\mathbf{r}) d\mathbf{r} = \delta_{\lambda\lambda'} \quad . \tag{2.20}$$

In the groundstate, the $\mathcal{Z}$ lowest single-electron states are occupied. The groundstate wavefunction is a Slater determinant of the occupied $\psi_\lambda$, and the groundstate energy $\mathcal{E}^s_g$ and one-electron density $\rho^s_g(\mathbf{r})$ are respectively

$$\mathcal{E}^s_g = \sum_{\lambda=1}^{\mathcal{Z}} E_\lambda \quad , \tag{2.21}$$

$$\rho^s_g(\mathbf{r}) = \sum_{\lambda=1}^{\mathcal{Z}} \psi^*_\lambda(\mathbf{r}) \psi_\lambda(\mathbf{r}) \quad . \tag{2.22}$$

In sums such as these, it is understood that the $\psi_\lambda(\mathbf{r})$ are present in degenerate pairs, corresponding to the two spin states for each electron.

The next step is to forget the Schrödinger solution just presented, and apply density functional theory to the noninteracting system. The constrained search program is the same as defined in Eqs. (2.13) and (2.14), but now the variational set of system functions is a single Slater determinant, made up from $\mathcal{Z}$ orthonormal variational functions $\phi_\lambda(\mathbf{r}), \lambda = 1, \cdots, \mathcal{Z}$. This means that the one-electron density, and the various energy functionals, are less general than in the interacting electron system, because they are defined on a restricted class of functions. The one-electron density is

$$\rho^s(\mathbf{r}) = \sum_{\lambda=1}^{\mathcal{Z}} |\phi_\lambda(\mathbf{r})|^2 \quad , \tag{2.23}$$

and the energy functional (2.17) becomes

$$\mathcal{E}^s[\rho^s] = \mathcal{T}^s[\rho^s] + \int \rho^s(\mathbf{r}) V^s(\mathbf{r}) d\mathbf{r} \quad , \tag{2.24}$$

where

$$\mathcal{T}^s[\rho^s] = \sum_{\lambda=1}^{\mathcal{Z}} \left\langle \phi_\lambda \left| -\frac{\hbar^2 \nabla^2}{2m} \right| \phi_\lambda \right\rangle \quad . \tag{2.25}$$

Density functional theory now tells us that the groundstate energy is $\mathcal{E}_g^s = \min \mathcal{E}^s[\rho^s]$, and the minimizing $\rho^s(\mathbf{r})$ is the groundstate density $\rho_g^s(\mathbf{r})$.

Kohn and Sham now assume that the groundstate density $\rho_g(\mathbf{r})$ for an interacting system is *noninteracting V-representable*, which means $\rho_g(\mathbf{r})$ is identical to the density $\rho_g^s(\mathbf{r})$ for a noninteracting system with *some* $V^s(\mathbf{r})$. To appreciate the importance of this step, notice that the form written in (2.23) is a very weak restriction on the one-electron density, but if we were trying to solve the Schrödinger equation for the electronic groundstate, limiting the wavefunction to a Slater determinant would be a very serious restriction. The condition $\rho_g(\mathbf{r}) = \rho_g^s(\mathbf{r})$ implies that the functional variations of both $\mathcal{E}[\rho]$ and $\mathcal{E}^s[\rho]$ are zero at the same density:

$$\frac{\delta \mathcal{E}[\rho]}{\delta \rho} = \frac{\delta \mathcal{E}^s[\rho]}{\delta \rho} = 0, \qquad \text{at } \rho(\mathbf{r}) = \rho_g(\mathbf{r}) \quad . \tag{2.26}$$

With $\mathcal{E}[\rho]$ and $\mathcal{E}^s[\rho]$ from (2.17) and (2.24) respectively, the above variation leads to the equation for $V^s(\mathbf{r})$,

$$V^s(\mathbf{r}) = \mathcal{V}(\mathbf{r}) + e^2 \int \frac{\rho_g(\mathbf{r}')}{|\mathbf{r} - \mathbf{r}'|} d\mathbf{r}' + V_{xc}(\mathbf{r}) \quad , \tag{2.27}$$

where $V_{xc}(\mathbf{r})$ is the exchange-correlation potential, given by

$$V_{xc}(\mathbf{r}) = \left. \frac{\delta \mathcal{E}_{xc}[\rho]}{\delta \rho(\mathbf{r})} \right|_{\rho_g} \quad , \tag{2.28}$$

with (see problem 2.1)

$$\mathcal{E}_{xc}[\rho] = \mathcal{T}_E[\rho] - \mathcal{T}^s[\rho] + \frac{e^2}{2} \iint \frac{\rho(\mathbf{r}) \rho(\mathbf{r}') h(\mathbf{r}, \mathbf{r}')}{|\mathbf{r} - \mathbf{r}'|} d\mathbf{r}\, d\mathbf{r}' \quad . \tag{2.29}$$

The groundstate energy of the interacting system is given by Eq. (2.17), as $\mathcal{E}_g = \mathcal{E}[\rho_g]$. Likewise the groundstate energy of the noninteracting system

is given by Eq. (2.24), as $\mathcal{E}_g^s = \mathcal{E}^s[\rho_g]$. By writing $\mathcal{E}_g = \mathcal{E}_g^s + (\mathcal{E}_g - \mathcal{E}_g^s)$, it follows (see problem 2.2)

$$\mathcal{E}_g = \sum_{\lambda=1}^{\mathcal{Z}} E_\lambda - \frac{e^2}{2} \iint \frac{\rho_g(\mathbf{r})\rho_g(\mathbf{r}')}{|\mathbf{r}-\mathbf{r}'|} d\mathbf{r}\, d\mathbf{r}' + \mathcal{E}_{xc}[\rho_g] - \int \rho_g(\mathbf{r}) V_{xc}(\mathbf{r}) d\mathbf{r} \quad . \tag{2.30}$$

This expresses the groundstate energy of the interacting system in terms of the Schrödinger solution (2.21) and (2.22) for the noninteracting system, plus two small terms representing exchange and correlation effects. Notice $\mathcal{E}_{xc}[\rho]$, Eq. (2.29), which is commonly referred to as the exchange-correlation energy, contains the configurational exchange-correlation energy from Eq. (2.12), and contains also a kinetic energy term specific to the Kohn-Sham formulation.

Operationally, the Kohn-Sham procedure for calculating $\mathcal{E}_g$ is as follows. Initial information consists of the potential $\mathcal{V}(\mathbf{r})$ due to the nuclei, and some approximation for the universal functional $\mathcal{E}_{xc}[\rho]$, Eq. (2.29). A guess is made for the groundstate density, $\rho_g^s(\mathbf{r})$, then $V^s(\mathbf{r})$ is calculated from (2.27), the noninteracting-system equations (2.19) and (2.20) are solved, and $\rho_g^s(\mathbf{r})$ is calculated from Eq. (2.22). The process is iterated to self-consistency in $\rho_g^s(\mathbf{r})$, and then $\mathcal{E}_g$ is evaluated from (2.30).

The equations which define $\mathcal{E}_{xc}[\rho]$, starting with Eq. (2.13) for $\mathcal{E}[\rho]$, are hopelessly complicated. The utility of the Kohn-Sham formulation is that the exchange-correlation terms in $\mathcal{E}_g$, Eq. (2.30), are small, so an approximation is acceptable. The *local density* approximation consists of writing the exchange-correlation energy in the form

$$\mathcal{E}_{xc}[\rho] = \int \rho(\mathbf{r}) X(\rho(\mathbf{r})) d\mathbf{r} \quad , \tag{2.31}$$

where $X(\rho(\mathbf{r}))$ is a function of $\rho(\mathbf{r})$, not a functional. Then from (2.28), the exchange-correlation potential $V_{xc}(\mathbf{r})$ also becomes a function of the local density $\rho(\mathbf{r})$,

$$V_{xc}(\mathbf{r}) = \frac{d[\rho(\mathbf{r})X(\rho(\mathbf{r}))]}{d\rho(\mathbf{r})} \quad . \tag{2.32}$$

Kohn and Sham (1965) pointed out that the local density approximation is correct for a uniform electron gas, and in fact they limited their original derivation to the local density approximation.

### *Current Applications of Density Functional Theory*

Density functional theory for the electronic groundstate of condensed matter systems has been under active development since the papers of Hohenberg and Kohn (1964), and Kohn and Sham (1965). The focus has been to find a reliable approximation for the exchange-correlation functional, and the work has been done through a great many studies in which theory and experiment are compared for a wide variety of crystal properties. The Kohn-Sham formulation in local density approximation (LDA) has become the standard technique for band structure calculations, and currently provides respectable *ab initio* results for most crystals. The word "respectable" here means that calculations agree with experiment to within a few times the experimental error. In recent years, the theory has been extended beyond LDA, by means of the generalized gradient approximation (GGA), which includes gradients of the local one-electron density. Often but not always, GGA results are in better agreement with experiment than LDA results.

The current status of density functional theory is illustrated by examples from the recent literature. Calculations of cohesive energies, equilibrium lattice parameters, and bulk moduli are common. Calculations for various crystal structures of a given element almost always confirm the experimentally observed stable crystal structure, and similar calculations for elements under compression almost always confirm experimentally observed phase transitions as function of pressure. Elastic constants and phonon frequencies are calculated, as well as vacancy formation energies and pressure-induced changes in c/a ratios. Spin-dependent density functional theory is able to account for the crystal structures of Fe, Co, and Ni. A current frontier in electronic structure theory is the f-electron metals, the lanthanides and actinides, which are characterized by complicated crystal structures, temperature-induced phase transitions, and the availability of both localized and delocalized f-electron states. Calculations account for the observed crystal structures and equilibrium volumes of the light actinides (Th, Pa, U, Np, and Pu), while the high-temperature phases of Pu, and all crystal phases of the heavy actinides, are influenced by f-electron localization, a process whose physical origin is currently under study. Many results of density functional theory will be presented at appropriate places in this monograph.

Work has also proceeded to extend density functional theory to excited

electronic states. Mermin (1965) gave a formal density functional theory for the free energy of a system of interacting electrons in the presence of a fixed external potential. Individual excited states have been studied by Theophilou (1979), Görling (1999), and Levy and Nagy (1999). These papers make use of the stationary property of an excited state eigenfunction, when it is restricted to be orthogonal to all lower lying eigenfunctions. But the problem is extremely complicated, and we shall have to take an alternate approach in the following sections, in order to construct a practically useful condensed matter Hamiltonian.

The development of density functional theory was recognized by the award of the Nobel Prize in Chemistry to Walter Kohn in 1998.

*Problems*

*2.1* Starting from Eq. (2.26), derive (2.27) – (2.29).
*2.2* Derive Eq. (2.30). Notice the first term on the right expresses $\mathcal{E}_g^s$.

## 3 ELECTRONIC EXCITED STATES IN METALS

### *What Kind of Theory is Needed*

The essential characteristic of a metal is its unfilled conduction band. In the electronic groundstate, one-electron states are filled up to the Fermi energy, and are empty above the Fermi energy, hence there are many low-lying excited states available to the electronic system. At finite temperatures, thermal excitation of the electrons will contribute to the thermal energy and the entropy of a metal. This electronic-excitation contribution dominates the energy and entropy at very low temperatures, and continues to make a small to moderate contribution at higher temperatures, so that it is almost always larger than experimental error in the measured thermal energy and entropy. Therefore, we require a theory for the thermal excitation of electrons in metals. The same theory will also apply to semimetals, the main difference being that a semimetal has an unusually small density of electronic states at the Fermi energy. On the other hand, in an insulator, the lowest excited electronic states lie above the groundstate by a gap, of an eV or so, hence the electronic excitations give a negligible contribution to the thermal energy and entropy. Qualitatively, the same is true in a semiconductor. Nevertheless, one can use the same formal theory as we shall

develop for metals, to calculate electronic excitation effects in insulators and semiconductors, should it become of interest to do so.

If one could calculate the electronic groundstate, and the excited states as well, for the nuclei located at a fixed configuration, one could then evaluate the electronic free energy with the nuclei at that configuration. The free energy density functional theory of Mermin (1965) offers a technique for doing this in principle. However, such an electronic free energy, even if it could be evaluated for *any* configuration of the nuclei, and even if it could be averaged over the nuclear configurations, does not in principle give us the excitation free energy of a condensed matter system. This is because, in a complete treatment of the system, one has to allow the nuclei to move, that is to have kinetic energy, and this kinetic energy induces transitions among the electronic states. In other words, the nuclear kinetic energy perturbs the electronic states, and this perturbation is not present in any calculation of electronic states where the nuclei are at fixed positions. The process just described, of inducing electronic transitions by the nuclear motion, constitutes the nonadiabatic part of the system motion. To treat the nonadiabatic part, one requires the complete system Hamiltonian, expressing *simultaneous coupled motion* of the nuclei and electrons.

In this section, a tractable approximation is constructed for the electronic excited states in metals, when the nuclei are at arbitrary fixed locations. In Sec. 4, the coupled nuclear and electronic motion will be analyzed.

### *One-Electron Approximation: The Groundstate*

The term *one-electron approximation* generally indicates a model in which the system wavefunctions are constructed from single-electron functions. It is applied to the electronic groundstate, by minimizing $\langle\Psi|\mathcal{H}_E|\Psi\rangle$, where $\Psi$ is some variational representation of the total wavefunction. The Hartree approximation results when $\Psi$ is a product of single-electron functions, and exhibits kinetic energy, potential energy due to the external potential $\mathcal{V}(\mathbf{r})$, and uncorrelated electron Coulomb energy. Hartree-Fock results when $\Psi$ is a Slater determinant, and exhibits one additional term, the exchange Coulomb energy. But the Hartree-Fock equations are complicated to solve for condensed matter systems, so Slater proposed to replace the exchange terms in the Hartree-Fock equations by a one-electron potential depending on the local one-electron density. Later, the local exchange potential was modified with the intention of including correlation energy as well.

The latter procedure, with an arbitrary form for the exchange-correlation potential, is presented in *Thermodynamics of Crystals*, Sec. 22, and will be followed here. Excellent discussions of the one-electron approximations may be found in Kittel (1963, Ch. 5), Slater (1974), and Harrison (1989, App. A).

The starting point is an orthonormal set of one-electron variational functions $\psi_\lambda(\mathbf{r})$, $\lambda = 1, \cdots, \mathcal{Z}$. The groundstate energy is supposed to be

$$\begin{aligned} \mathcal{E}_g &= \sum_\lambda \int \psi_\lambda^*(\mathbf{r}) \left[ -\frac{\hbar^2 \nabla^2}{2m} + \mathcal{V}(\mathbf{r}) \right] \psi_\lambda(\mathbf{r}) d\mathbf{r} \\ &\quad + \frac{1}{2} \sum_{\lambda\lambda'} \iint \psi_\lambda^*(\mathbf{r}) \psi_{\lambda'}^*(\mathbf{r}') \frac{e^2}{|\mathbf{r} - \mathbf{r}'|} \psi_\lambda(\mathbf{r}) \psi_{\lambda'}(\mathbf{r}') d\mathbf{r} d\mathbf{r}' \\ &\quad + \sum_\lambda \int \psi_\lambda^*(\mathbf{r}) X(\rho_g(\mathbf{r})) \psi_\lambda(\mathbf{r}) d\mathbf{r} \quad , \end{aligned} \tag{3.1}$$

where the groundstate one-electron density is

$$\rho_g(\mathbf{r}) = \sum_\lambda \psi_\lambda^*(\mathbf{r}) \psi_\lambda(\mathbf{r}) \quad . \tag{3.2}$$

In (3.1), the first term is kinetic energy, and $\mathcal{V}(\mathbf{r})$ is the potential each electron sees due to the nuclei at fixed positions. The double sum is the uncorrelated Coulomb energy, the same as the first term in (2.12), and the last term is the exchange-correlation energy, where the function $X(\rho(\mathbf{r}))$ will eventually be calibrated to get the result of density functional theory for $\mathcal{E}_g$. Now the variation of $\mathcal{E}_g$ is set to zero,

$$\delta \mathcal{E}_g = \sum_\lambda \int \left[ \frac{\partial \mathcal{E}_g}{\partial \psi_\lambda^*(\mathbf{r})} \delta \psi_\lambda^*(\mathbf{r}) + \frac{\partial \mathcal{E}_g}{\partial \psi_\lambda(\mathbf{r})} \delta \psi_\lambda(\mathbf{r}) \right] d\mathbf{r} = 0 \quad , \tag{3.3}$$

subject to the condition that the variational functions remain normalized,

$$\delta \int \psi_\lambda^*(\mathbf{r}) \psi_\lambda(\mathbf{r}) d\mathbf{r} = \int \left[ \delta \psi_\lambda^*(\mathbf{r}) \psi_\lambda(\mathbf{r}) + \psi_\lambda^*(\mathbf{r}) \delta \psi_\lambda(\mathbf{r}) \right] d\mathbf{r} = 0 \quad . \tag{3.4}$$

The last equation is multiplied by the real Lagrange multiplier $E_\lambda$, and is summed over $\lambda$ and subtracted from Eq. (3.3), to give

$$\sum_\lambda \int \left[ \frac{\partial \mathcal{E}_g}{\partial \psi_\lambda^*(\mathbf{r})} - E_\lambda \psi_\lambda(\mathbf{r}) \right] \delta \psi_\lambda^*(\mathbf{r}) d\mathbf{r} + \text{complex conjugate} = 0 \quad . \tag{3.5}$$

Since $\delta\psi_\lambda(\mathbf{r})$ is an arbitrary complex function, then in (3.5) the coefficients of both $\delta\psi_\lambda(\mathbf{r})$ and $\delta\psi^*_\lambda(\mathbf{r})$ must vanish everywhere, and this gives the one-electron wave equations,

$$\frac{\partial \mathcal{E}_g}{\partial \psi^*_\lambda(\mathbf{r})} - E_\lambda \psi_\lambda(\mathbf{r}) = 0 \quad . \tag{3.6}$$

Since $\mathcal{E}_g$ and $E_\lambda$ are real, the complex conjugate equations contain the same information.

Equations (3.6) are transformed to the one-electron Schrödinger equation with Hamiltonian $h$ (see problem 3.1),

$$h\psi_\lambda(\mathbf{r}) = \left[-\frac{\hbar^2\nabla^2}{2m} + V_g(\mathbf{r})\right]\psi_\lambda(\mathbf{r}) = E_\lambda\psi_\lambda(\mathbf{r}) \quad , \tag{3.7}$$

where $V_g(\mathbf{r})$ is the self consistent one-electron potential,

$$V_g(\mathbf{r}) = \mathcal{V}(\mathbf{r}) + e^2\int \frac{\rho_g(\mathbf{r}')}{|\mathbf{r}-\mathbf{r}'|}d\mathbf{r}' + \frac{d\rho_g(\mathbf{r})X(\rho_g(\mathbf{r}))}{d\rho_g(\mathbf{r})} \quad . \tag{3.8}$$

The system of equations (3.2), (3.7), and (3.8) have to be solved self consistently. The total groundstate energy (3.1) can now be expressed in terms of the one-electron eigenvalues $E_\lambda$ (see problem 3.2),

$$\begin{aligned}\mathcal{E}_g &= \sum_\lambda E_\lambda - \frac{e^2}{2}\iint \frac{\rho_g(\mathbf{r})\rho_g(\mathbf{r}')}{|\mathbf{r}-\mathbf{r}'|}d\mathbf{r}d\mathbf{r}' \\ &\quad + \sum_\lambda \int \psi^*_\lambda(\mathbf{r})\left[X(\rho_g(\mathbf{r})) - \frac{d\rho_g(\mathbf{r})X(\rho_g(\mathbf{r}))}{d\rho_g(\mathbf{r})}\right]\psi_\lambda(\mathbf{r})d\mathbf{r} \quad .\end{aligned} \tag{3.9}$$

The second and third terms on the right are corrections of the Coulomb energy and the exchange-correlation energy, respectively, for multiple counting which appears in $\Sigma_\lambda E_\lambda$. The above equations prescribe the groundstate in the one-electron approximation, where the function $X(\rho_g(\mathbf{r}))$ is still arbitrary.

### *One-Electron Approximation: Excited States*

For crystal and liquid metals in the condensed matter regime, thermal energy constitutes only a small perturbation in the electronic structure problem. In particular, for any set of nuclear positions, the electronic charge density at all temperatures of interest remains close to its value at zero temperature. Hence the potential an electron sees, due to the nuclei *and*

due to the the other electrons as well, is to first approximation independent of temperature, and equal to its evaluation in the electronic groundstate. This is the approximation we shall make, in treating the electronic excited states in metals.

Suppose the self consistent one-electron groundstate has been obtained, for a given external potential $\mathcal{V}(\mathbf{r})$, and for appropriate boundary conditions. The process has given us a one-electron Hamiltonian $h$, defined in (3.7), based on the potential $V_g(\mathbf{r})$ defined in (3.8). We shall assume that the excited electronic states are given in this one-electron approximation, with $V_g(\mathbf{r})$ fixed. Then $h$ has a complete set of wavefunctions $\psi_\lambda(\mathbf{r})$, $\lambda = 0, 1 \cdots$, which satisfy

$$h\psi_\lambda(\mathbf{r}) = E_\lambda \psi_\lambda(\mathbf{r}) \quad , \tag{3.10}$$

$$\int \psi^*_\lambda(\mathbf{r})\psi_{\lambda'}(\mathbf{r}) = \delta_{\lambda\lambda'} \quad . \tag{3.11}$$

To enumerate the states of the $\mathcal{Z}$-electron system, let us introduce the occupation numbers $f_\lambda = 0, 1$. For any system state, the set of occupied $\psi_\lambda$ have $f_\lambda = 1$, the set of unoccupied $\psi_\lambda$ have $f_\lambda = 0$, and the number of occupied states is always $\mathcal{Z}$, so that

$$\sum_\lambda f_\lambda = \mathcal{Z} \quad . \tag{3.12}$$

The $\mathcal{Z}$-electron system now has energy levels $\mathcal{E} = \Sigma_\lambda f_\lambda E_\lambda$. But we want to apply this description to the excited states only, and not to the groundstate. Let us use a different symbol, namely $g_\lambda = 0, 1$, for the occupation numbers when the system is in its groundstate. Then the system excited states have excitation energies given by

$$\mathcal{E} - \mathcal{E}_g = \sum_\lambda (f_\lambda - g_\lambda) E_\lambda \quad . \tag{3.13}$$

The operator equivalent to (3.13), *i.e.* the Hamiltonian which has the same energy levels, is the *electronic excitation* Hamiltonian $\mathcal{H}_{EX}$, given by

$$\mathcal{H}_{EX} = \sum_\alpha h(\mathbf{r}_\alpha) - \sum_\lambda g_\lambda E_\lambda \quad , \tag{3.14}$$

where $h(\mathbf{r})$ is given by Eq. (3.7). For a prescribed set of nuclear positions, $\mathcal{H}_{EX}$ has a complete set of $\mathcal{Z}$-electron states, each wavefunction is a Slater

determinant, and the lowest lying state has zero energy. While $\mathcal{H}_{EX}$ is expressed entirely in the one-electron approximation, the groundstate energy $\mathcal{E}_g$ of the many-electron system is independent of $\mathcal{H}_{EX}$, hence we are free to find $\mathcal{E}_g$ from the best theory available, or even from experimental data.

### *Calibration from Density Functional Theory*

Through the introduction of the function $X(\rho_g(\mathbf{r}))$ in Eq. (3.1), the groundstate energy in the one-electron approximation has been rendered an uncontrolled approximation, since it is no longer in the form $\langle\Psi|\mathcal{H}_E|\Psi\rangle$ for some wavefunction $\Psi$. Hence $\mathcal{E}_g$ is no longer an upper bound for the true groundstate energy. The same property holds for the Kohn-Sham formulation of density functional theory, whenever an approximation is made for the unknown functional $\mathcal{E}_{xc}[\rho]$ of Eq. (2.29). In fact, the common result of Kohn-Sham calculations for a real material is to place the groundstate energy *below* the experimental value. It is possible to calibrate the one-electron approximation so that its groundstate energy, Eq. (3.1), is the same as the energy obtained from density functional theory. Let us do this here for the Kohn-Sham formulation in the local density approximation. The calibration is accomplished merely by setting the function $X(\rho_g(\mathbf{r}))$ in (3.1) equal to the function $X(\rho(\mathbf{r}))$ in (2.31) (see problem 3.3). Under this condition, the one-electron Hamiltonian in (3.7), with potential given by (3.8), is the same as the Kohn-Sham Hamiltonian (2.18), with potential given by (2.27). Hence a Kohn-Sham calculation in local density approximation provides all the parameters, namely the groundstate potential $V_g(\mathbf{r})$ and the set of $E_\lambda$, which appear in the electronic excitation Hamiltonian of (3.14). We shall assume that these parameters are available for any metallic system of interest, and will use them to construct the total system Hamiltonian, including both adiabatic and nonadiabatic contributions, in Sec. 4 below.

Regarding numerical aspects of electronic structure calculations, note that one ordinarily uses a set of basis functions sufficient for a good representation of the $\psi_\lambda(\mathbf{r})$ which are occupied in the groundstate. This basis set will normally give low-lying excited states accurately for a metal, but at some level of excitation, the groundstate basis set will not be sufficient, because every higher lying $\psi_\lambda(\mathbf{r})$ has to be orthogonal to all lower $\psi_\lambda(\mathbf{r})$. Hence to find accurate values for the excited energies $E_\lambda$, or what is equivalent, for the electronic density of states above the Fermi energy, the basis

set has to be augmented from that used for an ordinary groundstate calculation. The same problem is encountered, and presumably solved, when wavefunctions of electronic excited states are used to calculate optical properties of a crystal.

*Problems*

*3.1* Derive Eqs. (3.7) and (3.8) from (3.6). Note $\partial\rho_g(\mathbf{r})/\partial\psi^*_\lambda(\mathbf{r}) = \psi_\lambda(\mathbf{r})$, from Eq. (3.2).

*3.2* Derive Eq. (3.9) from (3.1).

*3.3* When $X(\rho_g(\mathbf{r}))$ in (3.1) is the same as $X(\rho(\mathbf{r}))$ in (2.31), show that the two expressions (3.1) and (2.30) for $\mathcal{E}_g$ are the same.

## 4 TOTAL HAMILTONIAN

### *Nuclear Motion Hamiltonian*

Our condensed matter system is composed of $N$ similar nuclei and $\mathcal{Z}$ electrons. The nuclei have mass $M$, charge $ze$, and positions $\mathbf{r}_K$, with $K = 1, \cdots, N$, while the electrons have positions $\mathbf{r}_\alpha$, with $\alpha = 1, \cdots, \mathcal{Z}$, and $\mathcal{Z} = zN$. The Hamiltonian is the sum of kinetic energies and Coulomb potentials:

$$\mathcal{H} = \mathcal{T}_N + \mathcal{T}_E + \Omega + NI \quad , \tag{4.1}$$

where

$$\mathcal{T}_N = -\sum_K \frac{\hbar^2\nabla_K^2}{2M} \quad , \tag{4.2}$$

$$\mathcal{T}_E = -\sum_\alpha \frac{\hbar^2\nabla_\alpha^2}{2M} \quad , \tag{4.3}$$

$$\Omega = \frac{1}{2}{\sum_{KL}}' \frac{z^2e^2}{|\mathbf{r}_K - \mathbf{r}_L|} - \sum_{\alpha K} \frac{ze^2}{|\mathbf{r}_\alpha - \mathbf{r}_K|} + \frac{1}{2}{\sum_{\alpha\beta}}' \frac{e^2}{|\mathbf{r}_\alpha - \mathbf{r}_\beta|} \quad , \tag{4.4}$$

and where $I$ is the total ionization energy of a single atom. The term $NI$ is included in $\mathcal{H}$ so that the system energy levels are measured with respect to a set of infinitely separated neutral atoms. Though the above

Hamiltonian explicitly represents an elemental material, the derivations can be done as well for a mixture of atoms representing an alloy or a compound. Finally, while one usually thinks of a system in a box with periodic boundary conditions, other geometries and boundary conditions are equally permissible.

For the electronic problem, discussed in Secs. 2 and 3, the nuclei are fixed at their positions $\mathbf{r}_K$, making $\mathcal{T}_N = 0$, and reducing $\mathcal{H}$ to $\mathcal{H}_E = \mathcal{T}_E + \Omega$. The Coulomb terms in (4.4) for $\Omega$ are respectively nuclear-nuclear, electron-nuclear, and electron-electron. The first two terms in $\Omega$ combine to form the potential $\Sigma_\alpha \mathcal{V}(\mathbf{r}_\alpha)$ written in (2.3), and the last term in $\Omega$ is $\Omega_{EE}$ of (2.2). Now the point of the whole exercise of trying to solve for the electronic groundstate is this: the groundstate energy $\mathcal{E}_g(\{\mathbf{r}_K\})$, the energy of the entire system when the nuclei are fixed and the electrons are in their groundstate, is an excellent approximation for the potential which governs the motion of the nuclei. To this approximation, the nuclear motion is described by the Hamiltonian

$$\mathcal{H}_N = \mathcal{T}_N + \Phi(\{\mathbf{r}_K\}) \quad , \tag{4.5}$$

$$\Phi(\{\mathbf{r}_K\}) = \mathcal{E}_g(\{\mathbf{r}_K\}) + NI \quad . \tag{4.6}$$

This is the nuclear motion Hamiltonian, where $\Phi(\{\mathbf{r}_K\})$ is called the groundstate adiabatic potential, or simply the adiabatic potential.

Suppose we have an exact solution for the many-electron groundstate energy $\mathcal{E}_g(\{\mathbf{r}_K\})$. By adding and subtracting $\mathcal{E}_g$ to the total Hamiltonian (4.1), and by using (4.5) and (4.6), it follows

$$\mathcal{H} = \mathcal{H}_N + (\mathcal{H}_E - \mathcal{E}_g) \quad . \tag{4.7}$$

Obviously, the electronic part $\mathcal{H}_E - \mathcal{E}_g$ expresses only *excitation* of the electronic system from its groundstate. At this point, let us replace $\mathcal{H}_E - \mathcal{E}_g$ by its one-electron approximation $\mathcal{H}_{EX}$, Eq. (3.14), so that

$$\mathcal{H} \doteq \mathcal{H}_N + \mathcal{H}_{EX} \quad . \tag{4.8}$$

Now the nuclear motion Hamiltonian $\mathcal{H}_N$ contains in principle the exact adiabatic potential $\Phi = \mathcal{E}_g + NI$. From all of our experience in studying nuclear motion, illustrated by the evidence to be presented in the following chapters, $\mathcal{H}_N$ is the most accurate nuclear-motion Hamiltonian we know

how to make. On the other hand, the electronic excitation Hamiltonian $\mathcal{H}_{EX}$ is intrinsically approximate, through its formulation in terms of the one-electron approximation. Nevertheless, the evidence so far, also to be reported in the following chapters, indicates that $\mathcal{H}_{EX}$ is accurate to the same level as the overall experimental error in the thermal excitation properties of metals.

***Electrons at the Reference Structure***

A nuclear configuration is specified by the set of nuclear positions $\{\mathbf{r}_K\}$. In the nuclear configuration space, the potential surface is $\Phi(\{\mathbf{r}_K\})$, and the forces are gradients of $\Phi(\{\mathbf{r}_K\})$. An equilibrium configuration is one where the force on each nucleus vanishes, and a *structure* is a locally stable equilibrium configuration, *i.e.* the configuration at the bottom of a many-particle valley. Structures are representative of the configurations found in condensed matter systems. In a crystal the nuclei move in the vicinity of a single crystal structure, while in an amorphous solid the nuclei move in the vicinity of a single random structure. In a liquid the nuclei move among many random valleys, but these valleys are all equivalent, and are represented by a single random structure. Hence for a given state of condensed matter, one can choose a *reference structure*, where the electronic excitations are representative of the excitations in all the most popular nuclear configurations found in that state of matter. It will then be very useful to split the electronic excitation Hamiltonian into a part evaluated at the reference structure, and the remaining part which sees the motion of the nuclei.

Positions of the nuclei in the reference structure are denoted $\mathbf{R}_K$, $K = 1, \cdots, N$. The potential of an electron at $\mathbf{r}$, due to the nuclei in configuration $\{\mathbf{r}_K\}$, has been denoted $\mathcal{V}(\mathbf{r})$, and is more completely specified as $\mathcal{V}(\mathbf{r};\{\mathbf{r}_K\})$. Let us write $\mathcal{V}^\sigma(\mathbf{r})$ to denote evaluation at the nuclear reference structure, so that $\mathcal{V}^\sigma(\mathbf{r}) = \mathcal{V}(\mathbf{r};\{\mathbf{R}_K\})$. Then $\mathcal{V}(\mathbf{r})$ can be expanded about the reference structure,

$$\mathcal{V}(\mathbf{r}) = \mathcal{V}^\sigma(\mathbf{r}) + \delta\mathcal{V}(\mathbf{r}) \quad , \tag{4.9}$$

where this equation defines $\delta\mathcal{V}(\mathbf{r})$, *i.e.*

$$\delta\mathcal{V}(\mathbf{r}) = \mathcal{V}(\mathbf{r};\{\mathbf{r}_K\}) - \mathcal{V}(\mathbf{r};\{\mathbf{R}_K\}) \quad . \tag{4.10}$$

In the same way the one-electron potential $V_g(\mathbf{r})$, which depends explicitly

*and* implicitly on the nuclear configuration, can be expanded about the reference structure,

$$V_g(\mathbf{r}) = V_g^\sigma(\mathbf{r}) + \delta V_g(\mathbf{r}) \quad . \tag{4.11}$$

Then in Eq. (3.7), the one-electron Hamiltonian becomes $h = h^\sigma + \delta V_g$, and the one-electron energies become $E_\lambda = E_\lambda^\sigma + \delta E_\lambda$. Let us finally expand $\mathcal{H}_{EX}$, Eq. (3.14), about the reference structure:

$$\mathcal{H}_{EX} = \mathcal{H}_{EX}^\sigma + \delta\mathcal{H}_{EX} \quad , \tag{4.12}$$

where

$$\mathcal{H}_{EX}^\sigma = \sum_\alpha h^\sigma(\mathbf{r}_\alpha) - \sum_\lambda g_\lambda E_\lambda^\sigma \quad , \tag{4.13}$$

$$\delta\mathcal{H}_{EX} = \sum_\alpha \delta V_g(\mathbf{r}_\alpha) - \sum_\lambda g_\lambda \delta E_\lambda \quad . \tag{4.14}$$

At the reference structure, the one-electron wavefunctions are $\psi_\lambda^\sigma(\mathbf{r})$, and each system wavefunction is a Slater determinant of the occupied $\psi_\lambda^\sigma(\mathbf{r})$. Determinantal matrix elements can be used to express $\mathcal{H}_{EX}$ in the basis of reference structure electrons. The result for $\mathcal{H}_{EX}^\sigma$ is

$$\mathcal{H}_{EX}^\sigma = \sum_\lambda E_\lambda^\sigma (C_\lambda^+ C_\lambda - g_\lambda) \quad , \tag{4.15}$$

where $C_\lambda^+$ and $C_\lambda$ are respectively the creation and annihilation operators for electrons at the reference structure. The eigenvalues of $C_\lambda^+ C_\lambda$ are $f_\lambda$, and the condition (3.12) that the total number of electrons is $\mathcal{Z}$ becomes

$$\sum_\lambda C_\lambda^+ C_\lambda = \mathcal{Z} \quad . \tag{4.16}$$

The result for $\delta\mathcal{H}_{EX}$ is

$$\delta\mathcal{H}_{EX} = \sum_{\lambda\lambda'} \delta V_{\lambda\lambda'} C_\lambda^+ C_{\lambda'} - \sum_\lambda g_\lambda \delta E_\lambda \quad , \tag{4.17}$$

where

$$\delta V_{\lambda\lambda'} = \langle \psi_\lambda^\sigma | \delta V_g | \psi_{\lambda'}^\sigma \rangle \quad . \tag{4.18}$$

Notice once again that both $\delta V_{\lambda\lambda'}$ and $\delta E_\lambda$ depend parametrically on the nuclear positions, and they also have an implicit dependence on the reference structure itself.

The total Hamiltonian (4.8) can now be written

$$\mathcal{H} \doteq \mathcal{H}_N + \mathcal{H}^\sigma_{EX} + \delta\mathcal{H}_{EX} \quad . \tag{4.19}$$

This is a valuable result. First, since the nuclear positions do not appear *as variables* in $\mathcal{H}^\sigma_{EX}$, then $\mathcal{H}_N$ and $\mathcal{H}^\sigma_{EX}$ commute, which means there is no interaction between the motion of the nuclei and the excitation of reference structure electrons. Hence $\mathcal{H}_N$ and $\mathcal{H}^\sigma_{EX}$ represent two *independent* systems, and this simplifies the dynamics and statistical mechanics. Second, speaking generally of condensed matter systems, the three terms on the right of (4.19) are ordered in strongly decreasing importance. Hence the interaction between nuclear motion and electronic excitation is isolated in the smallest term in (4.19), and in the dynamics and statistical mechanics of metals, this term can ordinarily be treated as a perturbation.

### *Notes on the Resolution of the Total Hamiltonian*

The total Hamiltonian expressed in Eq. (4.19) will be the starting point for all subsequent developments in this monograph. We need to discuss some subtle points associated with this Hamiltonian, and for this purpose we can limit our consideration to a metal crystal. The general idea is contained in this observation: electron-phonon interactions are not defined until the electrons and phonons are defined, and then, electron-phonon interactions are uniquely defined, through the (unique) total Hamiltonian.

The smallest Hamiltonian contribution, $\delta\mathcal{H}_{EX}$, expresses the interaction between motion of the nuclei and excitation of the electrons. In a crystal, the nuclear motion is analyzed into phonons, and $\delta\mathcal{H}_{EX}$ constitutes the electron-phonon interaction. In Eq. (4.17), $\delta\mathcal{H}_{EX}$ is expressed in terms of reference structure electrons, for which the total electronic wavefunctions are $\Psi(\{\mathbf{r}_\alpha\},\{\mathbf{R}_K\})$. In the total system Schrödinger equation, the nuclear motion will give rise to terms which do not mix these electronic states, and terms which do mix them. Let us define these terms respectively as *adiabatic* and *nonadiabatic*. Their contributions to the free energy of a metallic crystal will be studied in Sec. 18. A formal separation of adiabatic and nonadiabatic effects for nonmetallic crystals, applicable in principle to metallic crystals as well, is given by Born and Huang (1954, Appendix VIII). Born

and Huang work with the electronic wavefunctions $\Psi(\{\mathbf{r}_\alpha\},\{\mathbf{r}_K\})$, which are valid for arbitrary positions of the nuclei, and they define adiabatic (nonadiabatic) nuclear motion as that which does not mix (does mix) these electronic states. Obviously the present definition of adiabatic and nonadiabatic effects, in terms of the wavefunctions $\Psi(\{\mathbf{r}_\alpha\},\{\mathbf{R}_K\})$, is nontrivially different from the definition of Born and Huang. As a practical note, working in the basis of reference structure electrons gives us the ability to evaluate matrix elements of the electron-phonon interaction, which would be virtually impossible in the representation of Born and Huang.

A still more subtle point arises. The "adiabatic" potential $\Phi(\{\mathbf{r}_K\})$ is $\mathcal{E}_g(\{\mathbf{r}_K\})+NI$, and $\mathcal{E}_g(\{\mathbf{r}_K\})$ is the electronic groundstate energy when the nuclei are fixed at $\{\mathbf{r}_K\}$. But when the nuclei are *moving*, as they are in all quantum states of the total system, $\delta\mathcal{H}_{EX}$ becomes an *operator* in phonon space, hence $\delta\mathcal{H}_{EX}$ gives a small correction to the groundstate energy, say $\delta\mathcal{E}_g(\{\mathbf{r}_K\})$. So the true groundstate energy is $\mathcal{E}_g+\delta\mathcal{E}_g$, and is by definition adiabatic. Born and Huang (1954) recognize $\mathcal{E}_g+\delta\mathcal{E}_g$ as the true adiabatic groundstate potential. However, we do not include $\delta\mathcal{E}_g$ in our nuclear motion potential $\Phi$, because $\delta\mathcal{E}_g$ is extremely small and is virtually impossible to calculate or to measure. Instead we keep all components of the electron-phonon interaction, present in all electronic states including the groundstate, in the Hamiltonian $\delta\mathcal{H}_{EX}$. Our procedure has the advantage, both practical and aesthetic, of treating all contributions to $\delta\mathcal{H}_{EX}$ on the same footing.

Since the electrons, phonons, and all interactions among them are described by one global Hamiltonian, there is a consistency condition among them, namely that all their separate energy operators must add up to the total Hamiltonian of Eq. (4.1), or Eq. (4.7). But in condensed matter research, various excitations are almost always studied separately, and consistency conditions implied by the global Hamiltonian are rarely observed. Electron-phonon interactions are usually studied through $\mathcal{H}_E$, but according to Eq. (4.7) these interactions are contained in the operator $\mathcal{H}_E-\mathcal{E}_g$, not $\mathcal{H}_E$. The fact that the electron-phonon Hamiltonian must contain only *excited* electronic sates, and not the electronic groundstate, is sometimes crucial, but is almost always overlooked.

It is quite satisfactory to be able to present such a simple derivation as that going from (4.1) to (4.19). The result here is identical to that obtained from a much more tortuous procedure in *Thermodynamics of Crys-*

*tals*. Present equations are the same as those in Sec. 24 of *Thermodynamics of Crystals*, as follows: (4.7) is (24.13), (4.15) is (24.20), and (4.19) expressed specifically for crystals is (24.22).

## 5 NEARLY-FREE-ELECTRON METALS

### *Pseudopotential Perturbation Theory*

The nearly-free-electron metals can be represented approximately by a collection of rigid closed-shell ions, plus their valence electrons, which interact weakly with one another and with the ions. If these interactions were *not* weak, the electronic structure problem would be intractable, and could only be solved by computer. On the other hand, if the interactions were neglected entirely, the valence electrons would be a free electron system, possessing kinetic energy and Fermi statistics, and missing all the remaining interesting properties of real metals. But by treating the interactions in perturbation theory, the electronic structure problem is tractable, yet exhibits all the important properties of real metals within a single unified theoretical framework. Further, when properly calibrated, this theory will give an accurate account of a wide range of experimental properties of metals. Extensive treatments may be found in Harrison (1989, Chaps. 15–17), and in *Thermodynamics of Crystals* (Chap. 6 and Sec. 34).

The theory starts with the interaction of a valence electron with an ion core. In an accurate electronic structure calculation, the complications within the core, namely the deep Coulomb well and the orthogonalization of valence electrons to core electrons, are handled numerically. Here these complications are replaced by a weak local *pseudopotential*, allowing the valence electrons to have the right energies, and to have wavefunctions which are correct *outside* the core, but not *inside* the core. The interaction of an electron at $\mathbf{r}$ with a spherically symmetric ion core centered at the origin is represented by the bare pseudopotential $w_b(|\mathbf{r}|)$. The interaction of an electron at $\mathbf{r}$ with all the ion cores, located at $\mathbf{r}_K$, is

$$W_b(\mathbf{r}) = \sum_K w_b(|\mathbf{r} - \mathbf{r}_K|) \quad . \tag{5.1}$$

The total potential seen by one electron is then

$$W(\mathbf{r}) = W_b(\mathbf{r}) + W_s(\mathbf{r}) + W_{xc}(\mathbf{r}) \quad , \tag{5.2}$$

where the screening potential $W_s(\mathbf{r})$ is due to the Coulomb interaction with all the other valence electrons, and where the potential $W_{xc}(\mathbf{r})$ is an approximation for exchange and correlation effects among the valence electrons. The one-electron Hamiltonian is

$$h = -\frac{\hbar^2\nabla^2}{2m} + W(\mathbf{r}) \quad , \tag{5.3}$$

and $W(\mathbf{r})$ is considered a perturbation. $W(\mathbf{r})$ will be evaluated self-consistently in the electronic groundstate, so that $W(\mathbf{r}) = W_g(\mathbf{r})$, and the subscript $g$ will not be needed. Henceforth we shall refer to the valence electrons simply as "the electrons", and to $W(\mathbf{r})$ as "the pseudopotential".

The system is composed of $N$ ion cores, each with charge $ze$, together with $\mathcal{Z} = zN$ electrons, all in a cubical box of volume $V$, with periodic boundary conditions at the box surface. A plane wave which satisfies the boundary conditions is $|\mathbf{p}\rangle$,

$$|\mathbf{p}\rangle = \frac{1}{\sqrt{V}} e^{i\mathbf{p}\cdot\mathbf{r}} \quad , \tag{5.4}$$

where the wavevectors $\mathbf{p}$ form a discrete infinite set. The plane waves are orthonormal,

$$\langle \mathbf{p}'|\mathbf{p}\rangle = \frac{1}{V}\int e^{i(\mathbf{p}-\mathbf{p}')\cdot\mathbf{r}} d\mathbf{r} = \delta_{\mathbf{p}\mathbf{p}'} \quad , \tag{5.5}$$

and they are complete in the space of functions which satisfy the boundary conditions,

$$\sum_{\mathbf{p}} |\mathbf{p}\rangle\langle\mathbf{p}| = \frac{1}{V}\sum_{\mathbf{p}} e^{i\mathbf{p}\cdot(\mathbf{r}-\mathbf{r}')} = \delta(\mathbf{r}-\mathbf{r}') \quad . \tag{5.6}$$

Planewave matrix elements of a function $f(\mathbf{r})$ yield the Fourier transform,

$$f(\mathbf{q}) = \langle \mathbf{p}+\mathbf{q}|f|\mathbf{p}\rangle = \frac{1}{V}\int f(\mathbf{r}) e^{-i\mathbf{q}\cdot\mathbf{r}} d\mathbf{r} \quad . \tag{5.7}$$

The inverse transform is obtained by applying the completeness relation (5.6), to find

$$f(\mathbf{r}) = \sum_{\mathbf{q}} f(\mathbf{q}) e^{i\mathbf{q}\cdot\mathbf{r}} \xrightarrow[V\to\infty]{} \frac{V}{(2\pi)^3}\int f(\mathbf{q}) e^{i\mathbf{q}\cdot\mathbf{r}} d\mathbf{q} \quad . \tag{5.8}$$

The transformation to the integral uses that $V/(2\pi)^3$ is the density of vectors in $\mathbf{q}$-space. Note the transformation between (5.7) and (5.8) is asymmetric in the factors of $2\pi$. Finally, the convolution formula works out to be

$$\frac{1}{V}\int f(\mathbf{r})g(\mathbf{r})d\mathbf{r} = \sum_{\mathbf{q}} f(\mathbf{q})g(-\mathbf{q}) \quad . \tag{5.9}$$

Let us return to the electronic structure problem, defined by the Hamiltonian (5.3) and the periodic boundary condition. In zeroth order, the solutions are free electrons,

$$-\frac{\hbar^2\nabla^2}{2m}|\mathbf{p}\rangle = e_{\mathbf{p}}|\mathbf{p}\rangle \quad , \qquad e_{\mathbf{p}} = \frac{\hbar^2 p^2}{2m} \quad . \tag{5.10}$$

With $W(\mathbf{r})$ treated as a perturbation, the solutions are still indexed by the wavevectors $\mathbf{p}$, and they satisfy

$$h\psi_{\mathbf{p}} = E_{\mathbf{p}}\psi_{\mathbf{p}} \quad , \qquad \langle\psi_{\mathbf{p}'}|\psi_{\mathbf{p}}\rangle = \delta_{\mathbf{p}\mathbf{p}'} \quad . \tag{5.11}$$

The wavefunctions to first order, and the energies to second order, are

$$\psi_{\mathbf{p}} = |\mathbf{p}\rangle + \sum_{\mathbf{q}}{}' \frac{W(\mathbf{q})|\mathbf{p}+\mathbf{q}\rangle}{(e_{\mathbf{p}} - e_{\mathbf{p}+\mathbf{q}})} \quad , \tag{5.12}$$

$$E_{\mathbf{p}} = e_{\mathbf{p}} + W(\mathbf{q}=0) + \sum_{\mathbf{q}}{}' \frac{|W(\mathbf{q})|^2}{(e_{\mathbf{p}} - e_{\mathbf{p}+\mathbf{q}})} \quad , \tag{5.13}$$

where the prime on $\Sigma'_{\mathbf{q}}$ means to omit the $\mathbf{q}=0$ term. Since $W(\mathbf{r})$ is real, then $W(\mathbf{q})^* = W(-\mathbf{q})$.

### *Groundstate Electron Density*

In the groundstate, the electrons occupy the one-electron states up to the Fermi energy $E_F$. The Fermi energy specifies a constant-energy surface in $\mathbf{p}$-space, the Fermi surface. In zeroth order, the constant-energy surfaces are spheres, and the Fermi energy is

$$e_F = \frac{\hbar^2 f^2}{2m} \quad , \tag{5.14}$$

where $f$ is the zeroth-order (free electron) Fermi wave vector. The Fermi surface is at $|\mathbf{p}| = f$. The Fermi sphere must contain exactly $zN$ electrons, and this determines $f$, according to

$$zN = \frac{2V}{8\pi^3}\int_0^f d\mathbf{p} = \frac{Vf^3}{3\pi^2} \quad , \tag{5.15}$$

where the factor 2 in the integral expression accounts for spin degeneracy. The volume per atom is $V_A = V/N$, the average electron density is $\rho_0 = z/V_A$, and in these terms $f$ is given by

$$f^3 = \frac{3\pi^2 z}{V_A} = 3\pi^2\rho_0 \quad . \tag{5.16}$$

The total kinetic energy in zeroth order is the total free-electron energy, given by

$$\frac{2V}{8\pi^3}\int_0^f d\mathbf{p}\frac{\hbar^2 p^2}{2m} = zN\left(\frac{3\hbar^2 f^2}{10m}\right) = zN\left(\frac{3}{5}e_F\right) \quad . \tag{5.17}$$

The electron density at $\mathbf{r}$ is $\rho(\mathbf{r})$,

$$\rho(\mathbf{r}) = \sum_{\mathbf{p}} g_{\mathbf{p}}\psi^*_{\mathbf{p}}(\mathbf{r})\psi_{\mathbf{p}}(\mathbf{r}) \quad , \tag{5.18}$$

where as usual $g_{\mathbf{p}}$ are the groundstate occupation numbers, and $\Sigma_{\mathbf{p}} g_{\mathbf{p}} = zN$. When a sum is restricted to the occupied one-electron states, as indicated by the presence of $g_{\mathbf{p}}$ in $\Sigma_{\mathbf{p}}$, it is understood that a factor 2 for spin is implicit in the sum. From Eq. (5.12) for the wavefunctions, $\rho(\mathbf{r})$ to first order is

$$\rho(\mathbf{r}) = \frac{1}{V}\sum_{\mathbf{p}} g_{\mathbf{p}}\left\{1 + \sum_{\mathbf{q}}{}' \left[\frac{W(-\mathbf{q})e^{-i\mathbf{q}\cdot\mathbf{r}}}{(e_{\mathbf{p}} - e_{\mathbf{p}-\mathbf{q}})} + \frac{W(\mathbf{q})e^{i\mathbf{q}\cdot\mathbf{r}}}{(e_{\mathbf{p}} - e_{\mathbf{p}+\mathbf{q}})}\right]\right\} \quad . \tag{5.19}$$

The $\mathbf{q} = 0$ component is just the average electron density,

$$\rho(\mathbf{q} = 0) = \rho_0 = \frac{z}{V_A} \quad . \tag{5.20}$$

For the $\mathbf{q} \neq 0$ components, the two terms in (5.19) can be combined by interchanging $\mathbf{q}$ with $-\mathbf{q}$ inside the sum, to obtain

$$\rho(\mathbf{q}) = \frac{2}{V}\sum_{\mathbf{p}} g_{\mathbf{p}}\frac{W(\mathbf{q})}{(e_{\mathbf{p}} - e_{\mathbf{p}+\mathbf{q}})} \quad , \qquad \mathbf{q} \neq 0 \quad . \tag{5.21}$$

We only want to evaluate this to leading order, which means the $\Sigma_{\mathbf{p}}$, after transforming to an integral, needs to be evaluated only over the zeroth-order Fermi sphere. The result is

$$\rho(\mathbf{q}) = \frac{q^2}{4\pi e^2} W(\mathbf{q})[1 - H(q)] \quad , \qquad \mathbf{q} \neq 0 \quad , \tag{5.22}$$

where $H(q)$ is the static Hartree dielectric function, given by

$$H(q) - 1 = \frac{2me^2 f}{\pi\hbar^2 q^2} \left[ \frac{1 - (q/2f)^2}{2(q/2f)} \ln \left| \frac{1 + (q/2f)}{1 - (q/2f)} \right| + 1 \right] \quad . \tag{5.23}$$

Equation (5.22) begins to reveal how the electrons respond to the potential field, represented by $W(\mathbf{q})$. The next step is to calculate the field self consistently.

### *Screening and Exchange-Correlation Potentials*

The screening potential is the Coulomb potential arising from the electron density $\rho(\mathbf{r})$,

$$W_s(\mathbf{r}) = e^2 \int \frac{\rho(\mathbf{r}')}{|\mathbf{r} - \mathbf{r}'|} d\mathbf{r}' \quad , \tag{5.24}$$

and this function obeys Poisson's equation, so that

$$W_s(\mathbf{q}) = \frac{4\pi e^2}{q^2} \rho(\mathbf{q}) \quad , \qquad \mathbf{q} \neq 0 \quad . \tag{5.25}$$

In the present formulation, the $\mathbf{q} = 0$ component of $W_s(\mathbf{q})$ is not defined, and it need not be defined, since all "Coulomb divergences" sum to zero. The theory could otherwise be constructed by replacing the Coulomb interaction $1/r$ with $e^{-\kappa r}/r$, with $\kappa$ small and positive, and then the denominator in (5.25) would be $q^2 + \kappa^2$, and the $\mathbf{q} = 0$ term is defined. In physically meaningful quantities, the $\mathbf{q} = 0$ terms will cancel and the limit $\kappa \to 0$ will exist. Notice also that the nonphysical Coulomb interaction of each electron with itself will be contained here in the total Coulomb energy $\int \rho(\mathbf{r}) W_s(\mathbf{r}) d\mathbf{r}$. In a theory where the electrons are approximately plane waves, this self energy is of relative order $N^{-1}$ in the total energy, hence is negligible.

By eliminating $\rho(\mathbf{q})$ between (5.22) and (5.25), the screening potential is simply related to the total potential,

$$W_s(\mathbf{q}) = W(\mathbf{q})[1 - H(q)] \quad . \tag{5.26}$$

This constitutes a solution for the screening potential, and is a key result of electron response theory.

Let us write the exchange-correlation potential $W_{xc}(\mathbf{r})$, which appears in Eq. (5.2), through its Fourier components, as a local field correction to the screening potential,

$$W_{xc}(\mathbf{q}) = -W_s(\mathbf{q})Y(\mathbf{q}) = -\frac{4\pi e^2}{q^2}\rho(\mathbf{q})Y(\mathbf{q}) \quad . \tag{5.27}$$

As usual, all the intractable many-electron effects are represented by the unknown function $Y(\mathbf{q})$. Here we shall take a simple model for $Y(\mathbf{q})$, which will serve to illustrate the construction of the complete theory,

$$Y(\mathbf{q}) = Y(q) = \frac{q^2}{2(q^2 + \xi f^2)} \quad , \tag{5.28}$$

where $\xi$ is a positive density-dependent parameter. Arguments for this form are as follows. Since exchange and correlation operate to keep electrons apart, they reduce the (positive) Coulomb energy, so that $W_s + W_{xc}$ must be less than $W_s$. This accounts for the minus sign in (5.27). Further, $W_{xc}$ should go to a finite function of density as $\mathbf{q} \to 0$, and, as observed by Hubbard (1958), exchange alone should make $Y(q)$ approach $\frac{1}{2}$ at large $q$. From Eqs. (5.27) and (5.28), it is apparent that $W_{xc}(q)$ represents a screened Coulomb potential. In fact $\mathcal{E}_{xc}$, the total exchange-correlation energy corresponding to $W_{xc}$, is a functional of the electron density $\rho(\mathbf{r})$,

$$\mathcal{E}_{xc} = \int \rho(\mathbf{r})X(\mathbf{r})d\mathbf{r} \quad , \tag{5.29}$$

where $X(\mathbf{r})$ is *also* a functional of $\rho(\mathbf{r})$,

$$X(\mathbf{r}) = -\frac{e^2}{4}\int \rho(\mathbf{r}')\frac{e^{-\kappa|\mathbf{r}-\mathbf{r}'|}}{|\mathbf{r}-\mathbf{r}'|}d\mathbf{r} \quad . \tag{5.30}$$

Because $\mathcal{E}_{xc}$ is quadratic in $\rho(\mathbf{r})$, the exchange-correlation potential becomes (see Eq. (2.28)

$$W_{xc}(\mathbf{r}) = 2X(\mathbf{r}) \quad . \tag{5.31}$$

The Fourier transform of $W_{xc}(\mathbf{r})$ is given by Eqs. (5.27) and (5.28), with $\kappa = \xi f^2$.

There are various ways to calibrate $\xi$. As $\mathbf{q} \to 0$, the above equations reduce to a local density approximation for a homogeneous electron system at density $\rho_0$. If we set $\mathcal{E}_{xc}[\rho_0]$ equal to the exchange energy of the uniform electron gas, then $\xi = 4/9$. Instead, one can use the compressibility sum rule, which expresses that the system compressibility must be the same whether calculated from the velocities of long wavelength acoustic phonons, or from homogeneous deformation (the derivation is given in Chap. 3). From the compressibility of the uniform electron gas, one finds $\xi = 2$ for exchange only, minus a small density-dependent correction for correlation (see *e.g.* Wallace, 1968). On the other hand, the compressibility calculated from density functional theory gives $\xi = 1.2$ in a pseudopotential model for Al (Straub *et al.*, 1994). More sophisticated models for the exchange-correlation contribution to electron response are discussed by Singwi and Tosi (1981, Secs. 5 and 6), and by Mahan (1981, Sec. 5.5).

The total pseudopotential $W(\mathbf{q})$ is now determined. From (5.26) and (5.27), the screening and exchange-correlation contribution amount to

$$W_s(\mathbf{q}) + W_{xc}(\mathbf{q}) = W(\mathbf{q})[1 - H(q)][1 - Y(q)] \quad . \tag{5.32}$$

Now since $W = W_b + W_s + W_{xc}$, the screening and exchange-correlation contributions can be eliminated to find

$$W(\mathbf{q}) = \frac{W_b(\mathbf{q})}{1 + [H(q) - 1][1 - Y(q)]} \quad . \tag{5.33}$$

So the total potential seen by any single electron is the bare potential from all the ions, screened collectively by all the electrons, where the screening function is controlled by the Coulomb interaction and the exchange-correlation effects among the electrons. If $Y(q)$ is set zero, then $W(\mathbf{q})$ reduces to $W_b(\mathbf{q})/H(q)$, exhibiting the meaning of $H(q)$ as a dielectric function.

### *Electron-Ion Interaction*

The heart of our theory is the bare pseudopotential $w_b(r)$, representing the interaction of one electron with one ion. The ion has charge $+ze$, so that outside the ion core $w_b(r)$ is $-ze^2/r$. Then the bare interaction can be

written

$$w_b(r) = -\frac{ze^2}{r} + w_c(r) \quad , \tag{5.34}$$

where the core potential $w_c(r)$ is localized to the core region. Inside the core, an electron sees a strong negative Coulomb potential from the nucleus, but the electron also has a large positive kinetic energy due to its orthogonalization to core electrons. The sum of these energies is represented by a relatively weak local potential, hence the name pseudopotential. In this monograph, $w_c(r)$ is viewed as a function to be modeled so as to achieve a good overall theory for nearly-free-electron metals. The Harrison model takes $w_c(r)$ proportional to a $1s$ electron density, so that $w_c(r) = \beta e^{-r/r_c}$, where $\beta$ and $r_c$ are positive parameters. The Heine-Abarenkov model is a well of depth $\beta$ inside the core, plus the ion Coulomb potential outside the core:

$$w_b(r) = -\beta \text{ for } r \le r_c \quad , \qquad w_b(r) = -\frac{ze^2}{r} \text{ for } r > r_c \quad . \tag{5.35}$$

The Ashcroft empty core model results from setting $\beta = 0$ in the Heine-Abarenkov model.

Since $W_b(\mathbf{r})$ is a sum of single ion pseudopotentials, then $W_b(\mathbf{q})$ factors in an important way:

$$\begin{aligned} W_b(\mathbf{q}) &= \frac{1}{V}\int W_b(\mathbf{r}) e^{-i\mathbf{q}\cdot\mathbf{r}} d\mathbf{r} \\ &= \frac{1}{V}\sum_K e^{-i\mathbf{q}\cdot\mathbf{r}_K} \int w_b(|\mathbf{r}-\mathbf{r}_K|) e^{-i\mathbf{q}\cdot(\mathbf{r}-\mathbf{r}_K)} d\mathbf{r} \\ &= S(\mathbf{q}) w_b(q) \quad , \end{aligned} \tag{5.36}$$

where $S(\mathbf{q})$ is the structure factor,

$$S(\mathbf{q}) = \frac{1}{N}\sum_K e^{-i\mathbf{q}\cdot\mathbf{r}_K} \quad , \tag{5.37}$$

and $w_b(q)$ is the single-ion bare pseudopotential,

$$w_b(q) = \frac{1}{V_A}\int w_b(r) e^{-i\mathbf{q}\cdot\mathbf{r}} d\mathbf{r} \quad . \tag{5.38}$$

Notice that $S(\mathbf{q})$ is normalized to 1 at $\mathbf{q} = 0$, and also that $w_b(q)$ is normalized by the volume per atom $V_A$, which is appropriate since $w_b(r)$ belongs to a single ion. The importance of the decomposition (5.36) is that all

dependence of $W_b(\mathbf{q})$ on the ion positions $\mathbf{r}_K$ is contained in the structure factor $S(\mathbf{q})$. Further, since $W(\mathbf{q})$ is proportional to $W_b(\mathbf{q})$, from Eq. (5.33), then the factorization of $W_b(\mathbf{q})$ carries over to the total potential, so that

$$W(\mathbf{q}) = S(\mathbf{q})w(q) \quad , \tag{5.39}$$

where $w(q)$ is called the screened-ion form factor, or simply the form factor,

$$w(q) = \frac{w_b(q)}{1 + [H(q) - 1][1 - Y(q)]} \quad . \tag{5.40}$$

With the last two equations, it becomes apparent why pseudopotential perturbation theory can treat a wide variety of properties in a simple unified formulation. First, the dependence on ion positions is reduced to $S(\mathbf{q})$ in the wavefunctions to first order, and to $|S(\mathbf{q})|^2$ in the energies to second order. Hence the theory is ideal for calculating what happens when the ions move around, and it easily handles configurations appearing in crystal, amorphous solid, and liquid states. Second, again in the electron wavefunctions and energies, the effect of all interactions appears in the form factor $w(q)$. And since screening and exchange-correlation effects are evaluated in zeroth order, *i.e.* in the free-electron approximation, the functions $H(q)$ and $Y(q)$ in Eq. (5.40) depend only on the mean electron density, through the parameters $f$ and $\xi$.

A characteristic property of metals, resulting from the long-range divergence of electron Coulomb interactions, is that the dielectric function diverges as $q \to 0$. This property is contained in $H(q)$, Eq. (5.23), whose small-$q$ expansion is

$$H(q) - 1 = \frac{4me^2 f}{\pi\hbar^2 q^2} - \frac{me^2}{3\pi\hbar^2 f} + \cdots \quad . \tag{5.41}$$

But $w_b(q)$ has the same divergence with opposite sign, because $w_b(r)$ has an attractive Coulomb potential at large $r$, so that $w(q)$, Eq. (5.40), has the finite limit

$$\lim_{q\to 0} w(q) = -\frac{2}{3}e_F = -\frac{\hbar^2 f^2}{3m} \quad . \tag{5.42}$$

***Electronic Groundstate Energy***

The electronic groundstate energy in the one-electron approximation is written in Eq. (3.9), specifically with exchange-correlation effects given by

a local density approximation. The corresponding equation in pseudopotential perturbation theory reads

$$\mathcal{E}_g = \sum_{\mathbf{p}} g_{\mathbf{p}} E_{\mathbf{p}} - \frac{1}{2}\int \rho(\mathbf{r}) W_s(\mathbf{r}) d\mathbf{r} + \int \rho(\mathbf{r})[X(\mathbf{r}) - W_{xc}(\mathbf{r})] d\mathbf{r} \quad . \tag{5.43}$$

On the right side, the two integrals correct for what is "over counted" in the sum of one-electron energies. We shall continue to use the exchange-correlation model outlined in Eqs. (5.27) to (5.31), so that

$$\int \rho(\mathbf{r}) \left[X(\mathbf{r}) - W_{xc}(\mathbf{r})\right] d\mathbf{r} = -\frac{1}{2}\int \rho(\mathbf{r}) W_{xc}(\mathbf{r}) d\mathbf{r} \quad . \tag{5.44}$$

Notice that the direct ion-ion interaction energy is still not contained in Eq. (5.43), but will be added when the effective ion-ion potential is constructed below. With the aid of Eq. (5.13) for $E_{\mathbf{p}}$, the sum of one-electron energies is

$$\sum_{\mathbf{p}} g_{\mathbf{p}} E_{\mathbf{p}} = \sum_{\mathbf{p}} g_{\mathbf{p}} e_{\mathbf{p}} + zNW(\mathbf{q}=0) + {\sum_{\mathbf{q}}}' \sum_{\mathbf{p}} g_{\mathbf{p}} \frac{W(\mathbf{q})W(-\mathbf{q})}{(e_{\mathbf{p}} - e_{\mathbf{p}+\mathbf{q}})} \quad . \tag{5.45}$$

The first term on the right is the sum of free electron energies, given by Eq. (5.17) (see problem 5.1). In view of Eq. (5.21) for $\rho(\mathbf{q})$, the last term in (5.45) is

$$\frac{1}{2}V\sum_{\mathbf{q}} \rho(\mathbf{q}) W(-\mathbf{q}) - \frac{1}{2} V \rho(\mathbf{q}=0) W(\mathbf{q}=0) \quad , \tag{5.46}$$

where the $\mathbf{q} = 0$ term has been added and subtracted. With Eq. (5.44), the two integrals in (5.43) combine to yield

$$-\frac{1}{2}V\sum_{\mathbf{q}} \rho(\mathbf{q})[W_s(-\mathbf{q}) + W_{xc}(-\mathbf{q})] \quad . \tag{5.47}$$

Then since $W = W_b + W_s + W_{xc}$, the above contributions to $\mathcal{E}_g$ become

$$\mathcal{E}_g = zN\left[\frac{3}{5}e_F + \frac{1}{2}W(\mathbf{q}=0)\right] + \frac{1}{2}V\sum_{\mathbf{q}} \rho(\mathbf{q}) W_b(-\mathbf{q}) \quad , \tag{5.48}$$

where we used $\rho(\mathbf{q}=0) = \rho_0$, and $V\rho_0 = zN$.

The only term in Eq. (5.48) which depends on the ion positions is the last term, and that dependence can be made explicit through the structure

factor $S(\mathbf{q})$. This is done by using successively Eqs. (5.22), (5.33), and (5.36), to find

$$\frac{1}{2}V\sum_{\mathbf{q}}\rho(\mathbf{q})W_b(-\mathbf{q}) = N\sum_{\mathbf{q}}S(\mathbf{q})S(-\mathbf{q})F(q) \quad , \tag{5.49}$$

where $F(q)$ is the energy-wavenumber characteristic, given by

$$F(q) = \frac{q^2V_A}{8\pi e^2}\ \frac{[w_b(q)]^2[1-H(q)]}{1+[H(q)-1][1-Y(q)]} \quad . \tag{5.50}$$

Putting in for $S(\mathbf{q})$, from (5.37), the right side of (5.49) is transformed to

$$\frac{1}{2}{\sum_{KL}}' v_{ind}(|\mathbf{r}_K-\mathbf{r}_L|) + \sum_{\mathbf{q}}F(q) \quad , \tag{5.51}$$

where

$$v_{ind}(|\mathbf{r}|) = \frac{2}{N}\sum_{\mathbf{q}}F(q)e^{i\mathbf{q}\cdot\mathbf{r}} \quad . \tag{5.52}$$

Here $v_{ind}$ is the *indirect* ion-ion interaction, arising from ion-electron-ion interactions summed over intermediate electrons in the electronic ground-state.

The above equations for $\mathcal{E}_g$, and for $v_{ind}(r)$, were derived in *Thermodynamics of Crystals*, at a time when computer limitations required us to split these functions into real-space and Fourier-space contributions. It is now possible for computers to calculate all our functions entirely in real space, or in Fourier space, and the new formulation is enormously simpler. In the new algebra, the Coulomb divergences are handled differently from before. The undefined (infinite) terms in the above equations are the $\mathbf{q}=0$ component of $W_s$ in (5.47), and the $\mathbf{q}=0$ component of $W_b$ in (5.48) and (5.49). But these undefined components all appear inside sums, and the sums can be transformed to integrals, which are finite. There remains the bare Coulomb behavior $1/r$ at large $r$, present in $v_{ind}(r)$, but this will be canceled by the direct ion-ion interactions. It is possible to show that Eq. (5.48) for $\mathcal{E}_g$ is the same as Eq. (27.14) for $E_G$ in *Thermodynamics of Crystals*.

***Adiabatic Potential***

The groundstate energy contribution still missing from Eq. (5.48) is the sum of direct interactions among the ions. The ion cores are still considered rigid, in particular nonpolarizable, so the Coulomb energy between two nonoverlapping ions separated by $r$ is $z^2e^2/r$. The *effective* ion-ion potential $\phi(r)$ is therefore $z^2e^2/r + v_{ind}(r)$. Transforming (5.52) to an integral over $\mathbf{q}$, we have

$$\phi(r;V) = \frac{z^2e^2}{r} + \frac{V_A}{\pi^2}\int_0^\infty F(q)\frac{\sin qr}{qr}q^2dq \quad . \tag{5.53}$$

At large $r$, the leading dependence of the integral is $-z^2e^2/r$, hence $\phi(r)$ does not exhibit bare Coulomb behavior at large $r$. The volume dependence of $\phi(r;V)$ comes from the explicit appearance of $V_A$, and also from the volume dependences of $\xi$, $f$, and the parameters in $w_c(r)$.

The adiabatic potential $\Phi$ is defined in Eq. (4.6), and for $N$ rigid ions whose ionization energy is $I_z$, it follows $\Phi = \mathcal{E}_g + NI_z$. From Eqs. (5.48) to (5.53), we can write

$$\Phi(\{\mathbf{r}_K\}) = \Omega(V) + \frac{1}{2}{\sum_{KL}}' \phi(|\mathbf{r}_K - \mathbf{r}_L|;V) \quad , \tag{5.54}$$

correct to second order in the pseudopotential, where

$$\Omega(V) = NI_z + zN\left[\frac{3}{5}e_F + \frac{1}{2}W(\mathbf{q}=0)\right] + \frac{V}{2\pi^2}\int_0^\infty F(q)q^2dq \quad . \tag{5.55}$$

According to Eq. (5.42), $\frac{1}{2}W(\mathbf{q}=0) = -\frac{1}{3}e_F$. Except for the constant $NI_z$, the indicated volume dependence of $\Omega(V)$ is present in every term on the right of (5.55), and includes the volume dependences of $\xi$, $f$, and the parameters in $w_c(r)$. The ionization energy is positive and large, the term in square brackets is positive and relatively small, while the major contribution to $\Omega(V)$ is the integral, which is negative and expresses the metallic binding, dominated by the ion-electron Coulomb attraction. As pointed out in Sec. 1, in connection with Eq. (1.2), the sum of effective ion-ion potentials makes a relatively small contribution to $\Phi(\{\mathbf{r}_K\})$ in Eq. (5.54).

The leading dependence of $\phi(r)$ at large $r$ turns out to be (see *e.g.* Harrison, 1989, Eq. (17–12))

$$\phi(r) \propto \frac{\cos 2fr}{r^3} \quad , \quad \text{at large } r \quad . \tag{5.56}$$

The cosine factor produces the Friedel oscillations, and results from the discontinuity in the groundstate occupation of the electron states, at the Fermi energy. The convergence of $\phi(r)$ is sufficient to make the energy $\frac{1}{2}\Sigma_{KL}\phi(|\mathbf{r}_K - \mathbf{r}_L|)$ finite, that is, the energy $\phi_K = \frac{1}{2}\Sigma_L\phi(|\mathbf{r}_K - \mathbf{r}_L|)$ is finite for every ion $K$. But if we take strain and volume derivatives of the total energy, as in the calculation of stresses and elastic constants, and if we take those derivatives *inside the sum*, as we do in Secs. 10 and 14, then the derivative contributions arising from $\phi_K$ no longer converge in an infinite system. This is a spurious effect, since the energy itself is always finite, hence has finite strain derivatives. The problem is cured by cutting off $\phi(r)$ at some large $r$, such that the total energy is unaffected at the level of accuracy of the theory. Friedel oscillations in nearly-free-electron metals are generally smaller than a few $\mu$Ry, or say $1K$, and the whole theoretical construction cannot be meaningful at this energy. Original and damped forms of $\phi(r)$ for Na are shown in Fig. 1.1.

### *Electronic Excited States*

When we extend pseudopotential perturbation theory to electronic states above the groundstate, we make the same "weak excitation" approximation as in Sec. 3, namely that the potential seen by an electron, in this case the complete screened pseudopotential $W(\mathbf{r})$, will retain its groundstate evaluation, even as some electrons are excited out of the groundstate. This is accomplished by using the groundstate evaluations of the response functions $H(q)$ and $Y(q)$.

Let us consider the excitation of reference structure electrons. As we shall see in Sec. 7, the contribution to a thermodynamic function arising from excitation of reference structure electrons is expressed in terms of the electronic density of states, $n(E^\sigma)$. In pseudopotential perturbation theory, all the dependence on ion positions is in $W(\mathbf{r}) = W(\mathbf{r}; \{\mathbf{r}_K\})$. At the reference structure this is $W^\sigma(\mathbf{r}) = W(\mathbf{r}; \{\mathbf{R}_K\})$. Since $W$ is a perturbation, $n(E^\sigma)$ will be the free electron value $n(e)$, plus something small. In fact, whenever pseudopotential perturbation theory is a good description to begin with, then we expect the accurate $n(E^\sigma)$ from density functional theory to be reasonably well approximated by the free electron model. This turns out to be the case. The situation is illustrated, and the computational details are described, in Sec. 18.

When it comes to calculating *interactions* involving reference structure

electrons, the situation is different, because here the electron wavefunctions are needed. In some matrix elements, the perturbation part of the wavefunction can be as important as the free electron part. The Hamiltonian $\delta\mathcal{H}_{EX}$, describing interaction of the excited reference structure electrons with the motion of the ions, and the corresponding contribution to the free energy, are derived in pseudopotential perturbation theory in Sec. 18.

Finally, pseudopotential perturbation theory provides a conceptual simplification in the resolution of the total Hamiltonian. The exact electron excitation Hamiltonian is $\mathcal{H}_E - \mathcal{E}_g$, in Eq. (4.7), and this is approximated in Eq. (4.8), when it is replaced by its one-electron approximation $\mathcal{H}_{EX}$. But in pseudopotential perturbation theory, the one-electron description is exact in zeroth order, hence no separate one-electron approximation is required.

### *Calibration of Pseudopotential Models*

Pseudopotential perturbation theory is an approximate electronic structure theory, and is most useful when calibrated, either to more accurate theoretical results, or to experimental data. The general result for a real metal is that a calibrated pseudopotential model accounts for physical properties far beyond the data to which it is calibrated. The adiabatic potential expressed in Eqs. (5.53) to (5.55) produces an excellent total Hamiltonian for the alkali metals, when the exchange-correlation parameter $\xi$ is determined from the compressibility of the uniform electron gas, and when the core potential $w_c(r)$ is calibrated to experimental data. This is the pseudopotential model for Na whose effective ion-ion potential is shown in Fig. 1.1, and which is utilized throughout this monograph to illustrate what is achievable with a highly accurate Hamiltonian. The list of properties accurately accounted for by this model for Na includes the binding energy, the compressibility and elastic constants, thermal expansion, the phonon spectrum, the melting temperature, quasiharmonic and anharmonic contributions to thermodynamic functions from $T = 0$ to melt, electron-phonon interactions, and corresponding properties of the liquid as well.

In the old days, to test sensitivity to the form of $w_c(r)$, the parameters were adjusted on Harrison and Heine-Abarenkov models to obtain a good overall fit to the experimental phonon dispersion curves of Al (Wallace, 1969b). The best Heine-Abarenkov potential turned out to be an Ashcroft empty core potential. Dispersion curves are virtually identical for the two

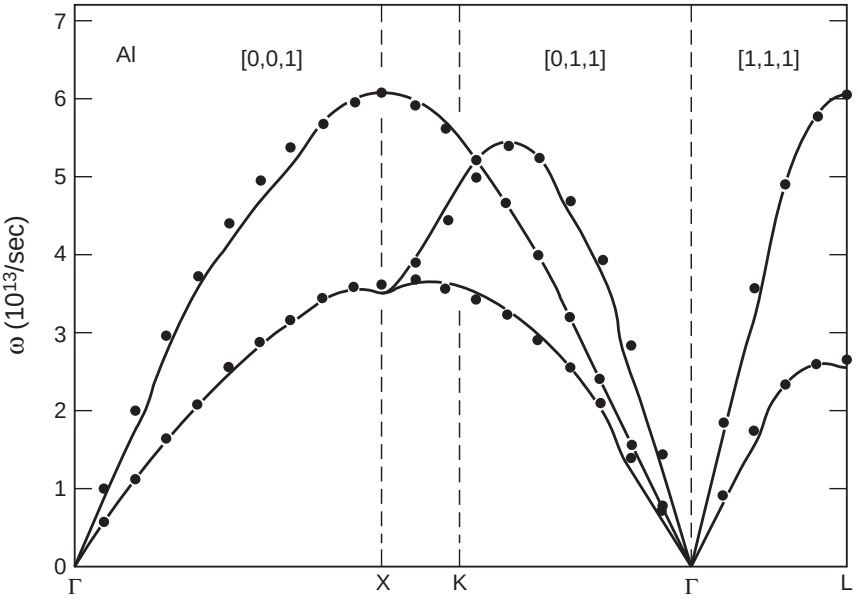


Figure 5.1. Calculated phonon dispersion curves (lines) for fcc Al, compared with experiment at 80K (points). In the theoretical curves, Kohn anomalies are artificially sharpened to make them clearly visible.

models, and are compared with experiment in Fig. 5.1. The form factors for the two models are compared in Fig. 5.2, and are seen to differ only at $q \gtrsim 2f$. We conclude that the phonon frequencies are only weakly dependent on $w(q)$ at large $q$. Values of $w(q)$ at the first two inverse lattice vectors, extracted from experimental Fermi surface data by Ashcroft (1963), are also shown in Fig. 5.2, and are in good agreement with our model form factors. These models for Al also give good results for quantities related to phonon-phonon and electron-phonon interactions.

However, these Al pseudopotential models give only qualitatively correct results for the binding energy and compressibility. This discrepancy was recognized by Ashcroft and Langreth (1967), as a general property of the theory, and was accounted for by adding another term into $\Omega(V)$, proportional to $V_A^{-1}$ and representing the $\mathbf{q} = 0$ component of contributions from higher order perturbation theory. In a more recent study of Al, Straub *et al.* (1994) calibrated a complete pseudopotential model, namely the core potential $w_c(r)$, the exchange-correlation parameter $\xi$, and the total $\Omega(V)$

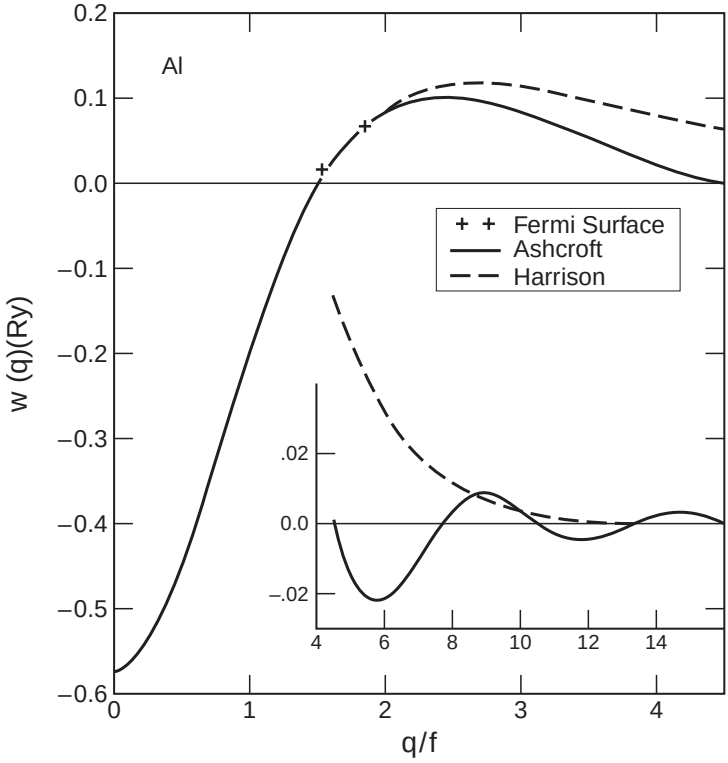


Figure 5.2. Screened form factors for the two pseudopotential models whose parameters were determined to give the best overall fit to the measured phonon frequencies for Al.

function, to density functional calculations of the static lattice potential and a small number of zone-boundary phonon frequencies. In this way, the pseudopotential perturbation theory serves as an interpolation formula for the entire $\Phi(\{\mathbf{r}_K\})$ surface, from just a few points on that surface calculated from a much more accurate theory.

Since we are interested in the equation of sate of condensed matter, the theory developed here is supposed to apply to metals under compression, even under extreme compression. Considering the various effects which are represented by the local core potential $w_c(r)$, mentioned in connection with Eq. (5.34), and considering that the valence electrons are increasingly forced into the core region as a metal is compressed, the parameters of $w_c(r)$ must in principle vary with the system volume $V$. This property was

accounted for in the Al model mentioned above (Straub *et al.*, 1994), since that model was independently calibrated to results of density functional theory at a series of volumes. However, in our models for the alkali metals (Wallace, 1968), we added an empirical Born-Mayer repulsion to $\phi(r)$, of the form $\alpha e^{-\gamma r}$, intended to account for the Pauli repulsion when the ion cores begin to overlap. As it turns out, the Born-Mayer term gives only a small contribution to the physical properties, in all the comparisons of theory and experiment presented in this monograph. Moreover, since the whole model was calibrated to experimental data, the Born-Mayer repulsion gives a proper *empirical* account of compression effects. Nevertheless, Born-Mayer repulsion is not consistent with the physical basis of pseudopotential perturbation theory. Instead, the pseudopotential parameters themselves should vary with $V$, and when a metal is compressed to the point where ion cores begin to overlap, the outer shell of core electrons should be removed and included with the valence electrons.

Pseudopotential perturbation theory is still being developed as a description from first principles of the electronic structure of nearly-free-electron metals. Ashcroft (1990) discussed effects in liquid metals, associated with nonrigid ion cores, and with transient clustering of the ions. Pollack *et al.* (1997) compared experiment and theory for zone-boundary phonons and elastic constants from a local pseudopotential in second order, and they also examined nonlocal and nonperturbative effects.

*Problem*

*5.1* In arriving at Eq. (5.48), the sum of free electron energies in (5.45) is evaluated over the zeroth order Fermi sphere. Is this the correct procedure? Show that the true Fermi surface differs from the free electron surface in second order in $W(\mathbf{q})$, and both surfaces enclose the same volume. Hence show the sum of free electron energies is the same to second order when evaluated over either volume.

*This page intentionally left blank*

# Chapter 2
# Statistical Mechanics

## 6 AVERAGING TECHNIQUES

### *Fluctuating Equilibrium State*

Imagine a monatomic liquid in a container, maintained at uniform boundary conditions, so that it is in an equilibrium state. For the moment assume the motion of the atoms is classical, hence is determined by Newtonian mechanics and the interatomic potential. Actually, the underlying Hamiltonian is that of Chap. 1, and the system corresponds to nuclei moving in the adiabatic potential, but in the present section it will be more in line with a century of statistical mechanics thinking to speak of atoms moving according to their interatomic potential. Consider, then, the condition of a particular atom in the interior of the liquid. This atom is in constant motion, is constantly being pushed and pulled by its neighboring atoms, which are also moving; in short, the atom can never rest. Through this motion, each atom explores all its accessible states of motion, and moreover, the collection of atoms explore their collective states of motion, and this constant motional exploration is perhaps the most important property of the equilibrium state of matter.

For the moment let us ignore the world outside our monatomic liquid, and ignore also the surface region of the liquid, where the motion is affected by the boundary conditions, and ask about the statistical properties of the atoms in the interior. Then, all atoms in the interior are equivalent, since over a sufficiently long period of time, each atom will pass through the same set of conditions as will every other atom in the interior. These conditions are the atom's kinetic and potential energy, its velocity and acceleration,

and so on. Hence, any single atom can serve as a statistical system, since over time its single-atom properties will average to values corresponding to the equilibrium state of the liquid.

Notice there are systems where all atoms are not equivalent, as for example a crystal with inequivalent lattice sites. In such a case, the above picture requires the trivial modification that each atom serves as a statistical system only for its particular equivalence class.

Let us next consider the subsystem composed of the atoms within a fixed subvolume in the interior of the liquid. The number of atoms in the subsystem fluctuates, as atoms move in and out of the subvolume, and indeed every property of the subsystem fluctuates, except its volume. The instantaneous configuration of the subsystem continually fluctuates away from the mean configuration of the equilibrium liquid, and with each such fluctuation, restoring forces develop to drive the configuration back toward the mean. Hence within the fluctuations of the equilibrium state, there is information on the forces which drive the liquid to its equilibrium. This is the physical basis for the fluctuation-dissipation theorem, and the Green-Kubo formulation of linear response theory, in which the regression of fluctuations in the equilibrium state provides a quantitative measure of the irreversible processes which move a nonequilibrium system toward equilibrium.

The same property of equilibrium fluctuations has an essential role in phase transitions. For example, suppose the temperature of the liquid is lowered. Small groups of atoms are constantly exploring all accessible configurations, including the crystal configuration, and when the correct temperature is reached, the atoms will choose to remain locally in the crystal configuration. Local seed crystals will then grow, converting the liquid into a polycrystalline solid. The physics of phase transitions will be discussed further in Chapter 6.

So far we have discussed the motion of individual atoms in an equilibrium liquid. In many systems it is appropriate to express the equilibrium motion in terms of approximate normal modes. This is true for crystalline or amorphous solids, where the atomic motion is described by weakly interacting vibrational modes. The normal mode description applies equally to quantum or classical motion, and accounts for both quantum and classical fluctuations. Quantum fluctuations express that an operator $\mathcal{A}$ can exhibit $\langle \mathcal{A}^2 \rangle \neq \langle \mathcal{A} \rangle^2$ for expectation values in a single quantum state, while classical fluctuations express the same relation for averages over a distribution

of quantum states. Quantum fluctuations dominate at low temperatures, where they give rise to zero-point motion, while classical fluctuations dominate at higher (classical) temperatures. Hence a many-atom condensed matter system has many normal modes of excitation, with interactions among them, so that each excitation fluctuates over its energy levels, and the equilibrium motion is just as complicated in the normal mode description as it is in the single-atom description.

### *Laboratory Systems and Theoretical Systems*

A laboratory system is a real $N$-atom system, with very large $N$, whose equilibrium motion is determined by its Hamiltonian and applied boundary conditions. Thermodynamic properties of the system are measured in laboratory experiments, and are averages over its motion in equilibrium states. Measured quantities might be $V/N$, the volume per atom, obtained perhaps from x-ray measurements of the crystal lattice parameter, or the internal energy $U$, whose increments are obtained from calorimeter measurements. There are two classes of boundary conditions, namely (a) those which fix certain thermodynamic variables, such as temperature and pressure, information which is reported as part of the experimental data, and (b) those which are merely surface effects, such as the surface-to-volume ratio in a powdered x-ray sample, and the nature of the thermal contact in a calorimeter. The latter information might be an important part of the experimental technique, but is not part of the thermodynamic data reported from an experiment, because surface effects vanish as $N \to \infty$. There are also effects such as gravity, which are not surface effects, but are still negligible in most thermodynamic experiments.

The program of equilibrium statistical mechanics is to construct a theoretical system, usually called a *mechanical system*, or just *system*, which accurately represents the laboratory system, and to calculate averages over the equilibrium motion of this mechanical system. In setting up the system, there are again two classes of boundary conditions, which have entirely different roles in the theory. Certain boundary conditions fix certain mechanical variables which are also thermodynamic variables, such as the number of particles $N$, and the total volume $V$, or the crystal lattice parameters. Often, but not always, the independent variables of theory are the dependent variables of experiment, and vice versa. Other boundary conditions are again surface effects, hence they do not determine thermodynamic vari-

ables, but still they have an important role in the computational technique. Once the mechanical system is constructed to have the desired values of independent variables $N$, $V$, and so on, then those boundary conditions which contribute only surface effects can be chosen at will. One can choose to facilitate solution for the equilibrium motion of the system, in classical or quantum mechanics, and one can also choose to minimize finite-$N$ effects. For some mechanical systems, such as perfect crystals, it is possible to do theoretical work in the limit $N \to \infty$, so that finite-$N$ effects can be ignored. For other systems, such as those used in computer simulations, our theoretical capabilities are limited to small values of $N$, and it is necessary to account for finite-$N$ effects in order to compare calculated averages with experiment.

Let us now describe a few simple mechanical systems, to illustrate the preceding observations. Consider a system of $N$ atoms in a cubical box of volume $V$, with periodic boundary conditions. The periodic boundary condition is equivalent to having space filled with identical boxes, with $N$ atoms undergoing identical motion in each box. Notice this is Hamiltonian motion from a periodic initial condition over all space. Since the repeating periodic units each contain $N$ atoms, it is believed the periodic boundary condition causes effects of $RO(N^{-1})$ at large $N$. The notation $RO(N^{-1})$ means of *relative order* $N^{-1}$, *i.e.* for a quantity $\mathcal{A}$ of any order in $N$, $RO(N^{-1})$ means of order $\mathcal{A}/N$. With the periodic boundary condition, total energy and total linear momentum are conserved under Hamiltonian motion. Since we are interested in thermodynamic properties, the total momentum is set zero. In a mechanical system where the momentum is not a constant of the motion, but fluctuates, the mean momentum will be set zero.

One can also consider a system of $N$ atoms in a cubical box of volume $V$ with perfectly reflecting walls, or $N$ atoms in a condensed system with a free surface. With reflecting walls, total energy and momentum fluctuate, while both are conserved with the free surface. Either of the these boundary conditions presumably produces effects of $RO(N^{-1/3})$ at large $N$, much larger than the effects of periodic boundary conditions.

A different mechanical system is the collection of atoms within a fixed cubical volume $V$ in the interior of a larger system, the interior being the region where the motion is indifferent to the boundary condition applied to the larger system. For this interior system, the instantaneous number of atoms fluctuates about the mean value $N$, and the total energy and

total momentum also fluctuate about their mean values. These fluctuations presumably contribute to statistical averages in $RO(N^{-1})$ at large $N$. For both the interior system, and the system with periodic boundary conditions, motional correlations with wavelength up to the system size, but not larger, should be properly contained in the solution for the motion.

### *Time Averages for a Molecular Dynamics System*

In molecular dynamics, the mechanical system is replicated on a computer, and its motion is calculated numerically. Because of the small size of molecular dynamics systems, it is necessary to average over time to get highly accurate average values. However, as we shall see, finite-$N$ effects are still present in time averages, even over arbitrarily long times. Since at present most molecular dynamics calculations are classical, our treatment of time averages is limited to classical statistical mechanics.

A dynamical variable $\mathcal{A}$ is a function of the instantaneous positions and momenta of all the atoms in the system. The variables of interest are those whose average represents a macroscopic physical property, as energy, pressure, or temperature. The average $\langle \mathcal{A} \rangle$ is the time average over the system motion,

$$\langle \mathcal{A} \rangle = \frac{1}{\theta} \int_0^\theta \mathcal{A}(t) dt \quad , \tag{6.1}$$

where the time interval $\theta$ is sufficiently long to yield an average of a specified accuracy. An estimate of accuracy is often an important part of the specification of a calculated average. The dynamical variable expressing a fluctuation is

$$\delta\mathcal{A} = \mathcal{A} - \langle \mathcal{A} \rangle \quad , \tag{6.2}$$

and the averages $\langle \delta\mathcal{A}^2 \rangle$ and $\langle \delta\mathcal{A}\delta\mathcal{B} \rangle$ are mean quadratic fluctuations, and are often called simply *fluctuations*. The term "dynamical variable" alone will not be used to mean a fluctuation, *i.e.* will not mean $\delta\mathcal{A}$, unless explicitly so stated.

The total energy is $\mathcal{H} = \mathcal{K} + \Phi$, where $\mathcal{K}$ and $\Phi$ are respectively the total kinetic and potential energies. While $\mathcal{H}$ might or might not be a constant of the motion, depending on the boundary condition, $\mathcal{K}$ and $\Phi$ both fluctuate, as the system exchanges energy between kinetic and potential components. A graph of $\mathcal{K}/N$ *vs* time for an equilibrium molecular dynamics system is

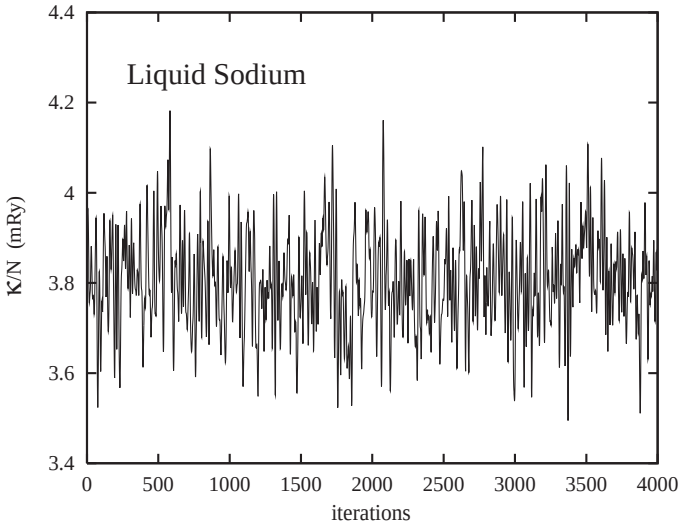


Figure 6.1. Kinetic energy per atom for pseudopotential sodium in equilibrium at 393 K and $V/N = 278a_0^3$, the atomic volume of liquid sodium at $T_m = 371K$. One iteration is the molecular dynamics timestep, 7.00 fs, and $N = 500$.

shown in Fig. 6.1. Through its equilibrium motion the system samples a *distribution* of $\mathcal{K}/N$, and a convenient way to represent a distribution is through its moments. The first moment is the mean value of $\mathcal{K}/N$, and the second moment is the variance, or mean fluctuation, which measures the average width of the distribution of $\mathcal{K}/N$ in Fig. 6.1. A graph such as Fig. 6.1 is called a *stationary time signal* by statisticians, because averages such as Eq. (6.1) are independent of where the zero of time is chosen. As a practical note, successively higher moments require averaging for much longer times to achieve a given level of accuracy, and correspondingly, moments beyond the second are seldom considered in statistical mechanics.

If now the system size increases, such that $N/V$ remains constant as $N$ increases, those effects which vanish as some inverse power of $N$, as $N \to \infty$, are finite-$N$ effects. To illustrate, consider the variable $\mathcal{K}/N$ graphed in Fig. 6.1. The mean of $\mathcal{K}/N$ approaches a nonzero limit, the thermodynamic limit, as $N \to \infty$. At finite $N$, the mean of $\mathcal{K}/N$ differs from its thermodynamic limit by a term going as some inverse power of $N$, depending on the boundary condition. On the other hand, the mean fluctuation of $\mathcal{K}/N$ is itself a finite-$N$ effect, since it goes to zero as some inverse

power of $N$, as $N \to \infty$. The only way to evaluate these finite-$N$ effects is numerically, by finding their dependence on $N$ through calculations for a range of $N$.

Let us relate the thermodynamic properties of a molecular dynamics system to its time averages. For a fixed number of atoms $N$, the system volume $V$ is a variable, and the thermodynamic internal energy $U$ is the mean energy $\langle \mathcal{H} \rangle$. Notice the custom in thermodynamics is to consider a fixed large number of atoms $N$, so that $V$ is the thermodynamic variable, though the physically meaningful variable is actually the atomic volume $V/N$. So $U$ and $V$ are determined, and these two variables specify an equilibrium state. One more thermodynamic variable will fix the entire equilibrium surface. Two points are important. First, there is no dynamical variable whose mean will give the entropy. The situation here is precisely the same as in experiment, where only increments of entropy are measured. Second, every *other* thermodynamic function has a corresponding dynamical variable, and the choice of which to use can be made on the basis of convenience. Let us choose the temperature $T$. From statistical mechanics based on phase-space averaging, the dynamical variable corresponding to temperature in classical statistics is $\mathcal{K}/N$, according to the relation derived in Eq. (10.8),

$$\langle \mathcal{K}/N \rangle = \frac{3}{2} kT \quad , \tag{6.3}$$

in the thermodynamic limit. With temperature determined, $U(V,T)$ is prescribed, and all thermodynamic functions are determined. For example, since $dU = TdS - PdV$, the entropy can be calculated up to a constant of integration from $dS_V = T^{-1} dU_V$. With entropy determined, the pressure is $P = -(\partial U/\partial V)_S$. Ultimately, the unknown entropy constant has to come from phase-space averaging.

### *Phase Space Averages for a Single System*

While the concept of an ensemble, being an infinite set of model systems in contact with reservoirs, is widely used to support the logic of statistical mechanics, the practical result of equilibrium statistical mechanics is the recipe for calculating statistical averages, by means of the partition function, as averages over the phase space of a single model system. It is then a separate assumption, or an hypothesis, that the averages so calculated

should be the same as the measured thermodynamic properties of a laboratory system. To test this assumption, one invariably applies the logic that the model system, for which the partition function is to be calculated, should match the laboratory system in its relevant properties, such as its Hamiltonian, its mean density, or perhaps its crystal structure. Within this logic, and through countless comparisons of statistical mechanical calculations with experimental thermodynamic data, the assumption in question has become one of the most universally verified in all of physics. It is therefore possible to omit the concept of ensemble, and simplify the formulation of statistical mechanics. The steps are as follows.

(a) Construct a mechanical system which accurately represents the laboratory system.

(b) Calculate phase space averages from the partition function.

(c) Assume the phase space averages are the same in the thermodynamic limit as averages over the equilibrium motion of the mechanical system, or what is equivalent, assume the phase space averages are the same as the measured thermodynamic properties of the laboratory system.

In phase space averaging, the role of the mechanical system is to determine the phase space. Averaging over this space is then carried out with a weight function, whose purpose is to enforce mean-value constraints. Thermodynamic variables such as volume are fixed by the phase space, while others such as the internal energy are fixed by the constraints. As usual, boundary conditions which do not control thermodynamic variables contribute finite-$N$ effects, and can be chosen at will. For example, for a quantum system, periodic boundary conditions will condition the wave functions, and will contribute finite-$N$ effects to all matrix elements. In the customary formulation of phase space averaging, it is assumed that one is working in the limit $N \to \infty$, so that finite-$N$ effects vanish. In principle, finite-$N$ effects can be accounted for if necessary.

The normalized weight function is the distribution of probability density over the phase space of the system, or simply *the distribution*. The four commonly used distributions are the microcanonical, canonical, grand canonical, and constant pressure distributions. In the thermodynamic limit, as will be shown below, all distributions yield identical results for thermodynamic functions, so ultimately the distribution can be chosen for mathematical convenience. The microcanonical distribution specifies the physically realistic conditions that $N$, $V$, and the total energy $\mathcal{H}$ are constants. But the constraint of constant $\mathcal{H}$ is difficult to work with, and it is much easier

to use the canonical distribution, in which this constraint is eliminated in favor of a Lagrange multiplier, which can be chosen to fix the mean energy $\langle \mathcal{H} \rangle$ at any desired value. The same mathematical convenience justifies the grand canonical distribution, which removes the constraint of constant $N$, and the constant pressure distribution, which removes the constraint of constant $V$.

Let us construct the microcanonical distribution for a classical system of $N$ atoms in a cubical volume $V$. The atoms have positions $\mathbf{r}_K$ and momenta $\mathbf{p}_K$ for $K = 1, \cdots, N$, and the phase space is the volume $V$ for each $\mathbf{r}_K$, and all momentum space for each $\mathbf{p}_K$. Let $x$ represent a phase space point $\{\mathbf{r}_K, \mathbf{p}_K\}$. The microcanonical distribution must specify that $\mathcal{H}(x)$ has the constant value $U$. To accomplish this, phase space is divided into incremental cells located at the points $x_n$, for $n = 1, 2, \cdots$. Notice the actual cell volume is unimportant, as long as it is small (see *e.g.* Reif, 1965, pp. 215–216). The finite dimensionless weight function $\Delta(\mathcal{H}(x) - U)$ is defined to have the value $\Delta_n$ throughout cell $n$, where $\Delta_n = 1$ if $\mathcal{H}(x) = U$ anywhere in cell $n$, and $\Delta_n = 0$ otherwise. The total volume of cells containing the constant energy surface is $\int \Delta(\mathcal{H}(x) - U)dx$. The average of a dynamical variable $\mathcal{A}(x)$ is

$$\langle \mathcal{A} \rangle = \frac{\int \mathcal{A}(x)\Delta(\mathcal{H}(x) - U)dx}{\int \Delta(\mathcal{H}(x) - U)dx} \quad . \tag{6.4}$$

This equation confirms $\langle \mathcal{H} \rangle = U$.

The thermodynamic quantity which has no corresponding dynamical variable, and which therefore cannot be calculated from the averaging prescription (6.4), is the entropy. But for the entropy we have the Boltzmann correspondence, that the entropy of a closed system is $k \ln \Omega$, where $\Omega$ is the number of microstates accessible to the system. The phase space volume accessible to the system is just the denominator of (6.4), so the question now is, how much of this volume is to be associated with each microstate? The answer is $h^{3N}$, a result which obviously has to come from quantum mechanics, and will be derived in Sec. 9, *e.g.* in Eq. (9.21). So the number of accessible microstates is $h^{-3N} \int \Delta(\mathcal{H}(x) - U)dx$. However, this counts all states equivalent by the $N!$ particle permutations in the $N$-atom system, and what one wants is the number $Z(N, V, U)$ of *distinguishable* accessible

microstates, or

$$Z(N,V,U) = \frac{1}{N!h^{3N}} \int \Delta(\mathcal{H}(x) - U)dx \quad . \tag{6.5}$$

This function is the classical microcanonical partition function, and the Boltzmann entropy is given by

$$S = k \ln Z \quad . \tag{6.6}$$

At this point, all thermodynamic quantities are determined, since they follow from the state function $U(V,S)$. For example, since $dU = TdS - PdV$, the temperature and pressure are given by

$$T = \frac{\partial U}{\partial S}\Big)_V \quad , \quad P = -\frac{\partial U}{\partial V}\Big)_S \quad . \tag{6.7}$$

***Internal Consistency***

If the total system energy is $E$, then in quantum or classical mechanics, the canonical weight function is $e^{-\beta E}$, the density of energy levels is $\Omega(E)$, and the canonical partition function is $\int \Omega(E)e^{-\beta E}dE$. As functions of increasing $E$, $\Omega(E)$ is strongly increasing, $e^{-\beta E}$ is strongly decreasing, so the integrand has a sharp peak. The important property is that the width of this peak is proportional to the mean fluctuation $\langle \delta E^2 \rangle$, and goes to zero in $RO(N^{-1})$ as $N \to \infty$. This property tells us how to relate different phase space distributions, as follows.

The discussion applies equally to classical mechanics, where the system phase space is the space of atomic positions and momenta, and to quantum mechanics, where the system phase space is its complete set of quantum states. The point is, several different distributions are commonly used, where each has its fully equivalent classical and quantum forms. Each distribution specifies the phase space probability distribution of a few dynamical variables, say one or two, hence various distributions are different in the variables which they allow to fluctuate. Consider the dynamical variables $\mathcal{N}$, $\mathcal{V}$, and $\mathcal{H}$. In the microcanonical distribution $\mathcal{N}$, $\mathcal{V}$, and $\mathcal{H}$ are constants, while $\mathcal{H}$ fluctuates in the canonical distribution, both $\mathcal{N}$ and $\mathcal{H}$ fluctuate in the grand canonical distribution, and $\mathcal{V}$ and $\mathcal{H}$ fluctuate in the constant pressure distribution. So in each partition function, the integrand has widths in various directions in phase space, and each width is proportional to the fluctuation in that particular direction, and since the mean

quadratic fluctuations all go to zero in $RO(N^{-1})$, then all phase space integrands collapse to the same thermodynamic equilibrium surface as $N \to \infty$. Hence all four distributions are the same in the thermodynamic limit. That mean fluctuations are of $RO(N^{-1})$ is demonstrated in Secs. 7 and 10.

To compare averages from different distributions, one first has to specify a common equilibrium state, say at given $V$ and $U$. Then, in the thermodynamic limit, every distribution will give the same value of the entropy, and of every other thermodynamic function as well. At finite $N$, the entropy and the dependent thermodynamic functions will differ in $RO(N^{-1})$ among different distributions. An equation for the differences in averages of a given dynamical variable is given in (10.50).

There is a point to make regarding consistency between thermodynamics and statistical mechanics. In the microcanonical distribution, for example, the quantities $V$, $U$, and $S$ can be obtained as independent data, according to Eqs. (6.4) – (6.6). These data completely specify the equilibrium surface, so that all other thermodynamic quantities are dependent data. There are two ways to calculate dependent quantities: they can be calculated by thermodynamic relations, from the function $U(V, S)$, or they can be calculated by averaging dynamical variables. But these two ways must give the same results in the thermodynamic limit, and this condition determines the dynamical variable corresponding to a given thermodynamic function. From Eq. (6.3), for example, the dynamical variable corresponding to $kT$ is $\frac{2}{3}\mathcal{K}/N$ in classical statistics. Additional examples will be derived throughout this chapter. Because of the equivalence of different distributions, the dynamical variable for a given thermodynamic function is the same in all distributions. The conclusion is that, with properly constructed dynamical variables, thermodynamics and statistical mechanics are consistent in all distributions, to $RO(N^{-1})$.

In the time averaging technique, $V$, $U$, and $T$ can be obtained as independent data, so that all remaining thermodynamic quantities are dependent. But to find temperature, we have to use the classical phase space relation between $\langle \mathcal{K}/N \rangle$ and $T$, Eq. (6.3). To justify this procedure, we make the kinetic-energy quasiergodic hypothesis: At given $V$ and $U$, the phase space average of $\mathcal{K}/N$ and the time average of $\mathcal{K}/N$ are the same in the thermodynamic limit. Then $T$ is the same function of $V$ and $U$ in both averaging techniques, hence the complete set of thermodynamic functions is likewise the same, except for the constant of entropy, which is still

undetermined in time averaging. The conclusion is that, under the stated hypothesis, time averaging and phase space averaging are consistent, again to $RO(N^{-1})$.

## 7 QUANTUM STATISTICAL MECHANICS

### *Canonical Distribution*

The quantum mechanical system is described by its Hamiltonian and boundary conditions. To be definite, we are considering the condensed matter Hamiltonian derived in Chap. 1, for a system of $N$ atoms, reduced to $N$ nuclei and $zN$ electrons, in a cubical box of volume $V$, with periodic boundary conditions. The Schrödinger equation has presumably been solved for the complete set of states $n = 1, 2, \cdots$, by

$$\mathcal{H}\psi_n = E_n\psi_n \quad , \qquad \langle\psi_{n'}|\psi_n\rangle = \delta_{nn'} \quad . \tag{7.1}$$

The solution is supposed to be highly accurate, exact in principle. The system phase space is the complete set of states, and for phase space averaging, each state is assigned a weight factor $f_n$. The $f_n$ are supposed to be normalized,

$$\sum_n f_n = 1 \quad , \tag{7.2}$$

so that they constitute a probability distribution over the set of states. The average of a dynamical variable $\mathcal{A}$ is therefore given by

$$\langle\mathcal{A}\rangle = \sum_n f_n \langle\psi_n|\mathcal{A}|\psi_n\rangle \quad . \tag{7.3}$$

It is understood in quantum mechanics that dynamical variables are operators.

Turning to the entropy, the basic ideas are found in the work of Boltzmann, and of Gibbs (for a historical review see Bailyn, 1994, Chaps. 10 and 11). Boltzmann thought of entropy as a measure of the distribution $f_n$ of a closed classical system over its microstates, and he included all distributions, both equilibrium and nonequilibrium distributions. An approach to equilibrium means the distribution becomes more uniform, until at equilibrium the distribution is perfectly uniform, all microstates have the same probability $f_n = f$, and the equilibrium entropy is $S = -k \ln f$.

Gibbs generalized this equilibrium entropy to $S = -k\,\Sigma_n f_n \ln f_n$ for all three canonical ensembles. Let us now consider a quantum system, let the normalized distribution over its quantum states be $\hat{f}_n$, where the hat signifies the distribution is completely general, equilibrium or nonequilibrium, and define the corresponding entropy $\hat{S}$ as

$$\hat{S} = -k \sum_n \hat{f}_n \ln \hat{f}_n \quad . \tag{7.4}$$

Then following the logic of Boltzmann, under all variations of the distribution $\hat{f}_n$, subject to its normalization and any other constraints, $\hat{S}$ is maximum at equilibrium, and is the equilibrium entropy $S$. So by properly choosing the phase space distribution, we have more than a prescription for evaluating the averages in Eq. (7.3), we have the great advantage of a formula for the entropy.

The canonical constraints on the distribution are that the average energy is the thermodynamic internal energy $U$, and that the distribution is normalized, *i.e.*,

$$\sum_n E_n \hat{f}_n = U \quad , \qquad \sum_n \hat{f}_n = 1 \quad . \tag{7.5}$$

To maximize $\hat{S}$, its variation $\delta\hat{S}$ is set zero, and subject to the above constraints, the result is

$$-k \sum_n \delta\hat{f}_n (\ln \hat{f}_n + 1 + \lambda + \beta E_n) = 0 \quad , \tag{7.6}$$

where $\lambda$ and $\beta$ are Lagrange multipliers. Since each $\delta\hat{f}_n$ is now arbitrary, its coefficient in (7.6) must vanish, and this yields the normalized equilibrium distribution $f_n$,

$$f_n = \frac{e^{-\beta E_n}}{Z} \quad , \qquad Z = \sum_n e^{-\beta E_n} \quad , \tag{7.7}$$

where $Z$ is the canonical partition function. The remaining Lagrange parameter $\beta$ is determined by the value of $U$, from

$$U = \sum_n E_n f_n \quad , \tag{7.8}$$

and the equilibrium entropy is

$$S = -k \sum_n f_n \ln f_n \quad . \tag{7.9}$$

The thermodynamics of the system is now completely specified, through the known function $U(V, S)$. The volume dependence is contained in $f_n$, through $E_n = E_n(V)$, and through the density of states contained in the $\Sigma_n$ in $Z$.

There is a simple relation between the distribution parameter $\beta$ and the temperature $T$, namely

$$\beta = \frac{1}{kT} \quad . \tag{7.10}$$

This will be derived shortly, as soon as we get into thermodynamics, but meanwhile it is needed to examine the $T \to 0$ limit of the entropy. This limit corresponds to $\beta \to \infty$, where all $f_n \to 0$ except for the groundstate probability $f_g$. Now the groundstate must be nondegenerate, hence it follows $f_g \to 1$ from Eq. (7.7), and the entropy goes to zero:

$$S \to -k f_g \ln f_g \to 0 \quad , \text{ as } T \to 0 \quad . \tag{7.11}$$

As a final note, system states related by continuous symmetries, such as uniform translations or rotations of the whole system, are considered indistinguishable, hence are counted only once in statistical mechanics.

***Thermodynamics***

The internal energy $U(V, S)$ is a *thermodynamic state function*, since all thermodynamic quantities can be derived from it. The combined first and second laws of thermodynamics is $dU = TdS - PdV$. From this, the dependent variables $T$ and $P$ are given by

$$T = \frac{\partial U}{\partial S}\Big)_V \quad , \qquad P = -\frac{\partial U}{\partial V}\Big)_S \quad . \tag{7.12}$$

The first equation now fixes the relation between $T$ and the distribution parameter $\beta$. From Eq. (7.8) we have $dU_V = \Sigma_n E_n df_n$, since $E_n = E_n(V)$, from Eq. (7.9) we have $dS_V = \beta k \Sigma_n E_n df_n$, where the normalization condition $\Sigma_n df_n = 0$ has been used. Comparing these results with $dU_V = TdS_V$, from Eq. (7.12), one immediately finds $\beta = 1/kT$, as written in Eq. (7.10).

In practice it is often more convenient to work from a different thermodynamic state function, the Helmholtz free energy $F(V,T)$. The two state functions are related by

$$F = U - TS \quad . \tag{7.13}$$

Entropy and pressure are given by the two independent first derivatives of $F$,

$$S = -\frac{\partial F}{\partial T}\Big)_V \quad , \qquad P = -\frac{\partial F}{\partial V}\Big)_T \quad . \tag{7.14}$$

Since $U$ and $S$ are given as phase space sums by Eqs. (7.8) and (7.9), then $F$ can be constructed as a phase space sum from Eq. (7.13), with the help of (7.14) for $S$, and the result is

$$F = -kT \ln Z \quad . \tag{7.15}$$

This equation is the most universally used connection between statistical mechanics and thermodynamics.

Several important thermodynamic functions, useful in our work, are as follows.

$$\begin{aligned}
C_P &= T\,\frac{\partial S}{\partial T}\Big)_P : \text{specific heat at constant pressure,} \\
C_V &= T\,\frac{\partial S}{\partial T}\Big)_V : \text{specific heat at constant volume,} \\
B_S &= -V\,\frac{\partial P}{\partial V}\Big)_S : \text{adiabatic bulk modulus,} \\
B_T &= -V\,\frac{\partial P}{\partial V}\Big)_T : \text{isothermal bulk modulus,} \\
\alpha &= \frac{1}{V}\,\frac{\partial V}{\partial T}\Big)_P : \text{thermal expansion coefficient,} \\
\gamma &= V\,\frac{\partial P}{\partial U}\Big)_V = \frac{\alpha V B_T}{C_V} : \text{Grüneisen parameter.}
\end{aligned} \tag{7.16}$$

The following relations among functions are also useful in our work.

$$\frac{C_P}{C_V} = \frac{B_S}{B_T} = 1 + \alpha T \gamma \quad . \tag{7.17}$$

Finally, thermodynamic stability requires

$$C_P > C_V > 0 \quad ,$$
$$B_S > B_T > 0 \quad . \tag{7.18}$$

The above relations are discussed in more detail in Sec. 1 of *Thermodynamics of Crystals* (see also problem 7.1).

As mentioned in Sec. 6, once the complete equilibrium surface is determined, through the function $U(V,S)$ say, or through $F(V,T)$, then all remaining thermodynamic functions *and* their corresponding phase space operators are dependent variables. Let us take pressure as an example, and see how its phase space operator is determined. $P$ is determined from $Z$, through $F$, by Eqs. (7.14) and (7.15), and since $Z = Tre^{-\beta\mathcal{H}}$, we have

$$P = -\frac{1}{Z} Tr\left(\frac{d\mathcal{H}}{dV} e^{-\beta\mathcal{H}}\right) = -\left\langle \frac{d\mathcal{H}}{dV} \right\rangle \quad . \tag{7.19}$$

Hence the operator whose mean value is $P$ is $-d\mathcal{H}/dV$. A similar but more extensive analysis, giving the complete stress tensor, is carried out in classical statistics in Sec. 10.

***Fluctuations***

The dynamical variable (operator) representing a fluctuation is $\delta\mathcal{A} = \mathcal{A} - \langle\mathcal{A}\rangle$, and the mean quadratic fluctuation of $\mathcal{A}$ and $\mathcal{B}$ is

$$\langle\delta\mathcal{A}\delta\mathcal{B}\rangle = \langle\mathcal{A}\mathcal{B}\rangle - \langle\mathcal{A}\rangle\langle\mathcal{B}\rangle \quad . \tag{7.20}$$

Common terminology is quite imprecise, since the term fluctuation can mean a variable $\delta\mathcal{A}$, or a quadratic variable $\delta\mathcal{A}\delta\mathcal{B}$, or its mean value as written above. Normally the meaning is clear from the context. The result to be shown here is that $\langle\delta\mathcal{A}\delta\mathcal{B}\rangle$ is of $RO(N^{-1})$, meaning it is of order $N^{-1}\langle\mathcal{A}\rangle\langle\mathcal{B}\rangle$. This is the result which ultimately leads to the conclusion that operator mean values, obtained by averaging with different distributions, differ only in $RO(N^{-1})$, as described in Sec. 6.

Let us denote by $\mathcal{N}$ the number operator in a quantum many-particle system. In the microcanonical distribution, denoted $MC$, the energy is fixed at $\mathcal{H} = U$, and the particle number is fixed at $\mathcal{N} = N$. This means that all fluctuations involving $\mathcal{H}$ or $\mathcal{N}$ vanish in the microcanonical distri-

bution:

$$\left\langle \delta\mathcal{N}^2 \right\rangle_{MC} = \langle \delta\mathcal{N}\delta\mathcal{H} \rangle_{MC} = \left\langle \delta\mathcal{H}^2 \right\rangle_{MC} = 0 \quad . \tag{7.21}$$

Notice $\mathcal{N}$ and $\mathcal{H}$ commute, so the ordering in $\delta\mathcal{N}\delta\mathcal{H}$ makes no difference. For operators $\mathcal{A}$ and $\mathcal{B}$ which do not commute, the symmetric average $\frac{1}{2}\langle \delta\mathcal{A}\delta\mathcal{B} + \delta\mathcal{B}\delta\mathcal{A} \rangle$ is usually taken to define the quadratic fluctuation.

In the canonical distribution, denoted $C$, $\mathcal{H}$ fluctuates about its mean value $\langle \mathcal{H} \rangle = U$, and $\mathcal{N}$ is fixed at $N$. Hence any fluctuation involving $\mathcal{N}$ vanishes in the canonical distribution:

$$\left\langle \delta\mathcal{N}^2 \right\rangle_{C} = \langle \delta\mathcal{N}\delta\mathcal{H} \rangle_{C} = 0 \quad . \tag{7.22}$$

The fluctuation of $\mathcal{H}$ is $\delta\mathcal{H} = \mathcal{H} - \langle \mathcal{H} \rangle$, and from the canonical partition function $Z_C = Tre^{-\beta\mathcal{H}}$ one finds $\langle \delta\mathcal{H}^2 \rangle_C = \partial^2 \ln Z_C / \partial\beta^2$. Then since $\ln Z_C = -\beta F$, the fluctuation may be written (see problem 7.2)

$$\left\langle \delta\mathcal{H}^2 \right\rangle_{C} = kT^2 C_V \quad . \tag{7.23}$$

Now the total Hamiltonian is of order $N$, hence both $\langle \mathcal{H} \rangle$ and $C_V$ are of order $N$, so the last equation tells us $\langle \delta\mathcal{H}^2 \rangle_C$ is of order $N^{-1}\langle \mathcal{H} \rangle^2$, or is of $RO(N^{-1})$.

In the grand canonical distribution, denoted $GC$, $\mathcal{H}$ fluctuates about $\langle \mathcal{H} \rangle = U$, and $\mathcal{N}$ fluctuates about $\langle \mathcal{N} \rangle = N$. Each mean-value constraint requires one Lagrange multiplier, and the grand canonical partition function becomes

$$Z_{GC} = Tre^{-\beta\mathcal{H}} e^{\beta\mu\mathcal{N}} \quad . \tag{7.24}$$

Again $\beta$ is $1/kT$, and $\mu$ is the chemical potential, the same in a one-component system as the Gibbs free energy per particle. The thermodynamic significance of the grand canonical partition function is shown by

$$PV = kT \ln Z_{GC} \quad . \tag{7.25}$$

Useful thermodynamic relations are (see problem 7.3)

$$V \frac{\partial P}{\partial U}\Big)_{N,V} = \gamma \quad , \tag{7.26}$$

$$V \frac{\partial P}{\partial N}\Big)_{U,V} = \frac{VB_T - \gamma(U + PV - \alpha TVB_T)}{N} \quad . \tag{7.27}$$

Notice the first equation is the same as the canonical expression for $\gamma$ in Eq. (7.16). Finally, the fluctuations are calculated in a manner similar to the derivation of Eq. (7.23) for $\langle \delta \mathcal{H}^2 \rangle_C$, and the results are (see problem 7.3)

$$\langle \delta \mathcal{N}^2 \rangle_{GC} = \frac{N^2 kT}{VB_T} \quad , \tag{7.28}$$

$$\langle \delta \mathcal{N} \delta \mathcal{H} \rangle_{GC} = \frac{NkT}{VB_T}(U + PV - \alpha TVB_T) \quad , \tag{7.29}$$

$$\langle \delta \mathcal{H}^2 \rangle_{GC} = kT^2 C_V + \frac{kT}{VB_T}(U + PV - \alpha TVB_T)^2 \quad . \tag{7.30}$$

In these three equations, all terms on the right are of order $N$, so that once again each quadratic fluctuation is of $RO(N^{-1})$.

In all the above fluctuation formulas, when results are compared for microcanonical, canonical, and grand canonical distributions, and ignoring the cases where zero is compared with zero, it is seen that a given mean fluctuation differs in $RO(1)$ in different distributions. Therefore, when a mean fluctuation is written, it is necessary to specify the distribution in which it is evaluated.

### *Trace Formulation and Particle Exchange Symmetry*

The canonical partition function is expressed in Eq. (7.7) in terms of the energy levels $E_n$, and since $E_n$ are the eigenvalues of $\mathcal{H}$, according to the Schrödinger equation (7.1), then the partition function can be written in terms of $\mathcal{H}$,

$$Z = \sum_n \langle \psi_n | e^{-\beta \mathcal{H}} | \psi_n \rangle = Tr e^{-\beta \mathcal{H}} \quad . \tag{7.31}$$

By operating with $\mathcal{H}$, the sum yields Eq. (7.7) for $Z$. But the sum is over a complete orthonormal set, hence the sum constitutes a trace, as indicated. In a similar way, the average of $\mathcal{A}$ expressed in Eq. (7.3) can be written

$$\langle \mathcal{A} \rangle = \frac{1}{Z} Tr \mathcal{A} e^{-\beta \mathcal{H}} \quad . \tag{7.32}$$

The useful relation $Tr \mathcal{A} e^{-\beta \mathcal{H}} = Tr e^{-\beta \mathcal{H}} \mathcal{A}$ is easily verified.

An important property of a quantum many-particle system is that the wavefunctions must satisfy particle exchange symmetries. Specifically, every wavefunction must be symmetric under the exchange of two identical bosons, and antisymmetric under the exchange of two identical fermions. These symmetries are supposedly built into the wavefunctions $\psi_n$. This means the same symmetry restrictions apply to any basis in which the trace may be evaluated. For suppose a linear transformation is made from the set $\psi_n$ to another complete orthonormal set $\phi_\alpha$, and the traces are then expressed in the forms

$$Z = \sum_\alpha \langle \phi_\alpha | e^{-\beta \mathcal{H}} | \phi_\alpha \rangle \quad , \quad \mathcal{A} = \frac{1}{Z} \sum_\alpha \langle \phi_\alpha | \mathcal{A} e^{-\beta \mathcal{H}} | \phi_\alpha \rangle \quad . \tag{7.33}$$

Since the $\phi_\alpha$ form a basis for the $\psi_n$, then each $\phi_\alpha$ must have the same particle exchange symmetries that are contained in the $\psi_n$. The general statement is that the traces in statistical mechanics have to be evaluated in a complete orthonormal set of appropriately symmetrized functions.

In condensed matter systems, exchange symmetries apply separately to the nuclei, and to the electrons, never to "atoms". Generally speaking, the importance of exchange decreases as the particle mass increases, as the interparticle separation increases, and as the temperature increases. In most solids and liquids the nuclei never approach one another very closely; this characteristic is apparent in the several graphs of pair correlation functions shown in Chap. 5. Because of this large internuclear separation, nuclear exchange effects are utterly negligible in most condensed matter systems. An exception is liquid helium, for which the nuclear exchange symmetry gives rise to superfluid behavior. On the other hand, because of their small mass, exchange symmetrization is of crucial importance for electrons in condensed matter systems.

### *Quantum Particle Statistics*

Real quantum particles, such as the electrons in a metal, are conserved in number. On the other hand, quantum *excitations*, such as the nuclear vibrational normal modes in a crystal, the phonons, are not conserved in number. But excitations are also called particles, and in calculating the energy levels of a system of quantum particles, conserved or not conserved, the only difference is the presence of a constraint in the case of conserved particles, requiring their total number to be fixed. The practical way to

enforce this constraint is to first extend the distribution to cover all possible particle numbers, weighted by means of a Lagrange multiplier, then determine the multiplier so that the mean number of particles is the correct number or particles. The corresponding distribution is the grand canonical distribution. The procedure is standard, and we shall provide merely an outline, sufficient for obtaining the results needed in this monograph. For further details see *e.g.* Reif (1965, Chap. 9), or McQuarrie (1985, Chaps. 3 and 4).

Consider a system of noninteracting particles in a box of volume $V$. The particles occupy single-particle states labeled $\lambda$, $\lambda = 1, 2, \cdots$, and each state has energy $E_\lambda(V)$. The number of particles in state $\lambda$ is $f_\lambda = 0, 1$ for fermions, and $f_\lambda = 0, 1, 2, \cdots$ for bosons. The total number of particles is $\Sigma_\lambda f_\lambda$, the total system energy levels are $\Sigma_\lambda f_\lambda E_\lambda$, hence the grand partition function is the product $\Pi_\lambda Z_\lambda$, where

$$Z_\lambda(V, \beta, \beta\mu) = \sum_{f_\lambda} e^{-\beta f_\lambda E_\lambda} e^{\beta\mu f_\lambda} \quad . \tag{7.34}$$

Here $\beta$ and $\beta\mu$ are Lagrange multipliers, and the eventual comparison of statistical mechanics with thermodynamics will tell us

$$\beta = \frac{1}{kT} \quad , \quad N\mu = G \quad , \tag{7.35}$$

where $G$ is the Gibbs free energy,

$$G = U - TS + PV \quad . \tag{7.36}$$

The identification $N\mu = G$ means that $\mu$ is the chemical potential. The mean number of particles in state $\lambda$ is $\bar{f}_\lambda = \langle f_\lambda \rangle$,

$$\bar{f}_\lambda = \frac{\partial \ln Z}{\partial \beta\mu}\Big)_{V,\beta} = \frac{1}{e^{\beta(E_\lambda - \mu)} \pm 1} \quad , \tag{7.37}$$

where the upper (lower) sign is for fermions (bosons). The mean number of particles in total is $N$, the mean total energy is $U$, and these quantities are obviously given by

$$N = \sum_\lambda \bar{f}_\lambda \quad , \tag{7.38}$$

$$U = \sum_\lambda \bar{f}_\lambda E_\lambda \quad . \tag{7.39}$$

When the theory is to be applied to a system with specified $N$, or with specified particle density $N/V$, Eq. (7.38) has to be solved for the corresponding value of $\beta\mu$.

With the grand canonical distribution, one has $PV = kT \ln \Pi_\lambda Z_\lambda$, or

$$PV = \pm kT \sum_\lambda \ln \left(1 \pm e^{-\beta(E_\lambda - \mu)}\right) \quad . \tag{7.40}$$

Now Eq. (7.36) can be solved for the entropy, and with $G = N\mu$, and the above equations for $N$, $U$, and $PV$, the entropy is expressed as follows. For fermions:

$$S = -k \sum_\lambda \left[\bar{f}_\lambda \ln \bar{f}_\lambda + (1 - \bar{f}_\lambda) \ln(1 - \bar{f}_\lambda)\right] \quad . \tag{7.41}$$

Here every term is positive, since $0 < \bar{f}_\lambda < 1$. For bosons:

$$S = k \sum_\lambda \left[(\bar{f}_\lambda + 1) \ln(\bar{f}_\lambda + 1) - \bar{f}_\lambda \ln \bar{f}_\lambda\right] \quad . \tag{7.42}$$

Here the contribution for every $\lambda$ is positive, since $\bar{f}_\lambda > 0$. All thermodynamic functions can be derived from the preceding results. The Helmholtz free energy is $F = G - PV$, or

$$F = \mu N \mp kT \sum_\lambda \ln \left(1 \pm e^{-\beta(E_\lambda - \mu)}\right) \quad . \tag{7.43}$$

Notice at the beginning, in the partition function (7.34), if we set $\mu = 0$, then $Z_\lambda(V, \beta)$ is the canonical partition function for nonconserved quantum particles. Hence all the above results apply to nonconserved quantum particles, by setting $\mu = 0$.

### *Excitation of Reference Structure Electrons*

The Hamiltonian for the excited states of reference structure electrons was derived in Sec. 4, and is written in Eq. (4.15). Here we shall adopt a more streamlined notation: for a set of $\mathcal{Z}$ independent electrons, the excitation Hamiltonian is $\mathcal{H}_{el}$,

$$\mathcal{H}_{el} = \sum_\lambda \epsilon_\lambda (C_\lambda^+ C_\lambda - g_\lambda) \quad , \tag{7.44}$$

where

$$\mathcal{Z} = \sum_\lambda C_\lambda^+ C_\lambda \quad . \tag{7.45}$$

Here $\lambda$ labels a one-electron state whose energy is $\epsilon_\lambda$, $\Sigma_\lambda$ is over all such states, and as usual $\Sigma_\lambda$ is understood to include two degenerate spin states for each $\lambda$. $C_\lambda^+$ and $C_\lambda$ are respectively fermion creation and annihilation operators. The eigenvalues of $C_\lambda^+ C_\lambda$ are $f_\lambda = 0, 1$, so that the system energy levels are $\Sigma_\lambda \epsilon_\lambda (f_\lambda - g_\lambda)$, and the total number of electrons is $\Sigma_\lambda f_\lambda$. In any metallic system, solid or liquid, element or alloy, $\mathcal{H}_{el}$ is independent of the rest of the system Hamiltonian, so that the corresponding statistical mechanics can be done independently of other statistical mechanics contributions. The free energy for this set of conserved fermions is therefore given by Eq. (7.43), plus the groundstate correction $-\Sigma_\lambda \epsilon_\lambda g_\lambda$ contained in Eq. (7.44).

In practice, the spectrum of one-electron energies $\epsilon_\lambda$, as determined for example from a density functional calculation, is expressed through the density of one-electron energy levels $n(\epsilon)$, also called the *density of states*. A sum $\Sigma_\lambda$ transforms to an integral $\int d\epsilon$, according to the formula for any function $G_\lambda = G(\epsilon_\lambda)$,

$$\sum_\lambda G_\lambda = \int n(\epsilon) G(\epsilon) d\epsilon \quad . \tag{7.46}$$

Then with the Fermi distribution denoted $\bar{f}(\epsilon)$,

$$\bar{f}(\epsilon) = \frac{1}{e^{\beta(\epsilon-\mu)} + 1} \quad , \tag{7.47}$$

the equation for $\mathcal{Z}$, which determines $\mu$, is

$$\mathcal{Z} = \int n(\epsilon) \bar{f}(\epsilon) d\epsilon \quad . \tag{7.48}$$

From previous equations, the primary thermodynamic functions can be written as follows:

$$F_{el} = \mu \mathcal{Z} - \int \epsilon n(\epsilon) g(\epsilon) d\epsilon - kT \int n(\epsilon) \ln \left(1 + e^{-\beta(\epsilon-\mu)}\right) d\epsilon \quad , \tag{7.49}$$

$$P_{el} = -\left(\partial F_{el} / \partial V\right)_T \quad , \tag{7.50}$$

$$U_{el} = \int \epsilon n(\epsilon) \left[\bar{f}(\epsilon) - g(\epsilon)\right] d\epsilon \quad , \tag{7.51}$$

$$S_{el} = -k \int n(\epsilon) \left[\bar{f} \ln \bar{f} + (1 - \bar{f}) \ln(1 - \bar{f})\right] d\epsilon \quad , \tag{7.52}$$

where in the last equation $\bar{f}$ stands for $\bar{f}(\epsilon)$. All these thermodynamic functions vanish at $T = 0$, as they must because they express only thermal excitations. While we shall apply this formulation only to metals, it is valid also for nonmetals.

The chemical potential at $T = 0$ is denoted $\mu_0$, and this is also the Fermi energy $\epsilon_F$. The nature of electronic excitations is controlled by the one-electron states in the vicinity of $\mu_0$, specifically those states within a few $kT$ of $\mu_0$. For metals, the Fermi energy lies in a near-continuum of electronic states, hence there are thermal excitations of electrons at arbitrarily low temperatures. The Sommerfeld expansion is the low temperature expansion of electronic excitation properties for metals, and is quite useful since the leading term is always accurate to tens of Kelvin, and is often accurate to thousands of Kelvin. If we set the zero of energy so that the lowest $\epsilon_\lambda$ is zero, then the prototypic expansion is (see *e.g.* Wilson, 1954, App. A4; also *Thermodynamics of Crystals*, p. 283–285)

$$\int_0^\infty n(\epsilon)\bar{f}(\epsilon)G(\epsilon)d\epsilon = \int_0^{\mu_0} n(\epsilon)G(\epsilon)d\epsilon + \frac{\pi^2}{6}(kT)^2 n(\mu_0) \left.\frac{dG(\epsilon)}{d\epsilon}\right|_{\mu_0} + \cdots \quad , \tag{7.53}$$

where $+\cdots$ represents terms of order $(kT)^4$ and higher. The leading low temperature term in the excitation free energy, Eq. (7.49), is then (see problem 7.5)

$$F_{el} = -\frac{\pi^2}{6}(kT)^2 n(\mu_0) \quad . \tag{7.54}$$

The corresponding entropy and internal energy are

$$S_{el} = \frac{\pi^2}{3} k^2 T n(\mu_0) \quad , \tag{7.55}$$

$$U_{el} = \frac{\pi^2}{6}(kT)^2 n(\mu_0) \quad . \tag{7.56}$$

Because $S_{el}$ is linear in $T$, the electronic specific heat $C_{el}$ satisfies $C_{el} = S_{el}$. Ultimately, as we shall see in Sec. 18, electron-phonon interactions will modify the coefficients, but not the leading temperature dependences, of the low-temperature electronic excitation properties.

The Sommerfeld expansion is developed from a Taylor series for $n(\epsilon)$ about $\epsilon_F$. However, in density functional calculations, $n(\epsilon)$ is commonly found to have significant variations over small ranges of $\epsilon$, *i.e.* $n(\epsilon)$ has fluctuations. For this reason we generally use only the leading term of the Sommerfeld expansion, and when temperature is sufficiently high that this leading term becomes inaccurate, we then use the complete integral formulation written in Eqs. (7.49)–(7.52).

### *Perturbation Expansion of the Free Energy*

Here we shall derive a useful perturbation expansion of the free energy of a many-particle system. The perturbation is defined through a small parameter, and the Hamiltonian is expanded in powers of that parameter, as

$$\mathcal{H} = \mathcal{H}^{(0)} + \mathcal{H}^{(1)} + \mathcal{H}^{(2)} + \cdots \quad . \tag{7.57}$$

Ordinary perturbation theory is used to find the energy levels to second order, giving

$$E_n = E_n^{(0)} + E_n^{(1)} + E_n^{(2)} \quad . \tag{7.58}$$

With this, the canonical partition function (7.7) is expanded to second order, then the Helmholtz free energy (7.15) is expanded to second order, and the result is (see problem 7.6)

$$F = F^{(0)} + \langle E^{(1)} \rangle + \left[ \langle E^{(2)} \rangle - \frac{1}{2} \beta \langle (\delta E^{(1)})^2 \rangle \right] \quad , \tag{7.59}$$

where

$$F^{(0)} = -kT \ln Z^{(0)} = -kT \ln \sum_n e^{-\beta E_n^{(0)}} \quad ; \tag{7.60}$$

$$\langle E^{(\nu)} \rangle = \frac{\Sigma_n E_n^{(\nu)} e^{-\beta E_n^{(0)}}}{Z^{(0)}}, \quad \text{for} \quad \nu = 1, 2 \quad ; \tag{7.61}$$

$$\langle(\delta E^{(1)})^2\rangle = \left\langle [E^{(1)} - \langle E^{(1)}\rangle]^2 \right\rangle \quad . \tag{7.62}$$

Notice that the mean fluctuation $\langle(\delta E^{(1)})^2\rangle$, being of $RO(N^{-1})$, is of order $N$, so that every perturbation term on the right of (7.59) is of order $N$, as it must be so that $F$ is of order $N$. Hence the perturbation expansion of $F$ is a cumulant expansion. Notice also that by working with the energy levels (7.58), one avoids the commutation algebra associated with expansion of the operator $e^{-\beta\mathcal{H}}$.

The nuclear motion free energy is the total free energy for insulators, and remains the dominant contribution for metals. For crystals, the leading term of this free energy represents independent phonons, and the perturbation expansion in powers of phonon-phonon interactions is discussed in Sec. 17. Electron-phonon interactions are also treated in perturbation theory, in Sec. 18. In both these problems of many-particle interactions, the Hamiltonian $\mathcal{H}^{(1)}$ has no diagonal elements, so that $\langle E^{(1)}\rangle$ vanishes, and the leading free energy contribution arising from the perturbation is of second order, according to Eq. (7.59). Further, both theories are *extremely* complicated beyond second order, and both are examples of our general conclusion regarding such theories: In any practical calculation where terms higher than second order are important in the free energy, one is well advised not to proceed to higher-order perturbation theory, but rather to search for a more accurate zeroth-order description, or else a nonpertubative numerical calculation.

*Problems*

*7.1* In Eq. (7.16), given the first equality as the definition of $\gamma$, derive the second equality by ordinary thermodynamics manipulations. Derive the two equalities in Eq. (7.17).

*7.2* Follow the outline preceding Eq. (7.23) to derive that expression for $\langle\delta\mathcal{H}^2\rangle_C$.

*7.3* Derive the Eqs. (7.26) and (7.27). Notice you can derive them with the grand canonical distribution, *or* you can derive them from canonical thermodynamic relations, such as (7.16). Then verify the grand canonical fluctuation formulas (7.28) – (7.30).

*7.4* For a system of independent fermions or bosons, equations one should derive if one hasn't previously done so, are (7.37) for $\bar{f}_\lambda$, and (7.41)

and (7.42) for the entropy.

*7.5* From Eq. (7.49) for $F_{el}$, use the Sommerfeld expansion (7.53) to derive the leading low temperature expression (7.54) for $F_{el}$ (not a trivial calculation). From Eq. (7.54), it *is* trivial to verify the following equations for $S_{el}$ and $U_{el}$.

*7.6* Derive Eq. (7.59) for the perturbation expansion of $F$. Work out the corresponding expansions of $S$ and $U$. Demonstrate the result for $U$ is consistent with $U = \langle \mathcal{H} \rangle$.

## 8 THERMOELASTICITY

### *Thermoelastic State Functions*

For completeness of the present monograph, thermoelasticity will be presented in outline form. A more extensive account of the historical development, and of the analysis of laboratory experiments, can be found in D. C. Wallace (1967, 1970). We consider a continuous homogeneous material whose equilibrium states depend only on the configuration, denoted by $\mathbf{x}$, and the temperature $T$ or the entropy $S$. The material can be a liquid, an isotropic solid, or a solid with any prescribed crystalline symmetry. When $T$ is an independent variable, the convenient state function is the Helmholtz free energy $F(\mathbf{x}, T)$, and dependent variables include the stresses and entropy. When $S$ is an independent variable, the convenient state function is the internal energy $U(\mathbf{x}, S)$, and dependent variables include the stresses and temperature. Even though it is customary in elasticity to work with energy and entropy per unit mass, because mass is conserved during elastic stains, while volume is generally not conserved, we shall nevertheless continue to write extensive functions for a system of $N$ atoms in a volume $V$, to maintain consistent usage throughout this work. In a partial derivative with respect to a given strain component, it is understood that all other strain components are held fixed.

We begin with a system in an initial equilibrium state, having configuration $\mathbf{X}$ in the presence of an applied stress. The applied stress is constant over the system surface, is therefore constant throughout the material, and surface effects are considered negligible. It is not necessary for the initial state to be obtained by elastic deformation from a state of zero stress. The theory can describe, for example, a crystal under pressure, which has undergone a phase transition during the application of the pressure. Now

from the initial configuration $\mathbf{X}$, the system undergoes a finite strain to a final configuration $\mathbf{x}$. If the final configuration is obtained by applying a small additional constant stress to the system, then the strain from $\mathbf{X}$ to $\mathbf{x}$ is homogeneous, *i.e.* constant throughout the material. If the final configuration corresponds to a wave (or several waves) propagating in the material, the strain from $\mathbf{X}$ to $\mathbf{x}$ is nonuniform in space and in the time $t$, and the equations derived below are local in $\mathbf{X}$ and $t$.

Let us extend the meaning of our notation: The position of a given material particle in the initial configuration is $\mathbf{X}$, and in the final configuration is $\mathbf{x}$. The deformation from $\mathbf{X}$ to $\mathbf{x}$ is specified by either of two sets of nine independent deformation parameters. The transformation coefficients $\alpha_{ij}$ are

$$\alpha_{ij} = \partial x_i / \partial X_j \quad , \quad \text{where} \quad x_i = x_i(\mathbf{X}, t) \quad . \tag{8.1}$$

The displacement gradients $u_{ij}$ are

$$u_{ij} = \partial u_i / \partial X_j \quad , \text{where} \quad x_i - X_i = u_i(\mathbf{X}, t) \quad . \tag{8.2}$$

The indices $i, j$ represent Cartesian coordinates, and each goes over three values. The two sets of deformation parameters are related by

$$\alpha_{ij} = \delta_{ij} + u_{ij} \quad . \tag{8.3}$$

The symmetric finite-strain parameters of Murnaghan (1951), also called Lagrangian strains, are

$$\eta_{ij} = \frac{1}{2} \sum_k \alpha_{ki} \alpha_{kj} - \delta_{ij} = \frac{1}{2} \left( u_{ij} + u_{ji} + \sum_k u_{ki} u_{kj} \right) \quad . \tag{8.4}$$

We treat the $\eta_{ij}$ as nine independent variables, but always make sure the calculations are consistent with $\eta_{ij} = \eta_{ji}$. If two material particles are separated by the vector $\Delta\mathbf{X}$ in the initial configuration, and $\Delta\mathbf{x}$ in the final configuration, and if $\eta_{ij}$ are constant over the region of $\Delta\mathbf{X}$, then

$$|\Delta\mathbf{x}|^2 - |\Delta\mathbf{X}|^2 = 2 \sum_{ij} \eta_{ij} \Delta X_i \Delta X_j \quad . \tag{8.5}$$

This is the important property of the Lagrangian strains, that the distances between all pairs of material particles, and hence the relative positions of all material particles, are completely specified by the initial configuration $\mathbf{X}$ and the $\eta_{ij}$, for constant $\eta_{ij}$.

Concerning the configuration, the state functions can depend only on the relative positions of all the material particles. Specifically, this requirement applies over distances of the order of the range of interactions within the material, and if the $\eta_{ij}$ are essentially constant over such distances, then $U$ and $F$ can depend on $\mathbf{x}$ only through $\mathbf{X}$ and the $\eta_{ij}$:

$$U(\mathbf{x}, S) = U(\mathbf{X}, \eta_{ij}, S) \quad , \quad F(\mathbf{x}, T) = F(\mathbf{X}, \eta_{ij}, T) \quad . \tag{8.6}$$

This dependence is necessary and sufficient to insure rotational invariance of $U$ and $F$, for any initial configuration $\mathbf{X}$. These relations are valid only when the strain is essentially constant over the range of interactions within the material. For wave propagation, for example, the wavelength must be long compared to the range of interactions. If the wavelength is noticeably shorter, dispersion occurs, and the atomic nature of the material has to be taken into account, as we shall do later in the theories of lattice dynamics and liquid dynamics. Because thermoelasticity treats only very long wavelength strains, it sees no formal difference between an isotropic polycrystalline solid, and an isotropic atomically-random solid, though these two isotropic solids have significantly different atomic vibrational properties.

### *Stresses and Elastic Constants*

Let us first consider the initial equilibrium state at configuration $\mathbf{X}$. For a continuous material, the mechanical equilibrium condition is that the net linear force, and the net torque, on each mass element must vanish. This requires that the Cauchy stress tensor, whose components are $\tau_{ij}$, be constant throughout the material, and be symmetric. The combined first and second laws of thermodynamics is $dU = TdS - đW$, where $đW$ is the work done by the material against the applied stress, in changing the configuration from $\mathbf{X}$ to $\mathbf{X} + d\mathbf{X}$. This is the strict analog to $đW = PdV$ for the usual pressure-volume variables. Evaluation of $đW$ for stress-strain variables leads to (see *e.g. Thermodynamics of Crystals*, p. 16–17)

$$dU = TdS + V \sum_{ij} \tau_{ij} d\eta_{ij} \quad . \tag{8.7}$$

Since $F = U - TS$, the differential of $F$ is

$$dF = -SdT + V \sum_{ij} \tau_{ij} d\eta_{ij} \quad . \tag{8.8}$$

Expressions for the dependent variables follow directly from these equations. For the internal energy,

$$\tau_{ij} = V^{-1}(\partial U/\partial \eta_{ij})_S \quad , \quad T = (\partial U/\partial S)_\eta \quad , \tag{8.9}$$

and for the Helmholtz free energy,

$$\tau_{ij} = V^{-1}(\partial F/\partial \eta_{ij})_T \quad , \quad S = -(\partial F/\partial T)_\eta \quad . \tag{8.10}$$

These equations for stresses, temperature, and entropy are the thermoelastic generalization of the usual thermodynamic equations for pressure, temperature, and entropy, as given for example in Eqs. (7.12) and (7.14). Notice that $T$ and $S$ are now given by derivatives of $U$ and $F$, respectively, at *constant configuration*, denoted constant $\eta$, and not merely at constant volume. The difference in sign in the equations for $\tau_{ij}$, and the equations for $P$, is due to a sign convention: A positive stress is exerted outward on a material mass element, while a positive pressure is exerted inward.

Let us now consider the final state as one of equilibrium at the configuration $\mathbf{x}$. In view of the functional dependence of the state functions, given by Eq. (8.6), and since the strains from $\mathbf{X}$ to $\mathbf{x}$ are small but not infinitesimal, the state functions may be expanded as

$$U(\mathbf{X}, \eta_{ij}, S) = U(\mathbf{X}, S) + V \sum_{ij} \tau_{ij}\eta_{ij} + \frac{1}{2} V \sum_{ijkl} C^S_{ijkl}\eta_{ij}\eta_{kl} + \cdots \quad , \tag{8.11}$$

$$F(\mathbf{X}, \eta_{ij}, T) = F(\mathbf{X}, T) + V \sum_{ij} \tau_{ij}\eta_{ij} + \frac{1}{2} V \sum_{ijkl} C^T_{ijkl}\eta_{ij}\eta_{kl} + \cdots \quad . \tag{8.12}$$

That the first order coefficients are the stresses, evaluated at $\mathbf{X}$, follows from the dependent-variable equations (8.9) and (8.10). The second order coefficients are defined as the second order elastic constants, evaluated at the (arbitrary) configuration $\mathbf{X}$, where the adiabatic and isothermal constants are respectively

$$C^S_{ijkl} = V^{-1}(\partial^2 U/\partial \eta_{ij}\partial \eta_{kl})_S \quad , \tag{8.13}$$

$$C^T_{ijkl} = V^{-1}(\partial^2 F/\partial \eta_{ij}\partial \eta_{kl})_T \quad . \tag{8.14}$$

Succeeding terms in the strain expansions, represented by $+\cdots$ in Eqs. (8.11) and (8.12), are of higher order in the Lagrangian strains, with higher order elastic constants as coefficients.

In view of their definitions, elastic constants of all orders have complete Voigt symmetry. Voigt symmetry means invariance under the interchange of $i$ and $j$ corresponding to a strain $\eta_{ij}$, and invariance under the interchange of $ij$ with $kl$ corresponding to strains $\eta_{ij}$ and $\eta_{kl}$. For the second order elastic constants, Voigt symmetry is

$$C_{ijkl} = C_{jikl} = C_{ijlk} = C_{klij} \quad . \tag{8.15}$$

It is convenient to use Voigt notation, in which a pair of Cartesian indices is replaced by a Voigt index $\alpha$, according to the scheme

$$\begin{array}{rcccccccc} ij & = & 11 & 22 & 33 & 32 \text{ or } 23 & 31 \text{ or } 13 & 21 \text{ or } 12 \\ \alpha & = & 1 & 2 & 3 & 4 & 5 & 6 \end{array} \tag{8.16}$$

Voigt symmetry is $C_{\alpha\beta} = C_{\beta\alpha}$, and so on for higher order elastic constants. Here and in the following, statements expressed without superscripts $S$ or $T$ are valid for either case.

### *Stress-Strain Relations*

In order to derive an equation for the variation of stress with strain, one has to evaluate $\tau_{ij}$ at two neighboring configurations, and subtract one stress tensor from the other. The calculation, for a state at arbitrary configuration $\mathbf{X}$, corresponding to an arbitrary applied stress, may be found in *Thermodynamics of Crystals* (p. 20 – 21). The result is

$$(\partial\tau_{ij}/\partial\eta_{kl})_S = B^S_{ijkl} \quad , \tag{8.17}$$

$$(\partial\tau_{ij}/\partial\eta_{kl})_T = B^T_{ijkl} \quad , \tag{8.18}$$

where the stress-strain coefficients $B^S_{ijkl}$, for adiabatic variations, are given by

$$B^S_{ijkl} = \frac{1}{2}\left(\tau_{il}\delta_{jk} + \tau_{jl}\delta_{ik} + \tau_{ik}\delta_{jl} + \tau_{jk}\delta_{il} - 2\tau_{ij}\delta_{kl}\right) + C^S_{ijkl} \quad , \tag{8.19}$$

with a corresponding equation for isothermal variations. The symbol $B_{ijkl}$ is introduced because these coefficients are complete generalizations of the

coefficients defined by Birch (1947), for the particular case of isothermal variations for a cubic crystal under isotropic pressure.

The stress-strain coefficients are generalized thermoelastic stiffnesses, and components of the inverse tensor are generalized thermoelastic compliances (generalized to the condition of applied stress in the initial state). The physical meaning of these various coefficients is both obvious and important: The stiffnesses relate variations in the stress, due to imposed variations in strain, and the compliances relate the inverse process. The stiffnesses determine the bulk modulus, and the compliances determine its inverse, the compressibility. Notice the applied stress appears explicitly in these coefficients, as for example in Eq. (8.19) for $B^S_{ijkl}$.

Since the $B_{ijkl}$ are symmetric in their first two indices, and also in their last two, as may be seen from Eqs. (8.17) and (8.18), they can be written in Voigt notation, as $B^S_{\alpha\beta}$, or $B^T_{\alpha\beta}$. In other words, all the independent $B_{ijkl}$ are contained in the set of $B_{\alpha\beta}$. However, $B_{\alpha\beta} \neq B_{\beta\alpha}$ in general. Only when the applied stress vanishes do the stress-strain coefficients reduce to the elastic constants. A mathematical point regarding inverse matrices appears in problem 8.1.

If the applied stress is isotropic pressure $P$, so that

$$\tau_{ij} = -P\delta_{ij} \quad , \tag{8.20}$$

then the stress-strain coefficients simplify to

$$B^S_{ijkl} = -P\left(\delta_{jl}\delta_{ik} + \delta_{il}\delta_{jk} - \delta_{ij}\delta_{kl}\right) + C^S_{ijkl} \quad , \tag{8.21}$$

with a corresponding equation for isothermal variations. Now the right side has complete Voigt symmetry, for arbitrary $P$, so that $B_{\alpha\beta} = B_{\beta\alpha}$. Please notice the important property that, when the tress tensor does not satisfy (8.20), then pressure is not defined. We make this point because in the literature the average diagonal element $-\frac{1}{3}\Sigma_i \tau_{ii}$ is often incorrectly called "the pressure". For when the stress is isotropic pressure, an increment $dP$ gives rise to a unique $dV$ (say at constant $T$), while with a nonisotropic stress there is no unique relation between $-\frac{1}{3}\Sigma_i d\tau_{ii}$ and $dV$ (see problem 8.2).

For a cubic crystal under isotropic pressure, there are only three independent second order elastic constants, namely $C_{11}$, $C_{12}$, and $C_{44}$ in Voigt notation, and the $B_{\alpha\beta}$ are given by

$$B_{11} = B_{22} \;=\; B_{33} \;=\; C_{11} - P \quad ,$$

$$B_{12} = B_{23} \;=\; B_{31} \;=\; \cdots \;=\; C_{12} + P \quad ,$$
$$B_{44} = B_{55} \;=\; B_{66} \;=\; C_{44} - P \quad . \tag{8.22}$$

The bulk modulus, defined in Eq. (7.16) as the volume derivative of pressure, is given by

$$B = -V \left.\frac{\partial P}{\partial V}\right) = \frac{1}{3}\left(B_{11} + 2B_{12}\right) = \frac{1}{3}\left(C_{11} + 2C_{12} + P\right) \quad . \tag{8.23}$$

These cubic-crystal relations can also be applied to an isotropic solid, or to a liquid, by including the following symmetry conditions:

$$B_{44} = \frac{1}{2}\left(B_{11} - B_{12}\right) \quad , \text{ for an isotropic solid,}$$
$$B_{44} = \frac{1}{2}\left(B_{11} - B_{12}\right) = 0 \quad , \text{ for a liquid.} \tag{8.24}$$

***Wave Propagation***

Let us now consider the propagation of small-amplitude long-wavelength thermoelastic waves. The initial configuration $\mathbf{X}$ still represents a homogeneous material in the presence of applied stress, but the strain from $\mathbf{X}$ to $\mathbf{x}$ is now explicitly dependent on time $t$ and location $\mathbf{X}$. The linear equation of motion for a stressed material was derived from a mechanical energy density by Huang (1950) and by Toupin and Bernstein (1961), and from a thermodynamic potential by Green (1962). The derivation is presented in *Thermodynamics of Crystals* (Sec. 3), and the result is

$$\rho \ddot{x}_i = \sum_{jkl} A_{ijkl}\left(\partial^2 x_k / \partial X_j \partial X_l\right) \quad , \tag{8.25}$$

where $\rho$ is the (constant) density of the initial configuration, and $A_{ijkl}$ are the propagation coefficients. For adiabatic propagation one uses

$$A^S_{ijkl} = \tau_{jl}\delta_{ik} + C^S_{ijkl} \quad , \tag{8.26}$$

and for isothermal propagation one uses

$$A^T_{ijkl} = \tau_{jl}\delta_{ik} + C^T_{ijkl} \quad . \tag{8.27}$$

The symmetry of the $A_{ijkl}$ follows from the symmetries of $\tau_{ij}$ and $C_{ijkl}$. The propagation coefficients do not have sufficient symmetry to be written in Voigt notation, unless the stress vanishes. The lack of Voigt symmetry

of the $A_{ijkl}$ led Huang (1950) to conclude that elastic constants can only be defined at zero applied stress. This untenable view has been circumvented by the development of thermoelasticity of stressed materials, where the elastic constants are defined by Eqs (8.13) and (8.14).

Solutions of the equation of motion (8.25) are planewaves. Consider the displacement

$$\mathbf{x} - \mathbf{X} = \mathbf{w} \sin(\mathbf{k} \cdot \mathbf{X} - \omega t) \quad , \tag{8.28}$$

where $\mathbf{k}$ is the wave vector, $\omega$ is the frequency, and $\mathbf{w}$ specifies the direction and magnitude of the displacement. With $\hat{\mathbf{k}}$ a unit vector in the direction of $\mathbf{k}$, and with $v$ the wave velocity,

$$\hat{\mathbf{k}} = \mathbf{k}/|\mathbf{k}| \ , \quad v = \omega/|\mathbf{k}| \quad , \tag{8.29}$$

the equation of motion is

$$\rho v^2 w_i = \sum_{jkl} A_{ijkl} \hat{k}_j \hat{k}_l w_k \quad . \tag{8.30}$$

This is an eigenvalue-eigenvector equation, which has three solutions, denoted by $s = 1, 2, 3$, for each direction of $\hat{\mathbf{k}}$. We define the real symmetric $3 \times 3$ propagation matrix $\mathbf{L}(\hat{\mathbf{k}})$ by

$$L_{ik} = \sum_{jl} A_{ijkl} \hat{k}_j \hat{k}_l \quad . \tag{8.31}$$

The eigenvalues and eigenvectors of $\mathbf{L}$ are $\rho v_s^2$ and $\mathbf{w}_s$ respectively, and the equation of motion which determines these solutions is

$$\rho v_s^2 w_{is} = \sum_k L_{ik} w_{ks} \quad . \tag{8.32}$$

The eigenvectors are chosen to be normalized, and since $\mathbf{L}$ is real symmetric, the eigenvectors are orthonormal and complete. The diagonalization of $\mathbf{L}$ is expressed by

$$\sum_{ij} w_{is} L_{ij} w_{js'} = \rho v_s^2 \delta_{ss'} \quad . \tag{8.33}$$

Notice the applied stress appears explicitly in the wave propagation coefficients, according to Eqs. (8.26) and (8.27). The $A_{ijkl}$ also appear in expansions of the state functions in powers of the displacement gradients (see problem 8.3).

Again there are simplifications when the initial stress is isotropic pressure, when Eq. (8.20) holds. From Eq. (8.31), only the symmetric combination $A_{ijkl} + A_{ilkj}$ contributes to the propagation matrix. When the stress is isotropic pressure, this combination of propagation coefficients equals the same combination of stress-strain coefficients, so that $A_{ijkl}$ can be replaced by $B_{ijkl}$ in the propagation matrix. Moreover, $B_{ijkl}$ can then be replaced with elastic constants from (8.21), to find

$$L_{ik} = \sum_{jl} C_{ijkl} \hat{k}_j \hat{k}_l - P\delta_{ik} \quad . \tag{8.34}$$

Hence, through the diagonalization (8.33), the initial applied pressure appears explicitly in the thermoelastic wave velocities of a material under pressure.

***Thermoelasticity Extension Notes***

Stability of a material requires the energies of all its long-wavelength thermoelastic waves to be positive, *i.e.* $[\omega_s(\hat{\mathbf{k}})]^2 > 0$ for all $\hat{\mathbf{k}}$ and $s$. This is the same as the requirement for stability against static homogeneous strains. That the initial applied stress appears explicitly in the stability condition, through its appearance in the propagation coefficients, was observed in *Thermodynamics of Crystals* (p. 38–41). Recently, Wang and coworkers (1993) have carried out molecular dynamics calculations for stressed crystals, to compare the stability condition from *Thermodynamics of Crystals* with the Born condition involving only elastic constants, and have verified that the applied stress actually does appear in the stability limits.

The thermoelastic waves which actually propagate in condensed matter are sound waves, and are very nearly adiabatic. Apparently, isothermal waves do not exist. The stability condition of positive energy for adiabatic waves is therefore the condition for stable sound waves in a real material. The stability condition for isothermal waves has no corresponding interpretation. Nevertheless, the isothermal stability condition does have physical significance, since as mentioned above, it is also the condition for stability against isothermal homogeneous strains.

The thermoelastic waves studied here travel without attenuation. This is a good approximation for most real crystals, and most solids and liquids in general, since the lifetime of a sound wave is generally very long compared to its vibrational period. Of course, there are always higher-order elastic

effects which cause interactions among the waves, and there are dissipative effects which cause attenuation, so that sound waves are never purely harmonic, and never perfectly adiabatic. An interesting property of liquids is that, while both of the static shear coefficients $B_{44}$ and $\frac{1}{2}(B_{11}-B_{12})$ vanish, as indicated in Eq. (8.24), shear stresses *can* be established for very short times, so that shear sound waves *will* propagate at very high frequencies.

The relation of thermoelastic waves to long wavelength acoustic phonons will be discussed in Sec. 14. Topics discussed further in *Thermodynamics of Crystals* (Secs. 2 and 3), and in Wallace (1970), include the crystal symmetry classes, thermodynamic functions in stress-strain variables, adiabatic-isothermal differences, transcription of finite initial stress effects to higher order elastic constants at zero stress, and experimental determination of third- and fourth-order elastic constants. A discussion of thermodynamics in stress-strain variables is also given by Barron and White (1999, Sec. 2.8). In order to construct the theory of dynamic deformation processes in materials, thermoelasticity is combined with continuum mechanics and irreversible thermodynamics, a theory presented for solids and liquids by D. C. Wallace (1985).

*Problems*

*8.1* The strain-stress relation is $(\partial\eta_{ij}/\partial\tau_{kl}) = S_{ijkl}$, where the $9\times 9$ matrix $[S_{ijkl}]$ is the inverse of $[B_{ijkl}]$. Show that if one writes $S_{ijkl}$ in Voigt notation, the resulting $6\times 6$ matrix is *not* the inverse of $[B_{\alpha\beta}]$. Define the matrix $[S_{\alpha\beta}]$ as the inverse of $[B_{\alpha\beta}]$, and find the relations between $S_{\alpha\beta}$ and $S_{ijkl}$.

*8.2* Consider a crystal of prescribed symmetry, say cubic, tetragonal, *etc.*, at zero stress, or in the presence of a nonzero stress consistent with the crystal symmetry. Show that there exists a continuous range of increments in $\bar{P} = -\frac{1}{3}\Sigma_i\tau_{ii}$ for which the increment in $V$ is unique, in other words show that $\partial\bar{P}/\partial V$ is not defined. Show that $\partial P/\partial V$ is unique when $\tau_{ij} = -P\delta_{ij}$.

*8.3* Expand the free energy in displacement gradients, as

$$F(\mathbf{X}, u_{ij}, T) = F(\mathbf{X}, T) + V\sum_{ij} A_{ij}u_{ij} + \frac{1}{2}V\sum_{ijkl} A^T_{ijkl}u_{ij}u_{kl} + \cdots \quad .$$

Use Eq. (8.4) to transform to $\eta_{ij}$, compare with Eq. (8.12) to find $A_{ij} = \tau_{ij}$, and to recover the relation (8.27) between $A^T_{ijkl}$ and $C^T_{ijkl}$.

## 9 CLASSICAL STATISTICS: DERIVATION

### *Partition Function for Quantum Nuclear Motion*

In this monograph, the term classical statistical mechanics will refer only to the nuclear motion. The system consists of $N$ similar nuclei in a cubical box of volume $V$, the nuclear motion is governed by the adiabatic potential $\Phi(\{\mathbf{r}_K\})$, and is constrained by periodic boundary conditions at the surface of the box. We shall denote the Hamiltonian by $\mathcal{H}$, in place of $\mathcal{H}_N$, when it is clear that only nuclear motion is considered:

$$\mathcal{H} = \mathcal{T} + \Phi \quad , \quad \mathcal{T} = -\sum_K \frac{\hbar^2 \nabla_K^2}{2M} \quad . \tag{9.1}$$

The nuclei may be either bosons or fermions, and additional degrees of freedom, such as spin, are not considered explicitly. Our objective in this section is to construct the partition function in quantum statistical mechanics, and then transform this in the appropriate high-temperature regime to the classical partition function. Our hope is to clarify the following important points.

(a) How classical statistics emerges as a high temperature limit of quantum statistics.

(b) How the normalization of the classical partition function comes about, and therefore how the entropy is determined in classical statistics.

(c) What is the contribution of particle exchange symmetry in classical statistics.

(d) What is the contribution of the interaction between electronic excitation and nuclear motion in classical statistics.

A clear understanding of these matters can only be obtained by following through the algebra of the derivation. The key steps of the derivation will therefore be presented.

Let us first develop notation. The set of nuclear positions $\{\mathbf{r}_K\}$ is ordered from $\mathbf{r}_1$ to $\mathbf{r}_N$. $\{P\mathbf{r}_K\}$ is a permutation of the ordered set. There are $N!$ permutations, including the identity, and $\Sigma_P$ is the sum over all permutations. $P$ operates on particle positions, so $Pf(\{\mathbf{r}_K\}) = f(\{P\mathbf{r}_K\})$. The set $\{\mathbf{q}\}$ is all wavevectors allowed by periodic boundary conditions, including $\mathbf{q} = 0$, and the set $\{\mathbf{q}\}$ is ordered. $\{\mathbf{q}_K\}$ is an ordered finite subset $\mathbf{q}_1, \cdots, \mathbf{q}_N$. Only distinct subsets are considered, which means only one set out of the $N!$ permutations of $\mathbf{q}_1, \cdots, \mathbf{q}_N$. In $\{\mathbf{q}_K\}$, each $\mathbf{q}$

appears $n_{\mathbf{q}}$ times, $n_{\mathbf{q}} = 0, 1, \cdots, N$, and the $n_{\mathbf{q}}$ are constrained by the condition $\Sigma_{\mathbf{q}} n_{\mathbf{q}} = N$. An unnormalized one-particle planewave is $e^{i\mathbf{q}\cdot\mathbf{r}}$. These planewaves satisfy the orthogonality and completeness relations of Eqs. (5.5) and (5.6). An unnormalized $N$-particle planewave is denoted $\phi_P$,

$$\phi_P\left(\{\mathbf{q}_K\};\ \mathbf{r}_1 \cdots \mathbf{r}_N\right) = \prod_K e^{iP\mathbf{q}_K\cdot\mathbf{r}_K} \quad . \tag{9.2}$$

A normalized symmetrized eigenfunction of the operator $\mathcal{T}$ is $\psi$,

$$\psi(\{\mathbf{q}_K\};\ \mathbf{r}_1 \cdots \mathbf{r}_N) = \frac{1}{\mathcal{D}} \sum_P (\pm 1)^P \phi_P\left(\{\mathbf{q}_K\};\ \mathbf{r}_1 \cdots \mathbf{r}_N\right) \quad , \tag{9.3}$$

where $+1$ is for bosons and $-1$ is for fermions, and $\mathcal{D}$ is the normalization factor. Two such functions are orthogonal unless they have the same set $\{\mathbf{q}_K\}$ of wavevectors, and normalization requires (see problem 9.1)

$$\mathcal{D}^2 = V^N N! \sum_{\mathbf{q}} n_{\mathbf{q}}! \tag{9.4}$$

Notice for fermions, if any two $\mathbf{q}$ vectors are the same, *i.e.* if any $n_{\mathbf{q}} > 1$, the wave function $\psi$ vanishes.

Let us write the canonical partition function as a trace in the basis of the wavefunctions $\psi$,

$$Z = \sum_{\{\mathbf{q}_K\}} \int \cdots \int \psi^* e^{-\beta\mathcal{H}} \psi \ d\mathbf{r}_1 \cdots d\mathbf{r}_N \quad , \tag{9.5}$$

where the sum is over all distinct subsets $\{\mathbf{q}_K\}$. The next step is to insert the symmetrized planewave expression (9.3) for $\psi$, and then to replace the restricted wavevector sum by a set of independent sums over all wavevectors. The result is (see problem 9.2)

$$Z = \frac{\Sigma_{PP'}(\pm 1)^{P+P'}}{V^N (N!)^2} \sum_{\mathbf{q}_1} \cdots \sum_{\mathbf{q}_N} \int \cdots \int \phi^*_{P'} e^{-\beta\mathcal{H}} \phi_P \ d\mathbf{r}_1 \cdots d\mathbf{r}_N \quad . \tag{9.6}$$

The last step is to transform sums to integrals, with the general relation $\Sigma_{\mathbf{q}} \to (V/8\pi^3) \int d\mathbf{q}$ from Eq. (5.8), and then change variables from the wavevector $\mathbf{q}$ to momentum $\mathbf{p} = \hbar\mathbf{q}$. The partition function becomes

$$Z = \frac{\Sigma_{PP'}(\pm 1)^{P+P'}}{(N!)^2 h^{3N}} \int \cdots \int \phi^*_{P'} e^{-\beta\mathcal{H}} \phi_P \ d\mathbf{p}_1 \cdots d\mathbf{p}_N \ d\mathbf{r}_1 \cdots d\mathbf{r}_N \quad . \tag{9.7}$$

Notice $h^{3N}$ in the denominator comes from the change of variables from $\mathbf{q}$ to $\mathbf{p}$. The quantum partition function is now expressed in the appropriate form to find the classical limit.

### *Expansion in Quantum Corrections*

This expansion follows the work of Kirkwood (1933), by means of a different algebraic path. The two quantum effects in (9.7) for $Z$ are (a) the noncommutation of $\mathcal{T}$ and $\Phi$ in $\mathcal{H}$, and (b) the particle exchange symmetries in the permutation sums. In the classical limit, all commutators become negligible, and all permutations except $P' = P$ give negligible contribution. The expansion to make is therefore in powers of commutators, and in powers of pair permutations. The formal expansion parameter is $\hbar$, and the result will also turn out to be a high-temperature expansion.

An expansion of $e^{-\beta\mathcal{H}}$ can be achieved from the Baker-Campbell-Hausdorf formula (see *e.g.* Sudarshan and Mukunda, 1974, pp. 204 and 220). That formula can be manipulated into the form

$$e^{a+b} = e^c e^b e^a,\ c = -\tfrac{1}{2}[b,a] - \tfrac{1}{6}[2b+a,[b,a]] + \cdots \quad . \tag{9.8}$$

The expansion we need is therefore

$$\begin{aligned} e^{-\beta\mathcal{H}} &= e^{-\beta(\mathcal{T}+\Phi)} = e^c e^{-\beta\Phi} e^{-\beta\mathcal{T}} \quad , \\ e^c &= 1 + \tfrac{1}{2}\beta^2[\mathcal{T},\Phi] + \tfrac{1}{8}\beta^4[\mathcal{T},\Phi]^2 - \tfrac{1}{6}\beta^3[2\Phi+\mathcal{T},[\mathcal{T},\Phi]] + \cdots \ . \end{aligned} \tag{9.9}$$

There are various ways to proceed. Here we shall calculate $e^{-\beta\mathcal{H}}\phi_P$, by operating to the right on $\phi_P$. Notice

$$\nabla_K \phi_P = \frac{i}{\hbar}\mathbf{p}_K \phi_P \quad , \quad e^{-\beta\mathcal{T}}\phi_P = e^{-\beta\Sigma_K \mathbf{p}_K^2/2M}\phi_P \quad . \tag{9.10}$$

It remains to calculate $e^c e^{-\beta\Phi}\phi_P$. To do this, commute $e^c$ through $e^{-\beta\Phi}$ and keep terms to order $\hbar^2\phi_P$, to order $\hbar^3\nabla_K\phi_P$, and to order $\hbar^4\nabla_K\nabla_L\phi_P$. The result is

$$e^c e^{-\beta\Phi}\phi_P = e^{-\beta\Phi}\phi_P g(\{\mathbf{p}_K\}) \quad , \tag{9.11}$$

where

$$g(\{\mathbf{p}_K\}) \quad = \quad 1 - \frac{i\hbar\beta^2}{2m}\sum_K \mathbf{p}_K\cdot\nabla_K\Phi - \frac{\hbar^2\beta^2}{4m}\sum_K \nabla_K^2\Phi$$

$$+\frac{\hbar^2\beta^3}{6m}\sum_K(\nabla_K\Phi)^2+\frac{\hbar^2\beta^3}{6m^2}\sum_{KL}\mathbf{p}_K\cdot\nabla_K\mathbf{p}_L\cdot\nabla_L\Phi$$
$$-\frac{\hbar^2\beta^4}{8m^2}\sum_{KL}(\mathbf{p}_K\cdot\nabla_K\Phi)(\mathbf{p}_L\cdot\nabla_L\Phi) \quad . \tag{9.12}$$

This equation agrees with Kirkwood's Eq. (16). At this point the partition function has the form

$$Z=\frac{\Sigma_{PP'}(\pm1)^{P+P'}}{(N!)^2h^{3N}}\int\cdots\int\phi^*_{P'}e^{-\beta\Sigma_K\mathbf{p}_K^2/2M}e^{-\beta\Phi}\phi_P g(\{\mathbf{p}_K\})\prod_{K=1}^N d\mathbf{p}_K d\mathbf{r}_K \tag{9.13}$$

Now the momentum integrals can be done, and this has the effect of replacing $g(\{\mathbf{p}_K\})$ by its canonical average $\langle g(\{\mathbf{p}_K\})\rangle$. Terms linear in $p_{Kx}$ average to zero, terms in $p_{Kx}p_{Ly}$ average to zero, and the only surviving terms contain

$$\langle p_{Lx}p_{Kx}\rangle = MkT\delta_{KL} \quad . \tag{9.14}$$

Let us first evaluate the permutations having $P'=P$. There are $N!$ such permutations, and the contribution to $Z$ becomes

$$\frac{1}{N!h^{3N}}\int\cdots\int e^{-\beta\mathcal{H}}\left\{1-\frac{\hbar^2\beta^2}{12M}\sum_K\left[\nabla_K^2\Phi-\frac{\beta}{2}(\nabla_K\Phi)^2\right]+\cdots\right\}$$
$$\times\prod_K d\mathbf{p}_K d\mathbf{r}_K \quad , \tag{9.15}$$

where $\mathcal{H}$ is the classical Hamiltonian *function*, given by

$$\mathcal{H}=\sum_K\frac{\mathbf{p}_K^2}{2M}+\Phi(\{\mathbf{r}_K\}) \quad . \tag{9.16}$$

In the end, it will turn out that both terms in the $\Sigma_K$ in (9.15) have the same $\beta$ dependence.

Next there is a series in pair permutations, another series in three-particle permutations, and so on. The leading term at small $\beta$ is from pair permutations. Let us set $P=P'+P_{KL}$, where $P_{KL}$ interchanges $\mathbf{r}_K$ and $\mathbf{r}_L$. The $\Sigma_P$ reduces to $\Sigma'_{KL}$, where the prime means to omit the term $K=L$, and the $\Sigma_{P'}$ gives a factor $N!$. Also, the leading term in the expansion of $e^{-\beta\mathcal{H}}$, Eq. (9.9), is just $e^c=1$. To this order the pair

permutation contribution to $Z$ is

$$\frac{\pm 1}{N!h^{3N}} \sum_{KL}{}' \int \cdots \int e^{-\beta \mathcal{H}} \phi^* P_{KL} \phi \prod_K d\mathbf{p}_K d\mathbf{r}_K \quad . \tag{9.17}$$

Notice both $P_{KL}$ and $P_{LK}$ are counted in the sum. Again the momentum integrals can be evaluated, and the last expression is transformed to

$$\frac{\pm 1}{N!h^{3N}} \int \cdots \int e^{-\beta \mathcal{H}} \sum_{KL}{}' e^{-M r_{KL}^2/\beta\hbar^2} \prod_K d\mathbf{p}_K d\mathbf{r}_K \quad , \tag{9.18}$$

where $r_{KL} = |\mathbf{r}_K - \mathbf{r}_L|$.

Let us collect the leading quantum corrections from (9.15) and (9.18) into the function $f(\{\mathbf{r}_K\})$, and write

$$Z = \frac{1}{N!h^{3N}} \int \cdots \int e^{-\beta \mathcal{H}} \left[1 + f(\{\mathbf{r}_K\})\right] \prod_K d\mathbf{p}_K d\mathbf{r}_K \quad , \tag{9.19}$$

where

$$f(\{\mathbf{r}_K\}) = -\frac{\hbar^2 \beta^2}{12M} \sum_K \left[\nabla_K^2 \Phi - \frac{\beta}{2} \left(\nabla_K \Phi\right)^2\right] \pm \sum_{KL}{}' e^{-M r_{KL}^2/\beta\hbar^2} \quad . \tag{9.20}$$

These results agree with Kirkwood's Eq. (21), where Kirkwood also keeps the first commutator correction within the pair permutation contribution. Kirkwood does not have the $N!$ normalization constant appearing in Eq. (9.19), presumably because he considered each nucleus to move in a single local region. In (9.19), the $N!$ cancels the complete set of particle permutations which are present in the $N$ spatial integrals over the box. This $N!$ is common in liquid theory (see *e.g.* Hansen and McDonald, 1986). On the other hand, in classical lattice dynamics, each nucleus can be located permanently in the vicinity of its own lattice site, and the $N!$ can be removed from Eq. (9.19).

### *Nuclear Motion Free Energy*

The classical partition function $Z^{cl}$ is the leading term of Eq. (9.19),

$$Z^{cl} = \frac{1}{N!h^{3N}} \int \cdots \int e^{-\beta \mathcal{H}} \prod_K d\mathbf{p}_K d\mathbf{r}_K \quad , \tag{9.21}$$

and the corresponding free energy is

$$F^{cl} = -kT \ln Z^{cl} \quad . \tag{9.22}$$

These equations constitute the foundation of classical statistical mechanics. The expression for $Z^{cl}$ could have been derived much more simply by merely setting $[\mathcal{T}, \Phi] = 0$, and by neglecting the particle exchange symmetries in the wave functions. However, that procedure would not give us the quantum corrections. In Eq. (9.21), the normalization factor $h^{3N}$ appears when changing from $N$ integrals over wavevectors, where those integrals express the trace in quantum mechanics, to $N$ integrals over classical momenta. The ultimate source of this $h^{3N}$ factor is the de Broglie relation $\mathbf{p} = \hbar\mathbf{q}$. The normalization of (9.21) correctly determines the entropy in classical statistics. We used this normalization in advance of deriving it, to construct the classical microcanonical partition function in Eq. (6.5).

Let us next consider the leading quantum corrections. Notice that

$$\int \cdots \int \nabla_K^2 e^{-\beta\Phi} d\mathbf{r}_1 \cdots d\mathbf{r}_N = 0 \quad , \tag{9.23}$$

since the volume integral becomes a surface integral by Green's theorem, and the surface integral vanishes because of the periodic boundary condition. This allows us to combine the two terms in gradients of $\Phi$, in Eq. (9.20), to write

$$f(\{\mathbf{r}_K\}) = -\frac{\hbar^2\beta^2}{24M} \sum_K \nabla_K^2 \Phi \pm \sum_{KL}{}' e^{-Mr_{KL}^2/\beta\hbar^2} \quad . \tag{9.24}$$

The total partition function (9.19) can be written

$$Z = Z^{cl} \left[1 + \langle f(\{\mathbf{r}_K\})\rangle\right] \quad , \tag{9.25}$$

where $\langle f \rangle$ is the classical canonical average,

$$\langle f(\{\mathbf{r}_K\})\rangle = \frac{\int \cdots \int f(\{\mathbf{r}_K\}) e^{-\beta\mathcal{H}} \, \Pi_K d\mathbf{p}_K d\mathbf{r}_K}{\int \cdots \int e^{-\beta\mathcal{H}} \, \Pi_K d\mathbf{p}_K d\mathbf{r}_K} \quad . \tag{9.26}$$

Then the leading order expansion of the free energy is

$$F = F^{cl} - kT\langle f(\{\mathbf{r}_K\})\rangle = F^{cl} + F^q \quad , \tag{9.27}$$

where the second equality defines the leading quantum correction $F^q$. While the magnitude of $F^{cl}$ increases with temperature, approximately as $T \ln T$, the above equations tell us that $F^q$ decreases approximately as $T^{-1}$. Hence

$F^{cl}$ is indeed the high temperature limit of the free energy. The most valuable property of the expression for $F^q$, in Eq. (9.27), is that it can tell us how accurate the classical approximation is. This is useful in connection with purely classical computer simulations, such as molecular dynamics calculations.

To further analyze the quantum corrections, let us approximate the adiabatic potential as a sum of central potentials:

$$\Phi(\{\mathbf{r}_K\}) = \frac{1}{2}{\sum_{KL}}' \phi(|\mathbf{r}_K - \mathbf{r}_L|) = \frac{1}{2}{\sum_{KL}}' \phi_{KL} \quad . \tag{9.28}$$

The results will also be valid for the form $\Phi = \Omega(V) + \frac{1}{2}\Sigma'_{KL}\phi_{KL}$, derived in Sec. 5 for nearly-free-electron metals. Then

$$f(\{\mathbf{r}_K\}) = {\sum_{KL}}' \left[ -\frac{\hbar^2\beta^2}{24M}\nabla_K^2\phi_{KL} \pm e^{-Mr_{KL}^2/\beta\hbar^2} \right] \quad . \tag{9.29}$$

The summand is a function only of the distance $|\mathbf{r}_K - \mathbf{r}_L|$, and for any function $\theta_{KL} = \theta(|\mathbf{r}_K - \mathbf{r}_L|)$, the relation holds

$${\sum_{KL}}' \langle\theta_{KL}\rangle = N\rho_A \int_0^\infty \theta(r)g(r)4\pi r^2 dr \quad , \tag{9.30}$$

where $\rho_A = N/V$ is the particle density, and $g(r)$ is the pair correlation function. The algebra associated with this transformation is presented in more detail in Sec. 21. The leading quantum contribution to the high temperature free energy now takes the form

$$F^q = NkT\rho_A \int_0^\infty \theta(r)g(r)4\pi r^2 dr \quad , \tag{9.31}$$

where

$$\theta(r) = \frac{\hbar^2\nabla^2\phi(r)}{24M(kT)^2} \mp e^{-Mr^2kT/\hbar^2} \quad . \tag{9.32}$$

This very simple formula applies to monatomic systems in any condensed-matter phase, i.e. crystal, amorphous solid, or liquid.

For all condensed matter systems we shall consider, the nuclear motion in first approximation consists of vibrations within one or more nearly-harmonic many-particle potential energy valleys. For this motion, a mean vibrational frequency $\langle\omega\rangle$ is defined, and the first term of $\theta(r)$ in Eq. (9.32) becomes proportional to $(\hbar\langle\omega\rangle/kT)^2$. In the vibrational approximation, and

at the temperature $kT = \hbar\langle\omega\rangle$, $F^q$ is approximately 2% of $F^{cl}$. Roughly, the characteristic temperature $\hbar\langle\omega\rangle$ is around room temperature for elements in condensed phases.

Again for the condensed matter systems we shall consider, the closest distance of approach of two nuclei is around $0.75R_1$, where $R_1$ is the mean nearest-neighbor distance. From Eq. (9.32), the exponential argument in the exchange term of $\theta(r)$ at $r = 0.75R_1$, is approximately $(R_1/\Lambda)^2$, where $\Lambda$ is the thermal de Broglie wavelength, given by

$$\Lambda^2 = \frac{2\pi\hbar^2}{MkT} \quad . \tag{9.33}$$

Hence exchange effects are negligible when $\Lambda^2 << R_1^2$. At the classical temperatures $kT \gtrsim \hbar\langle\omega\rangle$, the exchange correction is utterly negligible for materials of interest to us. For Li at $kT = \hbar\langle\omega\rangle$, the exchange contribution to $F^q$ relative to $F^{cl}$ is approximately one part in $e^{200}$. The fact that the nuclear wave functions have virtually zero overlap will keep exchange negligible down to $T = 0$. For this we have to thank the Pauli repulsion among valence electrons, which keeps the nuclei well separated in condensed matter systems.

***Electronic Excitation plus Nuclear Motion***

In the present derivation, we need the complete notation of Chap. 1, since both nuclei and electrons are treated. The total Hamiltonian is written in Eq. (4.8),

$$\mathcal{H} = \mathcal{H}_N + \mathcal{H}_{EX} \quad , \tag{9.34}$$

where $\mathcal{H}_N$ describes the nuclear motion, and $\mathcal{H}_{EX}$ expresses the electronic excited states in the one-electron approximation. Calculation of the partition function is complicated by the fact that $\mathcal{H}_N$, specifically $\mathcal{T}_N$, does not commute with $\mathcal{H}_{EX}$, because $\mathcal{H}_{EX}$ depends on the nuclear positions. In calculating the total free energy in quantum statistical mechanics, this complication will be handled by expanding $\mathcal{H}_{EX}$ about the reference structure, as in Eq. (4.19), and by treating the difference as a perturbation. This procedure will be carried out in Sec. 18. When the nuclear motion approaches classical, however, the noncommutation of $\mathcal{T}_N$ becomes a quantum correction, and this provides a different way to expand the electronic excitation contribution, as follows.

In evaluating the nuclear motion partition function, from the beginning of Sec. 9, commutators involving $\mathcal{T}_N$ and $\Phi$ are considered a quantum correction. A similar procedure can be used to treat the electronic excitations. Here we shall evaluate only the leading term, obtained by neglecting entirely the commutators between $\mathcal{T}_N$ and the electronic sector. In the first step, we commute $\mathcal{T}_N$ and $\mathcal{H}_{EX}$ to write

$$Z = Tre^{-\beta(\mathcal{H}_N+\mathcal{H}_{EX})} \doteq Tre^{-\beta\mathcal{H}_N}e^{-\beta\mathcal{H}_{EX}} \quad . \tag{9.35}$$

The trace can be factored to $Tr_N Tr_E$, where $Tr_E$ is over all electronic states with the nuclei fixed at some positions, and $Tr_N$ is over the eigenfunctions of $\mathcal{T}_N$ for all nuclear positions, as in Eq. (9.5). We commute the electronic wavefunctions through the operator $\mathcal{T}_N$, and write

$$Tr_E e^{-\beta\mathcal{H}_{EX}} = e^{-\beta F_{EX}} \quad , \tag{9.36}$$

where $F_{EX}$ is the free energy for the electronic excitations, and is a function of the nuclear positions. Then

$$Z = Tr_N e^{-\beta\mathcal{H}_N}e^{-\beta F_{EX}} \quad . \tag{9.37}$$

The derivation is only consistent with setting $[\mathcal{T}_N, F_{EX}] = 0$, hence the complete partition function corresponds to a system of nuclei moving in the "effective potential" $\Phi + F_{EX}$. This result was derived by Zwanzig (1957). Of course, the function $\Phi + F_{EX}$ is temperature dependent, and does not correspond to the potential appearing in any Hamiltonian (see problem 9.3).

The result of the last paragraph is interesting, but Eq. (9.37) is still much too complicated to evaluate for any physically realistic model. Let us therefore expand once again about the reference structure, where now it is only necessary to expand the *function* $F_{EX}$, and not the *operator* $\mathcal{H}_{EX}$. The excitation free energy in the one-electron approximation was written in Eq. (7.49), for reference structure electrons, and the same formula is valid here, when the nuclear positions are arbitrary,

$$F_{EX} = \mu\mathcal{Z} - \sum_\lambda g_\lambda E_\lambda - kT\sum_\lambda \ln(1 + e^{-\beta(E_\lambda-\mu)}) \quad , \tag{9.38}$$

where $E_\lambda = E_\lambda(\{\mathbf{r}_K\})$. The one-electron energies are now written as

$$E_\lambda(\{\mathbf{r}_K\}) = E_\lambda^\sigma + \delta E_\lambda(\{\mathbf{r}_K\}) \quad , \tag{9.39}$$

where as usual the reference structure electron energies are $E_\lambda^\sigma = E_\lambda(\{\mathbf{R}_K\})$. Then, to leading order in $\delta E_\lambda$ the free energy (9.38) is

$$F_{EX} = F_{EX}^\sigma + \sum_\lambda (\bar{f}_\lambda - g_\lambda)\delta E_\lambda \quad . \tag{9.40}$$

With this, the partition function (9.37) is expanded to leading order in $\delta E_\lambda$, and the total free energy $F = -kT \ln Z$ becomes (see problem 9.4)

$$F = F_N + F_{EX}^\sigma + \sum_\lambda (\bar{f}_\lambda - g_\lambda)\langle \delta E_\lambda \rangle \quad , \tag{9.41}$$

where $\langle \delta E_\lambda(\{\mathbf{r}_K\})\rangle$ is the classical canonical average over nuclear positions, as shown in Eq. (9.26).

Recalling our discussion at the end of Sec. 4, the interaction between nuclear motion and electronic excitation, as contained in $\delta\mathcal{H}_{EX}$, has both adiabatic and nonadiabatic components. Each component makes a contribution to the free energy, and in Sec. 18 we shall derive detailed formulas for these separate contributions. In Eq. (9.41), on the other hand, $\delta E_\lambda$ belongs to a specific one-electron state, namely the state $\lambda$, and since the average $\langle \delta E_\lambda \rangle$ is only over the nuclear motion, electronic states are not mixed in $\Sigma_\lambda(\bar{f}_\lambda - g_\lambda)\langle \delta E_\lambda \rangle$. We have therefore shown that, when the nuclear motion is classical, the free energy contribution due to interaction between nuclear motion and electronic excitation is purely adiabatic. Our current estimate for elemental metals is that this purely adiabatic contribution is small compared to $F_{EX}^\sigma$, the free energy arising from excitation of reference structure electrons, at all (classical) temperatures of the condensed matter regime defined in Sec. 1. But this is only an estimate, and further study is needed.

### *Notes on Classical Statistical Mechanics*

Classical statistical mechanics is not a theory which stands alone, it is merely quantum statistical mechanics at sufficiently high temperature that the motion is classical. In condensed matter physics, there is a well defined regime in which the nuclear motion is classical, hence classical statistical mechanics applies, and indeed is very useful. For the elements, this regime includes most crystals and liquids, at all temperatures above a few tenths of the melting temperature. More precise specification of the classical regimes for individual elements will be provided in Chaps. 4 and 5. Notice on the other hand that electrons are never classical in condensed matter physics.

A classical regime does exist for electrons, but that is in plasmas, at very low densities, and/or at very high temperatures.

Recall that $h$ appears as a normalization factor in the classical partition function (9.21). Any multiplying constant in the partition function, classical or quantum, appears as an additive constant in the entropy, and appears in no other thermodynamic function. From Eq. (9.21), the classical entropy contains the additive term $3Nk \ln h$, and this is the only place in classical thermodynamics where $h$ appears. Of course, $h$ is ubiquitous in thermodynamic functions at quantum temperatures, but terms in $h$ all vanish at classical temperatures, except for the entropy constant. So this measure from quantum mechanics, the entropy constant containing $\ln h$, remains at all temperatures, and remains important at all temperatures, even to the interior of stars, because it determines the entropy.

*Problems*

*9.1* Verify the normalization constant in Eq. (9.4).

*9.2* Carry out the steps mentioned before Eq. (9.6), to verify that result.

*9.3* "Temperature-dependent Hamiltonians" are currently popular. A genuine Hamiltonian $\mathcal{H}$ satisfies two equations, namely $\mathcal{Z} = Tre^{-\beta\mathcal{H}}$, and $U = \langle\mathcal{H}\rangle$. If $\mathcal{H} = \mathcal{H}(\beta)$, show these two equations are inconsistent, hence that $\mathcal{H}(\beta)$ is not a Hamiltonian.

*9.4* Starting with Eqs. (9.37) and (9.38), derive (9.40) and (9.41).

## 10 CLASSICAL STATISTICS: APPLICATIONS

### *Canonical Distribution*

The system consists of $N$ similar nuclei in a cubical box of volume $V$, with classical motion governed by the Hamiltonian $\mathcal{H}$. The total kinetic and potential energies are $\mathcal{K}$ and $\Phi$ respectively, so that

$$\mathcal{H} = \mathcal{K} + \Phi = \sum_K \frac{\mathbf{p}_K^2}{2M} + \Phi(\{\mathbf{r}_K\}) \quad . \tag{10.1}$$

Cartesian coordinates are indicated by subscripts $i$, $j$, $k$, $l$, where each stands for $x$, $y$, or $z$. Coordinates of the total system momentum are $\mathcal{M}_i$,

$$\mathcal{M}_i = \sum_K p_{Ki} \quad . \tag{10.2}$$

The classical canonical partition function is written in Eq. (9.21), and when the momentum integrals are done, the partition function reduces to

$$Z = \frac{V^N Q}{N! \Lambda^{3N}} \quad . \tag{10.3}$$

Here $\Lambda$ is the thermal de Broglie wavelength, given by Eq. (9.33), and $Q$ is the *configuration integral*,

$$Q = \frac{1}{V^N} \int \cdots \int e^{-\beta \Phi} \prod_K d\mathbf{r}_K \quad . \tag{10.4}$$

The factor $V^N$ was multiplied and divided in $Z$, merely to make $Q$ dimensionless, so that $\ln Q$ is defined. The dynamical variable $\mathcal{A}(\{\mathbf{p}_K, \mathbf{r}_K\})$ has mean value defined by

$$\langle \mathcal{A} \rangle = \frac{1}{N! h^{3N} Z} \int \cdots \int \mathcal{A}(\{\mathbf{p}_K, \mathbf{r}_K\}) e^{-\beta \mathcal{H}} \prod_K d\mathbf{p}_K d\mathbf{r}_K \quad . \tag{10.5}$$

If $\mathcal{A}$ is a function only of the nuclear positions $\mathbf{r}_K$, then $\langle \mathcal{A} \rangle$ reduces to

$$\langle \mathcal{A} \rangle = \frac{1}{V^N Q} \int \cdots \int \mathcal{A}(\{\mathbf{r}_K\}) e^{-\beta \Phi} \prod_K d\mathbf{r}_K \quad . \tag{10.6}$$

Two useful mean values are calculated by doing the momentum integrals indicated in Eq. (10.5):

$$\langle \mathcal{M}_i \rangle = 0 \quad , \tag{10.7}$$

$$\langle \mathcal{K} \rangle = \tfrac{3}{2} N k T \quad . \tag{10.8}$$

The mean momentum vanishes by symmetry of the phase-space distribution, but the total momentum still fluctuates, as we shall see. The relation between mean kinetic energy and temperature is important in classical statistics. This relation was used in Eq. (6.3), to relate thermodynamics to time averages over the system motion.

By differentiating the mean value $\langle \mathcal{A} \rangle$ in Eq. (10.5), one finds

$$\langle \delta \mathcal{A} \delta \mathcal{H} \rangle = -\frac{\partial \langle \mathcal{A} \rangle}{\partial \beta} \quad . \tag{10.9}$$

Applying this to $\langle \mathcal{H} \rangle = U$ leads again to Eq. (7.23), since

$$\langle \delta \mathcal{H}^2 \rangle_C = -\frac{\partial U}{\partial \beta} = k T^2 C_V \quad , \tag{10.10}$$

where $C_V = (\partial U/\partial T)_V$ is the constant-volume specific heat, defined in Eq. (7.16). Here is a list of important classical canonical fluctuations.

$$\begin{aligned}
\langle \delta\mathcal{K}^2\rangle_C &= \frac{3}{2}N(kT)^2 \\
\langle \delta\mathcal{K}\delta\Phi\rangle_C &= 0 \\
\langle \delta\Phi^2\rangle_C &= N(kT)^2\left(\frac{C_V}{Nk}-\frac{3}{2}\right) \\
\langle \delta\mathcal{M}_i\delta\mathcal{H}\rangle_C &= 0 \\
\langle \delta\mathcal{M}_i\delta\mathcal{M}_j\rangle_C &= \langle \mathcal{M}_i\mathcal{M}_j\rangle_C \;=\; NMkT\delta_{ij} \quad .
\end{aligned} \tag{10.11}$$

Here $\langle\delta\mathcal{K}^2\rangle_C$ is calculated by doing the momentum integrals, $\langle\delta\mathcal{K}\delta\Phi\rangle_C$ vanishes because $\mathcal{K}$ depends only on momenta while $\Phi$ depends only on positions, and $\langle\delta\Phi^2\rangle_C$ is calculated by differencing from $\langle\delta\mathcal{H}^2\rangle_C$. The momentum fluctuations in the last line exemplify a special case where $\delta\mathcal{A} = \mathcal{A}$ because $\langle\mathcal{A}\rangle = 0$. The quantity $\langle\delta\mathcal{M}_i\delta\mathcal{M}_j\rangle_C$ is still a fluctuation, and possesses the properties of one, even though the equal form $\langle\mathcal{M}_i\mathcal{M}_j\rangle_C$ might not look like a fluctuation. Finally notice the above formulas again demonstrate that average fluctuations are of $RO(N^{-1})$.

### *Stresses and Elastic Constants*

For this derivation we need to simplify the form of the potential $\Phi(\{\mathbf{r}_K\})$, so that we can maintain insight into the physical content of the theory. Let us take the form appropriate for nearly-free-electron metals, Eq. (5.54), derived from pseudopotential perturbation theory,

$$\Phi(\{\mathbf{r}_K\}) = \Omega(V) + \frac{1}{2}{\sum_{KL}}' \phi(r_{KL};V) \quad , \tag{10.12}$$

where $r_{KL} = |\mathbf{r}_K - \mathbf{r}_L|$, and let us continue to speak of nuclear motion, though this potential was in fact derived for rigid ions. It is convenient to abbreviate the sum over pairs as

$$\frac{1}{2}{\sum_{KL}}' \phi(r_{KL};V) = {\sum}' \phi(r;V) \quad . \tag{10.13}$$

Expressions for the partition function and configuration integral, Eqs. (10.3) and (10.4), are

$$Z = \frac{e^{-\beta\Omega(V)} V^N Q}{N! \Lambda^{3N}} \quad , \tag{10.14}$$

$$Q = \frac{1}{V^N} \int \cdots \int e^{-\beta \Sigma \phi} \prod_K d\mathbf{r}_K \quad . \tag{10.15}$$

The system is supposed to be large enough that surface effects are negligible. The next step is to evaluate the first two strain derivatives of $\ln Z$.

Define a uniform lattice of integration points located at $\mathbf{s}_\lambda$ throughout the volume $V$, with $\lambda = 1, 2, \cdots, \Gamma$, where the volume per point is $V/\Gamma$. To represent the coupled integrals in $Q$, nucleus $K$ is summed over integration points $\kappa$, nucleus $L$ is summed over integration points $\lambda$, and so on to the last nucleus $M$ which is summed over points $\mu$. Then

$$Q = \frac{1}{\Gamma^N} \sum_\kappa \sum_\lambda \cdots \sum_\mu e^{-\beta \Sigma \phi(s;V)} \quad , \tag{10.16}$$

where $s$ stands for $s_{\kappa\lambda} = |\mathbf{s}_\kappa - \mathbf{s}_\lambda|$. Consider two patterns of the integration lattice, the initial pattern with lattice-vector components $\bar{s}_{\kappa i}$, and the final pattern with lattice-vector components $s_{\kappa i}$. The two patterns are connected by a homogeneous deformation, represented by the transformation matrix $\alpha$,

$$s_{\kappa i} = \sum_j \alpha_{ij} \bar{s}_{\kappa j} \quad , \tag{10.17}$$

and distances in the final pattern are related to the initial pattern by

$$s^2_{\kappa\lambda} = \sum_{ij} (2\eta_{ij} + \delta_{ij})\, \bar{s}_{\kappa\lambda i} \bar{s}_{\kappa\lambda j} \quad , \tag{10.18}$$

where $\eta_{ij}$ are the Lagrangian strains. For definitions and properties of homogeneous strain parameters, see Sec. 8 on thermoelasticity. Strain derivatives of any function of $s$ and $V$ can be calculated with the aid of Eq. (10.18). For example,

$$\frac{\partial \phi(s;V)}{\partial \eta_{ij}} = \frac{\partial \phi}{\partial s} \frac{s_i s_j}{|\mathbf{s}|} + V \frac{\partial \phi}{\partial V} \delta_{ij} \quad . \tag{10.19}$$

In view of Eq. (10.16) for $Q$, strain derivatives of $\ln Q$ can be put into the form of statistical averages, according to

$$\frac{\partial \ln Q}{\partial \eta_{ij}} = -\beta \left\langle \frac{\partial \Sigma \phi(s;V)}{\partial \eta_{ij}} \right\rangle \quad . \tag{10.20}$$

The next strain derivative $\partial^2 \ln Q / \partial \eta_{ij} \partial \eta_{kl}$ is straightforward.

The stresses $\tau_{ij}$ and the isothermal elastic constants $C^T_{ijkl}$ are defined in Eqs. (8.10) and (8.14), as strain derivatives of $F = -kT \ln Z$,

$$V\tau_{ij} = -kT \left( \frac{\partial \ln Z}{\partial \eta_{ij}} \right)_T \quad , \tag{10.21}$$

$$VC^T_{ijkl} = -kT \left( \frac{\partial^2 \ln Z}{\partial \eta_{ij} \partial \eta_{kl}} \right)_T \quad . \tag{10.22}$$

The following abbreviated notations will be used.

$$\begin{aligned}
\phi &= \phi(r;V) & \phi^* &= V(\partial\phi/\partial V) \\
\phi' &= r(\partial\phi/\partial r) & \phi^{**} &= V^2(\partial^2\phi/\partial V^2) \\
\phi'' &= r^2(\partial^2\phi/\partial r^2) & \Omega^* &= V(d\Omega/dV) \\
\phi'^* &= rV(\partial^2\phi/\partial V \partial r) & \Omega^{**} &= V^2(d^2\Omega/dV^2)
\end{aligned} \tag{10.23}$$

Cartesian components of the unit vector between two nuclei are $\hat{r}_i = r_i/r$, and the following tensors are defined:

$$\begin{aligned}
\phi_{ij} &= \phi^* \delta_{ij} + \phi' \hat{r}_i \hat{r}_j \quad , \\
\phi_{ijkl} &= (\phi^{**} + \phi^*)\, \delta_{ij}\delta_{kl} - \phi^* (\delta_{ik}\delta_{jl} + \delta_{il}\delta_{jk}) \\
&\quad + \phi'^* (\delta_{ij}\hat{r}_k\hat{r}_l + \delta_{kl}\hat{r}_i\hat{r}_j) + (\phi'' - \phi')\, \hat{r}_i\hat{r}_j\hat{r}_k\hat{r}_l \quad .
\end{aligned} \tag{10.24}$$

Then with all derivatives evaluated at $\eta_{ij} = 0$, the stresses and elastic constants are given by (see problem 10.1)

$$V\tau_{ij} = (\Omega^* - NkT)\, \delta_{ij} + \langle \Sigma \phi_{ij} \rangle \quad , \tag{10.25}$$

$$\begin{aligned}
VC^T_{ijkl} &= (\Omega^{**} + \Omega^*)\, \delta_{ij}\delta_{kl} + (NkT - \Omega^*)\, (\delta_{ik}\delta_{jl} + \delta_{il}\delta_{jk}) \\
&\quad + \beta \{ \langle \Sigma\phi_{ij} \rangle \langle \Sigma\phi_{kl} \rangle - \langle \Sigma\phi_{ij} \Sigma\phi_{kl} \rangle_C \} + \langle \Sigma\phi_{ijkl} \rangle .
\end{aligned} \tag{10.26}$$

The terms in $NkT$ arise from the nuclear kinetic energy. Both stresses and elastic constants contain averages of sums linear in $\phi(r;V)$, and in addi-

tion, the elastic constants contain fluctuations in the canonical distribution, namely those terms in the curly brackets.

Two separate procedures are available for calculating elastic constants: (a) calculate the stress tensor as a function of strain, from Eq. (10.25), and numerically differentiate to obtain the stress-strain coefficients $B^T_{ijkl}$, defined in Eq. (8.18), or (b) evaluate (10.26) for $C^T_{ijkl}$ directly. If a distribution other than canonical is used to evaluate (10.26), then the calculated fluctuations have to be corrected from that distribution to the canonical. Such fluctuation corrections will be studied in the remainder of this section.

Equations similar to (10.25) and (10.26) were derived by Squire, Holt, and Hoover (1969). Their derivation is restricted to a crystal having $\Phi = \frac{1}{2}\Sigma'_{KL}\phi(r_{KL})$, and in order to calculate strain derivatives of $Q$, they assume the nuclear trajectories scale uniformly with strain. As seen from our derivation, this assumption is unnecessary. The present derivation was given by Wallace, Schiferl, and Straub (1984), where in a fit of excessive caution, it was said that the expansion of $Q$ in powers of $\eta_{ij}$ would not be reliable for a crystal having strain-induced sublattice displacements. However, the expansion is correct in principle, and should be valid for any monatomic system, crystal, amorphous solid, or liquid. A still different derivation was given by Greeff and Moriarty (1999). Equation (10.26) was evaluated by molecular dynamics to calculate elastic constants *vs* temperature from pseudopotential models for bcc Na (Schiferl and Wallace, 1985), and for hcp Mg (Greeff and Moriarty, 1999).

### *Stress Fluctuations*

In Eqs. (7.21) – (7.30), mean quadratic fluctuations of the operators $\mathcal{N}$ and $\mathcal{H}$ are calculated in quantum statistics for the three canonical distributions. These fluctuations are easy to calculate, because they are explicitly specified by the phase space distributions. In the canonical distribution, for example, $\mathcal{N}$ is fixed at the value $N$, and therefore does not fluctuate, while $\mathcal{H}$ has the specified distribution proportional to $e^{-\beta\mathcal{H}}$. On the other hand, reverting now to classical notation, the fluctuation of an arbitrary variable $\mathcal{A}(\{\mathbf{p}_K, \mathbf{r}_K\})$ is difficult to calculate, since this requires evaluation of the phase space integral of $[\delta\mathcal{A}(\{\mathbf{p}_K, \mathbf{r}_K\})]^2$. Here we shall carry out this evaluation for classical stress fluctuations, following the theory presented by Wallace (2000).

Our procedure is a continuation of the analysis leading to Eqs. (10.25)

and (10.26). Two limitations will be imposed to simplify the presentation, without losing any essential features of the theory. First, the applied stress is isotropic pressure, which means the shear stresses $\tau_{ij}$ for $i \neq j$ vanish, and

$$\tau_{ij} = -P\delta_{ij} \quad . \tag{10.27}$$

Then Eq. (10.25) tells us

$$PV = -\Omega^* + NkT - \left\langle \Sigma \left( \phi^* + \frac{1}{3}\phi' \right) \right\rangle \quad . \tag{10.28}$$

Second, the system will have cubic or isotropic symmetry, so the Cartesian directions $x$, $y$, and $z$ are equivalent. This means the system will be a cubic crystal, an amorphous solid, or a liquid. Notice an amorphous solid is *atomically* random, and occupies a random potential energy valley, as described in Sec. 23 on liquid theory. When it comes to *fluctuations*, a polycrystalline solid is not equivalent to an amorphous solid, and the polycrystal is specifically omitted here.

The stress energy tensor is defined as $-V\tau_{ij}$. The corresponding dynamical variable is $\sigma_{ij}$,

$$\sigma_{ij} = -\Omega^*\delta_{ij} + M\sum_K v_{Ki}v_{Kj} - \frac{1}{2}{\sum_{KL}}' (\phi^*_{KL}\delta_{ij} + \phi'_{KL}\hat{r}_{KLi}\hat{r}_{KLj}) \quad , \tag{10.29}$$

where $\mathbf{v}_K = \mathbf{p}_K/M$. This is derived in Eq. (10.25), except for the kinetic term, whose average appears in Eq. (10.25). The usual derivation of the kinetic term is through the microscopic equation for conservation of linear momentum (e.g., Irving and Kirkwood, 1950). By taking the average and comparing with Eq. (10.28), it follows

$$\langle \sigma_{ij} \rangle = PV\delta_{ij} \quad . \tag{10.30}$$

With our standard abbreviated notation, the shear components of $\sigma_{ij}$ are expressed as $\sigma_{xy} = M\Sigma v_x v_y - \Sigma\phi_{xy}$. From Eq. (10.30), $\langle \sigma_{xy} \rangle = 0$. To calculate the fluctuation $\langle (\sigma_{xy})^2 \rangle$, we use the canonical averages (only the first equation is restricted to cubic or isotropic symmetry):

$$\left\langle (\Sigma M v_x v_y)^2 \right\rangle_C = N(kT)^2 \quad , \tag{10.31}$$

$$\langle (\Sigma M v_x v_y)\,(\Sigma\phi_{xy}) \rangle_C = 0 \quad , \tag{10.32}$$

and we solve for $\langle(\Sigma\phi_{xy})^2\rangle_C$ from Eq. (10.26) for the elastic constant $C^T_{xyxy} = C^T_{44}$. The result is

$$\beta\langle(\sigma_{xy})^2\rangle_C = NkT - VB^T_{44} + \frac{1}{15}\langle\Sigma(\phi'' + 4\phi') \quad , \tag{10.33}$$

where the stress-strain coefficient $B^T_{44}$ is $C^T_{44} - P$, from Eq. (8.22). The average on the right side can be transformed to an integral, weighted with the pair correlation function $g(r)$, according to the general relation (9.30), leading to

$$\beta\langle(\sigma_{xy})^2\rangle_C = NkT - VB^T_{44} + \frac{2\pi}{15}N\rho_A\int_0^\infty [\phi''(r) + 4\phi'(r)]\, g(r)r^2 dr \quad . \tag{10.34}$$

For an isotropic solid, $B^T_{44} = \frac{1}{2}(B^T_{11} - B^T_{12})$, and $B^T_{44} = 0$ for a liquid. Also we shall find shortly, in Eq. (10.62), that this particular fluctuation is the same in every distribution.

The dynamical variable representing the isotropic stress energy is

$$\frac{1}{3}\sum_i \sigma_{ii} = \mathcal{Q} = \mathcal{P}V \quad , \tag{10.35}$$

where the first equality defines $\mathcal{Q}$, and the second defines the microscopic pressure variable $\mathcal{P}$. From Eq. (10.30), $\langle\mathcal{Q}\rangle = PV$, hence $\langle\mathcal{P}\rangle = P$. From Eq. (10.29) for $\sigma_{ij}$, it follows

$$\mathcal{Q} = -\Omega^* + \frac{2}{3}\mathcal{K} - \mathcal{W} \quad , \tag{10.36}$$

where $\mathcal{K}$ is the total kinetic energy,

$$\mathcal{K} = \frac{1}{2}M\Sigma v^2 \quad , \tag{10.37}$$

and $\mathcal{W}$ is the generalized virial,

$$\mathcal{W} = \frac{1}{3}\sum_i \Sigma\phi_{ii} \quad . \tag{10.38}$$

Note that $\Omega^*$ in (10.36) does not contribute to fluctuations in $\mathcal{Q}$, since $\delta\Omega^* = 0$. The fluctuating variables are

$$\begin{aligned} \delta\mathcal{Q} &= \mathcal{Q} - PV = \tfrac{2}{3}\delta\mathcal{K} - \delta\mathcal{W} \quad , \\ \delta\mathcal{K} &= \mathcal{K} - \tfrac{3}{2}NkT \quad , \\ \delta\mathcal{W} &= \mathcal{W} - \langle\Sigma(\phi^* + \tfrac{1}{3}\phi')\rangle \quad . \end{aligned} \tag{10.39}$$

Now $\langle \delta \mathcal{K}^2 \rangle_C = \frac{3}{2} N (kT)^2$, from Eq. (10.11), and $\langle \delta \mathcal{K} \delta \mathcal{W} \rangle_C = 0$ because $\mathcal{K}$ is a function of velocities while $\mathcal{W}$ is a function of positions, so that

$$\langle \delta \mathcal{Q}^2 \rangle_C = \frac{2}{3} N (kT)^2 + \langle \delta \mathcal{W}^2 \rangle_C \quad . \tag{10.40}$$

Equations (10.25) and (10.26) can be written for the combination of elastic constants

$$V B_T = \frac{1}{3} V \left( B_{11}^T + 2 B_{12}^T \right) = \frac{1}{3} V \left( C_{11}^T + 2 C_{12}^T + P \right) \quad , \tag{10.41}$$

and this equation can be solved for $\langle \delta \mathcal{W}^2 \rangle_C$ to obtain

$$\begin{aligned} \beta \langle \delta \mathcal{Q}^2 \rangle_C \quad &= \quad \Omega^{**} - V B_T + \frac{5}{3} N k T \\ &\quad + \frac{2\pi}{9} N \rho_A \int_0^\infty [9\phi^{**}(r) + 6\phi'^{*}(r) + \phi''(r) - 2\phi'(r)] g(r) r^2 dr \quad . \end{aligned} \tag{10.42}$$

Thus we have found the expression for isotropic stress energy fluctuations in the canonical distribution. It is equivalent to pressure fluctuations, through the identity $V^2 \langle \delta \mathcal{P}^2 \rangle_C = \langle \delta \mathcal{Q}^2 \rangle_C$.

An extensive account of linear response in a quantum fluid, specifically of the relation between response to an external perturbation and time dependent correlations in the equilibrium fluid, was presented by Puff and Gillis (1968). They derived formulas for fluctuations among hydrodynamic variables in the grand canonical distribution, and when all the theoretical differences are accounted for, their results are in agreement with our classical equations for $\langle (\sigma_{xy})^2 \rangle_C$ and $\langle \delta \mathcal{Q}^2 \rangle_C$. The present theory also resolves a number of inconsistencies in pressure fluctuation formulas, which have persisted many years in the literature (for details see Wallace, 2000). Finally we note that the thermodynamic fluctuations of Landau and Lifshitz (1938, Sec. 40; 1980, Sec. 112) are not derived from a phase space distribution, and hence they differ essentially from statistical mechanical fluctuations, a difference not recognized in theoretical research for over 60 years (again see Wallace, 2000).

### *Relation Between Different Distributions*

This derivation is within classical mechanics, and is based on the work of Lebowitz, Percus, and Verlet (1967). The theory can be extended to quan-

tum mechanics, by accounting for the noncommutation of operators representing dynamical variables. Let $x$ represent a phase space point $\{\mathbf{p}_K, \mathbf{r}_K\}$, and let $V = \{V_\alpha\}$ be a set of extensive variables, for $\alpha = 1, 2, \cdots$. The unnormalized probability density, or statistical weight, at a given $x$ and $V$ is $W(x|V)$. In the canonical distribution, for example, the given $\{V_\alpha\}$ are the number of atoms and the system volume, and $W(x|V)$ is $e^{-\beta\mathcal{H}(x)}$. The partition function $W(V)$ is defined by

$$W(V) = \int W(x|V)dx \quad , \tag{10.43}$$

and the mean value of the dynamical variable $\mathcal{A}(x)$ is defined by

$$\langle \mathcal{A}|V\rangle = \frac{\int \mathcal{A}(x)W(x|V)dx}{W(V)} \quad . \tag{10.44}$$

Now perform a Legendre transformation to a set of intensive variables $X = \{X_\alpha\}$, where $X_\alpha$ and $V_\alpha$ are conjugate, and let $X \cdot V = \Sigma_\alpha X_\alpha V_\alpha$. The statistical weight $W(x|X)$ and partition function $W(X)$ are defined by

$$W(x|X) = \int W(x|V)e^{-X\cdot V}dV \quad , \tag{10.45}$$

$$W(X) = \int W(x|X)dx \quad . \tag{10.46}$$

The mean value of $\mathcal{A}(x)$ is first defined, then transformed, as follows,

$$\langle \mathcal{A}|X\rangle = \frac{\int \mathcal{A}(x)W(x|X)dx}{W(X)} = \frac{\int \langle \mathcal{A}|V\rangle W(V)e^{-X\cdot V}dV}{W(X)} \quad , \tag{10.47}$$

where the transformation is derived with Eqs. (10.45) and (10.44).

The next step is to make a fluctuation expansion of the mean value of a dynamical variable. In the distribution $W(x|V)$, the mean value of the set of extensive variables is $\langle V|X\rangle$, and is abbreviated $\bar{V} = \{\bar{V}_\alpha\}$, and the corresponding fluctuations are $\delta V = \{\delta V_\alpha\}$. Notice $\langle \delta V|X\rangle = 0$. The fluctuation expansion of $\langle \mathcal{A}|V\rangle$ is

$$\langle \mathcal{A}|V\rangle = \langle \mathcal{A}|\bar{V}\rangle + \sum_\alpha \delta V_\alpha \frac{\partial\langle \mathcal{A}|\bar{V}\rangle}{\partial \bar{V}_\alpha} + \frac{1}{2}\sum_{\alpha\beta}\delta V_\alpha \delta V_\beta \frac{\partial^2\langle \mathcal{A}|\bar{V}\rangle}{\partial \bar{V}_\alpha \partial \bar{V}_\beta} + \cdots \quad . \tag{10.48}$$

With Eq. (10.47), this is transformed to

$$\langle \mathcal{A}|X\rangle = \langle \mathcal{A}|\bar{V}\rangle + \frac{1}{2}\sum_{\alpha\beta}\langle \delta V_\alpha \delta V_\beta|X\rangle \frac{\partial^2\langle \mathcal{A}|\bar{V}\rangle}{\partial \bar{V}_\alpha \partial \bar{V}_\beta} + \cdots \quad . \tag{10.49}$$

The fluctuation term on the right side is small, and the remaining terms are smaller still (see problem 10.3), and will be neglected. The expansion can be inverted, and $\langle \mathcal{A}|\bar{V}\rangle$ can be replaced by $\langle \mathcal{A}|X\rangle$ in the fluctuation term, to write

$$\langle \mathcal{A}|\bar{V}\rangle = \langle \mathcal{A}|X\rangle - \frac{1}{2}\sum_{\alpha\beta}\langle \delta V_\alpha \delta V_\beta|X\rangle \frac{\partial^2\langle \mathcal{A}|X\rangle}{\partial \bar{V}_\alpha \partial \bar{V}_\beta} \quad . \tag{10.50}$$

A further transformation is possible to (see problem 10.5)

$$\langle \mathcal{A}|\bar{V}\rangle = \langle \mathcal{A}|X\rangle + \frac{1}{2}\sum_{\alpha} \frac{\partial}{\partial X_\alpha}\frac{\partial\langle \mathcal{A}|X\rangle}{\partial \bar{V}_\alpha} \quad . \tag{10.51}$$

The last two equations relate the means of $\mathcal{A}(x)$ in two different distributions, namely one where the extensive variables are fixed at the values $\bar{V}$, the left side, and one where the extensive variables fluctuate about the same mean values, the right side. It is apparent from these equations that the two means of $\mathcal{A}(x)$ differ in $RO(N^{-1})$, i.e. that $\langle \mathcal{A}|\bar{V}\rangle - \langle \mathcal{A}|X\rangle$ is of order $N^{-1}\langle \mathcal{A}|X\rangle$.

It is now possible to find the relation between mean quadratic fluctuations in different distributions. The mean of $\delta\mathcal{A}\delta\mathcal{B}$, with $V$ fixed at $\bar{V}$, is

$$\langle \delta\mathcal{A}\delta\mathcal{B}|\bar{V}\rangle = \langle \mathcal{A}\mathcal{B}|\bar{V}\rangle - \langle \mathcal{A}|\bar{V}\rangle\langle \mathcal{B}|\bar{V}\rangle \quad . \tag{10.52}$$

This is to be evaluated with Eq. (10.50), where in the leading fluctuation term, $\langle \mathcal{A}\mathcal{B}|X\rangle$ can be replaced by its zero-fluctuation value $\langle \mathcal{A}|X\rangle\langle \mathcal{B}|X\rangle$. The result to leading order is

$$\langle \delta\mathcal{A}\delta\mathcal{B}|\bar{V}\rangle = \langle \delta\mathcal{A}\delta\mathcal{B}|X\rangle - \sum_{\alpha\beta}\langle \delta V_\alpha \delta V_\beta|X\rangle \frac{\partial\langle \mathcal{A}|X\rangle}{\partial \bar{V}_\alpha}\frac{\partial\langle \mathcal{B}|X\rangle}{\partial \bar{V}_\beta} \quad , \tag{10.53}$$

where the omitted higher-order terms are of $RO(N^{-1/2})$ (see problem 10.4). Again a further transformation is possible to (see problem 10.5)

$$\langle \delta\mathcal{A}\delta\mathcal{B}|\bar{V}\rangle = \langle \delta\mathcal{A}\delta\mathcal{B}|X\rangle + \sum_{\alpha} \frac{\partial\langle \mathcal{A}|X\rangle}{\partial X_\alpha}\frac{\partial\langle \mathcal{B}|X\rangle}{\partial \bar{V}_\alpha} \tag{10.54}$$

The last two equations relate the mean of $\delta\mathcal{A}\delta\mathcal{B}$ in two different distributions, one at $V = \bar{V}$ on the left, and one at fluctuating $V$ on the right, and these equations demonstrate that $\langle\delta\mathcal{A}\delta\mathcal{B}|\bar{V}\rangle - \langle\delta\mathcal{A}\delta\mathcal{B}|X\rangle$ is of $RO(1)$. Another general result of these equations is that if either $\langle\mathcal{A}|X\rangle$ or $\langle\mathcal{B}|X\rangle$ is constant, then the derivatives on the right side vanish, and the fluctuations $\langle\delta\mathcal{A}\delta\mathcal{B}|\bar{V}\rangle$ and $\langle\delta\mathcal{A}\delta\mathcal{B}|X\rangle$ are equal.

***Three Canonical Distributions***

The three distributions are defined in Sec. 7. Equation (10.50) gives the relation of canonical averages, and of grand canonical averages, to microcanonical averages, as follows.

$$\langle\mathcal{A}\rangle_{MC} = \langle\mathcal{A}\rangle_C - \frac{1}{2}\langle\delta\mathcal{H}^2\rangle_C \frac{\partial^2\langle\mathcal{A}\rangle_C}{\partial U^2} \quad , \tag{10.55}$$

$$\begin{aligned}\langle\mathcal{A}\rangle_{MC} &= \langle\mathcal{A}\rangle_{GC} - \frac{1}{2}\langle\delta\mathcal{N}^2\rangle_{GC}\frac{\partial^2\langle\mathcal{A}\rangle_{GC}}{\partial N^2} - \frac{1}{2}\langle\delta\mathcal{H}^2\rangle_{GC}\frac{\partial^2\langle\mathcal{A}\rangle_{GC}}{\partial U^2} \\ &\quad -\langle\delta\mathcal{N}\delta\mathcal{H}\rangle_{GC}\frac{\partial^2\langle\mathcal{A}\rangle_{GC}}{\partial N\partial U} \quad .\end{aligned} \tag{10.56}$$

Notice the theory does not provide a direct relation between $\langle\mathcal{A}\rangle_C$ and $\langle\mathcal{A}\rangle_{GC}$, and to find this relation, one has to eliminate $\langle\mathcal{A}\rangle_{MC}$ between the above two equations.

Mean quadratic fluctuations in the three canonical distributions can be related by applying Eq. (10.53), with the following results.

$$\langle\delta\mathcal{A}\delta\mathcal{B}\rangle_{MC} = \langle\delta\mathcal{A}\delta\mathcal{B}\rangle_C - \langle\delta\mathcal{H}^2\rangle_C \frac{\partial\langle\mathcal{A}\rangle_C}{\partial U}\frac{\partial\langle\mathcal{B}\rangle_C}{\partial U} \quad , \tag{10.57}$$

$$\begin{aligned}\langle\delta\mathcal{A}\delta\mathcal{B}\rangle_{MC} &= \langle\delta\mathcal{A}\delta\mathcal{B}\rangle_{GC} - \langle\delta\mathcal{N}^2\rangle_{GC}\frac{\partial\langle\mathcal{A}\rangle_{GC}}{\partial N}\frac{\partial\langle\mathcal{B}\rangle_{GC}}{\partial N} \\ &\quad -\langle\delta\mathcal{N}\delta\mathcal{H}\rangle_{GC}\left[\frac{\partial\langle\mathcal{A}\rangle_{GC}}{\partial N}\frac{\partial\langle\mathcal{B}\rangle_{GC}}{\partial U} + \frac{\partial\langle\mathcal{A}\rangle_{GC}}{\partial U}\frac{\partial\langle\mathcal{B}\rangle_{GC}}{\partial N}\right] \\ &\quad -\langle\delta\mathcal{H}^2\rangle_{GC}\frac{\partial\langle\mathcal{A}\rangle_{GC}}{\partial U}\frac{\partial\langle\mathcal{B}\rangle_{GC}}{\partial U} \quad .\end{aligned} \tag{10.58}$$

Every term in these two equations is of the same order, namely of order $N^{-1}\langle\mathcal{A}\rangle\langle\mathcal{B}\rangle$.

Evaluation of the various terms in the above relations among different distributions is accomplished with the aid of standard thermodynamic and fluctuation formulas, such as Eqs. (7.21) – (7.30) in quantum statistics, and Eqs. (10.7) – (10.11) in classical statistics. Classical canonical fluctuations in kinetic and potential energy are listed in Eq. (10.11), and transforming these to microcanonical fluctuations, by means of Eq. (10.57), gives

$$\langle \delta \mathcal{K}^2 \rangle_{MC} = \langle \delta \mathcal{K}^2 \rangle_C - \frac{9(NkT)^2}{4C_V} = \frac{3}{2} N (kT)^2 \left( 1 - \frac{3Nk}{2C_V} \right) \quad , \tag{10.59}$$

$$\langle \delta \Phi^2 \rangle_{MC} = \frac{3}{2} N (kT)^2 \left( 1 - \frac{3Nk}{2C_V} \right) \quad , \tag{10.60}$$

$$\langle \delta \mathcal{K} \delta \Phi \rangle_{MC} = -\frac{3}{2} N (kT)^2 \left( 1 - \frac{3Nk}{2C_V} \right) \quad . \tag{10.61}$$

For a physically realistic condensed matter system, the potential energy $\Phi$ is nonzero, hence $C_V > \frac{3}{2}Nk$, and the squared fluctuations above are positive. Notice that $\langle \delta \mathcal{K} \delta \Phi \rangle_{MC}$ acquires a nonzero value, even though $\langle \delta \mathcal{K} \delta \Phi \rangle_C$ in Eq. (10.11) is zero (see problem 10.6). Finally, since $\mathcal{H} = \mathcal{K} + \Phi$, and since $\delta \mathcal{H} = 0$ in the microcanonical distribution, then $\delta \Phi = -\delta \mathcal{K}$ in the microcanonical distribution, so we must have $\langle \delta \mathcal{K}^2 \rangle_{MC} = \langle \delta \Phi^2 \rangle_{MC}$, and $\langle \delta \mathcal{H}^2 \rangle_{MC} = 0$. These fluctuation properties are indeed satisfied by the above three equations.

Classical canonical stress energy fluctuations are evaluated in Eqs. (10.34) and (10.42). For the shear components, since $\langle \sigma_{xy} \rangle = 0$, it follows from Eq. (10.53), or from (10.54), and the remarks following Eq. (10.54), that $\langle (\sigma_{xy})^2 \rangle$ is the same in every distribution:

$$\langle (\sigma_{xy})^2 \rangle_{MC} = \langle (\sigma_{xy})^2 \rangle_C = \langle (\sigma_{xy})^2 \rangle_{GC} \quad . \tag{10.62}$$

For the isotropic stress energy fluctuations, Eqs. (10.57) and (10.58) are worked out to find

$$\langle \delta \mathcal{Q}^2 \rangle_{MC} = \langle \delta \mathcal{Q}^2 \rangle_C - kT^2 \gamma^2 C_V \quad , \tag{10.63}$$

$$\langle \delta \mathcal{Q}^2 \rangle_{MC} = \langle \delta \mathcal{Q}^2 \rangle_{GC} - kTVB_T - kT^2 \gamma^2 C_V \quad , \tag{10.64}$$

where $\gamma$ is the Grüneisen parameter, defined in Eq. (7.16). So stress energy fluctuations, or equally stress fluctuations, can be calculated in the canonical distribution by Eqs. (10.34) and (10.42), and can be transformed to microcanonical and grand canonical distributions by Eqs. (10.62) – (10.64).

*Problems*

*10.1* Derive Eqs. (10.25) and (10.26) for the stresses and elastic constants. Useful intermediate results are (these need to be extended to second derivatives):

$$\begin{aligned} \frac{\partial \ln V}{\partial \eta_{kl}}\Big) &= \delta_{kl} - 2\eta_{kl} + \cdots \quad , \\ \frac{\partial \Omega}{\partial \eta_{ij}}\Big) &= \Omega^* \delta_{ij} \quad , \\ \frac{\partial \ln Q}{\partial \eta_{ij}}\Big) &= -\beta \langle \Sigma \phi_{ij} \rangle \quad . \end{aligned}$$

*10.2* Carry out the algebraic steps which are omitted in the text, to derive the fluctuation formulas (10.34) and (10.42).

*10.3* Show that the leading omitted term in Eq. (10.49) is of $RO(N^{-3/2})$, i.e. is of order $N^{-3/2}\langle \mathcal{A} \rangle$.

*10.4* Show that the leading omitted term on the right of Eq. (10.53) is $RO(N^{-1/2})$, *i.e.* is of order $N^{-1/2}\langle \delta\mathcal{A}\delta\mathcal{B}|X\rangle$.

*10.5* Derive the equation

$$\langle \delta V_\alpha \delta V_\beta | X \rangle = -\frac{\partial \bar{V}_\alpha}{\partial X_\beta} = -\frac{\partial \bar{V}_\beta}{\partial X_\alpha} \quad .$$

Hence verify Eqs. (10.51) and (10.54).

*10.6* Explain why $\langle \delta\mathcal{K}\delta\Phi \rangle_C$ must be zero, and why $\langle \delta\mathcal{K}\delta\Phi \rangle_{MC}$ must be nonzero in any system other than an ideal gas (for the microcanonical fluctuation, argue from the relation $\delta\mathcal{H} = \delta\mathcal{K} + \delta\Phi$).

*10.7* Derive Eqs. (10.63) and (10.64), relating $\langle \delta\mathcal{Q}^2 \rangle$ among the three canonical distributions.

## 11 INTERPRETATION OF STATISTICAL MECHANICS

### *Summary of the Formulation*

For all phase space distributions, the entropy and other thermodynamic functions are the same in the thermodynamic limit. Because time averaging does not provide a direct way to calculate entropy, phase space averaging is the more fundamental technique. If we make the kinetic-energy quasiergodic hypothesis, that at given $V$ and $U$ the phase space average and time average of $\mathcal{K}/N$ are the same in the thermodynamic limit, then in classical statistics $T(V,U)$ is the same in both averages. Hence in both averages, all the thermodynamic functions are the same, except that the constant of entropy is still undetermined in time averaging. To compare these statistical averages with experimental data, a second fundamental assumption is required, for which we choose the following entropy hypothesis: At a given $V$ and $U$, the entropy calculated in phase space averaging in the thermodynamic limit is in principle the same as the experimental entropy. Then theory and experiment are in principle the same for all thermodynamic functions.

Fluctuations are not covered by the above remarks, since they are a finite-$N$ effect; in particular, in phase space averages, $\langle \delta\mathcal{A}\delta\mathcal{B}\rangle$ is of order $N^{-1}\langle\mathcal{A}\rangle\langle\mathcal{B}\rangle$ as $N \to \infty$. As a result, a mean quadratic fluctuation normally differs in $RO(1)$ in different distributions, though examples where differences are smaller than $RO(1)$ can be found. However, this strong dependence of fluctuations upon the distribution does not present us with an essential difficulty, because it is always possible to calculate thermodynamic functions from dynamical variables, without resorting to fluctuations. If one nevertheless chooses to work with fluctuations, two observations become important. First, for purely theoretical work, it is straightforward to calculate the differences of mean fluctuations between different distributions, as illustrated in Sec. 10. Second, when it comes to comparing theory and experiment for mean fluctuations, a careful analysis is required. An example relating to elastic constants is discussed below, under the interpretation of molecular dynamics.

There are situations where the standard phase space averaging technique will fail to give the correct statistical properties of a system. One is near the critical point, where fluctuations remain important as $N \to \infty$, so that phase space integrands fail to sharpen, and the mean value is not the

most probable value, in the thermodynamic limit (see *e.g.* Callen, 1985, Chap. 10). This case is not treated here. Another example is the glassy state, where the condensed system samples only a limited region of phase space during the time of an experiment. This state is characterized by rate-dependent response, and requires a nonequilibrium theory, for which a model is presented in Sec. 27.

### *Meaning of Entropy*

Boltzmann's system was a classical ideal gas, where the only energy is the kinetic energy of each atom. He divided single-atom kinetic energy space into bins, and defined a microstate of the system as a specific placement of the atoms into bins. Boltzmann argued that, subject to the constraint of constant total energy, the equilibrium system has equal a priori probability to be found in any microstate, hence the equilibrium entropy is $k \ln \Omega$, where $\Omega$ is the number of accessible microstates. An excellent review of Boltzmann's entropy theory is given by Bailyn (1994, Chap. 10).

Of course, $\Omega$ is a number, and in classical mechanics there is no way to count the number of microstates, or what is equivalent, there is no way to find the correct energy bin size. This problem is solved in quantum mechanics, where every system, every subsystem, every independent particle or normal mode, has a discrete countable set of allowed states. A system microstate is now a quantum state $\psi_n$, in which every quantized degree of freedom is given a specific occupation number. The probability of finding the system in state $\psi_n$ is $f_n$, and the entropy is given by the Gibbs formula $S = -k \Sigma_n f_n \ln f_n$. But in the thermodynamic limit, Gibbs' formula is the same as Boltzmann's. In the canonical distribution, for example, phase space integrands narrow in the thermodynamic limit to a single energy level $E_n$, all the corresponding $f_n$ are equal and have the value $1/\Omega$, where $\Omega$ is the number of states at $E_n$, so the Gibbs formula becomes $S = -k \Sigma_n f_n \ln(1/\Omega) = k \ln \Omega$.

A profound fact of nature is that Boltmann's entropy has been found to agree with the measured thermodynamic entropy for every equilibrium system for which the comparison has been made. There is no doubt about the meaning of entropy: it is a measure of the number of quantum states accessible to, and therefore occupied by, a mechanical system in a fluctuating equilibrium state.

It is of interest to illustrate the role of entropy in equilibrium *processes*.

Consider a system in equilibrium at volume $V$ and internal energy $U$, being uniformly distributed over the $\Omega$ states on the energy surface. If the energy is increased by $dU$ at constant $V$, the system promptly redistributes itself over the $\Omega + d\Omega$ states at $U + dU$, and the entropy therefore increases by $dS = kd\ln\Omega$. Hence the universal law relating $\Omega$ with $U$ at constant $V$ is $d\ln\Omega = dU/kT$. Also, the balance between energy and entropy is decisive in certain equilibrium phase transitions. Suppose a many-atom system can move within a single crystalline potential energy valley, or can move among a large number of random valleys located at some higher potential energy. At low temperatures, states of lowest energy are stable, so the system moves in the crystal valley. Upon increasing the temperature, when the system has sufficient energy to roam freely among the random valleys, then it will spend all its time among the random valleys, simply because they are so numerous. This is why a crystal melts. Phase transitions will be studied in more detail in Chap. 6.

### *Interpretation of Molecular Dynamics Calculations*

Classical statistical mechanics for nuclear motion was derived in Sec. 9, and applies to any system in which the nuclear motion is classical. For real condensed matter, the nuclear motion approaches classical at high temperatures, and classical statistical mechanics applies, with small quantum corrections. On the other hand, for a molecular dynamics system, the nuclear motion is *pure classical at all temperatures*, hence pure classical statistical mechanics applies at all temperatures, even down to $T = 0$. To alleviate confusion here, one can think of mean kinetic energy in an equilibrium system, in place of temperature. Then for all values of the mean kinetic energy, equilibrium phase space averages for a molecular dynamics system are expressed through the classical partition function $Z^{cl}$, written in Eq. (9.21), or in Eq. (6.5).

Compared to laboratory systems, computer systems are notoriously small, and have much larger finite-$N$ effects. Experimental data for energy and entropy, for example, are usually accurate to around one part in $10^4$. So that terms of $RO(N^{-1})$ are on the same order as experimental error, one therefore has to work with a molecular dynamics system having $N = 10^4$ or so. To eliminate terms of $RO(N^{-1/3})$ from molecular dynamics results, a numerical extrapolation for $N \to \infty$ is required. As long as finite-$N$ effects in molecular dynamics calculations are negligible, or are

eliminated by extrapolation, then boundary conditions can be chosen at will. Periodic boundary conditions are popular because they are easy to apply, and because they are presumed to give finite-$N$ effects of $RO(N^{-1})$.

Let us consider the entropy constant, which remains undetermined in molecular dynamics calculations. There are two reasons for needing this information, either to test a model theory for entropy, or else to calculate the equilibrium boundary between two phases. Notice that, even though a molecular dynamics system can decide for itself to change phases, the occurrence will not provide a reliable location of the coexistence curve, because boundary conditions strongly influence phase transitions in a molecular dynamics system. For an accurate phase boundary, one needs the free energy of each phase, hence one needs the entropy constant for each phase separately. The entropy constant can be determined numerically, by integrating $dS$ from some reference state, where the entropy is calculated by phase space averaging. Some useful references are Hansen and McDonald (1986, Sec. 6.2), Allen and Tildesley (1990, Sec. 7.2), and deKoning, Antonelli, and Yip (1999).

An important question regarding fluctuations needs to be addressed. Suppose one uses phase space averaging theory to develop an equation containing fluctuations, then what correction is necessary if the fluctuations are actually evaluated by molecular dynamics? For clarity of discussion, we shall answer this question for a specific example, namely for Eq. (10.26), which expresses isothermal elastic constants in terms of quantities related to stress fluctuations, and which was derived in the canonical distribution. First notice that surface effects were neglected in the derivation, and this is possible, according to a theorem developed in Sec. 12, because stresses are local functions, i.e. stresses can be evaluated in the interior of a large system, where surface effects are not felt. This argument applies to any system, so that stresses, and stress fluctuations as well, are independent of the boundary conditions for a molecular dynamics system in the thermodynamic limit. When boundary conditions are neglected, the distribution representing a molecular dynamics system is the constant energy surface, i.e. the microcanonical distribution. So stress fluctuations calculated in molecular dynamics are the same in the thermodynamic limit as stress fluctuations in the microcanonial distribution.

For a monatomic system with cubic or isotropic symmetry, the independent elastic constants are $C_{11}^T$, $C_{12}^T$, and $C_{44}^T$. The fluctuation corrections from microcanonical to canonical distribution are calculated from

Eq. (10.57), with the following result: If the fluctuations are evaluated in the microcanonical distribution, or in molecular dynamics with surface effects eliminated, the correction $\Delta_{\alpha\beta}$ should be added to $VC^T_{\alpha\beta}$, where

$$\Delta_{11} = \Delta_{12} = \frac{-T(\gamma C_V - Nk)^2}{C_V} \quad , \qquad \Delta_{44} = 0 \quad . \tag{11.1}$$

The same corrections were originally found by Wallace, Schiferl, and Straub (1984), by correcting directly from the molecular dynamics distribution (see also problem 11.1).

Depending on the boundary condition, the total momentum might or might not fluctuate in a molecular dynamics system. With periodic boundary conditions, the net force on the system is zero, so the total momentum is a constant of the motion. Let $\mathbf{M}$ be the total momentum, and let $\Sigma_K \mathbf{p}_K$ be the dynamical variable representing total momentum. Notice this dynamical variable does not correspond to a thermodynamic function. In their study of relations between different distributions, Lebowitz, Percus, and Verlet (1967) defined the microcanonical weight function as $\delta(\mathcal{H} - U)$ and the molecular dynamics weight function as $\delta(\mathcal{H} - E)\delta(\Sigma_K \mathbf{p}_K - \mathbf{M})$. When $\mathbf{M} = 0$, then $E$ is the thermodynamic internal energy $U$. Constant total momentum also implies that the location of the system center of mass is a prescribed function of time, and this constraint was added to the molecular dynamics weight function by Ray and Zhang (1999). But these center-of-mass constraints are effects of $RO(N^{-1})$, and they cannot contribute to thermodynamic properties, including fluctuations. Let us illustrate by comparing fluctuations in the microcanonical and molecular dynamics distributions. A dynamical variable representing a thermodynamic function is denoted $\mathcal{A}$, and is for example the kinetic energy $\mathcal{K}$ in the center of mass coordinate system, or the potential energy $\Phi(\{\mathbf{r}_K\})$, which does not depend on the location of the center of mass. Then since derivatives of $\langle \mathcal{A}|X\rangle$ with respect to center-of-mass position or velocity are zero, the difference term in Eq. (10.53) for fluctuations vanishes. Hence all mean quadratic fluctuations of dynamical variables representing thermodynamic functions are the same in the molecular dynamics and microcanonical distributions. The result can also be shown by explicit calculations for any given dynamical variables (see Wallace and Straub, 1983).

*Problem*

*11.1* Verify the microcanonical to canonical fluctuation corrections for the elastic constants, Eq. (11.1). Notice it is convenient in Eq. (10.57) to convert from derivatives with respect to $U$ to derivatives with respect to $T$.

*This page intentionally left blank*

# Chapter 3
# Lattice Dynamics

## 12 LATTICE STATICS

### *Displacement Expansion of the Potential*

The system is a static finite array of $N$ nuclei, and their associated electrons in the electronic groundstate, or it can be considered a static finite array of interacting ions, or interacting atoms. The system potential as function of the nuclear positions is $\Phi(\{\mathbf{r}_K\})$, and for the moment let the externally applied forces vanish. The configuration at a potential energy minimum is a locally stable equilibrium configuration, and is called a *structure*. The potential has an absolute minimum at a certain crystal structure, representing that the system will crystallize into that structure at low temperatures. The potential also has many other local minima, corresponding to structures that might be stable at higher temperatures. Nuclear positions at a structure are denoted $\mathbf{R}_K$, and it is convenient to write

$$\mathbf{r}_K = \mathbf{R}_K + \mathbf{U}_K \quad , \tag{12.1}$$

where $\mathbf{U}_K$ are displacements from equilibrium, and are considered small. To keep notation simple, our equations will be written for monatomic systems, and for primitive lattices when it is necessary to indicate the unit cell geometry. General lattice structures are treated in Born and Huang (1954), and in *Thermodynamics of Crystals*.

The theory of lattice dynamics is based on the expansion of the potential energy in powers of nuclear displacements from equilibrium:

$$\Phi = \Phi_0 + \sum_K \sum_i \Phi_{Ki} U_{Ki} + \frac{1}{2} \sum_{KL} \sum_{ij} \Phi_{Ki,Lj} U_{Ki} U_{Lj} + \cdots \quad . \tag{12.2}$$

The potential energy coefficients, $\Phi_{Ki}$ and so on, are derivatives of $\Phi(\{\mathbf{r}_K\})$ with respect to components of $\mathbf{r}_K$, evaluated at equilibrium, *i.e.* at the structure. By definition, these coefficients are symmetric in their index pairs,

$$\Phi_{Ki,Lj} = \Phi_{Lj,Ki} \quad . \tag{12.3}$$

It is often said that the linear coefficients $\Phi_{Ki}$ vanish by the equilibrium condition, but this is not true when external forces are applied to the crystal, as will be clarified shortly. In the expansion of $\Phi$, the terms quadratic in displacements are called harmonic, and the higher-order terms are anharmonic. So that $\Phi$ remains of order $N$, there is presumably a finite range of internuclear interactions, a range small compared to the size of the crystal, and the potential coefficients of second and higher orders are negligible at distances beyond this range. For physical reasons, the crystal potential cannot depend on the *actual* positions of the nuclei, but only on their *relative* positions, given by the distances $|\mathbf{R}_K + \mathbf{U}_K - \mathbf{R}_L - \mathbf{U}_L|$. But the formulation in terms of the actual positions is more convenient, and the correct physics will be recovered through subsidiary conditions of macroscopic translational and rotational invariance.

The leading term $\Phi_0$ in the potential energy expansion is called the static lattice potential, or the structural potential. We have $\Phi_0 = \Phi(\{\mathbf{R}_K\})$, so that $\Phi_0$ depends on the crystal symmetry and its lattice parameters. For the simplest crystals, *e.g.* fcc, bcc, and dia, there is only one lattice parameter $a$, equivalent to the volume $V$. In such cases we write $\Phi_0^{fcc}(a)$, or $\Phi_0^{fcc}(V)$. The simplest hexagonal or tetragonal crystals have two lattice parameters, $a$ and $c$, equivalent to $V$ and $c/a$. As a general reminder that $\Phi_0$ has such dependences, when the analysis is not restricted to any *particular* crystal structure, we write simply $\Phi_0(V)$.

### *Surface Effects and Equilibrium Conditions*

First consider a finite crystal with free surfaces. The crystal has a distortion region near the surface, and the depth of this region is on the order of the range of the internuclear interaction. Our basic assumption is that surface effects are negligible, which ultimately means that the distortion region is small compared to the size of the crystal, and that the crystal in the interior is perfectly periodic. In principle, surface effects are eliminated merely by applying the theory of lattice statics and lattice dynamics to the perfectly

periodic interior. In practice, separating out the surface effects is not a trivial matter.

Next consider a finite crystal with externally applied forces, and let the forces be applied only to nuclei on the surface, so as to represent applied uniform stresses. The situation is essentially the same as before: there is a distortion region near the surface, and presumably a perfectly periodic crystalline interior. In principle, the applied forces can be varied so as to vary the shape and volume of the crystal, hence to control the lattice parameters of the periodic interior. The crystal with free surfaces is just a particular case of the crystal with applied surface forces.

The force applied to nucleus $K$ is $\mathbf{f}_K$, and such forces are supposed to be derivable from a potential. Let $\mathcal{W}(\{\mathbf{R}_K\})$ be the work done by the applied forces, when they are brought from zero to the current values $\mathbf{f}_K$. Then the total potential of the crystal plus external forces is $\Psi$,

$$\Psi(\{\mathbf{R}_K\}) = \Phi(\{\mathbf{R}_K\}) - \mathcal{W}(\{\mathbf{R}_K\}) \quad . \tag{12.4}$$

The potential $\Psi$ represents a closed system, and in any *real* process in which the equilibrium configuration of the crystal is changed, by changing the external forces, $\Psi$ is conserved. In a *virtual* process, when the crystal is deformed while the external forces are held constant, $\Psi$ is not conserved. Since the work done by the external forces in a virtual displacement is $\Sigma_{Ki} f_{Ki} U_{Ki}$, then from Eqs. (12.2) and (12.4), the expansion of $\Psi$ for virtual displacements is

$$\Psi = \Psi_0 + \sum_K \sum_i (\Phi_{Ki} - f_{Ki}) U_{Ki} + \frac{1}{2} \sum_{KL} \sum_{ij} \Phi_{Ki,Lj} U_{Ki} U_{Lj} + \cdots \quad . \tag{12.5}$$

This is the potential energy for the combined system of crystal plus *constant* externally applied forces.

The equilibrium condition is that the total force on each nucleus must vanish when all nuclei are located at the equilibrium positions $\{\mathbf{R}_K\}$. From Eq. (12.5), this means

$$\Phi_{Ki} - f_{Ki} = 0, \quad \text{for all } K, i \quad . \tag{12.6}$$

Hence $\Psi$ is a stationary function with respect to all displacements from equilibrium. Neither $\Phi$ nor $\mathcal{W}$ is similarly stationary in general. The macroscopic equilibrium conditions are that the total externally applied

force, and total externally applied torque, must vanish:

$$\sum_K f_{Ki} = 0, \quad \text{for all } i \ ; \tag{12.7}$$

$$\sum_K f_{Ki} R_{Kj} \ \text{ is symmetric in } i, j, \ \text{for all } i, j \ . \tag{12.8}$$

Since $\Phi_{Ki} = f_{Ki}$, these conditions are equivalent to the conditions that the crystal must experience no net force, and no net torque, as a result of the interactions among the nuclei, that is, $\Sigma_K \Phi_{Ki} = 0$, and $\Sigma_K \Phi_{Ki} R_{Kj}$ is symmetric in $i, j$.

When material (not necessarily a crystal) is in static equilibrium in the presence of surface forces, such that the stress tensor is constant over the surface, then the stress tensor is constant throughout the material as well. Hence in principle, stresses can be calculated as a surface effect, or as an interior property. We state this as a theorem: Stresses can be calculated by summing the externally applied surface forces, or equivalently, stresses can be calculated in the interior from strain derivatives of the system potential. The proof is as follows. Imagine the material has the macroscopic shape of a cube, with external forces $\mathbf{f}_K$ applied only to surface atoms, and constant over each face of the cube. Components of the applied stress are given by Cartesian components of the applied force per unit area, on each material face. Hence the stresses $\tau_{ij}$ are calculated directly from surface forces. To transform this to an interior evaluation, it is necessary to probe the stress field with an infinitesimal deformation. This is done by making a change $\delta f_{Ki}$, constant on each material face, so that an infinitesimal strain $\delta\eta_{ij}$ results, where $\eta_{ij}$ is homogeneous up to (negligible) surface effects. Then $\delta\mathcal{W} = V\Sigma_{ij}\tau_{ij}\delta\eta_{ij}$, or $\delta\mathcal{W}/\delta\eta_{ij} = V\tau_{ij}$. But this is a real process, in which $\Psi$ is conserved, so $d\Psi/d\eta_{ij} = 0$, which implies $d\Phi/d\eta_{ij} = V\tau_{ij}$. Under the assumption that the surface distortion gives a negligible contribution to the total $\Phi$, then $\Phi$ can be evaluated in the perfectly periodic interior, and the stresses are given by strain derivatives of this function.

A useful theoretical model is the infinite lattice model, where one considers a finite portion of the system, a subcrystal, within an infinite lattice. Obviously the subcrystal is perfectly periodic throughout, and has no surface distortion region. Nevertheless, surface effects are still present in the infinite lattice model. For interactions between nuclei within and without the subcrystal constitute externally applied forces, applied to the

subcrystal nuclei near the surface, within the range of internuclear interactions. Failure to recognize this presence of external forces has led to the incorrect conclusion that the infinite lattice model is valid only under the condition that the stresses must vanish (Born and Huang, 1954, Sec. 23). The present formulation, with explicit treatment of surface forces, is due to Wallace (1965).

### *Invariance and Stability*

For a given crystal structure, the potential energy coefficients must be consistent with symmetries of the lattice. This gives rise to microscopic invariance conditions. A lattice symmetry operation is one which transforms the infinite lattice into itself. Every lattice is invariant under translation by a primitive lattice vector. Hence for a primitive lattice, the potential energy coefficients are invariant under the operation $\mathbf{R}_K \rightarrow \mathbf{R}_K + \mathbf{R}_M$, for all $K$. Many lattices have inversion symmetry, and a primitive lattice is invariant under inversion through any lattice site. Hence for a primitive lattice, the potential energy coefficients coupling an even (odd) number of displacements are even (odd) under the operation $\mathbf{R}_K \rightarrow -\mathbf{R}_K$. For the second order coefficients for a primitive lattice, translation and inversion symmetries lead to complete symmetry in lattice sites, and in Cartesian indices:

$$\Phi_{Ki,Lj} = \Phi_{Li,Kj} = \Phi_{Kj,Li} \quad . \tag{12.9}$$

Similar invariance conditions hold for higher-order potential coefficients.

Beyond translation and inversion symmetries, each lattice has point symmetries specific to its crystal structure, and these symmetries provide additional relations among potential coefficients of each order. In cubic lattices, for example, the point symmetry tells us that $x, y$ and $z$ are equivalent Cartesian indices. The point symmetries are helpful in setting up force constant models. A force constant model is a set of independently variable parameters, representing the complete set of potential coefficients, for a given crystal structure. A second-order force constant model represents the second-order potential coefficients, and hence parameterizes the elastic constants and the phonon spectrum.

The macroscopic invariance conditions are that the total potential $\Psi$ is invariant under arbitrary translation or rotation of the entire system of nuclei and external forces. This is equivalent to requiring that the crystal

potential $\Phi$ is invariant under translation or rotation, without deformation, of the crystal alone. These conditions reduce the dependence of $\Phi$ from the actual nuclear positions, to only the relative nuclear positions, as mentioned earlier, following Eq. (12.3). The derivation is accomplished by requiring that the displacement expansion of $\Phi$, Eq. (12.2), is unaffected in every order by a rigid translation or rigid rotation of the crystal. For a primitive lattice, the second order translational invariance condition is

$$\sum_L \Phi_{Ki,Lj} = 0, \quad \text{for all } K, i, j \quad . \tag{12.10}$$

From the interchange symmetry (12.9), this is the same as

$$\sum_K \Phi_{Ki,Lj} = 0, \quad \text{for all } L, i, j \quad . \tag{12.11}$$

This condition is called the acoustic sum rule, since it makes the frequency of an acoustic phonon go to zero as its wavelength goes to infinity (Sec. 14). The second order rotational invariance condition for a primitive lattice is

$$\sum_L \Phi_{Ki,Lj} R_{Lk} + \Phi_{Kj}\delta_{ik} \ \text{ is symmetric in } j, k, \text{ for all } K, i \quad . \tag{12.12}$$

Again, similar invariance conditions hold for higher order potential coefficients (see problem 12.1).

We can now show how surface effects are eliminated from lattice sums. Each expression (12.10) to (12.12) is a sum over neighbors, and it can be evaluated in the perfectly periodic interior, where it converges with no influence from the surface. Let us place the origin of coordinates at lattice site 0, in the interior: $\mathbf{R}_0 = 0$. Then for example (12.10) with surface effects eliminated becomes

$$\sum_L \Phi_{0i,Lj} = 0, \quad \text{for all } i, j \quad . \tag{12.13}$$

The equilibrium configuration of nuclei with external forces is a stable equilibrium if the total potential $\Psi$ is minimum with respect to arbitrary small displacements of the nuclei from equilibrium. With the equilibrium condition (12.6), the expansion of $\Psi$ to second order is

$$\Psi = \Psi_0 + \frac{1}{2} \sum_{KL} \sum_{ij} \Phi_{Ki,Lj} U_{Ki} U_{Lj} \quad . \tag{12.14}$$

The stability condition is that the homogeneous quadratic form is positive definite, *i.e.* positive for any set of displacements not all zero. For a system of nuclei moving in this potential, this means that all normal vibrational modes, *i.e.* all phonons, must have positive energies. With one exceptional circumstance, all real crystals possess this stability property. That circumstance is where the harmonic potential has some unstable modes, but the crystal is stabilized by the anharmonic potential. An example of such stabilization at elevated temperatures is discussed in Sec. 26.

### *Stresses and Elastic Constants*

For the present application, the external forces are restricted to the surface region, and represent stresses applied to the crystal. Then since the applied forces vanish in the interior, the equilibrium condition (12.6) allows us to write

$$f_{Ki} = \Phi_{Ki} = 0, \quad \text{for all } K, i \text{ in the interior} \quad . \tag{12.15}$$

In an approximation referred to as the *potential approximation*, the crystal potential $\Phi$ is considered an approximation to the thermodynamic state functions:

$$\Phi \approx U; \ \Phi \approx F \quad . \tag{12.16}$$

In fact, as we shall see in Chap. 4, $\Phi$ is a very good approximation to $U$ and $F$ at zero temperature, while $\Phi$ completely misses the thermal contributions to $U$ and $F$. But thermal contributions to stresses and elastic constants are usually small for crystals, so the potential contribution constitutes a leading approximation for stresses and elastic constants.

The commonly used strain parameters, and the different types of elastic coefficients, are defined in Sec. 8. Expansions of $U$ and $F$ in powers of the Lagrangian strains $\eta_{ij}$ are given respectively in Eqs. (8.11) and (8.12), and the potential approximation to *either* expansion is

$$\Phi = \Phi_0 + V \sum_{ij} \tilde{C}_{ij} \eta_{ij} + \frac{1}{2} V \sum_{ijkl} \tilde{C}_{ijkl} \eta_{ij} \eta_{kl} + \cdots \quad . \tag{12.17}$$

The tilde is used to denote the potential approximation to a thermoelastic coefficient, *i.e.* $\tilde{C}_{ij}$ is the potential approximation to $\tau_{ij}$, and $\tilde{C}_{ijkl}$ is the potential approximation to either $C^T_{ijkl}$ or $C^S_{ijkl}$. The algebra is a little simpler if we expand in powers of the displacement gradients $u_{ij}$, in which

the coefficients are the wave propagation coefficients, according to problem 8.3. Hence we write

$$\Phi = \Phi_0 + V \sum_{ij} \tilde{A}_{ij} u_{ij} + \frac{1}{2} V \sum_{ijkl} \tilde{A}_{ijkl} u_{ij} u_{kl} + \cdots \quad . \tag{12.18}$$

The two sets of coefficients are related by (problem 8.3)

$$\tilde{A}_{ij} = \tilde{C}_{ij} \tag{12.19}$$

$$\tilde{A}_{ijkl} = \tilde{C}_{ijkl} + \tilde{C}_{jl}\delta_{ik} \quad . \tag{12.20}$$

Then from the complete Voigt symmetry of the elastic constants, the symmetries of the wave propagation coefficients are found to be

$$\tilde{A}_{ij} = \tilde{A}_{ji} \quad , \tag{12.21}$$

$$\tilde{A}_{ijkl} = \tilde{A}_{klij} \quad , \tag{12.22}$$

$$\tilde{A}_{ijkl} + \tilde{A}_{il}\delta_{jk} = \tilde{A}_{jikl} + \tilde{A}_{jl}\delta_{ik} \quad . \tag{12.23}$$

For a primitive lattice, the nuclear displacements corresponding to the homogeneous strain $u_{ij}$ are given by

$$U_{Ki} = \sum_j u_{ij} R_{Kj} \quad . \tag{12.24}$$

With this, the displacement expansion (12.2) of $\Phi$ becomes an expansion in the $u_{ij}$, and comparison with Eq. (12.18) yields the following for the coefficients:

$$\tilde{A}_{ij} = \frac{1}{V} \sum_K \Phi_{Ki} R_{Kj} \quad , \tag{12.25}$$

$$\tilde{A}_{ijkl} = \frac{1}{V} \sum_{KL} \Phi_{Ki,Lk} R_{Kj} R_{Ll} \quad . \tag{12.26}$$

It is instructive to show that the expressions on the right sides satisfy the symmetries of the $\tilde{A}$ coefficients, written in Eqs. (12.21) – (12.23) (see problem 12.2).

We now wish to eliminate surface effects. First note the coefficients $\tilde{A}_{ij} = \tilde{C}_{ij}$ are the potential approximation to the stresses $\tau_{ij}$. The expression (12.25) for $\tilde{A}_{ij}$ contains *essential* surface contributions, since the $\Phi_{Ki}$ vanish in the interior. In other words, Eq. (12.25) gives $\tilde{A}_{ij}$ as a sum over surface forces. The way to eliminate surface effects from $\tilde{A}_{ij}$ is to first evaluate $\Phi$ in the interior, then set $\tilde{A}_{ij} = V^{-1}(\partial\Phi/\partial u_{ij})$. To eliminate surface effects from the second order coefficients, we first define the combination of $\tilde{A}_{ijkl}$ symmetric in $j, l$:

$$\hat{A}_{ikjl} = \frac{1}{2}\left(\tilde{A}_{ijkl} + \tilde{A}_{ilkj}\right) \quad . \tag{12.27}$$

This coefficient is constructed from Eq. (12.26), translational invariance conditions (12.10) and (12.11) are used to transform to a sum over neighbors, and this sum is evaluated in the interior to find (see problem 12.3)

$$\hat{A}_{ikjl} = -\frac{1}{2V_A}\sum_K \Phi_{0i,Kk} R_{Kj} R_{Kl} \quad . \tag{12.28}$$

Equation (12.20) can be solved for $\tilde{C}_{ijkl}$, and the above two equations can then be used to eliminate surface effects, with the result

$$\tilde{C}_{ijkl} = \hat{A}_{ikjl} + \hat{A}_{jkil} - \hat{A}_{ijkl} - \tilde{C}_{jl}\delta_{ik} - \tilde{C}_{il}\delta_{jk} + \tilde{C}_{kl}\delta_{ij} \quad . \tag{12.29}$$

Equation (12.20) can be used again to eliminate surface effects from $\tilde{A}_{ijkl}$. Finally, the stress-strain coefficients are related to elastic constants in Eq. (8.19), and the corresponding relation in the potential approximation with surface effects eliminated is

$$\begin{aligned} \tilde{B}_{ijkl} \quad = \quad & \hat{A}_{ikjl} + \hat{A}_{jkil} - \hat{A}_{ijkl} \\ & + \frac{1}{2}\left(\tilde{C}_{ik}\delta_{jl} - \tilde{C}_{il}\delta_{jk} + \tilde{C}_{jk}\delta_{il} - \tilde{C}_{jl}\delta_{ik} + 2\tilde{C}_{kl}\delta_{ij} - 2\tilde{C}_{ij}\delta_{kl}\right) \quad . \end{aligned} \tag{12.30}$$

These equations are sometimes required in theoretical work, and they *will* eliminate surface effects (see problem 12.4).

To calculate elastic constants for a nonprimitive lattice, the primitive lattice vectors are displaced according to a homogeneous strain, precisely as in the preceding analysis, and the corresponding motion of the equilibrium positions *within* a unit cell, the sublattice displacements, have to be solved for. The algebra is rather involved, and is given in Born and Huang (1954, Chap. III), and also in *Thermodynamics of Crystals* (Sec. 7).

***Wave Propagation***

The equation of motion for sound waves is derived in Sec. 8, in terms of the wave propagation coefficients. Equation (8.32) is an eigenvalue-eigenvector equation for the velocities $v_s$, and in the potential approximation that equation reads

$$\rho v_s^2 w_{is} = \sum_{jmn} \tilde{A}_{imjn} \hat{k}_m \hat{k}_n w_{js} \ , \quad s = 1, 2, 3, \tag{12.31}$$

where $\rho$ is the crystal density, $\mathbf{k}$ is the wavevector, and $\mathbf{w}_s$ are the eigenvectors. To compare this equation with lattice dynamics, in Sec. 14, we use $\rho = M/V_A$, and $\omega_s = v_s|\mathbf{k}|$, and notice that only the combination of $\tilde{A}_{imjn}$ symmetric in $m, n$ contributes to the sum, so that

$$M\omega_s^2 w_{is} = V_A \sum_{jmn} \hat{A}_{ijmn} k_m k_n w_{js} \ , \tag{12.32}$$

where $\hat{A}_{ijmn}$ is defined in Eq. (12.27). The interior evaluation of $\hat{A}_{ijmn}$ is given by (12.28), hence in (12.32), surface effects are eliminated from the theory of long wavelength sound waves.

Mechanical stability of the crystal against excitation of long wavelength sound waves requires the energy of all such waves to be positive, or

$$\left[\omega_s(\mathbf{k})\right]^2 > 0 \ , \quad \text{for all } \mathbf{k}s \ . \tag{12.33}$$

Notice the condition depends only on the direction of $\mathbf{k}$, not on its magnitude. This is just the long wavelength acoustic part of the complete harmonic stability requirement, that all phonons must have positive energies, as mentioned following Eq. (12.14).

*Problems*

*12.1* Derive the invariance conditions (12.10) – (12.12). These and the equivalent higher-order conditions are derived in *Thermodynamics of Crystals*, p. 64–69.

*12.2* Show the symmetries (12.21) – (12.23) of the $\tilde{A}$ coefficients are satisfied by their lattice definitions in Eqs. (12.25) and (12.26). This is done in *Thermodynamics of Crystals*, p. 75–76.

*12.3* Transform the lattice expression for $\hat{A}_{ikjl}$ to the interior, and hence find Eq. (12.28).

*12.4* Derive Eqs. (12.29) and (12.30). This is done in *Thermodynamics of Crystals*, p. 75–78.

## 13 QUASIHARMONIC PHONONS

### *Historical Note*

From the beginning, the motivation for studying the motion of the atoms in a solid was to understand the thermal energy associated with this motion. The empirical rule of Dulong and Petit, that the specific heat of a solid at room temperature is around 3R per mole, was published in 1819. This property seems to have motivated a long slow development of the idea that the atoms of a solid undergo classical harmonic vibrations. But later, the specific heat of solids was observed to decrease toward zero at low temperatures, and this was explained by Einstein in 1907 as an effect of quantum statistics. Einstein (1907) presumed that the atomic vibrational normal modes have a distribution of frequencies, but he modeled the distribution with a single frequency, and this gave a specific heat curve which is classical at high temperatures, and goes to zero approximately exponentially as temperature goes to zero. But the experimentalists were not satisfied, as it was becoming clear that the low temperature specific heat behavior is actually more like $T^3$. This was explained by Debye in 1912, as due to the presence of vibrational modes which have frequency, hence energy, going to zero. Debye (1912) treated the solid as an isotropic elastic medium, whose vibrational modes are elastic waves quantized in the volume $V$, with one longitudinal and two transverse waves for each wavevector, and with $N$ wavevectors allowed when the volume contains $N$ atoms. This model gives a universal form for the frequency distribution, hence gives a universal curve of specific heat *vs* temperature, scaled for each material by its own characteristic (Debye) temperature, and Debye showed in his original paper that his model gave an excellent account of the measured specific heat for many solids. So well did Debye's elastic continuum model agree with experiment, that it had the effect of removing motivation for further theoretical work for the next twenty years.

At the same time, there was also published a theory which takes into account the (discrete) atomic structure of real solids. This was the paper of Born and von Karman (1912), who solved the prototype lattice dynamics problem of a linear diatomic chain with nearest-neighbor harmonic forces.

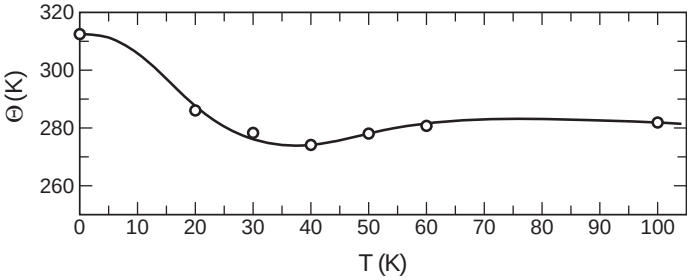


Figure 13.1. Effective Debye temperature $\Theta(T)$ for NaCl. Solid line is from experimental specific heat, and points are the lattice dynamics calculations of Kellermann [from E. W. Kellermann, Proc. R. Soc. Lond. A**178**, 17(1941)].

In the following year they also showed that their atomic model in three dimensions will give the same low temperature $T^3$ behavior of the specific heat as does the Debye model. But every theory is an approximation, and physicists have a strong tendency to use the simplest theory as long as it agrees with experiment. Not until the early 1930s did measured specific heats show deviations from the Debye model. Such deviations were customarily shown in graphs of the effective Debye temperature $\Theta$, as a function of temperature, where $\Theta(T)$ is the characteristic temperature required in a Debye model to fit the experimental specific heat at temperature $T$. The convincing explanation was given by Blackman (1935, 1937), who showed by numerical calculations that atomic models could give variations in $\Theta(T)$, similar to the variations observed in experiments. In other words, the experimental specific heat curves were showing the effect of phonon dispersion. It is interesting to note that Blackman was encouraged in his work by the ubiquitous Born. Finally came Kellermann's calculations on NaCl. Kellermann (1940, 1941) took realistic forces between rigid ions, namely Coulomb interactions between point charges, plus nearest-neighbor central repulsion, and calculated the frequency distribution and hence the specific heat. His result, shown in Fig. 13.1, shows the variation of effective Debye temperature due to phonon dispersion in the NaCl acoustic branches, and the calculation is in beautiful agreement with experiment. With this work, the discipline of lattice dynamics was securely established.

Of the many lattice dynamics calculations which followed, one is of special interest because of its artistic ingenuity. Leighton (1948) wrote down the secular equation for a two-force-constant model for an fcc lattice, and then proceeded to carve the shapes of constant frequency surfaces in

plaster of Paris. By weighing the plaster carvings in air, and in water, Leighton measured the volumes enclosed between successive surfaces, and from this he determined the frequency distribution. Leighton was able to account for phonon dispersion effects in the measured specific heat of silver.

An event of great importance was the announcement by Brockhouse and Stewart (1955, 1958) of the first measurement of a phonon frequency and wavevector by inelastic neutron scattering. Since that time, this technique has provided a great amount of highly accurate information, through the measurement of phonon spectra in a wide variety of crystals. These data allow the most direct test of harmonic lattice dynamics theory, and consequently, the emphasis of theory has shifted away from computing the specific heat, toward detailed studies of the phonon dispersion curves in high symmetry directions. But we can still learn much from highly accurate thermodynamic data. For such data, together with the accurate harmonic lattice dynamics calculations which are possible today, yield a direct measure of anharmonic contributions to thermodynamic functions, as we shall see in Chap. 4.

The development of neutron spectroscopy was recognized by the award of the Nobel Prize in Physics to Bertram Brockhouse in 1994.

### *Lattice Vibration Problem*

In a real material, as we have discussed in Sec. 6, the nuclei are in a state of continual motion, and this motion constitutes the thermal energy of the material. In a crystal, the nuclear motion consists of small vibrations about the equilibrium lattice sites. It is convenient to express this motional problem in terms of the nuclear displacements $\mathbf{U}_K$, and velocities $\dot{\mathbf{U}}_K$. Their commutators are contained in the ordinary position and momentum commutators (see *e.g.* Dirac, 1947),

$$\left[U_{Ki}, M\dot{U}_{Lj}\right] = i\hbar\delta_{KL}\delta_{ij} \quad , \tag{13.1}$$

$$[U_{Ki}, U_{Lj}] = \left[\dot{U}_{Ki}, \dot{U}_{Lj}\right] = 0 \quad . \tag{13.2}$$

The kinetic energy of all the nuclei in the crystal is $\mathcal{K}$,

$$\mathcal{K} = \frac{1}{2}\sum_K \sum_i M\left(\dot{U}_{Ki}\right)^2 \quad . \tag{13.3}$$

The Hamiltonian of the crystal plus external forces is $\mathcal{K} + \Psi$, where $\Psi$ is expanded in powers of the nuclear displacements in Eq. (12.5), and where the equilibrium condition (12.6) holds. To get the Hamiltonian of the crystal alone, we need to add $\mathcal{W}_0$, the work done by external forces in bringing the crystal to its initial equilibrium configuration (structure). Hence the crystal Hamiltonian is

$$\mathcal{H} = \Phi_0 + \mathcal{H}_2 + \Phi_3 + \Phi_4 + \cdots \quad , \tag{13.4}$$

where $\Phi_0$ is the static lattice potential, $\mathcal{H}_2$ is the quasiharmonic vibrational Hamiltonian $\mathcal{K} + \Phi_2$, or

$$\mathcal{H}_2 = \frac{1}{2} \sum_K \sum_i M \left( \dot{U}_{Ki} \right)^2 + \frac{1}{2} \sum_{KL} \sum_{ij} \Phi_{Ki,Lj} U_{Ki} U_{Lj} \quad , \tag{13.5}$$

and where $\Phi_3$ and $\Phi_4$ are potential energy terms of third and fourth order in displacements.

For $\mathcal{H}_2$, the term quasiharmonic is used, instead of harmonic, to remind us that the potential coefficients depend on the crystal volume and lattice parameters. For nearly all real crystals, at all densities, $\mathcal{H}_2$ is the dominant motional part of the crystal Hamiltonian, while the anharmonic terms $\Phi_3 + \Phi_4 + \cdots$ give a relatively small contribution. The anharmonic terms constitute phonon-phonon interactions, which will be studied in Sec. 16.

The analysis of $\mathcal{H}_2$ into a set of normal vibrational modes is presented in Born and Huang (1954, Chap. 4), and also in *Thermodynamics of Crystals*, Chap. 3. The procedure is outlined as follows. One works with a finite subcrystal containing $N$ atoms, within an infinite lattice, and with periodic boundary conditions on the nuclear motion. The lattice sites of the subcrystal, which are equilibrium positions for the nuclei, are denoted $\mathbf{R}_L$ for $L = 1, \cdots, N$. The (infinite) inverse lattice is defined by the vectors $\mathbf{Q}_M$, such that $\mathbf{Q}_M \cdot \mathbf{R}_L = 2\pi n$, where $n$ is an integer. The wavevectors $\mathbf{k}$ consistent with periodic boundary conditions form a grid in inverse lattice space, with $N$ such vectors in one unit cell of the inverse lattice, and this set of $N$ wavevectors forms a complete orthonormal set of planewaves. The condition of orthonormality is

$$\frac{1}{N} \sum_L \exp\left(i(\mathbf{k} - \mathbf{k}') \cdot \mathbf{R}_L\right) = \Delta(\mathbf{k} - \mathbf{k}') \quad . \tag{13.6}$$

The right side is a Kroneker delta, having $\Delta = 1$ if $\mathbf{k} - \mathbf{k}'$ is any reciprocal

lattice vector, including zero, and $\Delta = 0$ otherwise. Since $\mathbf{Q}_M \cdot \mathbf{R}_L = 2\pi n$, then

$$\exp\left(i(\mathbf{k} + \mathbf{Q}_M) \cdot \mathbf{R}_L\right) = \exp(i\mathbf{k} \cdot \mathbf{R}_L) \quad , \tag{13.7}$$

for any $\mathbf{Q}_M$, which tells us that the set of planewaves is identical for the set of $\mathbf{k}$ vectors lying in any unit cell of the inverse lattice. An equivalent complete set of wavevectors is commonly used, namely those in the first Brillouin zone. Notice for a complete set, $\mathbf{k}$ and $\mathbf{k}'$ are not both included if $\mathbf{k} - \mathbf{k}'$ is a nonzero reciprocal lattice vector. This condition eliminates half the vectors on the Brillouin zone surface, with further restrictions on zone edges and corners (geometrical details may be found in *Thermodynamics of Crystals*, App. 1).

Completeness of the wavevector set means that any function $f(\mathbf{R}_L)$ can be represented by the complete set of planewaves:

$$f(\mathbf{R}_L) = \frac{1}{\sqrt{N}} \sum_{\mathbf{k}} g(\mathbf{k}) \exp(i\mathbf{k} \cdot \mathbf{R}_L) \quad , \text{ for every } L \quad . \tag{13.8}$$

This can be inverted with Eq. (13.6), to find

$$g(\mathbf{k}) = \frac{1}{\sqrt{N}} \sum_{L} f(\mathbf{R}_L) \exp(-i\mathbf{k} \cdot \mathbf{R}_L) \quad . \tag{13.9}$$

The completeness relation implied by the last two equations is

$$\frac{1}{N} \sum_{\mathbf{k}} \exp\left(i\mathbf{k} \cdot (\mathbf{R}_L - \mathbf{R}_K)\right) = \delta_{LK} \quad . \tag{13.10}$$

A useful property is that $\mathbf{k} \cdot \mathbf{R}_L$ is invariant under homogeneous deformation of the crystal, for any wavevector $\mathbf{k}$ and any lattice vector $\mathbf{R}_L$.

### *Transformation to Phonons*

Diagonalization of $\mathcal{H}_2 = \mathcal{K} + \Phi_2$ requires simultaneous diagonalization of $\mathcal{K}$ and $\Phi_2$. Since $\mathcal{K}$ is already diagonal in nuclear coordinates, according to Eq. (13.3), we can concentrate on $\Phi_2$. The planewave transformation will bring $\Phi_2$ into block diagonal form, with $N$ dynamical matrices $\mathbf{D}(\mathbf{k})$ arranged along the diagonal. Let us first set out the properties of these matrices.

For a primitive lattice, $\mathbf{D}(\mathbf{k})$ is a $3 \times 3$ matrix whose elements are

$$\mathbf{D}_{ij}(\mathbf{k}) = \frac{1}{MN} \sum_{KL} \Phi_{Ki,Lj} \exp\left(i\mathbf{k} \cdot (\mathbf{R}_L - \mathbf{R}_K)\right) \quad . \tag{13.11}$$

Since the sum over $L$ is the same for every $K$ in the interior, surface effects can be eliminated by setting $K = 0$,

$$D_{ij}(\mathbf{k}) = \frac{1}{M} \sum_{L} \Phi_{0i,Lj} \exp\left(i\mathbf{k} \cdot \mathbf{R}_L\right) \quad . \tag{13.12}$$

The sum is real, since for every $\mathbf{R}_L$ there is a $-\mathbf{R}_L$, so that

$$D_{ij}(\mathbf{k}) = \frac{1}{M} \sum_{L} \Phi_{0i,Lj} \cos(\mathbf{k} \cdot \mathbf{R}_L) \quad . \tag{13.13}$$

Finally, because of the translational invariance condition (12.13), the $L = 0$ term can be separated, to write

$$D_{ij}(\mathbf{k}) = \frac{1}{M} {\sum_{L}}' \Phi_{0i,Lj} [\cos(\mathbf{k} \cdot \mathbf{R}_L) - 1] \quad . \tag{13.14}$$

This last is an especially convenient form for numerical evaluations.

Since $\mathbf{D}(\mathbf{k})$ is a real symmetric matrix, it is diagonalized by an orthogonal matrix of eigenvectors $\mathbf{v}(\mathbf{k}s)$, for $s = 1, 2, 3$, and the eigenvalues $[\omega(\mathbf{k}s)]^2$ are real. The set of equations which determine the eigenvalues and eigenvectors is

$$\sum_{j} D_{ij}(\mathbf{k}) v_j(\mathbf{k}s) = [\omega(\mathbf{k}s)]^2 v_i(\mathbf{k}s) \quad , \quad \text{for } s = 1, 2, 3 \quad . \tag{13.15}$$

The eigenvectors then satisfy

$$\sum_{i} v_i(\mathbf{k}s) v_i(\mathbf{k}s') = \delta_{ss'} \quad , \quad \text{orthonormality} \quad ; \tag{13.16}$$

$$\sum_{s} v_i(\mathbf{k}s) v_j(\mathbf{k}s) = \delta_{ij} \quad , \quad \text{completeness} \quad . \tag{13.17}$$

Also since $\mathbf{D}(-\mathbf{k}) = \mathbf{D}(\mathbf{k})$, from Eq. (13.13), the eigenvalues and eigenvectors can be chosen to have the same symmetry:

$$[\omega(-\mathbf{k}s)]^2 = [\omega(\mathbf{k}s)]^2 \quad , \tag{13.18}$$

$$v_i(-\mathbf{k}s) = v_i(\mathbf{k}s) \quad . \tag{13.19}$$

With these results we can proceed to diagonalize $\mathcal{H}_2$.

Let us define the linear transformation between the displacements $U_{Li}$ and the (complex) phonon coordinates $q(\mathbf{k}s)$,

$$U_{Li} = \frac{1}{\sqrt{NM}} \sum_{\mathbf{k}s} q(\mathbf{k}s) \exp(i\mathbf{k}\cdot\mathbf{R}_L) v_i(\mathbf{k}s) \quad . \tag{13.20}$$

The time derivative is

$$\dot{U}_{Li} = \frac{1}{\sqrt{NM}} \sum_{\mathbf{k}s} \dot{q}(\mathbf{k}s) \exp(i\mathbf{k}\cdot\mathbf{R}_L) v_i(\mathbf{k}s) \quad . \tag{13.21}$$

These equations are inverted to give

$$q(\mathbf{k}s) = \sqrt{\frac{M}{N}} \sum_{Li} U_{Li} \exp(-i\mathbf{k}\cdot\mathbf{R}_L) v_i(-\mathbf{k}s) \quad , \tag{13.22}$$

$$p(\mathbf{k}s) = \sqrt{\frac{M}{N}} \sum_{Li} \dot{U}_{Li} \exp(i\mathbf{k}\cdot\mathbf{R}_L) v_i(\mathbf{k}s) \quad , \tag{13.23}$$

where we have defined the phonon momentum $p(\mathbf{k}s)$ according to

$$p(\mathbf{k}s) = \dot{q}(-\mathbf{k}s) \quad . \tag{13.24}$$

The commutators are then calculated from the position and momentum commutators given by Eqs. (13.1) and (13.2), with the results (see problem 13.1)

$$[q(\mathbf{k}s), p(\mathbf{k}'s')] = i\hbar\Delta(\mathbf{k}-\mathbf{k}')\delta_{ss'} \quad , \tag{13.25}$$

$$[q(\mathbf{k}s), q(\mathbf{k}'s')] = [p(\mathbf{k}s), p(\mathbf{k}'s')] = 0 \quad . \tag{13.26}$$

These commutators show that $q(\mathbf{k}s)$ and $p(\mathbf{k}s)$ are conjugate, for each $\mathbf{k}s$. Complex conjugation of these operators is accomplished from Eqs. (13.22) and (13.23), with (13.19),

$$q(\mathbf{k}s)^* = q(-\mathbf{k}s), \quad p(\mathbf{k}s)^* = p(-\mathbf{k}s) \quad . \tag{13.27}$$

Since $\mathbf{k}$ and $\mathbf{k}'$ are from the same complete set, then $\mathbf{k}-\mathbf{k}'=\mathbf{Q}_M$ only for $\mathbf{Q}_M=0$, so $\Delta(\mathbf{k}-\mathbf{k}')=\delta_{\mathbf{k},\mathbf{k}'}$ in Eq. (13.25).

Diagonalization of $\mathcal{H}_2$ is accomplished by inserting the displacement transformation (13.20) in $\Phi_2$, and its time derivative (13.21) in $\mathcal{K}$. The result is denoted $\mathcal{H}_{ph}$, where (see problem 13.2)

$$\mathcal{H}_{ph}=\frac{1}{2}\sum_{\mathbf{k}s}\left\{|p(\mathbf{k}s)|^2+[\omega(\mathbf{k}s)]^2|q(\mathbf{k}s)|^2\right\} \quad . \tag{13.28}$$

Thus $\mathcal{H}_{ph}$ is a set of $3N$ independent harmonic oscillator Hamiltonians, with each oscillator (phonon) labeled by the index set $\mathbf{k}s$, and having frequency $\omega(\mathbf{k}s)$. In the presence of a given phonon $\mathbf{k}s$, Eq. (13.20) tells us that the magnitude of the nuclear displacements corresponds to a planewave of wavevector $\mathbf{k}$, and the direction of the nuclear displacements is given by the polarization vector $\mathbf{v}(\mathbf{k}s)$.

### *Properties of Phonons*

For any crystal lattice, primitive or nonprimitive, there are exactly three phonons at $\mathbf{k}=0$ which have zero frequency. This is shown explicitly for a primitive lattice by Eq. (13.14), which gives $\mathbf{D}(\mathbf{k}=0)=0$. These three phonons represent uniform translation of the crystal, and this motion is specifically excluded from lattice dynamics theory. Hence it is understood that the zero-frequency phonons at $\mathbf{k}=0$ are excluded from all Brillouin zone sums, and from all other parts of the analysis.

The condition that the crystal be stable against all possible small nuclear displacements is that the second-order potential $\Phi_2$ be positive definite, as discussed following Eq. (12.14). In phonon coordinates, $\Phi_2$ is

$$\Phi_2=\frac{1}{2}\sum_{\mathbf{k}s}[\omega(\mathbf{k}s)]^2|q(\mathbf{k}s)|^2 \quad . \tag{13.29}$$

Since the $q(\mathbf{k}s)$ are independent modes, and since $|q(\mathbf{k}s)|^2$ is positive, then $\Phi_2>0$ if and only if

$$[\omega(\mathbf{k}s)]^2>0 \quad , \quad \text{for all } \mathbf{k}s \quad . \tag{13.30}$$

We will always take the positive square root, so that $\omega(\mathbf{k}s)>0$ by convention.

The sum of the eigenvalues of $\mathbf{D}(\mathbf{k})$ is $\Sigma_i D_{ii}(\mathbf{k})$. From Eq. (13.12) for $D_{ij}(\mathbf{k})$, the Cartesian trace can be summed over the Brillouin zone to give

the average of all phonon frequencies squared (see also problem 13.3),

$$\langle\omega^2\rangle_{BZ} = \frac{1}{3N}\sum_{\mathbf{k}s}[\omega(\mathbf{k}s)]^2 = \frac{1}{3M}\sum_i \Phi_{0i,0i} \quad . \tag{13.31}$$

Here we introduced the notation $\langle\cdots\rangle_{BZ}$ for an average over the Brillouin zone. Again the translational invariance condition (12.13) changes this to (compare Eq. (13.14))

$$\langle\omega^2\rangle_{BZ} = -\frac{1}{3M}\sum_L{}' \sum_i \Phi_{0i,Li} \quad . \tag{13.32}$$

This provides a simple expression for the second moment of the phonon frequency distribution, and the formula is useful for evaluating a global measure of the phonons without going through a complete lattice dynamics calculation.

Again for any crystal lattice, phonon theory is parameterized by the crystal structure and its lattice parameters. In the normal theoretical procedure, these parameters are the independent variables, and the phonon frequencies and eigenvectors depend on them. Hence the phonon free energy, and all other averaged phonon properties, depend explicitly on the crystal structure and its lattice parameters. All of this dependence is understood within the term *phonon*, even when the reminder *quasiharmonic* is nowhere in sight. Derivatives of the phonon frequencies with respect to crystal parameters have come to be called phonon Grüneisen parameters. An example is the set of strain derivatives $\partial\omega(\mathbf{k}s)/\partial\eta_{ij}$, appropriate when the crystal undergoes a homogeneous deformation. For cubic crystals under isotropic pressure, including zero pressure, there is only one crystal parameter, which can be taken as $V$. Then the Grüneisen parameters are the volume derivatives $\gamma(\mathbf{k}s)$, defined by

$$\gamma(\mathbf{k}s) = -\frac{d\ln\omega(\mathbf{k}s)}{d\ln V} \quad . \tag{13.33}$$

More extensive discussion of phonon Grüneisen parameters is provided in *Thermodynamics of Crystals*.

Lattice dynamics for nonprimitive lattices follows the same principles, step by step, as those outlined above for primitive lattices. A nonprimitive lattice is a space filling array of identical unit cells, where the unit cells define a primitive lattice, and the sites within a unit cell are located at $n$ prescribed sublattice vectors. For a crystal of $N$ unit cells, there are $3nN$

spatial degrees of freedom. Some common crystal structures with $n = 2$ are dia, hcp, fct, and bct. The inverse lattice, and the complete set of $\mathbf{k}$ vectors, belong to the primitive lattice, and the dynamical matrices $\mathbf{D}(\mathbf{k})$ are $3n \times 3n$ Hermitian matrices, whose eigenvalues are $[\omega(\mathbf{k}s)]^2$ for $s = 1, \cdots, 3n$. For a given $\mathbf{k}s$, the phonon eigenvector displays the direction and relative magnitude of the motion of each nucleus in the unit cell, superimposed on the planewave motion of the entire cell. The set of phonons for a given $s$ and all $\mathbf{k}$ is a phonon branch. There are three acoustic branches, defined as those for which $\omega(\mathbf{k}s) \to 0$ as $|\mathbf{k}| \to 0$, and these will be discussed in Sec. 14. The remaining $3(n-1)$ branches are optic, with $\omega(\mathbf{k}s) > 0$ at $\mathbf{k} = 0$. The photon dispersion curve $\omega = c|\mathbf{k}|$ crosses the optic branches at extremely small $|\mathbf{k}|$, hence photons often interact with optic phonons at $\mathbf{k} \approx 0$.

*Problems*

*13.1* Invert the displacement expansion to find Eqs. (13.22) and (13.23) for the phonon coordinates and momenta. Then derive the phonon commutators (13.25) and (13.26).

*13.2* Derive Eq. (13.28) for the quasiharmonic phonon Hamiltonian. Notice it helps to eliminate surface effects in the transformed $\Phi_2$.

*13.3* From Eq. (13.11) for $\mathbf{D}(\mathbf{k})$, show $\Sigma_{\mathbf{k}} Tr\mathbf{D}(\mathbf{k}) = \Sigma_K \nabla_K^2 \Phi$. Then eliminate surface effects to recover Eq. (13.31).

## 14 THEORY AND EXPERIMENT

### *Long Wavelength Acoustic Waves*

Here we shall study the long wavelength acoustic phonons, and will demonstrate their identity with sound waves in the potential approximation. Long wavelength phonons are isolated by making an expansion of the dynamical matrix for small $\mathbf{k}$. For a primitive lattice, the leading term in the expansion of Eq. (13.14) for $D_{ij}(\mathbf{k})$ is

$$D_{ij}(\mathbf{k}) = -\frac{1}{2M} {\sum_L}' \Phi_{0i,Lj} (\mathbf{k} \cdot \mathbf{R}_L)^2 \quad . \tag{14.1}$$

When this is used in the eigenvalue-eigenvector equation (13.15), it is

$$M[\omega(\mathbf{k}s)]^2 v_i(\mathbf{k}s) = -\frac{1}{2}\sum_L{}' \sum_{jmn} \Phi_{0i,Lj} R_{Lm} R_{Ln} k_m k_n v_j(\mathbf{k}s) \quad . \tag{14.2}$$

The prime can be removed from the $\Sigma'_L$, because $\mathbf{R}_0 = 0$, and then the wave propagation coefficient $\hat{A}_{ijmn}$ appears, by virtue of Eq. (12.28), allowing us to write

$$M[\omega(\mathbf{k}s)]^2 v_i(\mathbf{k}s) = V_A \sum_{jmn} \hat{A}_{ijmn} k_m k_n v_j(\mathbf{k}s) \quad . \tag{14.3}$$

This equation describes waves with $\omega(\mathbf{k}s)$ proportional to $|\mathbf{k}|$, hence it is convenient to define the wave velocities $c(\hat{\mathbf{k}}s)$, according to

$$\omega(\mathbf{k}s) = c(\hat{\mathbf{k}}s)|\mathbf{k}| \quad , \quad \text{for small } |\mathbf{k}| \text{ and } s = \text{ acoustic} \quad . \tag{14.4}$$

So the long wavelength acoustic phonons are dispersionless, and have velocities which depend on the wavevector direction. For a given crystal, and for each acoustic branch, the velocity $c(\hat{\mathbf{k}}s)$ observes the crystal symmetry in its dependence on the direction $\hat{\mathbf{k}}$. Ultimately, the reason for the linear $|\mathbf{k}|$ dependence in Eq. (14.4) is the translational invariance condition (12.13), which was used in transforming the dynamical matrix from (13.13) to (13.14).

Essentially the same procedure can be carried out for a nonprimitive lattice, with the complication that sublattice displacements are induced by long wavelength phonons, but when the sublattice displacements are solved for and eliminated, precisely the same Equation (14.3) results for the long wavelength acoustic phonons. Again the macroscopic translational invariance condition, or acoustic sum rule, ensures the property (14.4) for the three acoustic branches. For the optic phonons at $\mathbf{k} = 0$, the homogeneous strains are zero, but the sublattice displacements are not, and the motion corresponds to the sublattices remaining rigid and vibrating with respect to one another. Extensive discussions of the long wavelength solutions may be found in Born and Huang (1954), and in *Thermodynamics of Crystals.*

The equation (14.3) for long wavelength acoustic phonons is identical to (12.32) for sound waves in the potential approximation. The same result holds for nonprimitive lattices, and was discussed by Born and Huang (1954) as the equivalence between the methods of long waves and homogeneous deformation. The physical meaning is, for wavelength long compared

to the range of internuclear forces, the process within an acoustic phonon is nothing but a slowly oscillating homogeneous deformation. The equivalence holds only in the leading order of theory, but is important in crystal physics because it is the origin of approximate relations among physical phonons, sound waves, and low temperature thermodynamic quantities. We shall endeavor to clarify these relations, here and in the following sections. Here is a summary of modifications to the equivalence of long waves and homogeneous deformation, in real crystals.

(a) At zero temperature, a system resides in its groundstate, hence at $T = 0$ the Helmholtz free energy, the thermodynamic internal energy, and the groundstate energy are all the same function of the crystal structure. This function serves as the potential for long wavelength acoustic excitations, hence at $T = 0$ the adiabatic sound waves, the isothermal sound waves, and the long wavelength acoustic phonons are the same. This result was demonstrated for a primitive lattice, by applying anharmonic perturbation theory to all orders, by Götze (1967).

(b) At finite temperatures, adiabatic and isothermal sound waves in the potential approximation, and long wavelength acoustic phonons in the harmonic approximation, are the same for any crystal. The following results are derived in leading order anharmonic perturbation theory (*Thermodynamics of Crystals*, Sec. 17), and presumably hold in all orders of anharmonicity, for any crystal at any temperature: Adiabatic and isothermal sound waves and long wavelength acoustic phonons retain the property $\omega(\mathbf{k}s) \propto |\mathbf{k}|$, with one longitudinal and two transverse polarizations for each allowed $\mathbf{k}$. At a given $\mathbf{k}s$, the adiabatic frequency is greater than the isothermal frequency, while there is no general rule for the relative value of the acoustic phonon frequency.

(c) At finite temperatures, experimental sound waves are presumably adiabatic, and the properties of experimental sound waves can in principle be calculated exactly from strain derivatives of the internal energy $U$, or from strain derivatives of the free energy $F$, together with isothermal to adiabatic corrections. On the other hand, phonons are measured by inelastic neutron scattering, and beyond the leading (harmonic) order of theory, the interpretation of these experiments is imprecise, so that no exact relation between experimental phonons and sound waves is possible in principle. This point emerges from the neutron scattering analysis of Ambegaokar, Conway, and Baym (1965).

***Nearly-Free-Electron Metals***

The form of the crystal potential $\Phi(\{\mathbf{r}_K\})$ for the nearly-free-electron metals, derived in Eq. (5.54), is

$$\Phi = \Omega(V) + \frac{1}{2}{\sum_{KL}}' \phi(|\mathbf{r}_K - \mathbf{r}_L|; V) \quad . \tag{14.5}$$

It is instructive to apply this potential function to the lattice statics and lattice dynamics theories of Secs. 12 and 13. Let us do this for a primitive cubic crystal under isotropic pressure $P$, so the stress tensor in the potential approximation is

$$\tilde{C}_{ij} = -\tilde{P}\delta_{ij} \quad ; \quad \tilde{P} = -\frac{d\Phi_0}{dV} \quad . \tag{14.6}$$

For cubic symmetry, there are three independent elastic constants $\tilde{C}_{\alpha\beta}$, and three independent stress-strain coefficients $\tilde{B}_{\alpha\beta}$, related through

$$\tilde{B}_{11} = \tilde{C}_{11} - \tilde{P}, \quad \tilde{B}_{12} = \tilde{C}_{12} + \tilde{P}, \quad \tilde{B}_{44} = \tilde{C}_{44} - \tilde{P} \quad . \tag{14.7}$$

The bulk modulus is

$$\tilde{B} = \frac{1}{3}\left(\tilde{B}_{11} + 2\tilde{B}_{12}\right) = -V\frac{d\tilde{P}}{dV} \quad . \tag{14.8}$$

For the homogeneous deformation calculation, the potential is $\Phi(\{\mathbf{R}_K\})$, and we can set $\mathbf{R}_L = 0$ in $\phi(|\mathbf{R}_K - \mathbf{R}_L|; V)$, to write

$$\Phi = \Omega(V) + \frac{1}{2}N{\sum_{K}}' \phi(|\mathbf{R}_K|; V) \quad . \tag{14.9}$$

Two procedures are available for evaluating the pressure and elastic constants: (a) one can use the chain rule to differentiate $\Phi$ with respect to $\eta_{ij}$ and $V$, as in Sec. 10, or (b) one can differentiate $\Phi$ with respect to the three Fuchs strains to find three independent combinations of $\tilde{B}_{\alpha\beta}$ (see Wallace, 1969a, or *Thermodynamics of Crystals*, p. 326). Abbreviations for distance and volume derivatives are listed in Eqs. (10.23), where for example $\phi' = R(\partial\phi/\partial R)$, and $\phi^* = V(\partial\phi/\partial V)$, and here we use the abbreviation $\phi_K = \phi(|\mathbf{R}_K|; V)$. The following results are obtained (see problem 14.1).

$$V\tilde{P} = -\Omega^* - \frac{1}{2}N{\sum_{K}}' \left(\phi_K^* + \frac{1}{3}\phi_K'\right) \quad , \tag{14.10}$$

$$V\tilde{B} = \Omega^{**} + \frac{1}{2}N{\sum_K}' \left[\phi_K^{**} + \frac{2}{3}\phi_K'^{*} + \frac{1}{9}\left(\phi_K'' - 2\phi_K'\right)\right] \quad , \tag{14.11}$$

$$V(\tilde{B}_{11}-\tilde{B}_{12}) = \frac{1}{2}N{\sum_K}' \left[\frac{2}{3}\phi_K' + (\phi_K'' - \phi_K')(\hat{R}_{Kx}^4 - \hat{R}_{Kx}^2\hat{R}_{Ky}^2)\right] \quad , \tag{14.12}$$

$$V\tilde{B}_{44} = \frac{1}{2}N{\sum_K}' \left[\frac{1}{3}\phi_K' + (\phi_K'' - \phi_K')\hat{R}_{Kx}^2\hat{R}_{Ky}^2)\right] \quad . \tag{14.13}$$

The first two coefficients, $V\tilde{P}$ and $V\tilde{B}$, represent pure volumetric strain, while the last two *shear* constants represent pure volume-conserving shear strains. If we return to Eqs. (10.25) and (10.26), and there set $T = 0$ and omit the fluctuations, and evaluate all functions of $\{\mathbf{r}_K\}$ at the lattice sites $\{\mathbf{R}_K\}$, for a primitive cubic lattice, then those formulas reduce to the static lattice results above. Notice the combinations in (14.11) and (14.12) can be solved for $\tilde{B}_{11}$ and $\tilde{B}_{12}$ separately.

In lattice dynamics, phonons are solutions of the harmonic nuclear motion problem, subject to the crystal having a fixed volume, and periodic boundary conditions. With these boundary conditions, the volume dependence of $\Phi$ is irrelevant, and only the distance dependence in $\phi(r;V)$ is significant. For a primitive lattice, the dynamical matrix evaluated in the interior is written in Eq. (13.14), and with $\Phi\{\mathbf{r}_K\})$ given by (14.5), one finds

$$MD_{ij}(\mathbf{k}) = {\sum_K}' \left[\frac{\phi_K'}{R_K^2}\delta_{ij} + \frac{(\phi_K'' - \phi_K')R_{Ki}R_{Kj}}{R_K^4}\right][1 - \cos(\mathbf{k}\cdot\mathbf{R}_K)] \quad . \tag{14.14}$$

The small-$\mathbf{k}$ expansion leads to the equation of motion (14.3) for long wavelength acoustic phonons, where the wave propagation coefficients are given by

$$V\hat{A}_{ijmn} = \frac{1}{2}N{\sum_K}' \left[\phi_K'\delta_{ij} + (\phi_K'' - \phi_K')\hat{R}_{Ki}\hat{R}_{Kj}\right]\hat{R}_{Km}\hat{R}_{Kn} \quad . \tag{14.15}$$

The last two equations are valid for any primitive lattice, not necessarily cubic. Now Eq. (12.30) is solved for the three cubic-lattice $\tilde{B}_{\alpha\beta}$, in terms

of $\hat{A}_{ijmn}$, and the results can be put in the form (see problem 14.2)

$$V\tilde{B} = \frac{1}{2}N{\sum_K}' \left[\frac{1}{9}(\phi''_K - 2\phi'_K)\right] \quad , \tag{14.16}$$

$$V(\tilde{B}_{11}-\tilde{B}_{12}) = \frac{1}{2}N{\sum_K}' \left[\frac{2}{3}\phi'_K + (\phi''_K - \phi'_K)(\hat{R}^4_{Kx} - \hat{R}^2_{Kx}\hat{R}^2_{Ky})\right] \quad , \tag{14.17}$$

$$V\tilde{B}_{44} = \frac{1}{2}N{\sum_K}' \left[\frac{1}{3}\phi'_K + (\phi''_K - \phi'_K)\hat{R}^2_{Kx}\hat{R}^2_{Ky}\right] \quad . \tag{14.18}$$

Again these three combinations are equivalent to the three independent $\tilde{B}_{\alpha\beta}$.

The above equations for the two shear coefficients, from the method of long waves, are precisely the same as the homogeneous deformation equations (14.12) and (14.13). But the corresponding equations (14.16) and (14.11) for the bulk modulus are not identical, and they will be the same only if

$$\Omega^{**} + \frac{1}{2}N{\sum_K}' \left(\phi^{**}_K + \frac{2}{3}\phi'^{*}_K\right) = 0 \quad . \tag{14.19}$$

Notice this function arises entirely from the explicit volume dependence of the potential $\Phi(\{\mathbf{r}_K\})$. We shall now discuss the nature of volume-dependent potentials in condensed matter, with particular reference to the equivalence of the methods of long waves and homogeneous deformation.

### *Note on Volume Dependent Potentials*

The general arguments here apply to any condensed matter phase, crystal, amorphous solid, or liquid. Of course, the dependence of potentials in condensed matter is on density $N/V$, not on $V$ alone. In a real material, the density dependence can only be local, and reflects a dependence on the mean density over the range of effective forces. Hence within a very long wavelength wave, the interatomic potentials at each location correspond to the density of the material at that location.

The same property is supposed to be present in theoretical potentials. If we could compute $\Phi(\{\mathbf{r}_K\})$ for a very large system with a slowly varying density, then $\Phi(\{\mathbf{r}_K\})$ should contain the correct local-density dependence

of the interatomic potentials. Or, if we compute $\Phi(\{\mathbf{r}_K\})$ for the same $N$-atom system at two different volumes, then the entire many-atom potential function will be different for the two volumes. Suppose we compute the static lattice potential $\Phi_0$, and some phonon dispersion curves, for a system representing a crystal of a given element, at different values of $V/N$. The results will certainly be volume dependent, and if we fit a model form for $\Phi(\{\mathbf{r}_K\})$ to these results, for example the form given in Eq. (14.5), then we will find the explicit $V$ dependence indicated in that equation. So when we apply condensed matter theory to materials under compression, we must deal with volume dependent potentials, and the equivalence of long waves and homogeneous deformation, as expressed for example by Eq. (14.19), will be an important theoretical constraint.

A special subtlety arises from the use of pseudopotential perturbation theory. The volume dependence in Eq. (14.5) comes from several sources, including the volume dependences of the Fermi wavevector $f$ and the exchange-correlation parameter $\xi$, as mentioned following Eqs. (5.53) for $\phi(r;V)$ and (5.55) for $\Omega(V)$. These volume dependences contribute to $V\tilde{B}$ as calculated from homogeneous deformation, but not as calculated from long waves. But that information *would* appear in the long waves calculation, if the dynamical matrix were expressed to fourth order in the pseudopotential, and indeed for this very reason, certain fourth-order contributions to the dynamical matrix were worked out in *Thermodynamics of Crystals* (p. 336–340). But pseudopotential perturbation theory is approximate from the outset, and rather than carry it to complicated high orders, it is sensible to adjust the model parameters in low order, so as to satisfy Eq. (14.19). Since $\xi$ controls the compressibility of the valence electron system, it is natural to adjust this parameter to achieve agreement between the long waves and homogeneous deformation expressions for $V\tilde{B}$. This is the procedure used for Al by Sraub *et al.* (1994), as mentioned in Sec. 5.

The equivalence of long waves and homogeneous deformation will be automatically satisfied when $\Phi(\{\mathbf{r}_K\})$ has the correct physical properties. This means the effective internuclear potentials in $\Phi(\{\mathbf{r}_K\})$ must depend on some *local measure* of the material density, and not on the macroscopic average density. In pseudopotential perturbation theory, for example, the Fermi wavevector $f$, the exchange-correlation parameter $\xi$, and the parameters in the core potential $w_c(r)$, must all be local parameters, depending on the local material density. Initial theoretical work on this formulation can

be found in *Thermodynamics of Crystals*, pp. 313 – 315, and in Ashcroft (1990).

### *Theory and Experiment for Elastic Constants*

Sound velocities in crystals are measured to high accuracy by ultrasonic experiments. Errors are commonly 1 part in $10^4$, and are often much smaller. Pressure derivatives are also measured accurately, as well as derivatives with respect to anisotropic stresses. Excellent data compilations are given by Simmons and Wang (1971), and by Hearmon (1969). Experimental results continue to appear in the literature. One has to be careful about the meaning of reported pressure derivatives, and stress derivatives in general. What is reported as "$dC_{\alpha\beta}/dP$" is often $dB_{\alpha\beta}/dP$, and for a cubic crystal, for example, the two quantities differ by $\pm 1$, which can easily amount to 30% or so. There is room here for heroic work in straightening out the experimental data base. Extensive discussion of the interpretation of experiments is provided by Thurston and Brugger (1964), Brugger (1965), and Wallace (1970).

The major contribution to theoretical elastic constants arises from the potential approximation. Vibrational contributions are small, but not smaller than experimental errors, and sometimes not smaller than theoretical errors. Vibrational effects in the overall comparison of theory and experiment are discussed in Secs. 17 and 19.

In the old days, theoretical elastic constants for pseudopotential models of Na and K were compared with experiment, and those comparisons are reproduced here in Table 14.1. The experimental constants are evaluated at zero temperature and pressure, while the theoretical constants are from homogeneous deformation calculations, at the same temperature and pressure in the potential approximation. The model has been adjusted to reproduce the experimental volume at $\tilde{P} = 0$, and the experimental bulk modulus. For Na and K together, the calculated $\tilde{B}_{11}$, $\tilde{B}_{12}$, and $\tilde{B}_{44}$ differ from experiment by $2 - 10\%$, with an average error of 5%. This accuracy is comparable to current density functional calculations. The shear coefficient $\tilde{B}_{11} - \tilde{B}_{12}$ is especially small for the alkali metals, and that property is also captured by the pseudopotential model. In calibrating the model, the parameter $\xi$ was determined from the compressibility of the uniform electron gas, and was not adjusted to achieve agreement between long waves and homogeneous deformation. Hence there is a difference, which can be

denoted

$$\Delta = V_A\tilde{B} \text{ (homogeneous deformation)} - V_A\tilde{B} \text{ (long waves)} \quad . \qquad (14.20)$$

The quantity on the left side of Eq. (14.19) is $N\Delta$. Notice the homogeneous deformation calculation of $V_A\tilde{B}$ is correct to a higher order in the pseudopotential than is the long waves calculation. Values of $\Delta$ are also listed in Table 14.1, and these are rather small, being 6–8% of $V_A\tilde{B}$, hence indicating a rapid convergence of pseudopotential perturbation theory for Na and K. The theoretical pressure derivatives $d\tilde{B}_{\alpha\beta}/d\tilde{P}$ are also in excellent agreement with experiment, having an average error of 4%. For more details see Wallace (1969a), or *Thermodynamics of Crystals*, Sec. 34.

Table 14.1. Comparison of pseudopotential theory with experiment for the stress-strain coefficients of bcc Na and K, at zero temperature and pressure. Units are Ry/atom.

| | Na | | K | |
|---|---|---|---|---|
| Quantity | Theory | Experiment | Theory | Experiment |
| $V_A\tilde{B}$ | 0.129 | 0.129 | 0.121 | 0.121 |
| $V_A\tilde{B}_{11}$ | 0.139 | 0.145 | 0.131 | 0.138 |
| $V_A\tilde{B}_{12}$ | 0.124 | 0.121 | 0.116 | 0.113 |
| $V_A\tilde{B}_{44}$ | 0.094 | 0.104 | 0.087 | 0.094 |
| $V_A(\tilde{B}_{11} - \tilde{B}_{11})$ | 0.015 | 0.024 | 0.015 | 0.025 |
| $\Delta$ | –0.008 | | –0.010 | |

Density functional theory has been used for *ab initio* homogeneous deformation calculations for many crystals. For a primitive lattice, the procedure is to calculate the electronic groundstate energy as a function of the magnitude of a given unit-cell strain, then numerically differentiate the energy *vs* strain curve to obtain a component of stress *vs* strain, and numerically differentiate again to obtain an elastic coefficient. For a nonprimitive lattice, the procedure is the same, except at each value of the unit-cell strain, the nuclei within the cell are moved to locations which minimize the groundstate energy. This energy minimization gives the sublattice vectors as unique functions of strain, and is equivalent to solving for the sublattice displacements in the formal theory of homogeneous deformation, as mentioned in Sec. 12. Common practice is to compare these density functional calculations, which represent the potential approximation, with the exper-

imental crystal structure and lattice parameters, and elastic constants, at room temperature and zero pressure. Sometimes the comparison is made with experiment at zero temperature. The results are exemplified by a series of papers on the 3d, 4d, and 5d transition metals, where agreement with experimental elastic constants is in most cases within 10% (Söderlind *et al*, 1993, 1994; Fast *et al*, 1995).

### *Theory and Experiment for Phonons*

The early pseudopotential perturbation models for the alkali metals contain three parameters, and were calibrated by fitting to experimental data for the binding energy, the volume at zero pressure, and the bulk modulus, all at $T = 0$. Within this procedure, there was still enough room for adjustment to fit the experimental $\langle\omega^2\rangle_{BZ}$ exactly, and then the pseudopotential parameters were tightly constrained. The pseudopotential expression for $\langle\omega^2\rangle_{BZ}$ is given in problem 14.3. Comparison of the theoretical phonon dispersion curves with inelastic neutron scattering experiments is shown in Fig. 14.1 for Na, and Fig. 14.2 for K. The discrepancies between theory and experiment, apparent in these figures, can guide us to improvements in our models. On the other hand, the overall accuracy of those early model theories is comparable to what can be achieved by current density functional calculations. The one-parameter model for phonon dispersion curves of Al is shown in Fig. 5.1. For more details see Wallace (1968, 1969b), or *Thermodynamics of Crystals*, Sec. 34.

Several procedures have been developed for *ab initio* density functional calculations of phonon frequencies. The agreement with experiment reaches the 5% level at best, not far from the experimental accuracies of say 1–5%. Phonon dispersion curves were calculated in linear response theory for Si and Ge by Giannozzi *et al.* (1991), and for Au by Quong (1994). A supercell method was used to calculate the internuclear force constants, and then the dispersion curves, for Rh by Heid, Bohnen, and Ho (1998). Frozen phonon calculations are an extension of homogeneous deformation calculations. A supercell is prescribed, large enough to contain half the phonon wavelength, and the electronic groundstate energy is calculated as a function of the phonon amplitude. The second derivative of the energy *vs* amplitude curve is $M\omega^2$. It is necessary to know the phonon eigenvector in advance, but for $\mathbf{k}$ along symmetry directions, the eigenvector is determined by symmetry arguments. Four zone boundary phonons for Al at several volumes were

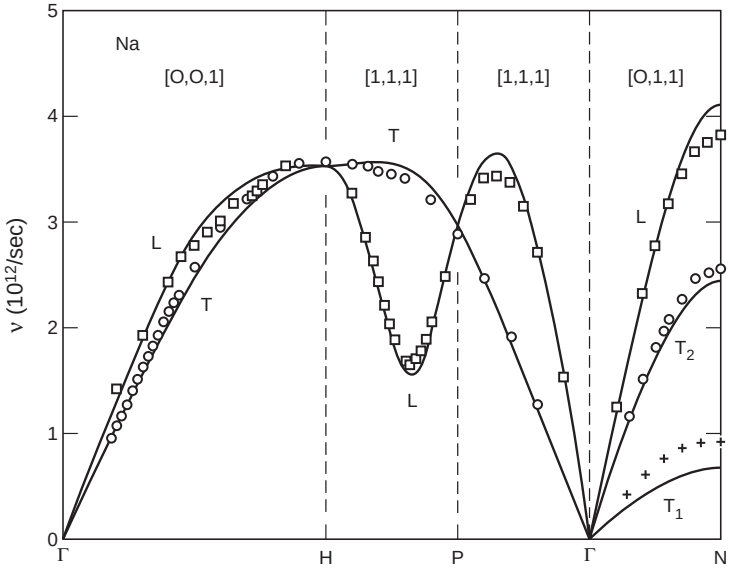


Figure 14.1. Phonon dispersion curves for bcc Na at 90 K, where $\nu = \omega/2\pi$. Points are experiment, lines are the pseudopotential model (Wallace, 1968).

calculated by John Wills, and at the volume of neutron scattering experiments, theory and experiment differ by 3–6% for these four phonons (see Straub *et al*, 1994).

*Problems*

*14.1* Find a way to convince yourself that the right sides of Eqs. (14.10) to (14.13) are correct.

*14.2* Write the set of independent $\hat{A}_{ijmn}$ for a primitive cubic lattice, from Eq. (14.15). Then use Eq. (12.30) to find the corresponding $\tilde{B}$ coefficients, and show they have complete Voigt symmetry, *e.g.* $\tilde{B}_{xyxy} = \tilde{B}_{xyyx}$. Then derive Eqs. (14.16) – (14.18).

*14.3* From Eq. (14.14) for the dynamical matrix, show that the mean phonon frequency squared for a primitive lattice is given by

$$M\langle\omega^2\rangle_{BZ} = \frac{1}{3}\sum_K{}' \left[\frac{\phi''_K + 2\phi'_K}{R_K^2}\right] \quad .$$

Demonstrate agreement with problem 13.3.

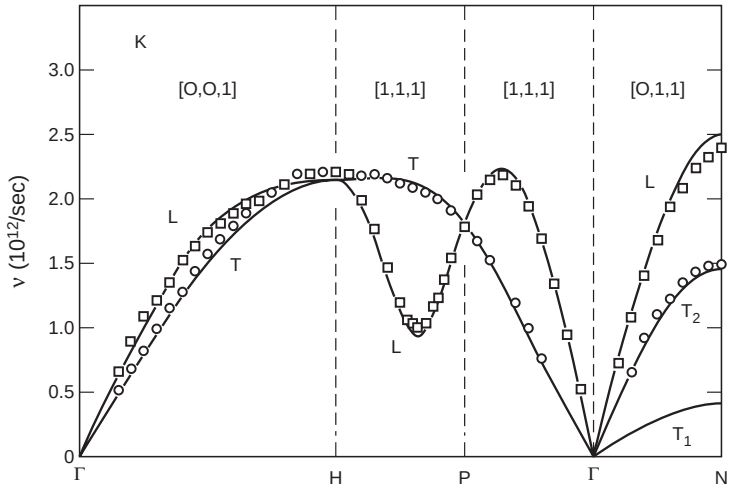


Figure 14.2. Phonon dispersion curves for bcc K at 9 K, where $\nu = \omega/2\pi$. Points are experiment, lines are the pseudopotential model (Wallace, 1968).

## 15 EXPERIMENTAL PHONON DATA

### *Phonon Dispersion Curves*

In inelastic neutron scattering experiments, the scattering cross section is proportional to the dynamic structure factor $S(\mathbf{q},\omega)$, where $\hbar\mathbf{q}$ and $\hbar\omega$ are respectively the momentum and energy transferred from the neutron to the system. Phonon data are obtained from measurements on large single crystals, and the discussion here applies to any crystal. In the leading theoretical approximation, the neutron interacts with a single quasiharmonic phonon, and $S(\mathbf{q},\omega)$ is a sum over all phonons $\mathbf{k}s$ of terms proportional to $\Delta(\mathbf{q}-\mathbf{k})\delta(\omega-\omega(\mathbf{k}s))$, each term describing the creation of one phonon at $\mathbf{k}s$, and terms proportional to $\Delta(\mathbf{q}-\mathbf{k})\delta(\omega+\omega(\mathbf{k}s))$, where each term describes the absorption of one phonon at $\mathbf{k}s$. In this theoretical approximation, the experiments can provide exact measurements of exact phonon frequencies. In higher theoretical approximation, $S(\mathbf{q},\omega)$ has corrections from anharmonicity, and from multiphonon scattering events. These corrections cause the phonon lines to shift, broaden, and become asymmetric, effects which generally increase as temperature increases. To interpret the experiment, one often fits $S(\mathbf{q},\omega)$ at fixed $\mathbf{q}$ to a Lorentzian function of $\omega-\omega_0$, where the fitted $\omega_0$ is taken to be the phonon frequency. At this

theoretical level, no phonon frequency can be measured exactly, as a matter of principle (see Ambegaokar, Conway, and Baym, 1965). The theory of inelastic neutron scattering is presented by Lovesey (1984), and by Glyde (1994).

Phonon frequencies are most often measured for $\mathbf{k}$ along symmetry directions of the inverse lattice, and the corresponding graphs of $\omega(\mathbf{k}s)$ *vs* $\mathbf{k}$ are called dispersion curves. Examples for primitive lattices are shown in Figs. 14.1 and 14.2, and Fig. 5.1. It is customary to fit the experimental dispersion curves with an empirical model, for example a Born-von Karman model, also called a force-constant model, or a shell model. Fitted models for primitive lattices generally have from 8 to 26 force constants. Such fitted models are useful extensions of the experimental data, because they provide an interpolation of the measured frequencies over the entire Brillouin zone, and because they also provide the phonon eigenvectors, or what is equivalent, they prescribe the set of dynamical matrices $\mathbf{D}(\mathbf{k})$ for all $\mathbf{k}$. From this information, all equilibrium statistical mechanical properties can be calculated in the quasiharmonic approximation. Extensive collections of experimental phonon data and fitted models may be found in Schober and Dederichs (1981), and in Bilz and Kress (1979).

In the early days, inelastic neutron scattering experiments were done at temperatures low compared to the melting temperature. The rare-gas crystals, and low-melting metals, were measured at around 10K, while the refractory metals were measured around room temperature. The measurements are quite accurate, having error bars in the range 1–5%. Higher temperature measurements are more difficult, because of the deterioration of the phonon lineshapes, but good measurements of phonon dispersion curves have recently been made, even to the melting temperature. In addition, experiments have been done for high temperature crystal phases, where the temperature has to be maintained continuously at an elevated level, while the crystal is grown and the measurements are accomplished. Examples include bcc Sr at 930K (Mizuki and Stassis, 1985), fcc La (Stassis *et al*, 1985), and bcc phases of Ti, Zr, Hf, La, and Sc (respectively Petry *et al*, 1991; Heiming *et al*, 1991; Trampenau *et al*, 1991; Güthoff *et al*, 1993; and Petry *et al*, 1993). Compression dependence of transverse acoustic phonon frequencies of Ge to 9.7 GPa has recently been measured (Klotz *et al*, 1997), and more such measurements will be welcome.

The temperature dependence of phonon data at 1 bar has two independent contributions, one being an explicit volume or lattice-parameter de-

pendence, resulting from thermal expansion, and the other an explicit temperature dependence resulting from anharmonicity. In these dependences, most elemental crystals display the same "ordinary" behavior, where the explicit temperature dependence is small and often negligible, and the lattice parameter dependence is understood theoretically, through quasiharmonic theory. This behavior is important in the analysis of experimental thermodynamic data in Chap. 4. The exception to ordinary behavior is the appearance of "soft phonons," marked by a strong temperature dependence of the frequencies in a small region of the Brillouin zone, and associated with an incipient crystal instability. Soft phonons are discussed in Sec. 26.

As wavelength increases for acoustic phonons, it is increasingly difficult to measure the frequency accurately, because the frequency decreases toward zero. The measured dispersion curves are often supplemented with initial slopes of $\omega$ *vs* $|\mathbf{k}|$, determined from more accurate elastic-constant data. This procedure is approximate, since acoustic phonons and sound waves are not the same at finite temperature, as discussed in Sec. 14. However, the approximation can always be improved with theoretical corrections, starting from the equivalence of acoustic phonons and sound waves at zero temperature. The inverse situation also occurs, where phonon dispersion curves are used to estimate the elastic constants, usually for a crystal for which no ultrasonic data exist. Such neutron scattering estimates were compared with Brillouin scattering measurements for Kr near melt, and indicate the difference between acoustic phonons and sound waves, also called the zero sound – first sound difference, amounts to 7–14% in the elastic constants (Landheer *et al*, 1976). Elastic constants of bcc Sr, of both high temperature phases of La, and of bcc Ti, Zr, Hf, and Sc were determined from the high temperature neutron scattering experiments mentioned above. It is often said that a change in slope of $\omega$ vs $|\mathbf{k}|$ at small $|\mathbf{k}|$, specifically an increase in slope with increasing $|\mathbf{k}|$, in a measured acoustic phonon dispersion curve, represents a change from first sound to zero sound. The statement is not correct. Such a change in slope can be achieved in a force constant model, or in pseudopotential theory, in the purely harmonic theory where zero sound and first sound are the same.

### *Phonon Frequency Distribution*

The normalized phonon frequency distribution $g(\omega)$ is defined in the same way for primitive and nonprimitive lattices, namely $g(\omega)d\omega$ is the number

of frequencies in $d\omega$ at $\omega$, normalized so that

$$\int g(\omega)d\omega = 1 \quad . \tag{15.1}$$

The standard procedure is to calculate $g(\omega)$ numerically, from a model which gives $\omega(\mathbf{k}s)$ over the entire zone. Of course, $g(\omega)$ contains much less information than the original model, since only a faint shadow of the dependence on wavevectors and polarizations remains in $g(\omega)$. The distribution is nevertheless useful in equilibrium statistical mechanics, because a quasiharmonic statistical average is the Brillouin zone average of a function $f(\omega)$, and for any lattice we have

$$\langle f(\omega)\rangle_{BZ} = \int f(\omega)g(\omega)d\omega \quad . \tag{15.2}$$

As we shall see in Sec. 16, all quasiharmonic thermodynamic functions are of this form, where each appropriate function $f(\omega)$ carries explicit temperature dependence. The statistical mechanical properties which cannot be put into the form of Eq. (15.2) are properties involving interactions of phonons with other particles, such as other phonons, electrons, or neutrons, because these interactions always depend on the phonon eigenvectors.

In Sec. 13, we mentioned the historical development of simple models for the phonon frequency distribution. In 1907, to demonstrate the relevance of the thermal energy of a harmonic oscillator to the specific heat of solids, it was sufficient for Einstein to take a single frequency $\omega_E$, so the normalized Einstein distribution is

$$g_E(\omega) = \delta(\omega - \omega_E) \quad . \tag{15.3}$$

The Debye model treats a solid as an isotropic elastic continuum, which gets the correct behavior $\omega \propto |\mathbf{k}|$ at small $|\mathbf{k}|$, but misses the dispersion, and misses the anisotropy of a crystalline solid. In terms of the Debye frequency $\omega_D$, the normalized Debye distribution is

$$\begin{aligned} g_D(\omega) &= \frac{3\omega^2}{\omega_D^3} \quad , \quad 0 \le \omega \le \omega_D \quad ; \\ g_D(\omega) &= 0 \quad , \quad \omega > \omega_D \quad . \end{aligned} \tag{15.4}$$

The Einstein and Debye distributions, separately or in combination, are too unrealistic to be useful in modern theoretical work. Moreover, what was understood 50 years ago but is not today, the Debye model is incapable of

replacing lattice dynamics in any realistic application. The superficial fact is that real crystalline solids indeed have $g(\omega) \propto \omega^2$, the same as $g_D(\omega)$ in Eq. (15.4), but only at very small $\omega$, while the profound truth is that the physically correct derivation of this property of $g(\omega)$ is provided by lattice dynamics theory, and *only* lattice dynamics theory can define the "Debye" frequency $\omega_D$. Lattice dynamics theory of the low frequency distribution is presented in Sec. 16, where we find $\hbar\omega_D \doteq k\Theta_D$, with $\Theta_D$ the experimental Debye temperature at $T = 0$.

Accurate phonon distributions $g(\nu)$, where $\nu = \omega/2\pi$, are shown for several elements in Fig. 15.1. These distributions are obtained from Born von Karman models fitted to experimental phonon dispersion curves. Debye distributions determined from experimental Debye temperatures are shown for comparison.

### *Phonon Moments*

*Phonon moments* are moments of the phonon frequency distribution, and they are important because almost all the quasiharmonic thermodynamic information is contained in just a few of the moments. Barron, Berg, and Morrison (1957) defined the following moments $\omega_n$, for $n \geq -3$:

$$\begin{aligned} \omega_n &= \left[\frac{n+3}{3}\int_0^\infty \omega^n g(\omega)d\omega\right]^{1/n} \quad , \quad n \neq 0 \text{ and } n \neq -3 \quad ; \\ \omega_0 &= \exp\left[\frac{1}{3} + \int_0^\infty \ln\omega g(\omega)d\omega\right] \quad ; \\ \omega_{-3} &= \lim_{n\to -3}\omega_n \quad . \end{aligned} \tag{15.5}$$

The numerical factors were chosen so that every moment of the Debye distribution is the same:

$$\omega_n[g_D(\omega)] = \omega_D \quad , n \geq -3 \quad . \tag{15.6}$$

The moments for $n < 0$ depend strongly on the smallest phonon frequencies, and the $-3$ moment only depends on the limiting character as $\omega \to 0$. Graphs of $\omega_n$ *vs* $n$ for the elemental metals are shown by Schober and Dederichs (1981). In these graphs, the maximum moment is either at $n = -3$, or at $n = \infty$, while the minimum moment is at $n$ in the range $-3$ to $+5$. The spread of moments from minimum to maximum is $10 - 40\%$ for metals at low temperatures, and becomes larger when temperature increases.

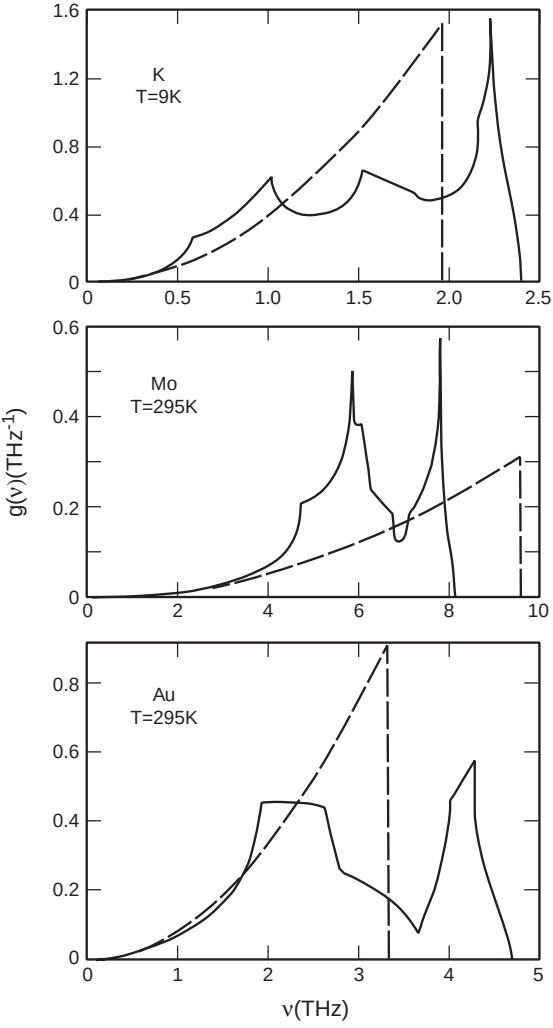


Figure 15.1. Experimental phonon distributions for three metals (solid lines, data from Schober and Dederichs, 1981), and Debye distributions determined from experimental Debye temperatures (dashed lines).

Lattice dynamics characteristic temperatures $\theta_n$ are defined from the phonon moments $\omega_n$, as follows. The Debye temperature in quasiharmonic

approximation is $\theta_{-3}$, where

$$k\theta_{-3} = \hbar\omega_{-3} \quad ; \tag{15.7}$$

the classical entropy temperature $\theta_0$ is

$$k\theta_0 = e^{-1/3}\hbar\omega_0 \quad ; \tag{15.8}$$

and the remaining $\theta_n$ are given by

$$k\theta_n = \hbar\omega_n \quad . \tag{15.9}$$

In quasiharmonic phonon statistical mechanics, specific characteristic temperatures possess the following properties:

$\theta_{-3}$ scales the thermal free energy at low temperature;

$\theta_{-2}$ scales the classical nuclear mean square displacement;

$\theta_0$ gives the classical entropy;

$\theta_1$ gives the zero-point vibrational free energy;

$\theta_2, \theta_4, \cdots$ give quantum corrections to the classical free energy.

Because it is difficult to measure accurately the frequencies of long wavelength acoustic phonons, by means of inelastic neutron scattering, it is difficult to obtain accurate values of $\omega_n$ for negative $n$, especially for $n = -3$. When one goes from neutron scattering experiments, through a force constant model to $g(\omega)$, and ultimately to $\theta_{-3}$, the result might be in error by more than 10% for an elemental crystal. Note the error here is determined by comparison with highly accurate values of $\Theta_D$ from low temperature specific heat measurements (see Sec. 16). In contrast to the moments at negative $n$, $\omega_n$ is quite accurate as $n \to \infty$, where the moment converges (slowly) to the highest phonon frequency. Most accurate of all are the *central* moments, at $n = 0, 1, 2$, since these have significant contribution from the entire experimental phonon spectrum. The accuracy of these moments for elemental crystals is such that, if respectable neutron scattering measurements are made in different countries in different years, on crystals grown in different laboratories, the results from separate force constant models will agree to around 0.1 – 0.5%.

Central characteristic temperatures from neutron scattering measurements, and Debye temperatures from low temperature specific heat measurements, are listed in Table 15.1. The crystal structure for the Debye temperature is listed when it is different from the crystal structure for the

central characteristic temperatures. The data are from the author's collection, assembled over the years and reported in Wallace (1991c, 1997a), where references to the sources can be found. A useful approximation, whose accuracy can be assessed from the tabulated data, is

$$\theta_1 \approx \theta_2 \approx e^{1/3}\theta_0 \quad . \tag{15.10}$$

We also have reliable information on the volume derivative of each $\theta_n$, to be presented in Sec. 19.

Table 15.1. Phonon characteristic temperatures $\theta_0, \theta_1$, and $\theta_2$, from neutron scattering measurements at temperature $T_{meas}$ and density $\rho_{meas}$, and Debye temperatures $\Theta_D$ from low temperature specific heat measurements.

| Element | $T_{meas}$ (K) | $\rho_{meas}$ $(g/cm^3)$ | Crystal | $\theta_0(K)$ | $\theta_1(K)$ | $\theta_2(K)$ | $\Theta_D(K)$ |
|---|---|---|---|---|---|---|---|
| Li | 98 | 0.546 | bcc | 265.5[a] | 388[a] | 400[a] | 371 |
| Na | 90 | 1.005 | bcc | 113.3 | 163 | 166 | 152.5 |
| K | 9 | 0.904 | bcc | 68.9 | 99.4 | 102.1 | 90.6 |
| Rb | 12 | 1.616 | bcc | 42.2 | 61.9 | 63.9 | 55.6 |
| Mg | 290 | 1.74 | hcp | 229.4 | 319 | 320 | 400 |
| Ca | 295 | 1.53 | fcc | 149 | 210 | 213 | 229 |
| Sr | 930 | 2.6 | bcc | 80.0 | 115 | 117 | 147(fcc) |
| Ba | 295 | 3.5 | bcc | 66.5 | 94.9 | 97.7 | 110.5 |
| Cu | 49 | 9.018 | fcc | 225.3 | 315 | 317 | 345 |
| Ag | 296 | 10.49 | fcc | 150.1 | 211 | 213 | 226 |
| Au | 295 | 19.27 | fcc | 124.5 | 179.3 | 184 | 162.5 |
| Zn | 80 | 7.270 | hcp | 161 | 235 | 242 | 326 |
| Hg | 80 | 14.46 | rhomb | 64.7 | 106 | (124) | 71.9 |
| Al | 80 | 2.731 | fcc | 283.5 | 399 | 404 | 428 |
| In | 77 | 7.43 | bct | 85.3 | 128 | (138) | 111 |
| Tl | 296 | 11.85 | hcp | 61.5 | 91.4 | (97) | 78.5 |
| Pb | 80 | 11.55 | fcc | 64.1 | 91.3 | 93.4 | 105 |
| Ar | 10 | 1.7705 | fcc | 59.1[b] | 82.9[b] | 83.4[b] | 92.0 |
| Kr | 10 | 3.091 | fcc | 46.03 | 64.6 | 65.0 | 71.9 |
| Xe | 10 | 3.780 | fcc | 39.92 | 56.0 | 56.3 | 64.0 |
| Ti | 295 | 4.505 | hcp | 255 | — | — | 427 |
| Zr | 295 | 6.507 | hcp | 178 | — | — | 294 |
| V | 296 | 6.12 | bcc | 250 | 347 | 347 | 400 |
| Nb | 296 | 8.58 | bcc | 198 | 278 | 280 | 272 |
| Ta | 296 | 16.68 | bcc | 162 | 226 | 226 | 259 |
| Cr | 300 | 7.19 | bcc | 338 | 464 | 459 | 600 |
| Mo | 296 | 10.22 | bcc | 273 | 377 | 374 | 470 |
| W | 298 | 19.26 | bcc | 225 | 310 | 307 | 390 |
| Fe | 295 | 7.87 | bcc | 301 | 420 | 421 | 470 |
| Ni | 298 | 8.91 | fcc | 275 | 383 | 385 | 470 |
| Pd | 120 | 12.07 | fcc | 200 | 284 | 289 | 272 |
| Pt | 90 | 21.56 | fcc | 163.5 | 232 | 237 | 236 |
| Th | 296 | 11.7 | fcc | 99.7 | 141 | 143 | 160 |
| Si | 296 | 2.34 | dia | 421 | 645 | 685 | 645 |
| Ge | 80 | 5.32 | dia | 245 | 373 | 396 | 374 |
| Sn | 300 | 7.30 | bct | 103.4 | 154 | 172 | 202(dia) |

[a]Data for $^7$Li was converted to atomic weight 6.939.

[b]Data for $^{36}$Ar was converted to atomic weight 39.948.

*This page intentionally left blank*

# Chapter 4

# Statistical Mechanics of Crystals

## 16 QUANTUM NUCLEAR MOTION

### *Interacting Phonon Description*

When we want to study the many-body properties of phonons, the most convenient formulation is in terms of phonon creation and annihilation operators. These operators are defined through a canonical transformation of the phonon coordinate and momentum operators of Sec. 13. It is convenient to streamline the notation by using the index $\kappa$ for the pair $\mathbf{k}s$, according to

$$\kappa = \mathbf{k}s \quad ; \quad -\kappa = -\mathbf{k}s \quad . \tag{16.1}$$

The phonon coordinates $q_\kappa$, and momenta $p_\kappa$, are given by Eqs. (13.22) and (13.23), respectively, and the phonon creation operators $A_\kappa^+$, and annihilation operators $A_\kappa$ are defined by

$$A_\kappa^+ = \frac{1}{\sqrt{2\hbar\omega_\kappa}}(\omega_\kappa q_{-\kappa} - ip_\kappa) \quad , \tag{16.2}$$

$$A_\kappa = \frac{1}{\sqrt{2\hbar\omega_\kappa}}(\omega_\kappa q_\kappa + ip_{-\kappa}) \quad . \tag{16.3}$$

Commutators are calculated with the help of Eqs. (13.25) and (13.26) for coordinate and momentum commutators, with the result

$$[A_\kappa, A_{\kappa'}^+] = \delta_{\kappa\kappa'} \quad , \tag{16.4}$$

$$[A_\kappa, A_{\kappa'}] = [A_\kappa^+, A_{\kappa'}^+] = 0 \quad . \tag{16.5}$$

Here $\delta_{\kappa\kappa'} = \Delta(\mathbf{k} - \mathbf{k}')\delta_{ss'}$, and as long as $\mathbf{k}$ and $\mathbf{k}'$ are both from the same Brillouin zone, then $\delta_{\kappa\kappa'} = \delta_{\mathbf{k}\mathbf{k}'}\delta_{ss'}$. The above equations, and most of those following in Sec. 16, are valid for any lattice, primitive or nonprimitive.

Expansion of the nuclear motion Hamiltonian in powers of displacements of the nuclei from equilibrium is written in Eq. (13.4). Here we shall write this expansion in the more descriptive "phonon notation," as

$$\mathcal{H} = \Phi_0 + \mathcal{H}_{ph} + \mathcal{H}_{anh} \quad , \tag{16.6}$$

where $\Phi_0$ is the static lattice potential, and (see problem 16.1)

$$\mathcal{H}_{ph} = \mathcal{H}_2 = \sum_\kappa \hbar\omega_\kappa \left( A_\kappa^+ A_\kappa + \frac{1}{2} \right) \quad , \tag{16.7}$$

$$\mathcal{H}_{anh} = \Phi_3 + \Phi_4 + \cdots \quad . \tag{16.8}$$

In terms of the operator $B_\kappa = A_\kappa + A_{-\kappa}^+$, $\Phi_3$ and $\Phi_4$ take the form

$$\Phi_3 = \sum_{\kappa\kappa'\kappa''} \Phi_{\kappa\kappa'\kappa''} B_\kappa B_{\kappa'} B_{\kappa''} \quad , \tag{16.9}$$

$$\Phi_4 = \sum_{\kappa\kappa'\kappa''\kappa'''} \Phi_{\kappa\kappa'\kappa''\kappa'''} B_\kappa B_{\kappa'} B_{\kappa''} B_{\kappa'''} \quad . \tag{16.10}$$

While $\mathcal{H}_{ph}$ is diagonal in phonons, $\mathcal{H}_{anh}$ is not, hence $\mathcal{H}_{anh}$ expresses interactions among phonons. Notice the terms *phonon-phonon interactions* and *anharmonicity* represent the same physics. The coefficients $\Phi_{\kappa\kappa'\kappa''}$, etc., are transforms of the potential energy coefficients of Sec. 12, and they contain lattice symmetry properties, as well as the requirements for conservation of total "crystal momentum." For example,

$$\begin{aligned} &\Phi_{\kappa\kappa'\kappa''} \text{ contains } \Delta(\mathbf{k} + \mathbf{k}' + \mathbf{k}'') \quad , \\ &\Phi_{\kappa\kappa'\kappa''\kappa'''} \text{ contains } \Delta(\mathbf{k} + \mathbf{k}' + \mathbf{k}'' + \mathbf{k}''') \quad . \end{aligned} \tag{16.11}$$

Unlike two-phonon terms, Umklapp processes appear in three- and four-phonon interactions, since the sum of three or four $\mathbf{k}$ vectors can equal a nonzero reciprocal lattice vector.

If $\sqrt{< U^2 >}$ is the rms nuclear displacement, and $R$ is a mean nearest neighbor distance, then $\epsilon = \sqrt{< U^2 >}/R$ is small, and the orders of magnitude of quantities entering $\mathcal{H}$ are as follows.

$$\begin{aligned} & A_\kappa \, , A_\kappa^+ \sim 1 \quad , \\ & \hbar\omega_\kappa \sim \epsilon^2 \quad , \\ & \sum_{\kappa'\kappa''} \Phi_{\kappa\kappa'\kappa''} \sim \epsilon\hbar\omega_\kappa \quad , \\ & \sum_{\kappa'\kappa''\kappa'''} \Phi_{\kappa\kappa'\kappa''\kappa'''} \sim \epsilon^2\hbar\omega_\kappa \quad . \end{aligned} \tag{16.12}$$

These orders of $\epsilon$ serve as the basis for the perturbation treatment of phonon interactions. In the early days, from Born and Huang (1954) through the seventies, anharmonicity was studied almost entirely by means of perturbation theory. Since the rms nuclear displacement increases with temperature, then so does $\epsilon$, and for this reason, great difficulty was encountered in pushing anharmonic perturbation theory to high temperatures, say to $T \gtrsim \frac{1}{2}T_m$. In the eighties we took a different approach, and began to study anharmonicity all the way to melting, through molecular dynamics simulations, and also through analysis of experimental data. This approach has given us a much better understanding of anharmonicity, and a much simpler picture of its role in thermodynamic properties of crystals. This new view of anharmonicity will be presented here, in Chap. 4, and along the way, we shall compare with results from perturbation theory.

### *Nuclear Motion Free Energy*

Since phonons are independent bosons, according to the commutators (16.4) and (16.5), the energy levels of $\mathcal{H}_{ph}$ are

$$\mathcal{E}_{ph}(\{n_\kappa\}) = \sum_\kappa \hbar\omega_\kappa \left( n_\kappa + \frac{1}{2} \right) \quad , \tag{16.13}$$

where $n_\kappa = 0, 1, \cdots$, for all $\kappa$. The Helmholtz free energy is given by Eq. (7.43) for bosons, where we must set $\mu = 0$ because phonons are not conserved, and where we must add the zero-point phonon energy appearing in Eq. (16.13), so that (see problem 16.2)

$$F_{ph} = \sum_\kappa \left[ \frac{1}{2}\hbar\omega_\kappa + kT \ln(1 - e^{-\beta\hbar\omega_\kappa}) \right] \quad . \tag{16.14}$$

The total nuclear motion free energy can then be written

$$F = \Phi_0 + F_{ph} + F_{anh} \quad , \tag{16.15}$$

where $F_{anh}$ is supposed to account fully for anharmonicity, as it is contained in $\mathcal{H}_{anh}$. The corresponding nuclear motion entropy $S$, and internal energy $U$, are

$$S = S_{ph} + S_{anh} \quad , \tag{16.16}$$

$$U = \Phi_0 + U_{ph} + U_{anh} \quad , \tag{16.17}$$

where the quasiharmonic contributions follow from Eq. (16.14) for $F_{ph}$,

$$S_{ph} = k \sum_{\kappa} [(\bar{n}_\kappa + 1) \ln(\bar{n}_\kappa + 1) - \bar{n}_\kappa \ln \bar{n}_\kappa] \quad , \tag{16.18}$$

$$U_{ph} = \sum_{\kappa} \hbar\omega_\kappa \left( \bar{n}_\kappa + \frac{1}{2} \right) \quad . \tag{16.19}$$

Here $\bar{n}_\kappa$ is the harmonic thermal average of the phonon occupation number $n_\kappa$,

$$\bar{n}_\kappa = \frac{1}{e^{\beta\hbar\omega_\kappa} - 1} \quad . \tag{16.20}$$

Let us derive the formal expression for $F_{anh}$ in leading order perturbation theory. In perturbation theory for the total system energy levels, $\Phi_3$ contributes in second order, $\Phi_4$ contributes in first order, both contributions are of order $\epsilon^4$, and their sum is denoted $\mathcal{E}_4(\{n_\kappa\})$. From the general perturbation expansion of the free energy, shown in Eq. (7.59), we can write

$$F_{anh} = \langle \mathcal{E}_4 \rangle + \cdots \quad , \tag{16.21}$$

where $\langle \mathcal{E}_4 \rangle$ is the harmonic phonon thermal average of $\mathcal{E}_4$, and $+\cdots$ represents terms of order higher than $\epsilon^4$.

Though anharmonic perturbation theory is extremely complicated, some results from the leading order theory, corresponding to Eq. (16.21), provide insights into the general effects of anharmonicity. First, the dynamic structure factor $S(\mathbf{q}, \omega)$ observed in inelastic neutron scattering is changed, so that the phonon peak at $\omega = \omega_\kappa$ is shifted to the "renormalized" frequency

$\Omega_\kappa = \omega_\kappa + \Delta_\kappa$, and is broadened to show a half width of $\Gamma_\kappa$, where $\Delta_\kappa$ and $\Gamma_\kappa$ are explicitly temperature dependent. Second, the entropy is given by the quasiharmonic entropy with $\omega_\kappa$ replaced by $\Omega_\kappa$, that is (see problem 16.3)

$$S_{ph} + S_{anh} = \hat{S}_{ph} = S_{ph}(\{\Omega_\kappa\}) \quad , \tag{16.22}$$

in leading order of anharmonicity, where the last equality defines $\hat{S}_{ph}$. This relation was shown by Barron (1965), and it will be useful in analyzing experimental data in Sec. 19. Third, no other thermodynamic function can be expressed in the fashion shown in Eq. (16.22) for the entropy. Finally, for the long wavelength acoustic phonons, the renormalized frequencies are still proportional to $|\mathbf{k}|$,

$$\Omega(\mathbf{k}s) = [c(\hat{\mathbf{k}}s) + \delta c(\hat{\mathbf{k}}s)]|\mathbf{k}| \quad , \tag{16.23}$$

and this holds at all temperatures, where the anharmonic shift $\delta c(\hat{\mathbf{k}}s)$ is temperature dependent. The dependence (16.23) was given by Wallace (1964) (or see *Thermodynamics of Crystals*, p. 202).

### *Theory and Experiment at Zero Temperature*

In trying to understand the physical nature of a condensed matter system, the first challenge is to understand its binding energy. At the level of accuracy of current theory, this problem is refined to the following: Find the crystal structure of lowest energy, calculate its equilibrium lattice parameters and energy at zero temperature and pressure, and demonstrate respectable agreement of these results with experiment. The theoretical basis for these calculations is the free energy at $T = 0$, equal to the internal energy at $T = 0$, and written from Eq. (16.15) as

$$F = U = \Phi_0 + \sum_\kappa \frac{1}{2}\hbar\omega_\kappa + U_{anh}(T = 0) \quad , \quad \text{at} \quad T = 0 \quad . \tag{16.24}$$

The curve of $F$ *vs* $V$ is minimum at the zero-pressure volume, and its curvature gives the bulk modulus. The cohesive energy is by definition positive, and is $|U|$ at zero temperature and pressure.

The second term in (16.24) is $U_{ph}(T = 0)$, and is the harmonic zero-point vibrational energy, while the last term represents the anharmonicity of the zero-point vibrations, or equivalently the interactions among zero-point phonons. In terms of the characteristic temperature $\theta_1$, listed in

Table 15.1, the harmonic zero-point energy for a monatomic crystal in any lattice structure is

$$\sum_{\kappa} \frac{1}{2}\hbar\omega_{\kappa} = \frac{9}{8}Nk\theta_1 \quad . \tag{16.25}$$

The first two terms in the expansion (16.24) are listed for several elements in Table 16.1. Considering the accuracy of current theoretical calculations, the anharmonic zero-point energy is negligible. If the anharmonicity must be accounted for, one should remember that the experimental $\theta_1$ already includes some anharmonicity, because it is determined from the renormalized phonon frequencies $\Omega_{\kappa}$ (theoretical details are provided in *Thermodynamics of Crystals*, Sec. 20).

Table 16.1. Contributions to the energy at zero temperature and pressure, evaluated from experimental data for several crystals.

| | | $\Phi_0$ | $\frac{9}{8}Nk\theta_1$ |
|---|---|---|---|
| Element | Structure | (mRy/atom) | |
| Ar | fcc | –6.47 | 0.59 |
| Kr | fcc | –9.00 | 0.46 |
| Xe | fcc | –12.2 | 0.40 |
| Li | bcc | –123 | 2.77 |
| Na | bcc | –83.0 | 1.17 |
| K | bcc | –69.3 | 0.71 |
| Rb | bcc | –63.0 | 0.44 |
| Cu | fcc | –259 | 2.24 |
| Ag | fcc | –218 | 1.55 |
| Au | fcc | –281 | 1.32 |

For most elemental crystals, density functional theory is the best we have. The standard procedure is to use $\Phi_0$ for $F$, that is, to work in the potential approximation, and calculate $\Phi_0(V)$ in the neighborhood of its minimum, for selected crystal structures. Yin and Cohen (1982) carried out a calculation in local density approximation for Si and Ge in several crystal structures, and found the dia structure to lie lowest, in accord with experiment. Their results are listed in Table 16.2, where it is seen that the lattice parameters are quite close to experiment, and the cohesive energy is larger than experiment by 5% for Si, and 11% for Ge. Ye *et al.* (1990) reported a calculation in local density approximation for bcc Na, and pro-

vided the comparison with experiment shown in Table 16.3. We added the harmonic zero-point energy to the static lattice energy of Ye *et al.*, and minimized the function $\Phi_0(V) + \frac{9}{8}Nk\theta_1(V)$, to find the results listed in the second line of Table 16.3. The zero-point energy expands the lattice, and decreases the cohesive energy, moving theory closer to experiment for bcc Na, but only a little closer. Very similar results are obtained when the zero-point energy is included for Al (Straub *et al.*, 1994)

Table 16.2. Calculations in local density approximation of Yin and Cohen (1982), for diamond-structure Si and Ge, compared with experiment.

| | | Lattice constant (Å) | Cohesive energy (eV) | Bulk modulus (Mbar) |
|---|---|---|---|---|
| Silicon | Theory | 5.451 | 4.84 | 0.98 |
| | Experiment | 5.429 | 4.63 | 0.99 |
| Germanium | Theory | 5.655 | 4.26 | 0.73 |
| | Experiment | 5.652 | 3.85 | 0.77 |

Table 16.3 Comparison of calculations in local density approximation with experiment for bcc Na. First and third lines are from Ye *et al.* (1980), and middle line is present results.

| | Lattice constant (Å) | Cohesive energy (mRy/atom) | Bulk modulus (kbar) |
|---|---|---|---|
| From $U = \Phi_0$ | 4.05 | 87.8 | 85.7 |
| From $U = \Phi_0 + \frac{9}{8}Nk\theta_1$ | 4.065 | 86.6 | — |
| Experiment | 4.225 | 83.3[a] | 73.6 |

[a] Cohesive energy from Table 16.1 is 81.8 mRy/atom.

For metals, the local density approximation usually overbinds, resulting in a lattice parameter which is too small, and a binding energy too large. Normally the generalized gradient approximation weakens the binding, allowing the lattice to expand, hence improving agreement with experiment for lattice parameters and binding energies in metals. On the other hand, the generalized gradient approximation for Si, and presumably also for Ge,

moves the binding energy closer to experiment, but moves the lattice parameter farther from experiment (Favot and Dal Corso, 1999). The local density approximation has an impressive record of confirming the correct most-stable crystal structure, i.e. the one observed by experiment, at zero temperature and arbitrary pressure. As the accuracy of density functional theory continues to improve, it will be increasingly important to include the harmonic zero-point energy at zero temperature.

### *Theory and Experiment in the Low Temperature Regime*

The nuclear motion free energy is given by Eq. (16.15), and if we subtract the free energy at $T = 0$, Eq. (16.24), the remaining part is the thermal free energy. The thermal free energy has a contribution from phonons, and one from anharmonicity, and we will show that both contributions go as $T^4$ in the low temperature limit.

Since $\kappa = \mathbf{k}s$, the quasiharmonic thermal free energy is

$$F_{ph}(\text{thermal}) \ = kT \sum_{\mathbf{k}s} \ln[1 - e^{-\hbar\omega(\mathbf{k}s)/kT}] \quad . \tag{16.26}$$

In the low temperature limit, only the long wavelength acoustic phonons contribute, since only these have arbitrarily small energies. Then $\omega(\mathbf{k}s)$ can be replaced by its long wavelength limit $c(\hat{\mathbf{k}}s)|\mathbf{k}|$ for $s =$ acoustic, and the sum over $\mathbf{k}$ can be replaced by an integral over $\mathbf{k}$ space, i.e. with $|\mathbf{k}|$ going to infinity, because the summand in (16.26) vanishes exponentially for $\hbar\omega(\mathbf{k}s) >> kT$. Therefore

$$\sum_{\mathbf{k}s} \rightarrow \frac{V}{(2\pi)^3} \sum_{\substack{s \\ \text{(acoustic)}}} \int_0^\infty d\mathbf{k} \quad , \quad \text{at low } T \quad , \tag{16.27}$$

since $V/(2\pi)^3$ is the density of allowed $\mathbf{k}$ vectors in reciprocal space. The velocity $c(\hat{\mathbf{k}}s)$ depends only on the direction of $\mathbf{k}$, so the angular integration can be separated by introducing the variable $x$,

$$x = \frac{\hbar c(\hat{\mathbf{k}}s)|\mathbf{k}|}{kT} \quad , \tag{16.28}$$

so that

$$d\mathbf{k} = |\mathbf{k}|^2 d|\mathbf{k}| d\alpha = \left[\frac{kT}{\hbar c(\hat{\mathbf{k}}s)}\right]^3 x^2 dx d\alpha \quad , \tag{16.29}$$

where $d\alpha$ is the increment of solid angle for $\hat{\mathbf{k}}$. The leading term in (16.26) at low temperature is

$$F_{ph}(\text{thermal}) = -\frac{\pi(kT)^4 V}{360\hbar^3} \sum_{\substack{s \\ (\text{acoustic})}} \int \frac{d\alpha}{[c(\hat{\mathbf{k}}s)]^3} \quad . \tag{16.30}$$

The $-3$ moment of the phonon distribution, and hence the characteristic temperature $\theta_{-3}$, is related to the angle average of $[c(\hat{\mathbf{k}}s)]^{-3}$, and the relation is such that (see problem 16.4)

$$F_{ph}(\text{thermal}) = -NkT\frac{\pi^4}{5}\left(\frac{T}{\theta_{-3}}\right)^3 \quad . \tag{16.31}$$

This formula holds for a monatomic system in any crystal lattice, and in fact holds as well for a polyatomic crystal (see *Thermodynamics of Crystals*, Eq. (18.19)).

Evaluation of the anharmonic thermal free energy at low temperature, in leading order perturbation theory, was done in *Thermodynamics of Crystals*, p. 213–217. This evaluation depends on the fact that the long wavelength acoustic phonons still have frequencies proportional to $|\mathbf{k}|$, as written in Eq. (16.23). It is widely said that the appearance of a renormalized Debye temperature follows from the Barron relation (16.22), but this is not the case, as Eq. (16.23) is crucial to the result. We are now prepared to carry the derivation to all orders. In Sec. 14, we observed that sound waves and long wavelength acoustic phonons are the same at $T = 0$, and the potential governing their motion is the exact groundstate energy, $U(T = 0)$. From thermoelasticity, we know these waves have frequencies given by $C(\hat{\mathbf{k}}s)|\mathbf{k}|$, where $C(\hat{\mathbf{k}}s)$ is the sound velocity, and $s =$ acoustic. In calculating the leading low-temperature dependence of the thermal free energy, only the phonon energies at $T = 0$ will enter, since the temperature dependence of phonon energies will give a higher-order free energy contribution. We therefore conclude that the quasiharmonic formulas become exact at low-temperatures, in terms of the sound velocities $C(\hat{\mathbf{k}}s)$, and the Debye temperature $\Theta_D$ as follows.

$$F(\text{thermal}) = -NkT\frac{\pi^4}{5}\left(\frac{T}{\Theta_D}\right)^3 \quad , \tag{16.32}$$

$$\frac{1}{[k\Theta_D]^3} = \frac{V_A}{18\pi^2\hbar^3} \sum_{\substack{s \\ \text{(acoustic)}}} \frac{1}{4\pi} \int \frac{d\alpha}{[C(\hat{\mathbf{k}}s)]^3} \quad . \tag{16.33}$$

The sound velocities can be calculated at all angles of $\mathbf{k}$ as eigenvalues of the propagation matrices, which in turn can be constructed from the measured set of independent propagation coefficients, as discussed in Sec. 8. To evaluate $\Theta_D$ at $T = 0$, the propagation coefficients must be extrapolated to $T = 0$, and this is easily accomplished from measurements down to a few K.

From the thermal free energy, the entropy and thermal energy are expressed as follows in the low-temperature regime.

$$S = Nk\frac{4\pi^4}{5}\left(\frac{T}{\Theta_D}\right)^3 \quad , \tag{16.34}$$

$$U(\text{thermal}) = NkT\frac{3\pi^4}{5}\left(\frac{T}{\Theta_D}\right)^3 \quad . \tag{16.35}$$

The low-temperature specific heat is $C_P = C_V = 3S$, where $C_P$ and $C_V$ are the same to order $T^3$ because $C_P - C_V$ goes as $T^7$ at low temperature. Also, $C_P$ measured at zero pressure is the same as $C_P$ at constant volume, to order $T^3$, since the difference is due to the volume dependence of $\Theta_D$, and again goes as $T^7$. So $\Theta_D$ can be measured from two independent experiments, and the important result here is that they are the same:

$$\Theta_D(\text{propagation coefficients}) = \Theta_D(\text{specific heat}) \quad . \tag{16.36}$$

Specific heat measurements give $\Theta_D$ to an accuracy of say 0.1 – 0.3%, while the value from propagation coefficients is usually more accurate still. Results from the two experiments are in excellent agreement, as shown in Table 16.4. In fact, these data are from Table 7 of *Thermodynamics of Crystals*, and sadly, we have not found time to update and extend this comparison. Finally, because our theory is valid for arbitrary equilibrium configuration of the crystal, Eq. (16.36) holds at any configuration, so the strain or volume derivatives of $\Theta_D$(propagation coefficients) and $\Theta_D$(specific heat) are also equal. This property is also experimentally verified, as shown in Table 8 of *Thermodynamics of Crystals*.

Table 16.4. Debye temperature calculated from experimental wave propagation coefficients, $\Theta_D(A_{ijkl})$, compared with that determined from experimental specific heat, $\Theta_D(C_P)$. All data are at $T = 0$.

| Material | $\Theta_D(A_{ijkl})(K)$ | $\Theta_D(C_P)(K)$ |
|---|---|---|
| K | 90.9 | 90.6 |
| Cu | 344.5 | 345 |
| Ag | 226.5 | 226 |
| Au | 161.6 | 162 |
| Al | 430.5 | 428 |
| Pb | 105.3 | 105 |
| NaCl | 321.0 | 321 |
| KCl | 236 | 235 |
| KBr | 172 | 174 |
| KI | 131 | 132 |
| Ar | 90.5 | 92.0 |

### *Thermodynamic Functions in the Dispersion Regime*

In the low temperature regime, phonon statistics depends only on the lowest lying modes, hence depends only on the lowest finite moment of the phonon distribution, namely on $\omega_{-3}$. As temperature increases, modes of higher energy contribute, so phonon dispersion becomes important, and the statistical mechanics depends on the higher moments $\omega_{-2}$, $\omega_{-1}$, and so on. Hence the phonon moment which most influences a given thermodynamic function will vary with temperature. In specific heat, for example, departure from the low-temperature behavior $(T/\Theta_D)^3$ becomes apparent at temperatures on the order of $0.01\Theta_D$. In the opposite extreme of high temperatures, the nuclear motion approaches classical, and the approach is characterized by the second moment $\omega_2$ (see Sec. 17). With increasing temperature, the phonon statistical mechanics has lost most of its dispersion dependence at a temperature around $0.5\theta_2$. We therefore define the dispersion regime by the condition $0.01\Theta_D \lesssim T \lesssim 0.5\theta_2$.

The specific heat $C_P$ is usually measured at 1bar, and thermodynamic data are then used to obtain $C_V$ from $C_P$, by means of Eq. (7.17). At temperatures in the dispersion regime, the experimental $C_V$ is often accurate to 0.1%. A graphical comparison of theory and experiment for $C_V$ *vs* $T$ in the dispersion regime is not useful, because a difference of 1% is theoretically meaningful, but cannot be seen on the graph. Dependence of $C_V(T)$

on phonon dispersion is magnified in the effective Debye temperature $\Theta$, defined such that $C_V(T) = C_D(\Theta/T)$. The experimental $\Theta(T)$ is highly accurate, and if anharmonicity is neglected, this function serves as a test of theory for the phonon frequency distribution. This is the test shown in Fig. 13.1, of Kellermann's calculations for NaCl. Many such comparisons have been made over the years, but the interpretation is always clouded by the same circumstance, namely that the experimental data contain quasiharmonic and anharmonic contributions, while the theory is quasiharmonic alone. The availability of experimental phonon dispersion curves now allows us to change our methods of comparing theory and experiment, so as to separate the quasiharmonic and anharmonic effects.

When all is said and done, the best test of theoretical phonon calculations is the experimental phonon dispersion curves. The experimental phonons have some anharmonic content, which is usually small, especially for phonons measured at low temperatures. On the other hand, the best way to test anharmonic theory is to use experimental data, as much as possible, to isolate the anharmonic contribution. In the dispersion regime, as temperature increases in the vicinity of $0.5\theta_2$, $\Theta(T)$ approaches $\theta_2$ in quasiharmonic theory, so the difference between $\Theta$ and $\theta_2$ expresses the anharmonic contribution to $C_V$. The most accurate value of $\theta_2$ available for this analysis comes from experimental phonon data. In analyzing the specific heat, or any thermodynamic data, for its nuclear motion content, it is necessary to remove the electronic excitation contribution for metals, and to make sure theory and experiment are evaluated at the same volume.

Regarding anharmonic contributions to thermal energy, or to entropy, in the dispersion regime, our current estimate is that it is on the order of a few percent in metals, and is noticeably larger in the rare gas crystals.

*Problems*

*16.1* Derive the phonon commutators and $\mathcal{H}_{ph}$ in terms of phonon creation and annihilation operators (Eqs. (16.4), (16.5), and (16.7)).

*16.2* Derive the quasiharmonic statistical mechanics results Eqs. (16.14) and (16.18) – (16.20).

*16.3* Does an equation analogous to (16.22) hold for the thermal energy? For the zero-point vibrational energy? Why does such a relation hold for the entropy, and for no other thermodynamic function?

*16.4* Derive Eq. (16.31) for a monatomic system in any crystal lattice,

and in the process verify that this is the leading term at low temperatures.

## 17 CLASSICAL NUCLEAR MOTION

### *Quantum Free Energy at High Temperatures*

The nuclear motion free energy is $F = \Phi_0 + F_{ph} + F_{anh}$, Eq. (16.15), correct at all temperatures for a crystal. At sufficiently high temperatures, the nuclear motion approaches classical, and $F$ approaches its classical limit. To study this behavior, we expand $\bar{n}_\kappa$ of Eq. (16.20), in powers of $\hbar\omega_\kappa/kT$:

$$\bar{n}_\kappa + \frac{1}{2} = \frac{kT}{\hbar\omega_\kappa} + \frac{1}{12}\frac{\hbar\omega_\kappa}{kT} - \frac{1}{720}\left(\frac{\hbar\omega_\kappa}{kT}\right)^3 + \cdots \quad , \tag{17.1}$$

where $+\cdots$ represents terms in higher odd powers of $\hbar\omega_\kappa/kT$. Notice there is no constant term, i.e. temperature independent term, on the right side of Eq. (17.1). The harmonic free energy, Eq. (16.14), then expands into

$$F_{ph} = -kT\sum_\kappa \left[\ln\left(\frac{kT}{\hbar\omega_\kappa}\right) - \frac{1}{24}\left(\frac{\hbar\omega_\kappa}{kT}\right)^2 + \frac{1}{2880}\left(\frac{\hbar\omega_\kappa}{kT}\right)^4 - \cdots\right] \quad . \tag{17.2}$$

Notice the zero-point energy $\Sigma_\kappa \frac{1}{2}\hbar\omega_\kappa$ no longer appears in $F_{ph}$ at high temperatures. The first term in Eq. (17.2) is the classical limit, and this is precisely the classical free energy derived in Sec. 9, and written in Eq. (9.22), evaluated for a crystal in harmonic lattice dynamics theory. The remaining terms are quantum corrections, which vanish as $T \to \infty$, and which also vanish if one sets $\hbar = 0$. The second term in Eq. (17.2), the leading quantum correction, is also the same in harmonic lattice dynamics theory as the leading quantum correction derived for a general condensed matter system in Sec. 9 (see problem 17.1).

The harmonic entropy and internal energy have the following high temperature expansions, derived from Eq. (17.2):

$$S_{ph} = k\sum_\kappa \left[\ln\left(\frac{kT}{\hbar\omega_\kappa}\right) + 1 + \frac{1}{24}\left(\frac{\hbar\omega_\kappa}{kT}\right)^2 - \frac{1}{960}\left(\frac{\hbar\omega_\kappa}{kT}\right)^4 + \cdots\right] \quad , \tag{17.3}$$

$$U_{ph} = kT \sum_{\kappa} \left[ 1 + \frac{1}{12} \left( \frac{\hbar\omega_\kappa}{kT} \right)^2 - \frac{1}{720} \left( \frac{\hbar\omega_\kappa}{kT} \right)^4 + \cdots \right] \quad . \tag{17.4}$$

In the entropy, the first two terms are classical, and $\hbar$ in the classical terms comes from the density of quantum states in the system phase space. As mentioned in Sec. 9, this is the only place where $\hbar$ enters classical statistical mechanics, and this $\hbar$ in the entropy remains important even as $T \to \infty$. One the other hand, the classical energy is just the sum of energies $kT$ for a set of independent classical harmonic oscillators. Again the terms which vanish as $T \to \infty$ are quantum corrections. The above equations, and most of those following in Sec. 17, are valid for any crystal.

It is convenient to write the high temperature expansions of harmonic thermodynamic functions in terms of the phonon characteristic temperatures $\theta_n$, defined in Sec. 15. For a monatomic crystal in any lattice structure, and also for a polyatomic $N$-atom crystal,

$$F_{ph} = -3NkT \left[ \ln\left( \frac{T}{\theta_0} \right) - \frac{1}{40} \left( \frac{\theta_2}{T} \right)^2 + \frac{1}{6720} \left( \frac{\theta_4}{T} \right)^4 - \cdots \right] \quad , \tag{17.5}$$

$$S_{ph} = 3Nk \left[ \ln\left( \frac{T}{\theta_0} \right) + 1 + \frac{1}{40} \left( \frac{\theta_2}{T} \right)^2 - \frac{1}{2240} \left( \frac{\theta_4}{T} \right)^4 + \cdots \right] \quad , \tag{17.6}$$

$$U_{ph} = 3NkT \left[ 1 + \frac{1}{20} \left( \frac{\theta_2}{T} \right)^2 - \frac{1}{1680} \left( \frac{\theta_4}{T} \right)^4 + \cdots \right] \quad . \tag{17.7}$$

As asymptotic series, these equations can be used for $T$ down to say $\frac{1}{2}\theta_2$. Since $\theta_4 \approx \theta_2$, the expansions with only terms to order $\theta_2$ are quite accurate for $T \gtrsim \theta_2$. The volume dependence, or more generally the crystal structure dependence, is entirely contained in the $\theta_n$. For example, the volume derivative of entropy is

$$\left. \frac{\partial S_{ph}}{\partial V} \right)_T = 3Nk \left[ -\frac{d \ln \theta_0}{dV} + \frac{1}{20} \left( \frac{\theta_2}{T} \right)^2 \frac{d \ln \theta_2}{dV} - \cdots \right] \quad . \tag{17.8}$$

Our formal definition of the high temperatures regime, or the regime of nearly classical nuclear motion, is $T \gtrsim \theta_2$. Here the anharmonic free energy has the following form: in leading order perturbation theory, $F_{anh} =$

$A_2T^2+A_0+\cdots$; in the next order perturbation theory it is $B_3T^3+B_1T+\cdots$; and so on, where the coefficients are functions of $V$. In each of these series the leading term is classical, while the following terms are quantum. The quantum terms are smaller by the order of a function $\chi$, which we estimate to be

$$\chi \sim \frac{1}{40}\left(\frac{\theta_2}{T}\right)^2 \quad . \tag{17.9}$$

Hence we can write

$$F_{anh} = (A_2T^2 + B_3T^3 + \cdots)[1 + O(\chi)] \quad . \tag{17.10}$$

This expansion is meaningful because, and only because, there is an upper limit to the temperature of its application, namely $T_m$. Several modifications of Eq. (17.10) have also been developed, through self-consistent phonon theory. The crucial question is whether or not any of these perturbation theories is of any practical value in the high temperature regime. Our answer follows.

### *Failure of Anharmonic Perturbation Theory*

For pseudopotential sodium in bcc structure, we carried out molecular dynamics calculations of the internal energy and pressure, for temperatures to melting, at several volumes (Swanson *et al.*, 1982). The temperature was calculated from Eq. (10.8), and the pressure from Eq. (10.28). These calculated data, $U_{MD}$ and $P_{MD}$, are pure classical and are fully anharmonic. In lattice dynamics theory, the classical expressions for internal energy and pressure are

$$U_{LD} = \Phi_0 + 3NkT + U^{cl}_{anh} \quad , \tag{17.11}$$

$$P_{LD} = -\frac{d\Phi_0}{dV} - 3NkT\frac{d\ln\theta_0}{dV} + P^{cl}_{anh} \quad , \tag{17.12}$$

where the terms linear in $T$ are classical quasiharmonic contributions. We also calculated $\Phi_0(V)$ and $\theta_0(V)$ from lattice dynamics theory, hence evaluated the volume dependent terms in (17.11) and (17.12), for the same

pseudopotential sodium model. We then extracted the classical anharmonic contributions by setting $U_{MD} = U_{LD}$, and $P_{MD} = P_{LD}$, and the results are graphed in Figs. 17.1 and 17.2.

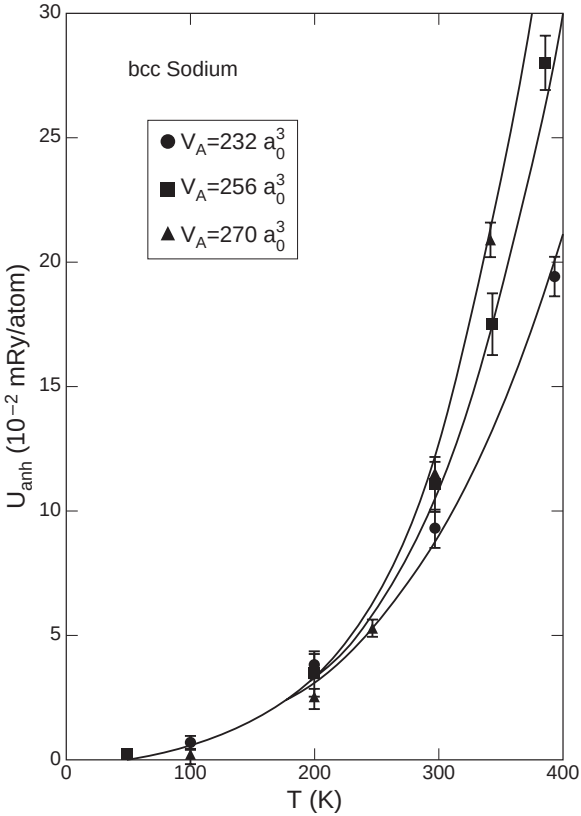


Figure 17.1. Classical anharmonic energy *vs* $T$ at three volumes, from molecular dynamics calculations for sodium. None of the curves goes as $T^2$ within estimated errors.

We learn two things from these molecular dynamics calculations for pseudopotential sodium. First, the anharmonic energy and pressure are very small, specifically, relative to the quasiharmonic thermal contributions in Eqs. (17.11) and (17.12), $U^{cl}_{anh}$ and $P^{cl}_{anh}$ are both $\lesssim 4\%$ for temperatures to melt. Second, the temperature dependences of $U^{cl}_{anh}$ and $P^{cl}_{anh}$ at constant volume are quite inconsistent with leading order anharmonic perturbation

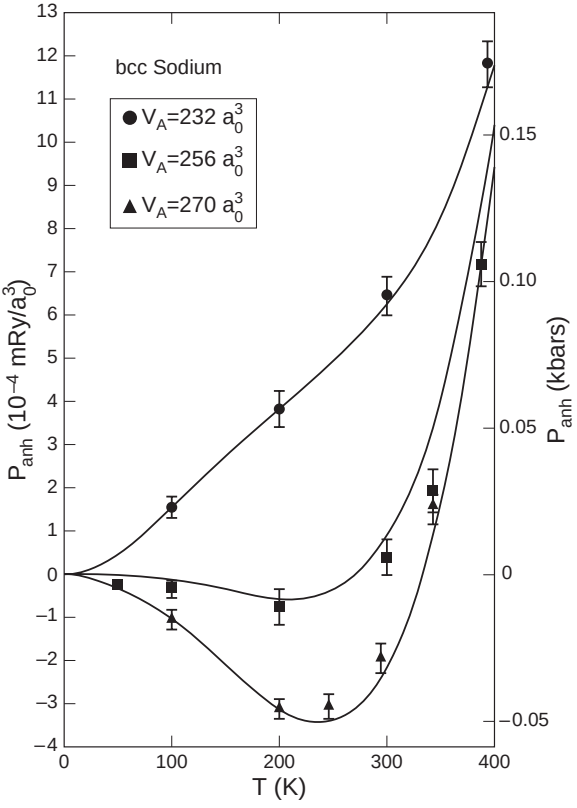


Figure 17.2. Classical anharmonic pressure *vs* $T$ at three volumes, from molecular dynamics calculations for sodium. None of the curves goes as $T^2$ within estimated errors.

theory. For in leading order, where the classical anharmonic free energy is $F^{cl}_{anh} = A_2 T^2$, the classical anharmonic energy and pressure are

$$U^{cl}_{anh} = -A_2 T^2 \quad , \quad P^{cl}_{anh} = -\frac{dA_2}{dV} T^2 \quad . \tag{17.13}$$

None of the data sets for $U^{cl}_{anh}$ or $P^{cl}_{anh}$ shown in Fig. 17.1 and 17.2 can be fitted to a $T^2$ curve within estimated errors. This result constitutes the strongest evidence we have for the failure of leading order anharmonic perturbation theory in the high temperature regime.

In related work, Glyde, Hansen, and Klein (1977) calculated the one-phonon contribution to the neutron scattering cross section $S(\mathbf{q}, \omega)$, for

a pseudopotential model for bcc potassium. They compared two theoretical procedures, namely (a) molecular dynamics, and (b) lattice dynamics, in the self-consistent-harmonic approximation plus cubic anharmonic contributions, at temperatures near $0.5T_m$ and $0.9T_m$. Since the phonon frequencies are primarily a quasiharmonic property, the two procedures should give nearly the same frequencies, and they do so within a few percent. On the other hand, the phonon widths (lifetimes) are a purely anharmonic effect, and here the two calculations are in reasonable agreement only at $T \approx 0.5T_m$. At $T \approx 0.9T_m$, the widths from molecular dynamics are about twice those from the anharmonic perturbation theory, and further, the molecular dynamics widths agree well with neutron scattering experiments on real potassium. The results demonstrate the failure of the particular anharmonic perturbation theory examined by Glyde, Hansen, and Klein.

Experimental data also provide information on the validity of anharmonic perturbation theory at high temperatures. In leading order perturbation theory, $F_{anh} = A_2T^2 + A_0 + \cdots$, and the corresponding entropy is $S_{anh} = -2A_2T + O(T^{-3})$. Over the years, we have carried out several studies of entropy at high temperatures, correcting the $S(T)$ curve from zero pressure to a fixed volume, and the results have always shown that $S_{anh}(T)$ at fixed volume is not of the form $AT$ for temperatures from around $\theta_2$ to $T_m$. This property is seen in the graphs of *Thermodynamics of Crystals*, Sec. 31, and in Fig. 1 of Wallace (1992b), and in unpublished graphs for transition metals, done in connection with Ericksson, Wills, and Wallace (1992).

Our general conclusion, implied here by the notation "failure of anharmonic perturbation theory," is as follows for the high temperature regime. First, when a reliable evaluation of an anharmonic property is needed, leading order perturbation theory will not provide it. Second, though theoretical procedures have been devised which will reproduce a specific computer simulation result for a specific interatomic potential, no theory of any order has been developed which is reliable for a general interatomic potential.

### *Classical Nuclear Motion from Computer Simulations*

For a given potential function $\Phi(\{\mathbf{r}_K\})$, statistical averages over the classical nuclear motion can be calculated from molecular dynamics or Monte Carlo techniques. In this way one obtains the total nuclear motion contribu-

tion, the classical quasiharmonic plus the classical anharmonic. There are two ways to use these computed results. First, by invoking lattice dynamics theory, one can extract the classical anharmonic part which is contained in the computer simulation data. This procedure can give reliable information on the nature of anharmonicity in crystals, as described in the last subsection. Second, the computer simulations can give accurate results for the thermodynamic properties of real crystals in the high temperature regime. For this application, the potential $\Phi(\{\mathbf{r}_K\})$ must be an accurate representation of the real potential in the real crystal. Let us illustrate the quality of results which can be obtained, by means of a detailed analysis of the entropy of bcc sodium at high temperatures.

The complete theory for the entropy of a crystal is

$$S = S_{ph} + S_{anh} + S_{el} + S_{ep} \quad . \tag{17.14}$$

The dominant term, which requires a highly accurate evaluation, is $S_{ph}$, given by Eq. (17.6) for high temperatures. To evaluate Eq. (17.6), we take $\theta_0$ and $\theta_2$ from neutron scattering measurements at 90 K, from Table 15.1, and we correct these for the temperature dependent volume change at $P = 0$, with the technique described in Sec. 19. Terms in (17.6) beyond $(\theta_2/T)^2$ are negligible here. The curve of $\theta_0(T, P = 0)$ is shown in the top panel of Fig. 17.3, and we estimate $\theta_0$ is accurate to better than 1% over the entire temperature range. The electronic excitation entropy $S_{el}$ is quite small, and is calculated in the Sommerfeld expansion, with $n(\epsilon_F)$ from electronic structure calculations, again with temperature dependent volume corrections applied. The electron-phonon interaction entropy $S_{ep}$ is neglected, as is appropriate for $T \gtrsim \theta_2$. Theoretical details regarding $S_{el}$ and $S_{ep}$ can be found in Sec. 18. The experimental entropy at $P = 0$ is $S_{expt}$, and the "experimental" anharmonic entropy is given by $S_{anh} = S_{expt} - S_{ph} - S_{el}$. We used two compilations of experimental data, those of Hultgren *et al.* (1973), and of Chase *et al.* (1985). Data for the crystal at $T_m = 371.0$ K, in units of $k$ per atom, are

$$\begin{aligned} S_{expt} &= 6.934 \text{ (Hultgren } et\, al.) \quad , \\ S_{expt} &= 6.964 \text{ (Chase } et\, al.) \quad , \\ S_{ph} &= 6.780 \pm 0.020 \quad , \\ S_{el} &= 0.053 \pm 0.005 \quad . \end{aligned} \tag{17.15}$$

The difference between the two experimental sources is an indication of the

experimental error. The two curves of $S_{anh}$ are shown in the lower panel of Fig. 17.3. Notice the experimental curves differ essentially by a constant, which is obviously traceable to a difference in specific heat data at some lower temperature.

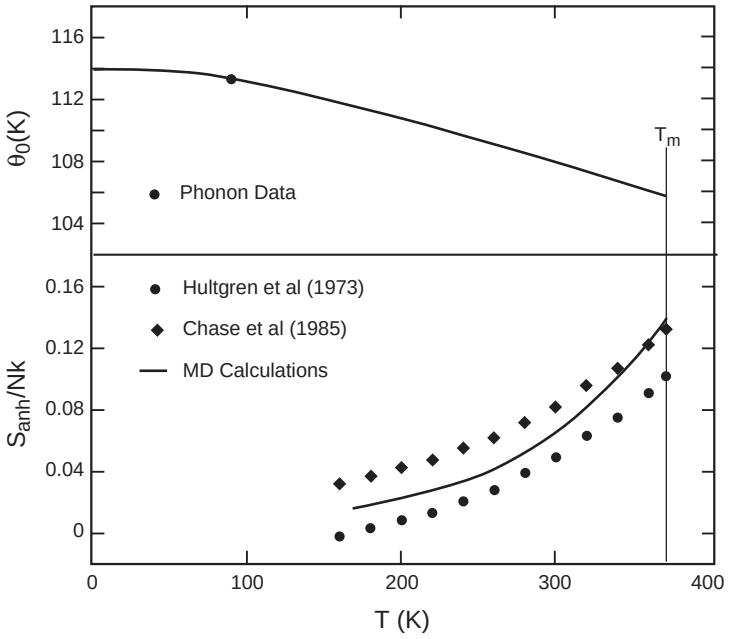


Figure 17.3. Upper panel: $\theta_0(T, P = 0)$ for bcc Na, calibrated at 90 K by experimental phonon data. Lower panel: anharmonic entropy of bcc Na from two experimental data compilations, and from molecular dynamics calculations (see text for details).

For pseudopotential sodium, we calculated the anharmonic entropy at high temperatures from the equation valid at a fixed volume,

$$S_{anh}(T) \approx S_{anh}(\theta_2) + \int_{\theta_2}^{T} \left( \frac{\partial U_{anh}^{cl}}{\partial T'} \right)_V d \ln T' \quad . \tag{17.16}$$

The classical anharmonic energy $U_{anh}^{cl}$ is from the molecular dynamics results shown in Fig. 17.1, and the small error in Eq. (17.16) is the replacement of $U_{anh}$ by $U_{anh}^{cl}$ at $T \geq \theta_2$. The unknown in Eq. (17.16) is the constant of integration, $S_{anh}(\theta_2)$. We have always estimated this as zero,

and here we shall take the average of the two experimental curves, so that

$$S_{anh}(\theta_2) = 0.018\ k/atom \quad , \quad \text{at } \theta_2 = 164K \quad . \tag{17.17}$$

Our theoretical $S_{anh}$ at $P = 0$ is also graphed in Fig. 17.3. We learn two things from this figure. First, the experimental anharmonic entropy is small, but is well outside experimental error, and amounts to around 0.12 k/atom, or 1.5% of the total entropy, at $T_m$. Second, given the experimental value of $S_{anh}(\theta_2)$, Eq. (17.17), the anharmonic entropy from molecular dynamics agrees with the experimental anharmonic entropy to around $\pm$ 0.02 k/atom, or $\pm$ 0.3% of the total entropy.

This entropy analysis for bcc sodium exemplifies theory and experiment at the high-accuracy level. In our experience, a single analysis at the high-accuracy level is more informative than many less accurate analyses. From extensive calculations over many years, we conclude that, given an accurate internuclear potential for an elemental crystal or liquid, molecular dynamics calculations of the nuclear motion statistical properties are highly accurate.

*Problem*

*17.1* Show that the leading quantum correction in Eq. (17.2) is the same as Kirkwood's result expressed in Eqs. (9.27) and (9.29), when the latter is evaluated with the nuclei located at crystal lattice sites. Note problem 13.3 is helpful here.

## 18 ELECTRONIC EXCITATIONS

### *Reference Structure Electrons*

For a normal (nonsuperconducting) metal at sufficiently low temperatures, the Sommerfeld expansion is valid, and according to Eq. (7.54), the theoretical free energy due to excitation of reference structure electrons is

$$F_{el} = -\frac{1}{2}\Gamma T^2 \quad , \quad \Gamma = \frac{\pi^2}{3}k^2 n(\epsilon_F) \quad , \tag{18.1}$$

where $n(\epsilon_F)$ is the density of states at the Fermi energy. Because the density of states is generally not suited to a Taylor expansion about $\epsilon_F$, we do not continue the Sommerfeld expansion to higher orders, but instead, at temperatures where Eq. (18.1) becomes inaccurate, we use the complete

integral formulation of thermodynamic functions. The electronic entropy is, from Eq. (7.52),

$$S_{el} = -k \int n(\epsilon)\{\bar{f}(\epsilon) \ln \bar{f}(\epsilon) + [1 - \bar{f}(\epsilon)] \ln[1 - \bar{f}(\epsilon)]\} d\epsilon \quad , \tag{18.2}$$

where

$$\bar{f}(\epsilon) = \frac{1}{e^{\beta(\epsilon - \mu)} + 1} \quad . \tag{18.3}$$

Notice the normalization of $S_{el}$ is carried in $n(\epsilon)$. When $n(\epsilon)$ is measured per atom, the chemical potential $\mu(\beta)$ is determined by

$$z = \int n(\epsilon) \bar{f}(\epsilon) d\epsilon \quad , \tag{18.4}$$

where $z$ is the number of electrons per atom. Modern electronic structure calculations of $n(\epsilon)$ for metals generally agree with one another to around 10%.

For nearly-free electron metals, reference structure electrons are approximately free electrons. For free electrons the energy is denoted $e$, the Fermi wavevector is $f$, and the Fermi energy $e_F$ and density of states $n(e)$ per atom are given by

$$e_F = \frac{\hbar^2 f^2}{2m} \quad , \quad \text{where } f^3 = \frac{3\pi^2 z}{V_A} \quad , \tag{18.5}$$

$$n(e) = \sqrt{\frac{e}{e_F}} n(e_F) \quad , \quad \text{where } \quad n(e_F) = \frac{3z}{2e_F} \quad . \tag{18.6}$$

Calculations in local density approximation of $n(\epsilon)$ for fcc and bcc Al, and the free electron $n(\epsilon)$, are all compared in Fig. 18.1. Presumably, the density of states for the random structures in liquid Al is approximately the same as the curves shown in the figure. We conclude that the free electron model will serve to calculate reference structure electronic excitation properties to an accuracy of around 10%, for crystal and liquid Al, at normal density and to temperatures of say 0.1 Ry. Conversion factors useful enough to remember are

$$\begin{aligned} 1 \text{ meV} &= 11.605K \quad , \\ 1 \text{ mRy} &= 157.89K \quad . \end{aligned} \tag{18.7}$$

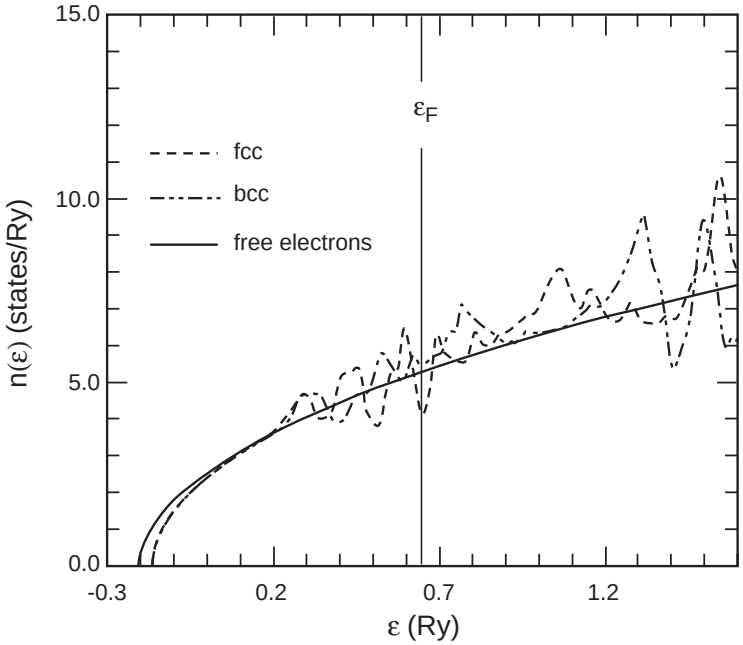


Figure 18.1. Electronic density of states for Al at $V_A = 112.0a_0^3$/atom ($\rho = 2.700 g/cm^3$), from density functional theory for fcc and bcc crystals, and from the free electron model.

Whether or not the free electron model will be of sufficient accuracy for a given metal has to be determined by comparing graphs of $n(\epsilon)$ and $n(e)$, as illustrated in Fig. 18.1. The same principle applies at all densities, since the electronic structure changes with compression. Generally for nearly-free-electron metals, the electronic excitation contribution to thermodynamic functions is relatively small, say a few percent at temperatures to melt, so that an error of 10 or 20 percent in the density of states can be acceptable. Moreover, to this kind of accuracy, the leading term in the Sommerfeld expansion is usually all that is needed for nearly-free-electron metals.

The transition metals are characterized by narrow partially-filled d bands. These bands have a large and rapidly varying density of states, for which departure from the leading low-temperature electronic entropy can be seen at temperatures as low as 300 K. Ericksson, Wills, and Wallace (1992) evaluated $S_{el}$ from Eq. (18.2) for 11 transition metals, from 300 K to melting, and at the zero-pressure density as function of temperature. If anharmonic-

ity, magnetism, and electron-phonon interactions are neglected, the total entropy is $S = S_{ph} + S_{el}$. Experimental data for $S - S_{ph}$ are compared with our theoretical $S_{el}$ in Fig. 18.2, for Pd and Pt. The figure illustrates the following general conclusions we are able to draw from our study of transition metals. First, $S_{el}$ is larger by a factor of 5–10 in transition metals than in nearly-free-electron metals. Second, the low temperature behavior where $S_{el}$ is linear in $T$ is in significant error for transition metals at temperatures above 300 K or so. Third, with certain notable exceptions, the error in the approximation $S \approx S_{ph} + S_{el}$ is on the order of 1%, the same order as the combined experimental and theoretical errors in the separate terms. A more extensive analysis of the entropy of elemental crystals is presented in Sec. 19.

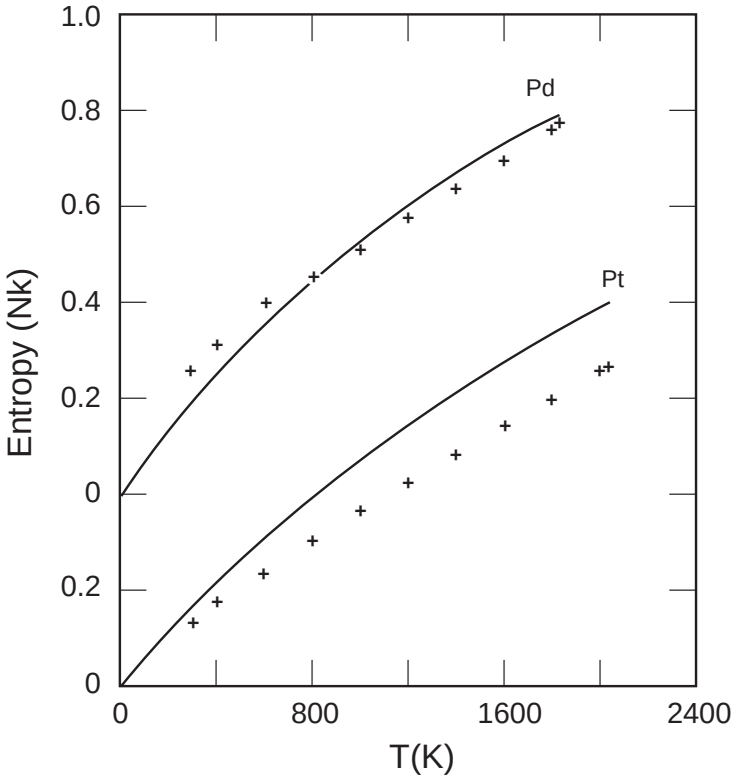


Figure 18.2. Entropy contributions for Pd and Pt, *vs* $T$ at $P = 0$. Solid lines are calculated $S_{el}$, and points are experimental $S - S_{ph}$.

***Interacting Electron-Phonon Description***

Our treatment of excited states of the electronic system, and their interaction with the nuclear motion, is in the one-electron approximation, as formulated in Secs. 3 and 4. The one-electron Hamiltonian is written in Eq. (3.7), as

$$h(\mathbf{r}) = -\frac{\hbar^2\nabla^2}{2m} + V_g(\mathbf{r}) \quad , \tag{18.8}$$

where $V_g(\mathbf{r})$ is the groundstate one-electron potential. $V_g(\mathbf{r})$ depends on the nuclear positions $\mathbf{r}_L$, $L = 1, \cdots, N$, and can in principle be obtained from density functional theory, as described in Sec. 3. The one-electron energies, eigenvalues of $h(\mathbf{r})$, are $E_\lambda$, $\lambda = 1, 2, \cdots$, and these energies also depend on the nuclear positions. For a set of electrons labeled $\alpha$, $\alpha = 1, \cdots, \mathcal{Z}$, the Hamiltonian expressing excitations from the ground state is given by Eq. (3.14),

$$\mathcal{H}_{EX} = \sum_\alpha h(\mathbf{r}_\alpha) - \sum_\lambda g_\lambda E_\lambda \quad , \tag{18.9}$$

where the last term is the system groundstate energy.

For notational simplicity, we restrict our analysis to a primitive crystal lattice. In the reference structure, the nuclei are located at the lattice sites $\mathbf{R}_L$, and the one-electron problem is solved by a complete orthonormal set of wavefunctions $\psi_\lambda(\mathbf{r})$, with corresponding energies $\epsilon_\lambda$. Only electrons which contribute to thermal excitation need to be considered, and these are presumed to lie in a single conduction band, so that $\lambda$ stands for a wavevector $\mathbf{p}$ and spin $\sigma$,

$$\lambda = \mathbf{p}\sigma \quad ; \quad \sum_\lambda = \sum_{\mathbf{p}} \sum_\sigma = 2 \sum_{\mathbf{p}} \quad . \tag{18.10}$$

The spin sum can be replaced by 2 because all matrix elements required here are independent of spin. The wavevector sum is *unrestricted*, meaning that $\mathbf{p}$ goes over all values consistent with periodic boundary conditions, as described in Sec. 5. The excitation Hamiltonian at the reference structure is $\mathcal{H}_{el}$,

$$\mathcal{H}_{el} = \sum_\lambda \epsilon_\lambda (C_\lambda^+ C_\lambda - g_\lambda) \quad . \tag{18.11}$$

This is the same as Eq. (4.15), but with simpler notation.

The general expression for $\delta\mathcal{H}_{EX}$, valid for arbitrary nuclear positions $\mathbf{r}_L$, and resolved into reference-structure electron matrix elements, is given in Eqs. (4.12)–(4.18). In current notation,

$$\mathcal{H}_{EX} = \mathcal{H}_{el} + \delta\mathcal{H}_{EX} \quad . \tag{18.12}$$

Here we shall express $\delta\mathcal{H}_{EX}$ for a crystal, by means of harmonic lattice dynamics theory. We write $\mathbf{r}_L = \mathbf{R}_L + \mathbf{U}_L$, and expand the one-electron potential $V_g(\mathbf{r})$ in powers of the displacements $\mathbf{U}_L$, to second order. The zeroth-order term gives the reference structure Hamiltonian, Eq. (18.11). The first-order term in the expansion of $V_g$ gives the following contribution to $\delta\mathcal{H}_{EX}$:

$$\sum_{\lambda\lambda'} \left\langle \psi_{\lambda'} \left| \sum_{Li} \frac{\partial V_g}{\partial R_{Li}} U_{Li} \right| \psi_\lambda \right\rangle C^+_{\lambda'} C_\lambda \quad . \tag{18.13}$$

The groundstate energy subtraction, present in Eq. (18.9), vanishes in first order in nuclear displacements, because the structure is an equilibrium configuration of the nuclei. The above matrix element is simplified by means of the Bloch theorem,

$$\psi_\lambda(\mathbf{r}) = e^{i\mathbf{p}\cdot\mathbf{R}_L}\psi_\lambda(\mathbf{r} - \mathbf{R}_L) \quad , \tag{18.14}$$

and $U_{Li}$ is expressed in terms of phonon operators by means of Eq. (13.20), then by Eqs. (16.2) and (16.3) for the creation and annihilation operators. The following electron-phonon interaction coefficient appears:

$$V(\mathbf{k}s, \mathbf{Q}, \lambda) = \sqrt{\frac{\hbar}{2NM\omega(\mathbf{k}s)}} \sum_i v_i(\mathbf{k}s)\theta_i(\lambda + \mathbf{k} + \mathbf{Q}, \lambda) \quad , \tag{18.15}$$

where $v_i(\mathbf{k}s)$ is a component of the phonon eigenvector, and where

$$\theta_i(\lambda'\lambda) = N \int \psi^*_{\lambda'}(\mathbf{r} - \mathbf{R}_L) \frac{\partial V_g}{\partial R_{Li}} \psi_\lambda(\mathbf{r} - \mathbf{R}_L) d\mathbf{r} \quad . \tag{18.16}$$

The notation is $\lambda = \mathbf{p}, \sigma$, and $\lambda + \mathbf{k} + \mathbf{Q} = \mathbf{p} + \mathbf{k} + \mathbf{Q}, \sigma$. The integral in (18.16) is of order 1, not $N$, because the $\psi_\lambda$ are normalized to the volume of the crystal, while $\partial V_g/\partial R_{Li}$ is appreciable only over a volume of order $V_A$. Additional properties are $\theta^*_i(\lambda'\lambda) = \theta_i(\lambda\lambda')$, and $\theta_i(\lambda'\lambda)$ contains $\delta_{\sigma\sigma'}$, and $\theta_i(\lambda'\lambda)$ is independent of $\mathbf{R}_L$.

In the contribution to $\delta\mathcal{H}_{EX}$ of second order in nuclear displacements, only diagonal electronic matrix elements need to be kept, and terms diagonal in phonon operators, in order to obtain the total energy levels correct to second order in the displacements. Here the electron-phonon interaction coefficient $W(\mathbf{k}s,\lambda)$ appears, where

$$W(\mathbf{k}s,\lambda) = \frac{\hbar}{2NM\omega(\mathbf{k}s)} \sum_{ij} v_i(\mathbf{k}s)\theta_{ij}(\mathbf{k},\lambda)v_j(-\mathbf{k}s) \quad , \tag{18.17}$$

$$\theta_{ij}(\mathbf{k},\lambda) = \sum_L e^{i(\mathbf{k}-\mathbf{p})\cdot(\mathbf{R}_M-\mathbf{R}_L)} N \int \psi^*_\lambda(\mathbf{r}-\mathbf{R}_M)\frac{\partial^2 V_g}{\partial R_{Mi}\partial R_{Lj}}\psi_\lambda(\mathbf{r}-\mathbf{R}_L)d\mathbf{r} \quad . \tag{18.18}$$

The second derivative of $V_g$ is presumably a local function, *i.e.* it vanishes for $|\mathbf{R}_M - \mathbf{R}_L|$ greater than a few nearest-neighbor distances, so the $\Sigma_L$ can be evaluated in the interior of the crystal. Then $\theta_{ij}$ is independent of $\mathbf{R}_M$, and $\theta_{ij}$ is of order 1, not $N$.

The total crystal Hamiltonian is $\mathcal{H} = \mathcal{H}_N + \mathcal{H}_{EX}$, Eq. (4.8). The nuclear motion Hamiltonian is expressed in the interacting phonon description in Eq. (16.6). Let us gather the terms in $\mathcal{H}_{EX}$, derived according to the preceding outline, and write the crystal Hamiltonian in the interacting electron-phonon description:

$$\mathcal{H} = \Phi_0 + \mathcal{H}_{ph} + \mathcal{H}_{el} + \mathcal{H}_{anh} + \mathcal{H}_{ep} \quad . \tag{18.19}$$

The independent-particle part describes quasiharmonic phonons in $\mathcal{H}_{ph}$, and reference structure electronic excitations in $\mathcal{H}_{el}$. Phonon-phonon interactions are contained in $\mathcal{H}_{anh}$. The terms coupling electronic excitations and phonons are called simply electron-phonon interactions, and are

$$\mathcal{H}_{ep} = \mathcal{H}^{(1)}_{ep} + \mathcal{H}^{(2)}_{ep} \quad , \tag{18.20}$$

$$\mathcal{H}^{(1)}_{ep} = \sum_\lambda \sum_{\mathbf{k}s}{}' \sum_{\mathbf{Q}} V(\mathbf{k}s,\mathbf{Q},\lambda)(A_{\mathbf{k}s} + A^+_{-\mathbf{k}s})C^+_{\lambda+\mathbf{k}+\mathbf{Q}}C_\lambda \quad , \tag{18.21}$$

$$\begin{aligned}\mathcal{H}_{ep}^{(2)} &= \sum_{\lambda}\sum_{\mathbf{k}s}{}' W(\mathbf{k}s,\lambda)\left(A_{\mathbf{k}s}^{+}A_{\mathbf{k}s}+\frac{1}{2}\right)(C_{\lambda}^{+}C_{\lambda}-g_{\lambda}) \\ &\quad -\sum_{\lambda}\sum_{\mathbf{k}s}{}'\sum_{\mathbf{Q}}|V(\mathbf{k}s,\mathbf{Q},\lambda)|^{2}\frac{g_{\lambda}(1-g_{\lambda+\mathbf{k}+\mathbf{Q}})}{(\epsilon_{\lambda}-\epsilon_{\lambda+\mathbf{k}+\mathbf{Q}})} \\ &\quad \times(A_{\mathbf{k}s}^{+}A_{\mathbf{k}s}+A_{-\mathbf{k}s}^{+}A_{-\mathbf{k}s}+1) \quad . \end{aligned} \tag{18.22}$$

The $\Sigma_{\lambda}$ is over all one-electron states, the $\Sigma'_{\mathbf{k}s}$ is over the phonons in one Brillouin zone, and the $\Sigma_{\mathbf{Q}}$ is over all reciprocal lattice vectors. Subtraction of the system groundstate energy, as it appears in Eq. (18.9), is expressed in Eq. (18.11) for $\mathcal{H}_{el}$, and in Eq. (18.22) for $\mathcal{H}_{ep}^{(2)}$, in the terms which contain the groundstate occupation numbers $g_{\lambda}$.

***Interaction Free Energy***

To calculate the interaction free energy, one first calculates the total system energy levels $\mathcal{E}_{ep}$ due to the perturbation $\mathcal{H}_{ep}$, correct to second order in nuclear displacements. Since $\mathcal{E}_{ep}$ contains no first order terms, the general perturbation expansion of the free energy, Eq. (7.59), yields

$$F_{ep} = \langle \mathcal{E}_{ep} \rangle \quad , \tag{18.23}$$

correct to second order, where the average is the zeroth-order thermal average over both electronic excitations and phonons. Thermal averages of the occupation numbers are denoted as usual by $\bar{f}_{\lambda}$ and $\bar{n}(\mathbf{k}s)$.

The calculation of $\mathcal{E}_{ep}$ was done in *Thermodynamics of Crystals*, Sec. 25, by first finding the individual electron and phonon energy shifts, then summing these with appropriate multiple-counting factors. The result is the same as an ordinary perturbation calculation of the total energy shift $\mathcal{E}_{ep}$. The average $\langle \mathcal{E}_{ep} \rangle$ then consists of two types of contribution, adiabatic and nonadiabatic, in which the nuclear motion respectively does not mix, and does mix, the reference structure one-electron states. Let us denote the adiabatic contribution with a subscript *ad*, the nonadiabatic contributions with subscript *na*, and write

$$F_{ep} = F_{na1} + F_{na2} + F_{ad} \quad . \tag{18.24}$$

The two nonadiabatic contributions are given by

$$F_{na1} = \sum_{\lambda}\sum_{\mathbf{k}s}{}'\sum_{\mathbf{Q}} |V(\mathbf{k}s,\mathbf{Q},\lambda)|^2(\bar{f}_\lambda - \bar{f}_{\lambda+\mathbf{k}+\mathbf{Q}}\left[\bar{n}(\mathbf{k}s)+\frac{1}{2}\right] \times\left[\frac{1}{\epsilon_\lambda-\epsilon_{\lambda+\mathbf{k}+\mathbf{Q}}+\hbar\omega(\mathbf{k}s)}-\frac{1}{\epsilon_\lambda-\epsilon_{\lambda+\mathbf{k}+\mathbf{Q}}}\right] \quad , \tag{18.25}$$

$$F_{na2} = \frac{1}{2}\sum_{\lambda}\sum_{\mathbf{k}s}{}'\sum_{\mathbf{Q}} |V(\mathbf{k}s,\mathbf{Q},\lambda)|^2\bar{f}_\lambda(1-\bar{f}_{\lambda+\mathbf{k}+\mathbf{Q}}) \times\left[\frac{1}{\epsilon_\lambda-\epsilon_{\lambda+\mathbf{k}+\mathbf{Q}}-\hbar\omega(\mathbf{k}s)}-\frac{1}{\epsilon_\lambda-\epsilon_{\lambda+\mathbf{k}+\mathbf{Q}}+\hbar\omega(\mathbf{k}s)}\right] \quad . \tag{18.26}$$

Notice each nonadiabatic contribution vanishes if one sets $\hbar\omega(\mathbf{k}s)=0$ in the denominators of terms in brackets, and indeed, this property is tantamount to the *meaning* of nonadiabatic in the perturbation formulation.

The adiabatic contribution has a simple interpretation in terms of the adiabatically "renormalized" one-electron energy levels. When the nuclear positions are arbitrary, the one-electron energy levels are $E_\lambda(\{\mathbf{r}_L\})$. The $E_\lambda$ may be expanded to second order in displacements of the nuclei from equilibrium, and averaged over the nuclear motion, a phonon average, to find

$$\langle E_\lambda\rangle = \epsilon_\lambda + \langle E_\lambda^{(2)}\rangle \quad , \tag{18.27}$$

where

$$\langle E_\lambda^{(2)}\rangle = \sum_{\mathbf{k}s}{}'\sum_{\mathbf{Q}} |V(\mathbf{k}s,\mathbf{Q},\lambda)|^2\frac{[2\bar{n}(\mathbf{k}s)+1]}{\epsilon_\lambda-\epsilon_{\lambda+\mathbf{k}+\mathbf{Q}}} + \sum_{\mathbf{k}s} W(\mathbf{k}s,\lambda)\left[\bar{n}(\mathbf{k}s)+\frac{1}{2}\right] \quad . \tag{18.28}$$

The adiabatic contribution to $F_{ep}$ is then

$$F_{ad} = \sum_\lambda (\bar{f}_\lambda - g_\lambda)\langle E_\lambda^{(2)}\rangle \quad . \tag{18.29}$$

This equation demonstrates the meaning of adiabatic, namely that the electrons continue to behave as independent particles, with the one-electron

energy levels merely averaged over the thermal nuclear motion. The entire electron-phonon groundstate subtraction is contained in the term in $g_\lambda$ in Eq. (18.29). This means the term quadratic in $g_\lambda$, in Eq. (18.22), vanishes identically in the average of $\mathcal{H}_{ep}^{(2)}$. That the groundstate subtraction appears entirely in the adiabatic part of $F_{ep}$ is obviously correct, since nuclear motion with the electrons in their groundstate is by definition adiabatic. Finally, in the high temperature regime, where the nuclear motion approaches classical, Eq. (18.29) is the same as the classical adiabatic free energy written in Eq. (9.41), when the latter is evaluated for a crystal in harmonic lattice dynamics.

Coffey and Pethick (1988) derived the interaction free energy in their Eq. (3), where of the two terms in brackets, the first is $F_{na2}$, and the second is $F_{na1} + F_{ad}$, without the adiabatic term in $W(\mathbf{k}s, \lambda)$, and without the adiabatic groundstate subtraction. Grimvall (1976) wrote the same interaction free energy, namely $F_{na}$ plus part of $F_{ad}$, in his Eq. (1), and went on to suggest a partial summation of the perturbation theory. The results here are the same as in *Thermodynamics of Crystals*, with the extension that $V_g(\mathbf{r})$ in Eq. (18.8) is general, and is not approximated by a sum of rigid ion potentials. The present formulation is applicable in principle to any elemental metal.

### *Nearly-Free-Electron Metals*

Pseudopotential perturbation theory is a perturbation expansion about free electrons. The one-electron Hamiltonian is

$$h(\mathbf{r}) = -\frac{\hbar^2 \nabla^2}{2m} + W(\mathbf{r}) \quad , \tag{18.30}$$

where the potential $W(\mathbf{r})$ is self-consistent with the electrons in their groundstate, and $W(\mathbf{r})$ is treated as a perturbation. The wavefunctions to first order, and energies to second order, are

$$\psi_{\mathbf{p}} = |\mathbf{p}\rangle + \sum_{\mathbf{q}}{}' \frac{W(\mathbf{q})|\mathbf{p}+\mathbf{q}\rangle}{(e_{\mathbf{p}} - e_{\mathbf{p}+\mathbf{q}})} \quad , \tag{18.31}$$

$$E_{\mathbf{p}} = e_{\mathbf{p}} + W(\mathbf{q}=0) + \sum_{\mathbf{q}}{}' \frac{|W(\mathbf{q})|^2}{(e_{\mathbf{p}} - e_{\mathbf{p}+\mathbf{q}})} \quad , \tag{18.32}$$

where $e_{\mathbf{p}} = \hbar^2\mathbf{p}^2/2m$, and where the constant $W(\mathbf{q}=0)$ will contribute nothing to our theory here. The pseudopotential $W(\mathbf{r})$ is a sum of screened potentials $w(|\mathbf{r}-\mathbf{r}_L|)$, which move rigidly with the ions,

$$W(\mathbf{r}) = \sum_L w(|\mathbf{r}-\mathbf{r}_L|) \quad . \tag{18.33}$$

It is only through $W(\mathbf{r})$ that the ion positions enter the electronic structure theory.

The versatility of pseudopotential perturbation theory occurs in large part because the above equations are valid for arbitrary positions $\mathbf{r}_L$ of the nuclei. However, the present application is formulated in terms of reference structure electrons, so we want the wavefunctions and energies evaluated at $\mathbf{r}_L = \mathbf{R}_L$. Now $W(\mathbf{q}) = S(\mathbf{q})w(|\mathbf{q}|)$, and for a perfect crystal $S(\mathbf{q}) = \Delta(\mathbf{q})$, hence for the reference structure electrons, the $\Sigma'_{\mathbf{q}}$ in pseudopotential perturbation theory reduces to a sum over reciprocal lattice vectors. While only the planewaves $|\mathbf{p}\rangle$ are required in evaluating the matrix element $\theta_i(\lambda'\lambda)$, Eq. (18.16), the first-order term in $\psi_{\mathbf{p}}$ is crucial for evaluating the matrix element $\theta_{ij}(\mathbf{k},\lambda)$, Eq. (18.18). The first-order interaction coefficient $V(\mathbf{k}s,\mathbf{Q},\lambda)$ simplifies to

$$V(\mathbf{k}s,\mathbf{Q}) = -i\sqrt{\frac{\hbar}{2NM\omega(\mathbf{k}s)}}[(\mathbf{k}+\mathbf{Q})\cdot\mathbf{v}(\mathbf{k}s)]w(|\mathbf{k}+\mathbf{Q}|) \quad . \tag{18.34}$$

The second-order interaction coefficient $W(\mathbf{k}s,\lambda)$ is

$$W(\mathbf{k}s,\mathbf{p}) = -\frac{\hbar}{NM\omega(\mathbf{k}s)}\sum_{\mathbf{Q}}{}' \frac{|\mathbf{Q}\cdot\mathbf{v}(\mathbf{k}s)|^2[w(|\mathbf{Q}|)]^2}{e_{\mathbf{p}} - e_{\mathbf{p}+\mathbf{Q}}} \quad . \tag{18.35}$$

The corresponding electron-phonon Hamiltonian is examined in problems 18.1 and 18.2.

Expressions for the interaction free energy contributions are as follows, correct to second order in the pseudopotential.

$$\begin{aligned} F_{na1} \quad = \quad & -\sum_{\mathbf{p}}\sum_{\mathbf{k}s}{}'\sum_{\mathbf{Q}}(\bar{f}_{\mathbf{p}} - \bar{f}_{\mathbf{p}+\mathbf{k}+\mathbf{Q}})\left[\bar{n}(\mathbf{k}s)+\frac{1}{2}\right] \\ & \times\frac{\hbar^2}{NM}\frac{|(\mathbf{k}+\mathbf{Q})\cdot\mathbf{v}(\mathbf{k}s)|^2[w(|\mathbf{k}+\mathbf{Q}|)]^2}{(e_{\mathbf{p}} - e_{\mathbf{p}+\mathbf{k}+\mathbf{Q}})(e_{\mathbf{p}} - e_{\mathbf{p}+\mathbf{k}+\mathbf{Q}} + \hbar\omega(\mathbf{k}s))} \quad , \end{aligned} \tag{18.36}$$

$$F_{na2} = \sum_{\mathbf{p}} \sum_{\mathbf{k}s}{}' \sum_{\mathbf{Q}} \bar{f}_{\mathbf{p}}(1 - \bar{f}_{\mathbf{p}+\mathbf{k}+\mathbf{Q}}) \times \frac{\hbar^2}{NM} \frac{|(\mathbf{k}+\mathbf{Q})\cdot\mathbf{v}(\mathbf{k}s)|^2 [w(|\mathbf{k}+\mathbf{Q}|)]^2}{(e_{\mathbf{p}} - e_{\mathbf{p}+\mathbf{k}+\mathbf{Q}})^2 - (\hbar\omega(\mathbf{k}s))^2} \quad , \tag{18.37}$$

$$F_{ad} = 2\sum_{\mathbf{p}} (\bar{f}_{\mathbf{p}} - g_{\mathbf{p}}) \langle E^{(2)}_{\mathbf{p}} \rangle \quad , \tag{18.38}$$

where

$$\langle E^{(2)}_{\mathbf{p}} \rangle = \sum_{\mathbf{k}s}{}' \frac{\hbar[\bar{n}(\mathbf{k}s) + \frac{1}{2}]}{NM\omega(\mathbf{k}s)} \left[ \sum_{\mathbf{Q}} \frac{|(\mathbf{k}+\mathbf{Q})\cdot\mathbf{v}(\mathbf{k}s)|^2 [w(|\mathbf{k}+\mathbf{Q}|)]^2}{e_{\mathbf{p}} - e_{\mathbf{p}+\mathbf{k}+\mathbf{Q}}} - \sum_{\mathbf{Q}}{}' \frac{|\mathbf{Q}\cdot\mathbf{v}(\mathbf{k}s)|^2 [w(|\mathbf{Q}|)]^2}{e_{\mathbf{p}} - e_{\mathbf{p}+\mathbf{Q}}} \right] \quad . \tag{18.39}$$

Recall the present derivation is for a primitive lattice, so $s$ labels three phonon branches, all of which are acoustic. The phonon wavevector $\mathbf{k}$ is from one Brillouin zone, $\Sigma_{\mathbf{Q}}$ is over all reciprocal lattice vectors, hence the vectors $\mathbf{k}+\mathbf{Q}$ are unrestricted. The electron momentum $\mathbf{p}$ is likewise unrestricted. Angle integrals in $F_{na2}$ and $F_{ad}$ are done in Eqs. (28.50) and (28.41), respectively, of *Thermodynamics of Crystals*. It is possible to make a much simpler derivation of $F_{ad}$ (see problem 18.3).

### *Properties of the Interaction Free Energy*

Here we shall summarize what is known or surmised about the magnitudes and temperature dependences of the three contributions to $F_{ep}$. First, while $F_{ad} = 0$ at $T = 0$, the two nonadiabatic contributions are nonzero at $T = 0$, and therefore constitute a correction to the electronic groundstate energy $\mathcal{E}_g(\{\mathbf{R}_L\})$. This correction is of relative order $m/M$, hence is formally negligible, in line with our discussion of the resolution of the total Hamiltonian in Sec. 4. To examine the temperature dependence, it is convenient to work with the entropy $S_{ep} = -(\partial F_{ep}/\partial T)_V$, and to assess its importance, we shall compare $S_{ep}$ with $S_{el}$.

Let us first consider the adiabatic electron-phonon entropy, $S_{ad}$. One can argue that the thermal average energy shift due to nuclear motion,

$\langle E_\lambda^{(2)} \rangle$, should be small compared to the reference structure energy $\epsilon_\lambda$, hence from Eqs. (18.29) or (18.38) for $F_{ad}$, one can expect

$$|S_{ad}| \ll S_{el} \quad . \tag{18.40}$$

The available theoretical calculations support this conclusion. In *Thermodynamics of Crystals*, Table 27, we listed estimates from pseudopotential models for Na, K, and Al, showing that $|S_{ad}|$ is of order $10^{-3} S_{el}$ at low temperatures, and $|S_{ad}|$ remains less than 1% of $S_{el}$ at all temperatures to melt. Allen and Hui (1980) considered specifically the adiabatic part of $F_{ep}$, but their Eq. (3) reads $F_{ad} = \Sigma_\lambda \bar{f}_\lambda \langle E_\lambda^{(2)} \rangle$ in the present notation, and this misses the groundstate subtraction present in Eq. (18.29). As a result, the adiabatic electron-phonon contributions to specific heat are seriously overestimated by Allen and Hui. Here we conclude that Eq. (18.40) holds, with say $|S_{ad}| \lesssim 0.1 S_{el}$, so that $S_{ad}$ can be neglected entirely, at temperatures from zero to melt. It is always possible that this conclusion will prove incorrect in some extraordinary case.

Next let us examine the leading temperature dependence at low temperatures, of all the contributions to the electronic entropy. The leading term of the Sommerfeld expansion yields $S_{el} = \Gamma T$, where $\Gamma = \Gamma(V)$ is given by Eq. (18.1). As $T \to 0$, the mean phonon occupation satisfies $\bar{n}(\mathbf{k}s) + \frac{1}{2} \to \frac{1}{2}$, and the Sommerfeld expansion also gives a linear temperature dependence for each of the three contributions to $S_{ep}$. In view of Eq. (18.40), we can continue to neglect $S_{ad}$. Further, $S_{na1}$ is formally of order $\langle \hbar\omega \rangle / \epsilon_F \times S_{na2}$, so that $S_{na1}$ can also be neglected. Then the only significant electron-phonon contribution is $S_{na2}$, which we write

$$S_{na2} = \Delta_2 \Gamma T \quad , \tag{18.41}$$

where $\Delta_2 = \Delta_2(V)$. So the total electronic entropy is

$$S_{el} + S_{ep} = \Gamma(1 + \Delta_2) T \quad . \tag{18.42}$$

Though derived for a primitive lattice, these results are expected to hold for elemental metals in any lattice. From Eq. (18.41), the leading temperature dependence of $F_{na2}$ is $T^2$, and the next higher dependence was shown to be $T^3 \ln T$ by Coffey and Pethick (1988).

Finally let us examine $S_{ep}$ in the high temperature regime, at $\theta_2 \lesssim T \leq T_m$, where the nuclear motion is essentially classical. From the statistical mechanics of metals with classical nuclear motion, derived in Sec. 9, and

discussed following Eq. (9.41), the free energy contribution arising from the interaction between electronic excitations and nuclear motion is pure adiabatic. Hence the formal implication is

$$F_{ad} \gg F_{na} \quad , \quad \text{at } T \gtrsim \theta_2 \quad . \tag{18.43}$$

Since $|S_{ad}|$ is already small compared to $S_{el}$, from Eq. (18.40), we conclude

$$|S_{ep}| \ll S_{el} \quad , \quad \text{at } T \gtrsim \theta_2 \quad . \tag{18.44}$$

The available model calculations agree with this conclusion (work in progress by Nicolas Bock, Dermot Coffey, and Duane Wallace).

### *Theory and Experiment for Electron-Phonon Interactions*

At low temperatures, the electronic entropy in a metal can be measured, since it is linear in $T$ and dominates the $T^3$ phonon entropy. Experiment sees only the total or "renormalized" entropy $\hat{S}_{el}$,

$$\hat{S}_{el} = S_{el} + S_{ep} \quad . \tag{18.45}$$

The renormalized electronic specific heat is $\hat{C}_{el}$, given by

$$\hat{C}_{el} = \hat{S}_{el} = \hat{\Gamma} T \quad , \tag{18.46}$$

where $\hat{\Gamma}$ is the total specific heat coefficient. From Eq. (18.42), we have

$$\hat{\Gamma} = \Gamma(1 + \Delta_2) \quad . \tag{18.47}$$

Accurate calculations of $\Gamma$ and $\Delta_2$ for pseudopotential Na, K, and Al are listed in Table 27 of *Thermodynamics of Crystals*, and theory and experiment are compared here for $\hat{\Gamma}$, in Table 18.1. We conclude that pseudopotential perturbation theory gives a respectable account of this small and very complicated electron-phonon entropy at low temperatures. The electron-phonon contribution to electronic thermal expansion has also been calculated, by evaluating the volume dependence of $\hat{\Gamma}$ (*Thermodynamics of Crystals*, Table 28).

Still at low temperatures, it is possible in principle to extract the electron-phonon entropy from the experimental entropy, with the help of a theoretical value of $\Gamma$. Let us denote the experimental coefficient $\hat{\Gamma}_{expt}$, and use the customary notation $\lambda$ for the electron-phonon enhancement, so that

$$\hat{\Gamma}_{expt} = \Gamma(1 + \lambda) \quad . \tag{18.48}$$

Table 18.1. Comparison of theory and experiment for the electronic specific heat of nearly-free-electron metals at low temperature and zero pressure. $\Gamma_{fe}$ is the free-electron coefficient for $zN$ electrons.

| Quantity | Na | K | Al |
|---|---|---|---|
| Structure (z) | bcc(1) | bcc(1) | fcc(3) |
| $\Gamma_{fe}/Nk(10^{-4}/K)$ | 1.315 | 2.016 | 1.085 |
| $\hat{\Gamma}/\Gamma_{fe}$ (theory) | 1.25 | 1.17 | 1.67 |
| $\hat{\Gamma}/\Gamma_{fe}$ (experiment) | 1.26 | 1.24 | 1.50 |

It follows that $S_{ep}/S_{el} = \lambda$. Data for $\hat{\Gamma}_{expt}$ are often accurate to around 1%, while all-electron calculations in local density approximation give values of $\Gamma$ which appear to be accurate to 5% or so. Tables of $\lambda$ for many metals are given by Allen (1987), and by Sanborn, Allen, and Papaconstantopolous (1989). Values of $\lambda$ for transition metals, from the work of Eriksson, Wills, and Wallace (1992), are listed here in Table 18.2. Very roughly, $0 \lesssim \lambda \lesssim 0.5$ for nearly-free-electron metals, and $0 \lesssim \lambda \lesssim 1.0$ for transition metals. Clearly electron-phonon interactions give an important contribution to the low-temperature thermal properties of metals. When $\lambda \gtrsim \frac{1}{2}$, one would reasonably suspect that leading-order perturbation theory is not accurate for $S_{ep}$, although the leading-order calculation for Al in Table 18.1 is not far off.

Table 18.2. Electron-phonon enhancement parameter $\lambda$ for transition metals, obtained by comparing $\hat{\Gamma}_{expt}$ with $\Gamma$ from electronic structure calculations. Data for Cr are for the paramagnetic state.

| Metal | Structure | $n(\epsilon_F)$ (states/atom ev) | $\hat{\Gamma}_{expt}/Nk$ $(10^{-4}/K)$ | $\lambda$ |
|---|---|---|---|---|
| V | bcc | 1.861 | 11.81 | 1.24 |
| Nb | bcc | 1.414 | 9.39 | 1.34 |
| Ta | bcc | 1.227 | 7.24 | 1.08 |
| Cr | bcc | 0.656 | 2.8 | 0.49 |
| Mo | bcc | 0.502 | 2.21 | 0.56 |
| W | bcc | 0.321 | 1.20 | 0.32 |
| Pd | fcc | 2.357 | 11.31 | 0.69 |
| Pt | fcc | 2.237 | 7.88 | 0.24 |
| Ti | hcp | 0.939 | 4.02 | 0.51 |
| Zr | hcp | 1.020 | 3.37 | 0.16 |

*Problems*

*18.1.* Derive the interaction coefficients (18.34) and (18.35). Use these to express the Hamiltonian, Eqs. (18.11), (18.21), and (18.22), correct to second order in the pseudopotential. Notice the same result is obtained by starting with Eq. (18.30), and proceeding as in the algebra following Eq. (18.8).

*18.2.* For nearly-free-electron metals, one might think to express electron-phonon interactions in terms of free electrons in place of reference structure electrons. If you do this, what terms of second order in the pseudopotential are missing from the Hamiltonian?

*18.3.* The one-electron energy $E_{\mathbf{p}}$ of Eq. (18.32) is valid for arbitrary positions of the nuclei. Expand $E_{\mathbf{p}}$ in powers of nuclear displacements from the lattice sites, and recover Eq. (18.39) for the thermal average of second-order terms. What does the term of zeroth order in displacements represent?

## 19 LEARNING FROM THERMODYNAMIC DATA

### *Thermal Expansion*

At any constant pressure, the volume of a condensed matter system changes with temperature, usually but not always increasing as temperature increases. The volume at the constant pressure $P_a$ is denoted $V(T, P_a)$, or sometimes simply $V(T)$. The volume at zero temperature and pressure is $V(0, 0) = V_0$. The relative volume expansion of a metal from $T = 0$ to melt is nominally around 7%. For 41 elements, for which we have been able to find sufficient highly-accurate data to carry out extensive thermodynamic analyses, crystal structures and phase transition temperatures, electronic valence type, and densities at several temperatures are listed in Table 19.1. Statistical analysis of the relative volume expansions from $T = 0$ to melt is discussed in problem 19.1.

Table 19.1. Crystal structures, phase transition temperatures, and related data for 41 elemental crystals at 1 bar. Densities at 0 and 293 K are respectively $\rho_0$ and $\rho_{293}$, and density of the crystal at melt is $\rho_{cm}$. $\gamma^*$ is the high-temperature Grüneisen parameter.

| Element | Crystal Structure | Valence Type | $T_m$ $(K)$ | $\rho_0$ $(g/cm^3)$ | $\rho_{293}$ $(g/cm^3)$ | $\rho_{cm}$ $(g/cm^3)$ | $\gamma^*$ |
|---|---|---|---|---|---|---|---|
| Li | hex/75/bcc | nfe | 453.7 | 0.547[a] | 0.533 | 0.523 | 0.88(bcc) |
| Na | hex/36/bcc | nfe | 371.0 | 1.013[a] | 0.967 | 0.948 | 1.24(bcc) |
| K | bcc | nfe | 336.4 | 0.904 | 0.858 | 0.849 | 1.24 |
| Rb | bcc | nfe | 312.6 | 1.616 | 1.526 | 1.516 | 1.26 |
| Cs | bcc | nfe | 301.6 | 2.02 | 1.91 | 1.89 | 1.14 |
| Mg | hcp | nfe | 922 | 1.76 | 1.74 | 1.64 | 1.5 |
| Ca | fcc/720/bcc | ae | 1113 | 1.55 | 1.53 | 1.41 | 1.1(fcc) |
| Sr | fcc/830/bcc | ae | 1042 | 2.62 | 2.58 | 2.57 | — |
| Ba | bcc | ae | 1002 | 3.55 | 3.5 | 3.33 | 0.9 |
| Cu | fcc | nfe | 1358 | 9.020 | 8.933 | 8.36 | 2.02 |
| Ag | fcc | nfe | 1235 | 10.62 | 10.49 | 9.82 | 2.42 |
| Au | fcc | nfe | 1338 | 19.46 | 19.27 | 18.26 | 2.95 |
| Zn | hcp | nfe | 692.7 | 7.29 | 7.14 | 6.87 | 2.2 |
| Cd | hcp | nfe | 594.2 | 8.84 | 8.65 | 8.38 | 2.3 |
| Hg | rhomb | nfe | 234.3 | 14.48 | — | 14.19 | 2.5 |
| Al | fcc | nfe | 933.5 | 2.734 | 2.700 | 2.551 | 2.25 |
| In | bct | nfe | 429.8 | 7.46 | 7.30 | 7.16 | 2.4 |
| Tl | hcp/507/bcc | nfe | 577 | 12.11 | 11.85 | 11.58 | 2.1(hcp) |
| Pb | fcc | nfe | 600.6 | 11.58 | 11.34 | 11.01 | 2.65 |
| Ar | fcc | vdW | 83.81 | 1.7710 | — | 1.622 | 2.6 |
| Kr | fcc | vdW | 115.76 | 3.0926 | — | 2.801 | 2.6 |
| Xe | fcc | vdW | 161.39 | 3.781 | — | 3.402 | 2.9 |
| Ti | hcp/1155/bcc | 3d | 1945 | 4.527 | 4.505 | 4.24 | 1.2(hcp) |
| Zr | hcp/1136/bcc | 4d | 2128 | 6.530 | 6.507 | 6.25 | 0.9(hcp) |
| V | bcc | 3d | 2202 | 6.15 | 6.12 | 5.69 | 1.5 |
| Nb | bcc | 4d | 2744 | 8.62 | 8.58 | 7.99 | 1.6 |
| Ta | bcc | 5d | 3293 | 16.74 | 16.68 | 15.30 | 1.6 |
| Cr | bcc | 3d | 2133 | 7.215 | 7.19 | 6.68 | (1.5) |
| Mo | bcc | 4d | 2896 | 10.25 | 10.22 | 9.56 | 1.6 |
| W | bcc | 5d | 3695 | 19.31 | 19.26 | 17.96 | 1.6 |
| Fe | bcc/1184/fcc 1665/bcc | 3d | 1811 | 7.92 | 7.87 | 7.26 | 1.7(bcc) |
| Ni | fcc | 3d | 1728 | 8.97 | 8.91 | 8.27 | 1.9 |
| Pd | fcc | 4d | 1827 | 12.09 | 12.01 | 11.18 | 2.3 |
| Pt | fcc | 5d | 2045 | 21.58 | 21.46 | 20.18 | 2.6 |
| Th | fcc/1636/bcc | 5f | 2031 | 11.8 | 11.7 | — | 1.4(fcc) |

Table 19.1 (Cont.)

| Element | Crystal Structure | Valence Type | $T_m$ $(K)$ | $\rho_0$ $(g/cm^3)$ | $\rho_{293}$ $(g/cm^3)$ | $\rho_{cm}$ $(g/cm^3)$ | $\gamma^*$ |
|---|---|---|---|---|---|---|---|
| Ga | orthorhomb | nfe | 302.9 | 5.96 | 5.91 | 5.90 | 1.5 |
| Si | dia | cov | 1687 | 2.34 | 2.34 | 2.28 | (0.5) |
| Ge | dia | cov | 1211 | 5.33 | 5.32 | 5.24 | 0.8 |
| Sn | dia/286/bct | cov/nfe | 505.1 | 7.40[b] | 7.30 | 7.18 | 2.2(bct) |
| Sb | rhomb | sm | 904 | 6.73 | 6.68 | 6.42 | 1.0 |
| Bi | rhomb | sm | 544.5 | 9.88 | 9.78 | 9.74 | 1.1 |

Valence type abbreviations: nfe (nearly-free-electron metal); ae (alkaline earth); vdW (van der Waals); 3d, 4d, 5d (transition metal); 5f (actinide); cov (covalent); sm (semimetal).

[a] Density in bcc structure.

[b] Density in bct structure.

At low temperatures, the free energy can be written

$$F(V,T) = F_0(V) - \frac{1}{2}\hat{\Gamma}(V)T^2 - D(V)T^4 \quad , \tag{19.1}$$

where $F_0(V)$ is the free energy at $T = 0$, Eq. (16.24), $\hat{\Gamma}(V)$ is the total electronic entropy coefficient from Eq. (18.46), and $D(V)T^4$ expresses the thermal nuclear vibrational contribution, where from Eq. (16.32),

$$D(V) = \frac{Nk\pi^4}{5[\Theta_D(V)]^3} \quad . \tag{19.2}$$

To find how volume varies with temperature at fixed pressure, one can calculate $P(V,T)$ from $F(V,T)$, set $P =$ constant, and solve for $V(T)$. At zero pressure, the result from Eq. (19.1) is (see problem 19.2)

$$\frac{V(T) - V_0}{V_0} = \frac{1}{B_0(V_0)}\left[\frac{\hat{\Gamma}T^2}{2}\left(\frac{d\ln\hat{\Gamma}}{d\ln V}\right) - 3DT^4\left(\frac{d\ln\Theta_D}{d\ln V}\right)\right]_{V_0} + \cdots \quad , \tag{19.3}$$

where $B_0(V_0)$ is the bulk modulus at zero temperature and pressure. Hence from a measurement of $V(T)$ at low temperatures, the volume derivatives of $\hat{\Gamma}$ and $\Theta_D$ can be found. The experimental technique was pioneered by Guy White, and a compilation of low-temperature data is given by Barron, Collins, and White (1980). A complete analysis of the temperature dependence at low temperatures of specific heat and thermal expansion,

accounting for the differences between data at $P = 0$ and at $V = V_0$, can be found in *Thermodynamics of Crystals*, pp. 346–351.

The thermal expansion coefficient is $\alpha$, defined by

$$\alpha = \frac{1}{V} \left. \frac{\partial V}{\partial T} \right)_P \quad . \tag{19.4}$$

Common terminology is imprecise, since any of the quantities $\Delta V = V(T) - V_0$, or $\Delta V/V_0$, or $\alpha$, might be called "thermal expansion." The standard way to calculate $\alpha$ is again through the pressure $P(V,T)$, by first solving for $V(T)$ at a constant $P$, then by differentiating. The thermodynamic identity $\alpha B_T = (\partial S/\partial V)_T$ is also useful. This equation makes clear that $\alpha = 0$ at $T = 0$. At high temperatures, the major contribution to $\alpha$ comes from the major contribution to $S$, namely $S_{ph}$, and with Eq. (17.3) for $S_{ph}$ we can write

$$\alpha = -\frac{k}{B_T} \sum_\kappa \frac{d \ln \omega_\kappa}{dV} + \cdots \quad , \quad \text{at high } T \quad , \tag{19.5}$$

where $+\cdots$ represents terms which are relatively small at high $T$. This equation shows that thermal expansion is a quasiharmonic effect, resulting from the volume dependence of the phonon frequencies $\omega_\kappa$. Thermal expansion occurs because it is possible to increase the entropy by increasing the volume, since an increase in volume causes the phonon frequencies to decrease. On the other hand, the above equation tells us that the thermal expansion is *negative* whenever an increase in volume causes (most of) the phonon frequencies to *increase*. While it is commonly said that thermal expansion is an effect of anharmonicity, it is actually a quasiharmonic effect, and anharmonicity will make only a small contribution within the $+\cdots$ in Eq. (19.5).

### *Thermodynamic Grüneisen Parameter*

The thermodynamic Grüneisen parameter $\gamma(V,T)$ can be written in many forms. The expression

$$\gamma = V \left. \frac{\partial P}{\partial U} \right)_V = \frac{V}{C_V} \left. \frac{\partial P}{\partial T} \right)_V \tag{19.6}$$

shows that $\gamma$ is a function only of the thermal excitation of a system. If we write

$$\frac{\partial S}{\partial \ln V}\Big)_T = \alpha V B_T \quad , \quad \frac{\partial S}{\partial \ln T}\Big)_V = C_V \quad , \tag{19.7}$$

then $\gamma$ is expressed in terms of the entropy,

$$\gamma = \frac{\alpha V B_T}{C_V} = \frac{(\partial S/\partial \ln V)_T}{(\partial S/\partial \ln T)_V} \quad . \tag{19.8}$$

It is from the middle expression here the $\gamma$ is usually evaluated from experimental data. Notice $\gamma$ has a finite (nonzero) limit as $T \to 0$.

The total entropy of a crystal is

$$S = S_{ph} + S_{anh} + S_{el} + S_{ep} \quad . \tag{19.9}$$

Though entropy is additive over these contributions, the Grüneisen parameter is not (see problem 19.3). For an insulator, the last two terms vanish, and since $S_{anh} \ll S_{ph}$, one has

$$\gamma \approx \gamma_{ph} \quad , \quad \text{for an insulator} \quad . \tag{19.10}$$

Here $\gamma_{ph}$ is given by Eq. (19.8), evaluated for phonons only,

$$\gamma_{ph} = \frac{(\partial S_{ph}/\partial \ln V)_T}{(\partial S_{ph}/\partial \ln T)_V} \quad . \tag{19.11}$$

For an insulator, $\gamma$ goes to $-d\ln\Theta_D/d\ln V$ at low temperatures. For a metal, one often finds the Grüneisen parameter written "$\gamma = \gamma_{ph} + \gamma_{el}$", an equation which is never correct, even if one neglects anharmonicity and electron-phonon interactions (see problem 19.3). For a metal, $\gamma$ goes to $d\ln\hat{\Gamma}/d\ln V$ as $T \to 0$.

At intermediate temperatures, where the crystal specific heat is dominated by the phonon contribution, $\gamma \approx \gamma_{ph}$ for metals and insulators alike. Here the experimental Grüneisen parameter shows significant variation with temperature, due to phonon dispersion.

A characteristic property of the experimental $\gamma$ is its insensitivity to temperature at high temperatures. For most elemental crystals, and for each separate crystal phase, the graph of $\gamma$ *vs* $T$ is constant to say $\pm$ 5% for $T \gtrsim \theta_2$. When we understand this near constancy, we shall uncover a most useful property of $\gamma$. With respect to Eq. (19.9) for the entropy of a crystal, by far the major contribution at high temperatures is $S_{ph}$,

comprising $\gtrsim 90\%$ of the total, as we shall see in the entropy analysis later in this section. Hence we have $S = S_{ph}$ + small terms, which implies $\gamma = \gamma_{ph}$ + small terms. From the high-temperature expansion of $S_{ph}$, Eq. (17.6), it follows $\gamma_{ph} = -(d\ln\theta_0/d\ln V)$ + quantum corrections. Since $\theta_0$ is a function of volume only, then in leading approximation so is $\gamma_{ph}$, and likewise $\gamma$, and since thermal expansion is a small effect, i.e. since $V$ is nearly constant in $T$, then $\gamma$ is nearly constant in $T$. The scatter in experimental data for $\gamma$ is reduced by working with $\gamma^*$, defined as the average of $\gamma(T)$ in the high-temperature regime. Our result is

$$\gamma^* = -\frac{d\ln\theta_0}{d\ln V} + \text{small terms} \quad . \tag{19.12}$$

We have estimated the small terms for elemental crystals, including those with large anharmonic entropy, and/or with large electronic entropy, and conclude they contribute less than 10% to the right side of (19.12).

Let us define the Grüneisen parameter for each phonon characteristic temperature,

$$\gamma_n = -\frac{d\ln\theta_n}{d\ln V} \quad , \tag{19.13}$$

where $\gamma_n = \gamma_n(V)$. We expect $\gamma_n$ to vary little for the central moments $n = 0, 1, 2$ (see problem 19.4). Therefore

$$\gamma_n \approx \gamma^* \quad , \quad n = 0, 1, 2 \quad . \tag{19.14}$$

We regard this approximation as accurate to say 5–10% for each elemental crystal phase. Starting with the characteristic temperature $\theta_n$ at density $\rho_{meas}$, listed in Table 15.1, one can find $\theta_n$ at nearby densities from

$$\theta_n(\rho) = \theta_n(\rho_{meas}) \left(\frac{\rho}{\rho_{meas}}\right)^{\gamma^*} \quad , \quad n = 0, 1, 2 \quad . \tag{19.15}$$

Without information on the density dependence of $\gamma^*$, application of this equation is limited to changes in $\theta_n$ up to say 20%. Values of $\gamma^*$ calculated from thermodynamic data at zero pressure are listed in Table 19.1. Statistical analysis of $\gamma^*$ for the elements is discussed in problem 19.5.

### *Regimes of Quantum and Classical Nuclear Motion*

The thermal part of the internal energy reveals the nature of the nuclear vibrational motion in a crystal. The complete theory for the internal energy

of a crystal is

$$U(V,T) = \Phi_0(V) + U_{ph}(V,T) + U_{anh}(V,T) + U_{el}(V,T) + U_{ep}(V,T) \ . \quad (19.16)$$

In tabulations of experimental data, the energy of a condensed matter system is customarily set zero at zero temperature and pressure, so that $U(V_0,0) = 0$. With Eqs. (16.24) and (16.25), this condition is written

$$0 = \Phi_0(V_0) + \frac{9}{8}Nk\theta_1(V_0) + U_{anh}(V_0,0) \ . \quad (19.17)$$

At low temperatures, the thermal part of the internal energy has a $T^2$ contribution from electronic excitations, and a $T^4$ contribution from nuclear vibrations. At high temperatures, and at $P = 0$, the temperature dependence of $U(V,T)$ is complicated by the volume dependences in Eq. (19.16), mainly by the volume dependence of $\Phi_0(V)$. Thermal expansion effects are eliminated by studying the internal energy at the fixed volume $V_0$. With the above equations, and with the high temperature expansion (17.7) of $U_{ph}$, the high temperature expansion of $U(V_0,T)$ is

$$\begin{aligned} U(V_0,T) &= -\frac{9}{8}Nk\theta_1 + 3NkT\left[1 + \frac{1}{20}\left(\frac{\theta_2}{T}\right)^2 + \cdots\right] \\ &\quad + U_{el}(V_0,T) + \delta U_{anh}(V_0,T) \ . \end{aligned} \quad (19.18)$$

Here $\theta_1$ and $\theta_2$ are evaluated at $V_0$, and $\delta U_{anh}$ is

$$\delta U_{anh}(V_0,T) = U_{anh}(V_0,T) - U_{anh}(V_0,0) \ . \quad (19.19)$$

In keeping with the conclusion of Sec. 18, $U_{ep}$ is neglected at high temperatures.

Analysis of the internal energy for sodium, from $T = 0$ to $T_m$, is shown in Fig. 19.1. The curve of $U(V,T) - U_{el}(V,T)$ is shown, and also that of $U(V_0,T) - U_{el}(V_0,T)$. $U(V,T)$ and $U(V_0,T)$ are from experiment (see problem 19.6), and $U_{el}$ is calculated from the Sommerfeld expansion, where $n(\epsilon_F)$ is from electronic structure theory and its volume dependence is from free-electron theory. At fixed volume, the dominant temperature dependence is known exactly, from Eq. (19.18):

$$\frac{U(V_0,T)}{Nk} - \frac{U_{el}(V_0,T)}{Nk} \to -\frac{9}{8}\theta_1(V_0) + 3T + \frac{\delta U_{anh}}{Nk} \quad , \quad \text{at high } T \ . \quad (19.20)$$

Notice, however, that data at the volume $V_0$ corresponds to a system with higher melting temperature than at $P = 0$. Relevant data for bcc Na are

$$\begin{aligned} &V_0 = 255 a_0^3/atom \quad ; \\ &\theta_1(\rho_{meas}) = 163K \quad , \quad \theta_1(V_0) = 164K \quad ; \\ &T_m(P=0) = 371.0K \quad , \quad T_m(V_0) = 405.4K \quad . \end{aligned} \tag{19.21}$$

Significant conclusions from Fig. 19.1 are as follows.

(a) In the internal energy curve, one clearly sees the quantum regime showing curvature at low $T$, and the classical regime of little curvature at high $T$, where the dividing temperature is around $\theta_2$.

(b) The experimental energy at fixed volume, in the form of the left side of (19.20), very nicely approaches the right side of (19.20), with $\delta U_{anh} \approx 0$, as $T$ increases above $\theta_2$. The difference between the two curves at $T \gtrsim \theta_2$ is essentially the quantum correction in $(\theta_2/T)^2$ in Eq. (19.18).

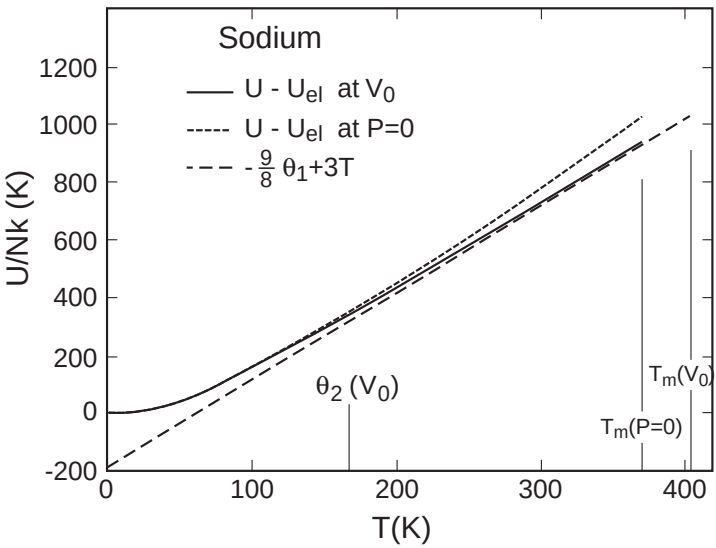


Figure 19.1. Nuclear motional part of the internal energy *vs* $T$ for Na, showing quantum and classical regimes in the experimental data, and showing the approach of experiment to classical quasiharmonic theory at high temperatures.

In connection with Fig. 19.1, it is often suggested that one can extrapolate experimental data from classical temperatures to $T = 0$, and thus determine the quantum zero-point contribution to the thermodynamic

quantity in question. With actual experimental data, however, such an extrapolation is sufficiently ambiguous that it cannot be used to obtain useful information (see problem 19.7).

### *Volume Effects and Temperature Effects*

Figure 19.2 presents two curves of volume *vs* temperature, at $P = 0$, for bcc Na. The lower curve is experimental, and shows the familiar quantum and classical regimes. The upper curve is calculated classically, from molecular dynamics, for pseudopotential Na, and hence does not possess a quantum regime. The two curves agree at $T = 0$ because the pseudopotential model, with quantum terms omitted, was fitted to experiment at $T = 0$. More specifically, the pressure at $T = 0$ is, from Eqs. (16.24) and (16.25),

$$P = -\frac{d\Phi_0}{dV} - \frac{9}{8}Nk\frac{d\theta_1}{dV} + P_{anh} \quad , \quad \text{at } T = 0 \quad . \tag{19.22}$$

In fitting the pseudopotential model to experiment, the potential approximation was used, in which $P = -d\Phi_0/dV$. Significant conclusions from Fig. 19.2 are as follows.

(a) Neglecting quantum terms in Eq. (19.22) is not good enough for highly accurate work. If fitting is done at $T = 0$, one should keep the term in $\theta_1$. If fitting is done at high temperatures, one should use the high-temperature expression for $P$. Either way, the model would be in better agreement with experiment for $V(T, P = 0)$.

(b) Since both curves in Fig. (19.2) have nearly the same slope at high temperatures, the theoretical thermal expansion coefficient is in good agreement with experiment at high temperatures.

Figure 19.3 compares theory and experiment for the isothermal bulk modulus of bcc Na. The theoretical curves are calculated from molecular dynamics, for pseudopotential Na, and hence do not contain quantum effects. The upper (lower) theoretical curve is evaluated at the experimental (theoretical) volume shown in Fig. 19.2. The slope of the theoretical curves is in respectable agreement with experiment at high temperatures. A similar agreement between theory and experiment for the adiabatic elastic constants is found for Na (Schiferl and Wallace, 1985), and for Mg (Greeff and Moriarty, 1999).

Metals in general display a highly uniform qualitative behavior in the temperature and volume dependences of elastic constants, and bulk and

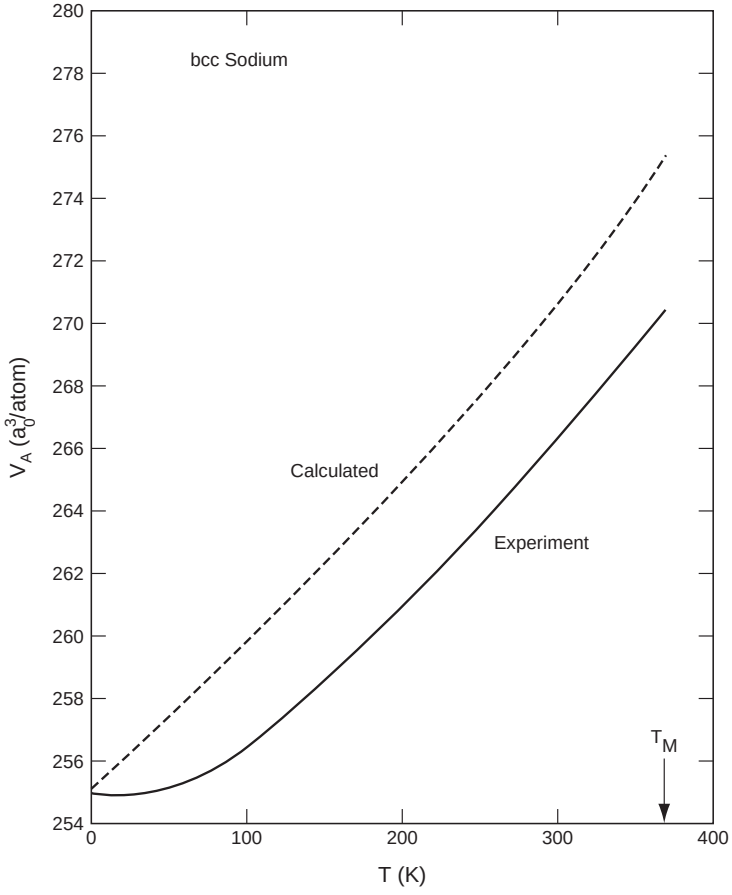


Figure 19.2. Molecular dynamics calculation of $V(T, P = 0)$ for sodium, compared with experiment, showing that neglecting quantum contributions in fitting theory to experiment is not the best one can do (figure from Swanson *et al.*, 1982).

shear moduli. With few exceptions, the following properties apply to curves of elastic constants *vs* temperature for elemental metals, and for alloys as well, for adiabatic *or* isothermal constants.

(a) Curves at $P = 0$ go to $T = 0$ with zero slope, and are roughly linear in $T$ at $T \gtrsim \theta_2$. The same properties hold for curves at fixed volume.

(b) The explicit temperature dependence, as observed at fixed volume, is normally small compared to the temperature dependence on the $P = 0$ curve, showing that the actual variation at $P = 0$ is largely a volume effect.

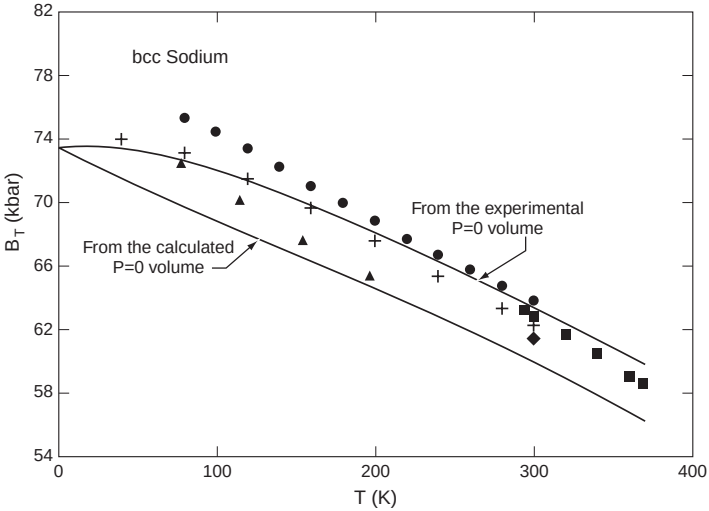


Figure 19.3. Molecular dynamics calculations (lines) of $B_T(V,T)$ for each of the $V(T)$ curves in Fig. 19.2, compared with experimental data (points) for $B_T$ *vs* $T$ at $P = 0$. This shows the difficulty in comparing theory and experiment at $P = 0$, when theoretical and experimental volumes are not the same at $P = 0$ (figure from Swanson *et al.*, 1982).

### *Anharmonic Entropy at High Temperatures*

Over the years, we have carried out an extensive analysis of the high-temperature entropy of elemental crystals, based on setting the experimental entropy equal to the total theoretical entropy,

$$S_{expt} = S_{ph} + S_{el} + S_{anh} \quad , \tag{19.23}$$

where from the conclusion of Sec. 18, $S_{ep}$ is neglected at high temperatures. Our procedure is to use this equation to find the anharmonic entropy. $S_{ph}$ is calculated from the high-temperature expansion (17.6), to order $(\theta_2/T)^2$, where $\theta_0$ and $\theta_2$ are taken from neutron scattering data, Table 15.1, and are corrected for thermal expansion with $\gamma^*$ and Eq. (19.15). $S_{el}$ is calculated from the Sommerfeld expansion for nearly-free-electron metals, where $n(\epsilon_F)$ is from available electronic structure calculations, otherwise from the free-electron model. For transition metals, $S_{el}$ is calculated from the complete integral, Eq. (18.2), with $n(\epsilon)$ from electronic structure calculations. $S_{ph}$ and $S_{el}$ are evaluated at the zero-pressure volume $V(T)$. The analysis was done for all elemental crystals for which we could find sufficient highly-

Table 19.2. Entropy contributions in units of k per atom for 23 elemental crystals at $T_m$ and atmospheric pressure.

| Element | Structure | $S_{expt}$ | $S_{ph}$ | $S_{el}$ | $S_{anh}$ |
|---|---|---|---|---|---|
| Li | bcc | 4.86 | 4.77 | 0.06 | 0.03 |
| Na | bcc | 6.93 | 6.79 | 0.05 | 0.09 |
| K | bcc | 8.23 | 8.00 | 0.08 | 0.15 |
| Rb | bcc | 9.42 | 9.25 | 0.09 | 0.08 |
| Mg | hcp | 7.70 | 7.45 | 0.12 | 0.13 |
| Cu | fcc | 8.93 | 8.81 | 0.12 | 0.00 |
| Ag | fcc | 9.84 | 9.82 | 0.09 | –0.07 |
| Au | fcc | 10.64 | 10.62 | 0.11 | –0.09 |
| Zn | hcp | 7.77 | 7.76 | 0.06 | –0.05 |
| Hg | rhomb | 7.13 | 7.02 | 0.03 | 0.08 |
| Al | fcc | 7.20 | 7.08 | 0.11 | 0.01 |
| In | bct | 8.19 | 8.13 | 0.06 | 0.00 |
| Pb | fcc | 10.17 | 10.10 | 0.11 | –0.04 |
| V | bcc | (10.97) | 9.86 | 0.95 | (0.16) |
| Nb | bcc | 12.06 | 11.23 | 0.92 | –0.09 |
| Ta | bcc | 13.40 | 12.46 | 1.01 | –0.07 |
| Mo | bcc | 11.78 | 10.41 | 0.65 | 0.72 |
| W | bcc | 13.02 | 11.74 | 0.69 | 0.59 |
| Pd | fcc | 10.95 | 10.19 | 0.79 | –0.03 |
| Pt | fcc | 11.78 | 11.12 | 0.81 | –0.15 |
| Si | dia | 7.44 | 7.21 | 0 | 0.23 |
| Ge | dia | 8.04 | 7.84 | 0 | 0.20 |
| Sn | bct | 7.98 | 7.87 | 0.09 | 0.02 |

accurate data. In Fig. 18.2, curves of $S_{expt} - S_{ph}$ and $S_{el}$ are compared for Pd and Pt, from 300K to $T_m$, showing that $S_{anh}$ is quite small over the entire temperature range. An indication of the relative magnitudes of the contributions in Eq. (19.23), throughout the range $\theta_2 \leq T \leq T_m$, is provided by the list of these contributions at $T_m$, in Table 19.2. The data are from Wallace (1991c, 1992b, 1997a), and Eriksson, Wills, and Wallace (1992), with a few minor changes to account for improved experimental results. In the table, and in the discussion here, entropy is in units of $k$ per atom. The error in $S_{expt}(T_m)$ generally increases as $T_m$ increases, and is estimated to be 0.02 – 0.06. The error in $S_{ph}(T_m)$ is estimated to be 0.03 – 0.06, and the error in $S_{el}$ is estimated to be around 10%.

Several general conclusions can be drawn from Table 19.2. First $S_{expt}$ at $T_m$ lies in the range 5–13, hence is of a common order of magnitude for all

elemental crystals at melt. Second, the dominant contribution in all cases is $S_{ph}$, and indeed $S_{ph}$ constitutes $\gtrsim 90\%$ of the total entropy at $T_m$. This is the reason we go to extremes to make the most accurate evaluation possible of the quasiharmonic phonon entropy. Third, at the level of accuracy of the present analysis, $S_{el}$ is never negligible for metals, and $S_{el}$ is even *important* for transition metals at $T_m$. Finally, $S_{anh}$ is always small.

Let us make a more precise discussion of $S_{anh}$. When $S_{anh}$ is not larger than its estimated error, we say $S_{anh} = 0$. This result holds for 19 of the 23 elements in Table 19.2. The average of $|S_{anh}|$ for these 19 elements is 0.07, and the average of $|S_{anh}|/S_{expt}$ is 0.008. For Si and Ge, $S_{anh} \approx 0.2$ and is marginally outside estimated errors, but is still only 3% of $S_{expt}$. The only other nonzero values of $S_{anh}$ in Table 19.2 are 0.7 for Mo and 0.6 for W, well outside of estimated errors, but still only 5–6% of $S_{expt}$. For the rare gas crystals, we are not able to analyze the entropy at atmospheric pressure, because the large thermal expansion makes our estimate of $\theta_0$ unreliable at $V(T_m)$. For compressed rare gases, at densities where we have an accurate evaluation of $\theta_0$, $S_{anh}$ is around –0.2 to –0.3 at $T_m$, marginally outside estimated errors, but only around 5% of $S_{expt}$ at $T_m$.

For those elements for which phonon moments are not available from inelastic neutron scattering experiments, useful estimates of $\theta_0$ can be made from the experimental entropy at $T \gtrsim \theta_2$ (see problem 19.8).

### *Special Entropy Analyses*

Nickel is ferromagnetic with a Curie temperature $T_c = 631K$. The experimental entropy shows a large magnetic anomaly in the vicinity of $T_c$. All our theory for $S_{el}$ describes a metal with conduction-electron spin degeneracy, and we shall continue with the same meaning here. An ordinary (spin-degenerate) density functional calculation gives $S_{el}$ for Ni, and real Ni then has an additional magnetic entropy $\delta S_{mag}$. Let us make the approximation $S_{anh} = 0$, reasonable in view of the preceding entropy study, so that the experimental entropy is given by

$$S_{expt} = S_{ph} + S_{el} + \delta S_{mag} \quad , \quad \text{at high } T \quad . \tag{19.24}$$

Figure 19.4 shows curves of $S_{expt} - S_{ph}$, and $S_{el}$, as functions of temperature at zero pressure. From the above equation, the difference between these curves is $\delta S_{mag}$. That $\delta S_{mag}$ is negative below $T_c$ presumably corresponds to the ferromagnetic state being more ordered than the spin-degenerate

state. Above $T_c$, $\delta S_{mag}$ is positive and quite significant. The entropy contributions for Ni at $T_m$ are listed in Table 19.3. The present results are very slightly different from results at constant density, in Fig. 8 of Ericksson *et al.* (1992). The theoretical challenge now is to understand the curve of $\delta S_{mag}$.

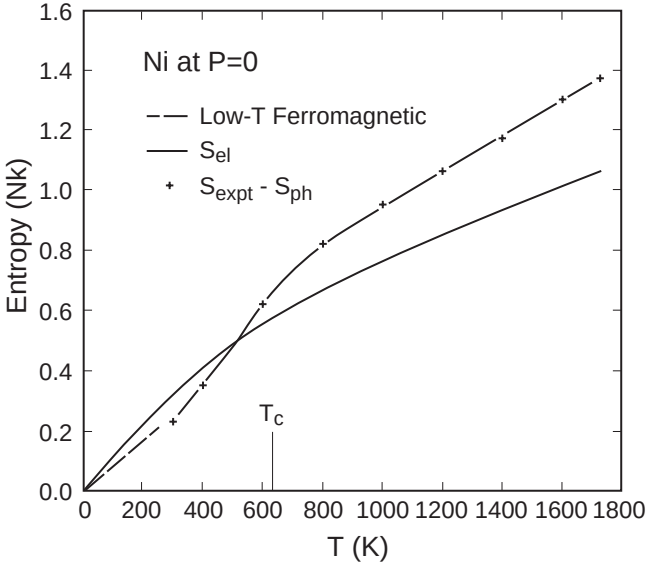


Figure 19.4. Entropy contributions for Ni at $P = 1$ bar. The difference between $S_{expt} - S_{ph}$ and $S_{el}$ is the magnetic entropy $\delta S_{mag}$.

Table 19.3. Entropy contributions for Ni and Cr at $T_m$, and for Ti and Zr at the highest temperature of each crystal phase. Entropy units are k per atom, and data are at atmospheric pressure.

| Element | State | $S_{expt}$ | $\hat{S}_{ph}$ | $S_{ph}$ | $S_{anh}$ | $S_{el}$ | $\delta S_{mag}$ |
|---|---|---|---|---|---|---|---|
| Ni | fcc at $T_m$ | 10.32 | — | 8.95 | 0[a] | 1.06 | 0.31 |
| Cr | bcc at $T_m$ | 10.53 | 9.44 | 8.86 | 0.58 | 0.75 | 0.34 |
| Ti | hcp at $T_{\alpha\beta}$ | 8.51[b] | 7.98 | 7.63 | 0.35 | 0.48 | 0 |
| Ti | bcc at $T_m$ | 10.93[b] | 9.80 | — | — | 1.23 | 0 |
| Zr | hcp at $T_{\alpha\beta}$ | 9.45[b] | 9.05 | 8.62 | 0.43 | 0.41 | 0 |
| Zr | bcc at $T_m$ | 12.20[b] | 11.07 | — | — | 1.09 | 0 |

[a] $S_{anh}$ for Ni is *assumed* zero.
[b] $S_{expt} \neq \hat{S}_{ph} + S_{el}$ since all three quantities are independent data.

Ti and Zr have a phase transition, from hcp to bcc with increasing temperature, at around 0.6 $T_m$. Each metal shows strong phonon softening, in both phases, associated with the transition. Phonon softening is explicit temperature dependence of some phonon frequencies, hence is explicit anharmonicity, and is accounted for in leading order perturbation theory by using renormalized frequencies in the harmonic phonon entropy formula, as expressed in Eq. (16.22). Let us test the same formula based on *experimental* phonon frequencies, instead of leading order perturbation frequencies, that is, let us test the equation

$$S_{ph} + S_{anh} = \hat{S}_{ph} \quad , \tag{19.25}$$

where $\hat{S}_{ph}(V,T) = S_{ph}(\{\Omega_\kappa(V,T)\})$, and where $\Omega_\kappa$ are the frequencies measured by inelastic neutron scattering. If (19.25) is correct, the high-temperature entropy of Ti and Zr will be given by

$$S_{expt} = \hat{S}_{ph} + S_{el} \quad . \tag{19.26}$$

Phonon dispersion curves have been measured at several temperatures in both phases for Ti(Stassis *et al.*, 1979, and Petry *et al.*, 1991), and for Zr (Stassis *et al.*, 1978, and Heiming *et al.*, 1991), and corresponding evaluations of $\hat{S}_{ph}(V,T)$ are given in these references. Figure 19.5, from Eriksson *et al.* (1992), compares the experimental $S_{expt} - \hat{S}_{ph}$ with calculations of $S_{el}$. For both phases of both metals, the agreement in Fig. 19.5 is remarkable, and indeed is within the combined estimated errors of the data. We are able to conclude for Ti and Zr that $\hat{S}_{ph}$ includes $S_{anh}$, to within errors involved in the analysis, those errors being $\lesssim 1\%$ of the experimental entropy at any temperature. Apparently something beyond leading order anharmonic perturbation theory is contained when the quasiharmonic phonon entropy is evaluated with experimental frequencies. Entropy contributions for Ti and Zr are listed in Table 19.3, for hcp at the transition temperature $T_{\alpha\beta}$, and for bcc at $T_m$. Phonon softening in Ti and Zr is discussed further in Sec. 26.

Chromium is antiferromagnetic with Néel temperature $T_N \approx 322K$, but the experimental entropy shows only an extremely small anomaly at $T_N$. Nevertheless, the high-temperature entropy of Cr is marvelously complicated. To analyze it, we need both contributions in Eq. (19.25) for the nuclear motion entropy, and we need a magnetic contribution as well:

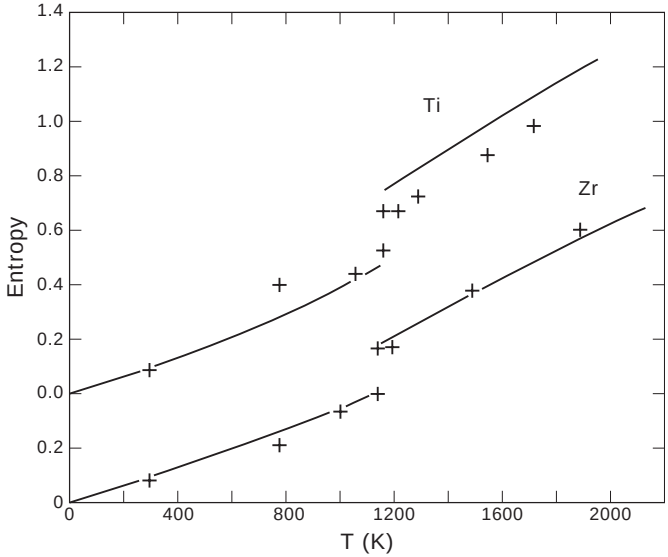


Figure 19.5. Entropy contributions for Ti and Zr at $P = 1$ bar, in the low-$T$ hcp and high-$T$ bcc phases. Symbols are $S_{expt} - \hat{S}_{ph}$ and lines are $S_{el}$.

$$\begin{aligned} S_{expt} &= \hat{S}_{ph} + S_{el} + \delta S_{mag} \quad , \\ &= S_{ph} + S_{anh} + S_{el} + \delta S_{mag} \quad . \end{aligned} \tag{19.27}$$

Phonon dispersion curves have been measured at several elevated temperatures by Trampenau *et al.* (1993), so that all four terms in Eq. (19.27) can be separated, with procedures used above for the other transition metals. Results at $T_m$ and atmospheric pressure are listed in Table 19.3. Again there is a slight difference from the graph for Cr at constant density, in Fig. 5 of Eriksson *et al.* (1992). For Cr at $T_m$, $S_{ph}$ is still dominant at 84% of $S_{expt}$, $S_{el}$ is 7%, $S_{anh}$ is 6% and is quite the same in magnitude and relative magnitude as for Mo and W (Table 19.2), while $\delta S_{mag}$ is still significant at 3%. A proposal to account for $\delta S_{mag}$ was made by Grimvall, Häglund, and Guillermet (1993).

*Problems*

*19.1.* The expansion at atmospheric pressure from $T = 0$ to $T_m$ is $\zeta = (V_{cm} - V_0)/V_0$. In Table 19.1, for the 21 metals in bcc, fcc, and hcp structures, the mean and variance of $\zeta$ implies $\zeta = 0.072 \pm 0.010$. Are the separate groups of bcc, fcc, and hcp metals consistent with this overall distribution? Can you understand the large $\zeta$ of Ar, Kr, and Xe from the physical nature of their binding? And the small $\zeta$ of Si and Ge? What would be your guess for $\zeta$ of a metal at 100 Mbar pressure?

*19.2.* Derive Eq. (19.3) for the volume expansion at low temperatures. In the $+\cdots$ of that equation are two very small terms going as $T^4$. Estimate the relative magnitude of these terms.

*19.3.* Given Eq. (19.9) for the entropy, show that

$$\gamma = \frac{C_{ph}\gamma_{ph} + C_{anh}\gamma_{anh} + C_{el}\gamma_{el} + C_{ep}\gamma_{ep}}{C_{ph} + C_{anh} + C_{el} + C_{ep}} \quad ,$$

where each contribution to $\gamma$ is given by an equation corresponding to (19.11) for $\gamma_{ph}$, and where $C_{ph}$ is the phonon contribution to $C_V$, and so on. Under what condition is one of the contributions negligible?

*19.4.* From the definition (19.13) of $\gamma_n$, show that

$$\gamma_n = \frac{\langle \gamma_\kappa \omega_\kappa^n \rangle_{BZ}}{\langle \omega_\kappa^n \rangle_{BZ}} \quad ,$$

where $\gamma_\kappa$ is the phonon Grüneisen parameter, written in Eq. (13.33). Hence show the approximation $\gamma_n \approx \gamma_0$ is the same as $\langle \gamma_\kappa \omega_\kappa^n \rangle_{BZ} \approx \langle \gamma_\kappa \rangle_{BZ} \langle \omega_\kappa^n \rangle_{BZ}$. How accurate is this approximation at $n = 2$ for the rare gas crystals, and for nearly-free-electron metals? (*Thermodynamics of Crystals*, Table 31).

*19.5.* For the single-phase elements in Table 19.1, find the mean and variance of $\gamma^*$ for the fcc metals, the bcc metals, the hcp metals, and the rare gas crystals. Which one of the other three groups is inconsistent with the fcc metals? Could you make a pure guess for $\gamma^*$ for a fcc metal? For a bcc metal?

*19.6.* Derive the expansion, useful for making volume corrections of the internal energy,

$$U(V_0, T) = U(V, T) + (V_0 - V)\Delta U(V, T) + \cdots \quad ,$$

where $\Delta U = \alpha T B_T - P$.

*19.7.* Suppose you do not know $\theta_1$, and wish to find it by extrapolating $U - U_{el}$ to $T = 0$ in Fig. 19.1. Use your transparent straight edge to discover that the extrapolation of the curve at $V(T)$ is ambiguous, while you can get a reasonable answer from the curve at $V_0$ only if you know the slope is 3, and if you *assume* $\delta U_{anh} = 0$. Note in trying to do such an extrapolation for thermodynamic functions other than the internal energy, the limiting quasiharmonic slope is an unknown quantity.

*19.8.* In the following table, use the data given for $S_{expt}(T)$, together with $S_{el}$ from the free electron model, and set $S_{anh} = 0$, to confirm the values of $\theta_0$ listed. From each $\theta_0$, estimate $\theta_1$, $\theta_2$, and $\langle \omega^2 \rangle_{BZ}$ (see Eq. (15.10)).

| Element | Structure | T(K) | $S_{expt}/Nk$ | $\approx \theta_0(K)$ |
|---|---|---|---|---|
| Cs | bcc | 298 | 10.235 | 27.5 |
| Cd | hcp | 298 | 6.233 | 103 |
| Ga | orthorh | 298 | 4.913 | 162 |
| Ca | fcc | 720 | 7.99 | 151 |
| Ca | bcc | 720 | 8.14 | 136 |
| Sr | fcc | 830 | 10.22 | 79 |
| Sr | bcc | 830 | 10.35 | 76 |
| Tl | hcp | 507 | 9.48 | 60.1 |
| Tl | bcc | 507 | 9.57 | 58.3 |
| Sn | dia | 286 | 5.18 | 140 |
| Sn | bct | 286 | 6.012 | 107 |

## 20 CRYSTAL EQUATION OF STATE

### *Form and Range of Validity*

By equation of state, we mean the complete set of thermodynamic functions on the equilibrium surface of a material. The Helmholtz free energy serves as a generating function for the equation of state. In practical applications, it is important to evaluate all thermodynamic functions from a single free energy, so as to achieve thermodynamic consistency among all the derived functions. For a crystal, the most useful thermodynamic functions are the internal energy, the entropy, and the stresses, with independent variables being the crystal structure and temperature. When the applied stress is isotropic pressure, the independent variables are volume and temperature.

The condensed matter regime is defined in Sec. 1, and the crystalline state belongs to this regime. Condensed matter theory is based on the exact many-particle Hamiltonian, with approximations appropriate to condensed matter (Chap. 1). The corresponding theories of statistical mechanics and lattice dynamics are valid at any density (Chaps. 2 and 3). Through extensive comparisons of theory and experiment at normal densities, a characteristic formulation of the equation of state of elemental crystals has emerged (Chap. 4). Since the underlying theory is valid at any compression, there is no reason to doubt that the same characteristic equation of state will also be valid at any compression. We therefore consider the discussion here, in Sec. 20, to apply to every crystal phase of every element, at all temperatures and volumes at which that phase is stable, or for that matter is even metastable (see Chap. 6). As a general rule, phonon frequencies increase with increasing density, and so does the melting temperature, although local exceptions are found in certain elements. The electronic structure changes as density increases, nonmetallic elements become metals, and there is a slow increase in the importance of electronic excitations relative to phonons in the equation of state.

The universal formulation we have developed for the free energy of a crystal, arranged in order of generally decreasing importance of terms for application to equations of state, is

$$F = \Phi_0 + F_{ph} + F_{el} + F_{anh} + F_{ep} \quad . \tag{20.1}$$

To construct an equation of state, one needs to calibrate the parametric functions contained in $F$. In practice we use all reliable information, both experimental and theoretical, in this calibration. An observation of primary importance is that the *form* of $F$ in Eq. (20.1), namely the explicit $V$ and $T$ dependences of its terms, expresses the correct physics for elemental crystals, and indeed when appropriately generalized, for *all* crystals. This form alone carries much information about the equation of state of crystals. Whatever we are able to accomplish, in trying to construct an equation of state for a real crystal, this is the best form to use. In other words, for a given set of input data, calibrating Eq. (20.1) will in principle produce the best possible equation of state.

Our practical experience supports the observation just made. Free energy functions of arbitrary form, including Mie-Grüneisen models and poly-

nomials in $V$ and $T$, even though calibrated to massive amounts of experimental data, are less accurate both for interpolation and extrapolation than free energy functions based on Eq. (20.1).

### *Calibration of the Static Lattice Potential*

The static lattice potential is a purely theoretical quantity, defined in Chap. 1 as the electronic groundstate energy when the nuclei are fixed at the crystal lattice sites. The nearest experimental quantity is the isothermal compression curve. For densities not far from normal density, the experimental compression curve is prescribed by the isothermal bulk modulus, normally available at various temperatures, including $T = 0$. For large compressions, room temperature diamond cell data are available, up to several Mbar. The experimental data always contain all the contributions implied by Eq. (20.1) for $F$, but the major contribution comes from $\Phi_0$, and the only other significant contribution is from $F_{ph}$. If we write $F = \Phi_0 + F_{ph}$, then at $T = 0$,

$$P = -\frac{d\Phi_0}{dV} - \frac{9Nk\theta_1}{8V}\,\frac{d\ln\theta_1}{d\ln V} \quad , \tag{20.2}$$

and at $T \gtrsim \theta_2$,

$$P = -\frac{d\Phi_0}{dV} - \frac{3NkT}{V}\left[\frac{d\ln\theta_0}{d\ln V} + \frac{1}{20}\left(\frac{\theta_2}{T}\right)^2 \frac{d\ln\theta_2}{d\ln V} + \cdots\right] \quad . \tag{20.3}$$

The dominant term $-d\Phi_0/dV$ is the pressure in the potential approximation.

For most elemental crystals at normal density, $\theta_2 \lesssim 300K$, and Eq. (20.3) applies at room temperature. However, under compression, $\theta_2$ increases and moves above 300 K. The curve of $P(T)$ at fixed volume is similar to the curve of $U(T)$ in Fig. 19.1. With this in mind, skillful use of Eqs. (20.2) and (20.3) allows one to estimate harmonic vibrational contributions to pressure at any $V$ and $T$.

Figure 20.1 shows diamond cell data for Na at 293 K, from Fritz and Olinger (1984), together with theoretical curves for pseudopotential sodium, of the pressure in the potential approximation, and of the pressure at 293 K calculated from Eq. (20.3). Recall that the pseudopotential model in the potential approximation was fitted to the experimental volume and bulk modulus at $T = 0$ and $P = 0$. Neglect of vibrational contributions in this

fitting procedure causes the small difference between theory and experiment at $P = 0$ in Fig. 20.1. This difference is the same as the volume difference at 293 K in Fig. 19.2. The following conclusions are drawn from Fig. 20.1.

(a) A meaningful comparison of theory and experiment, or what is equivalent, an accurate calibration of $\Phi_0(V)$ from the room temperature compression data, requires that the phonon vibrational pressure be included.

(b) The theoretical compression curve is in good agreement with experiment to compressions far beyond the range of a few percent, where the theoretical calibration from the bulk modulus is reliable, and this tells us that the $\Phi_0(V)$ curve from pseudopotential perturbation theory is quite accurate at the volumes shown.

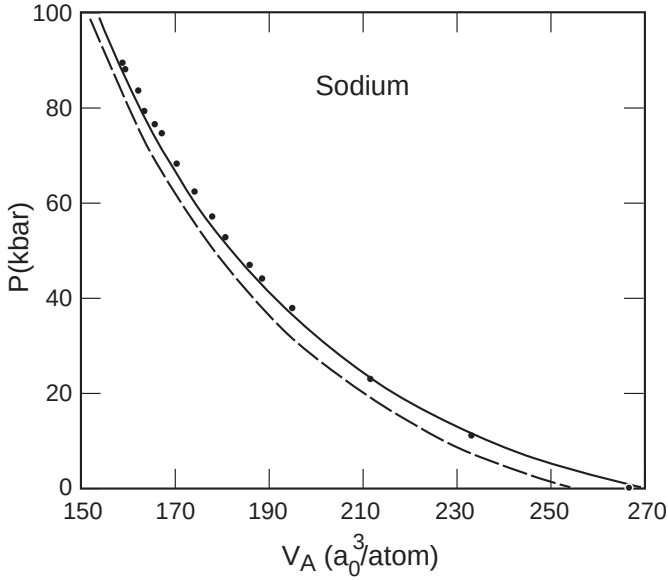


Figure 20.1. Compression curves for sodium at 293 K: points are diamond cell data and solid line is theory. Dashed line is $-d\Phi_0/dV$.

A metal for which extensive electronic structure calculations have been done, and far from Na in the periodic table, is Th. Work of Johansson *et al* (1995) shows that the fcc structure in Th is stabilized by itinerant f electrons, in contrast to the hcp structure of the d-electron metals in the same column, Ti, Zr, and Hf. Under compression at room temperature, Th exhibits a continuous phase transition in which c/a changes from its

fcc value of $\sqrt{2}$, to around 1.65 in a bct structure. This phase transition is explained by Söderlind *et al* (1995), as a result of an increased f-electron occupation and a concomitant Peierls distortion, with increasing compression. The theoretical c/a ratio as function of pressure is in remarkable agreement with experiment, as shown in Fig. 20.2. The theoretical curve of $-d\Phi_0/dV$ is compared with experimental P at room temperature in Fig. 20.3, and the agreement to 3 Mbar is rather good.

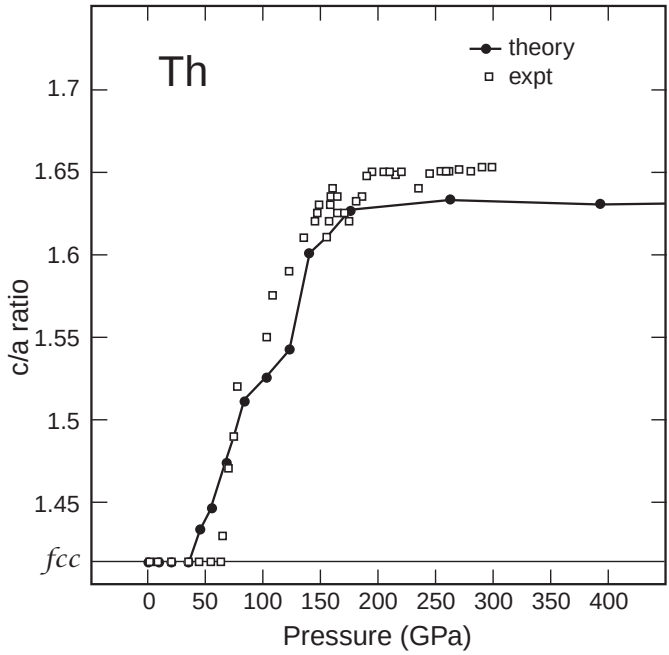


Figure 20.2. Comparison of electronic structure theory and experiment for c/a *vs* $P$ for Th at room temperature.

Figure 20.3 illustrates several points regarding the calibration of $\Phi_0(V)$. First, in order to rationalize density functional calculations of $-d\Phi_0/dV$ with experiment, a common practice is to rigidly shift the theoretical curve, so as to obtain better agreement with the measured volume and bulk modulus at $P = 0$. Figure 20.3 does not support this *ad hoc* procedure. Second, in the low-pressure region of Fig. 20.3, the vibrational contribution would move theory closer to experiment, but would reduce the discrepancy by only around 5%. Finally, to construct the most accurate possible $\Phi_0(V)$ func-

tion, it makes sense to use the most reliable data available, which means to use experimental compression data where it is available, and to interpolate smoothly to density functional calculations at higher compressions.

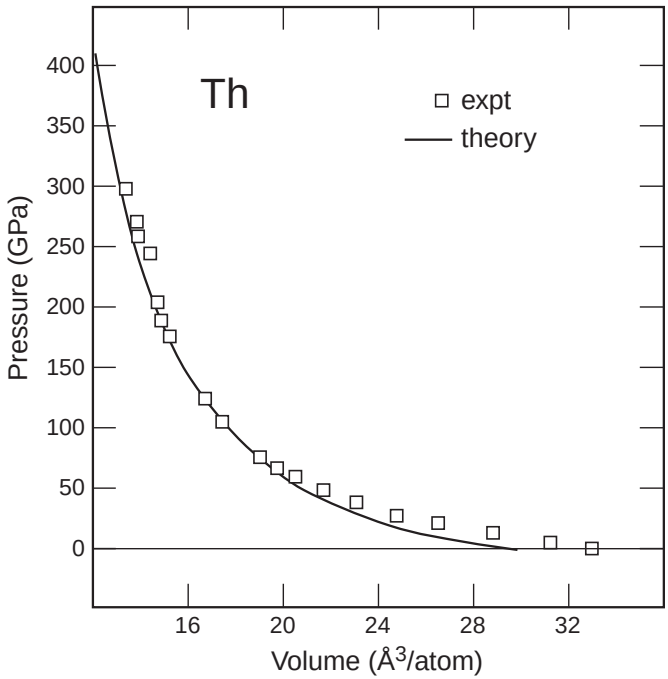


Figure 20.3. Comparison of electronic structure theory (potential aproximation) and experiment for room temperature compression of Th.

### *Calibration of the Thermal Part*

The free energy at $T = 0$ is given by Eq. (16.24),

$$F(T=0) = \Phi_0 + \frac{9}{8}Nk\theta_1 + U_{anh}(T=0) \quad . \tag{20.4}$$

In equation-of-state applications, the very small anharmonic contribution here is neglected. The small contribution in $\theta_1$ is part of the quasiharmonic phonon model, and will be determined when the thermal free energy is calibrated. The thermal free energy is

$$F(\text{thermal}) = F(V,T) - F(V,T=0) \quad . \tag{20.5}$$

In principle, $F(\text{thermal})$ and $S(V,T)$ contain the same information.

In the low-temperature regime, the nuclear motion free energy is written in Eq. (16.32),

$$(F_{ph} + F_{anh})(\text{thermal}) = -Nk\Theta_D \frac{\pi^4}{5} \left( \frac{T}{\Theta_D} \right)^4 \quad , \tag{20.6}$$

and the total electronic excitation free energy is written from Eq. (18.46) as

$$(F_{el} + F_{ep})(\text{thermal}) = -\frac{1}{2}\hat{\Gamma}T^2 \quad . \tag{20.7}$$

The coefficients $\Theta_D$ and $\hat{\Gamma}$ are volume dependent, and are measured in low-temperature specific heat experiments. Research is currently directed at understanding the small anharmonic contribution to $\Theta_D$, and the sizable electron-phonon interaction contribution to $\hat{\Gamma}$.

At intermediate temperatures, in the dispersion regime, the dominant thermal free energy contribution is $F_{ph}(\text{thermal})$, which can be calculated from the phonon density of states $g(\omega)$. The independent-electron excitation term $F_{el}$ is very small, but is easy to calculate, or to estimate. The contributions from anharmonicity and electron-phonon interactions are very small and difficult to calculate, and may be neglected in equation-of-state applications.

Most practical applications of equations of state are in the high-temperature regime, for $T \gtrsim \theta_2$. To express the relative importance of the various contributions, we make use of our extensive analysis of the entropy. From Sec. 18, $S_{ep}$ should be negligible even for highly accurate work. Then $S(V,T) = S_{ph} + S_{el} + S_{anh}$, and from Sec. 19 the three terms constitute the following proportions of the total, for temperatures from $\theta_2$ to $T_m$:

$$\begin{aligned} S_{ph} &\approx 90 - 100\% \quad , \\ S_{el} &\approx 0 - 10\% \quad , \\ S_{anh} &\approx 0 - 5\% \quad . \end{aligned} \tag{20.8}$$

An accurate evaluation of $S_{ph}$ requires data of similar accuracy for $\theta_0(V)$, and much less accurate data for $\theta_2(V)$, as can be seen from Eq. (17.6). At densities near normal, highly accurate experimental data are available for these phonon characteristic temperatures.

Let us consider what is possible at densities higher than normal, where experimental phonon data are not available. Phonon frequencies can be calculated at all densities from density functional theory, and $\theta_0(V)$ and $\theta_2(V)$ can be evaluated to an accuracy of say 5%, so that $S(V,T)$ is obtained to an accuracy ranging from 5% at $T = \theta_2$, to around 1% at $T_m$. $S_{el}$ can be calculated to an accuracy around 10%, from the free-electron model for nearly-free-electron metals, or better, from the electronic density of states for all metals. $S_{anh}$ can be calculated from molecular dynamics, if one has a reasonably accurate model for the adiabatic potential $\Phi(\{\mathbf{r}_K\})$. These calculations will provide the most accurate *ab initio* evaluation of $S(V,T)$ at high temperatures. On the other hand, at the risk of an additional error on the order of 5%, one can neglect $S_{anh}$. We then have a well-defined and simple procedure to calculate $S(V,T)$, to an overall accuracy estimated at 10% or better, from

$$S \approx S_{ph} + S_{el} \quad . \tag{20.9}$$

Should such an entropy function need to be corrected, to achieve agreement with any experimental data measuring thermal effects, the correction may be sought in the form of a small change in $\theta_0(V)$, or in a small $S_{anh}(V,T)$, or both.

The magnetic metals Ni and Cr have significant magnetic contributions, but they still remain phonon dominated. A theory for the magnetic entropy would be welcome.

Except at very low temperatures in metals, where electronic excitations dominate, by far the major thermal contribution to the equation of state of any crystal is the quasiharmonic phonon contribution. It is therefore always important to work with an accurate representation of the phonons. The functions entering the phonon thermodynamic formulas are uniquely defined, and one should not substitute other functions for them. Hence the Debye temperature has no role in the equation of state beyond the low temperature thermal part. In addition, Slater or Dugdale-McDonald formulas are unacceptable as approximations for the Grüneisen parameter. The classical free energy is discussed further in problems 20.1 and 20.2.

### *Planar Shocks in Solids*

Shocks in solids are usually generated by carefully controlled high-velocity plate impact experiments. Within the propagating shock front, material

is compressed and accelerated. A shock cannot exist without dissipation, and the major dissipative mechanisms in shocks in solids are plastic flow and heat transport. Hence the shock *process*, which takes place within the shock front, is irreversible, and requires irreversible thermodynamics for its theoretical description. On the other hand, the material behind the shock front is in a steady state of thermodynamic equilibrium, until the shock release wave arrives. Hence shock experiments allow us to measure certain equilibrium properties of compressed materials, in practice to pressures of several Mbar. For simplicity of discussion, we limit consideration to metals, in polycrystal or single crystal form.

When a weak shock propagates in a solid, the front exhibits a two-wave structure. The leading wave is the elastic precursor, which quickly decays to a stress level at the plastic yield strength, and a velocity at the longitudinal sound velocity. The second wave is the plastic wave, whose risetime is related to the plastic flow rate. The whole wave structure is nonsteady, and the only way to get information on the material within the shock front, and in the equilibrium state behind the front, is to integrate the hydrodynamic equations along the shock process. Hence, given a highly accurate equation of state to begin with, shock profile data can be analyzed to extract the irreversible component of the shock process, and thus to find the plastic constitutive behavior of the material at high strain rates (Wallace, 1980). It is possible to study the dynamics of shock driven phase transitions in the same way (Boettger and Wallace, 1997).

While the elastic precursor has a limiting amplitude and velocity, both the amplitude and velocity of the plastic wave increase as shock strength increases. At some shock strength, perhaps a few hundred kbar, the elastic precursor is negligible, and eventually the plastic wave overdrives (travels faster than) the elastic precursor. At these shock levels, the shock risetime is too short to be measured, and it is customarily assumed that the shock travels as a steady wave. We have applied steady wave theory to metals, and have concluded that heat conduction is necessary for the existence of steady overdriven shocks, and that the risetime of such shocks in metals is on the order of 1 ps (Wallace, 1981, 1982). The author is still hoping to see this risetime measured experimentally. The shock theory mentioned above is available in a reprint collection (Wallace, 1991a).

Let us consider shocks from an initial state labeled a, where density is $\rho_a$, internal energy is $U_a$, the applied stresses are zero, and the material velocity is $v_a = 0$. Often the initial state is the standard state at room

temperature and zero pressure. The equilibrium state behind a shock depends only on the initial state and the shock strength, hence as a function of shock strength, the shocked equilibrium states lie on a single curve on the equation-of-state surface. This curve is the *Hugoniot*. States on the Hugoniot are labeled $H$, and have density $\rho_H$, internal energy $U_H$, and normal compressive stress $\sigma_H$, where normal means in the shock propagation direction. The compression from initial to Hugoniot state is $\epsilon_H$,

$$\epsilon_H = 1 - \frac{\rho_a}{\rho_H} \quad . \tag{20.10}$$

If the shock is a steady wave, the continuum mechanics equations expressing conservation of mass, momentum, and energy can be used to derive the three Hugoniot jump conditions. These conditions are written in terms of the shock velocity $D$, and the material velocity $v_H$, also called the particle velocity,

$$\epsilon_H = v_H/D \quad , \tag{20.11}$$

$$\sigma_H = \rho_a D^2 \epsilon_H \quad , \tag{20.12}$$

$$U_H - U_a = \frac{1}{2} D^2 \epsilon_H^2 \quad , \tag{20.13}$$

where $U$ is energy *per unit mass*. Experiments are able to measure $D$ and $v_H$ to an accuracy of around $\frac{1}{2}\%$, and with this information the jump equations can be solved to find density, normal stress, and internal energy for the Hugoniot state.

If one neglects the difference between transverse and normal stresses in the shocked state, $\sigma_H$ becomes the pressure $P_H$. Standard practice in shock analysis is to replace $\sigma_H$ by $P_H$, and proceed as if the Hugoniot stress were always isotropic pressure. This approximation yields observable errors for weak shocks. The amount of work dissipated in a shock increases rapidly with shock strength, and correspondingly, the Hugoniot rises rapidly above the room temperature compression curve. The difference between these curves is a measure of thermal pressure, and thermal energy, and can in principle be used to calibrate the thermal free energy, or the entropy. It is also possible to measure velocities of shock release waves, for which the leading edge propagates at the longitudinal adiabatic sound velocity. This

information can be used to find the thermodynamic Grüneisen parameter on the Hugoniot. Observations of shock release waves can also locate crystal-crystal phase transitions, and melting, on the Hugoniot. This information is part of the material phase diagram, and is useful in finding the changes in thermodynamic quantities across phase boundaries.

*Problems*

*20.1.* A good aproximation for all crystals at high temperatures is the classical lattice dynamics free energy $F = \Phi_0(V) - 3NkT \ln (T/\theta_0(V))$. From this $F$, calculate the standard thermodynamic functions: (a) $S$, $U$, and $P$, related to first derivatives, (b) $B_T$, $C_V$, $\alpha$, and $\gamma$, related to second derivatives, and (c) the ratio $B_S/B_T$. Some results for checking are

$$\gamma = -\frac{d \ln \theta_0}{d \ln V} \quad , \quad \alpha = \frac{3Nk\gamma}{VB_T} \quad .$$

*20.2.* Show that the classical lattice dynamics pressure is

$$P = -\frac{d\Phi_0}{dV} + \frac{3NkT\gamma}{V} \quad .$$

Draw a curve of $\Phi_0(V)$, and visualize the sign and magnitude of each contribution to $P$ as a function of $V$ and $T$. Sketch the curve of $V(T, P = 0)$. Sketch the pressure isotherms for a set of temperatures.

*This page intentionally left blank*

# Chapter 5

# Liquid Dynamics and Statistical Mechanics

## 21 CONFIGURATIONAL CORRELATIONS IN A MONATOMIC LIQUID

### *Multiparticle Correlation Functions*

In this chapter we shall study monatomic liquids. Molecular liquids such as $H_2$ and $O_2$ are specifically omitted; however, under sufficient compression, these liquids become monatomic and are covered by our study. Our primary concern is with the nuclear motion, whose Hamiltonian is

$$\mathcal{H} = \sum_K \frac{\mathbf{p}_K^2}{2M} + \Phi(\{\mathbf{r}_K\}) \quad . \tag{21.1}$$

For most elemental liquids, the nuclear motion is classical at $T \geq T_m$. The leading quantum correction is significant for the light elements, say up to Ne, and it can be calculated from the Kirkwood expansion (9.27), or from Eq. (9.31) for central potentials. What makes He different from any liquid considered here is the importance of nuclear exchange. Valuable references on the theory of liquid He are Feenberg (1969), Campbell (1978), and Glyde (1994). For all the elements we have studied, structural and thermodynamic quantities for the liquid at melt are listed in Table 21.1. Some analysis of the liquid data is discussed in Problem 21.1.

Table 21.1. Data for 41 elemental liquids at melt. All but Ar, Kr, and Xe are metals, and z is listed for 22 nearly-free-electron metals. Density of the liquid at melt is $\rho_{lm}$, relative volume increase on melting is $\eta$, Eq. (22.1), number of atoms in the nearest-neighbor shell is $n_1$, and entropy units are $k$ per atom.

| Element | z | $\frac{T_m}{(K)}$ | $\frac{\rho_{lm}}{(g/cm^3)}$ | $\eta$ | $n_1$ | $S_{expt}$ | $S_1$ |
|---|---|---|---|---|---|---|---|
| Li | 1 | 453.7 | 0.515 | 0.015 | 9.5 | 5.66 | 8.11 |
| Na | 1 | 371.0 | 0.925 | 0.025 | 10.4 | 7.78 | 10.22 |
| K | 1 | 336.4 | 0.829 | 0.024 | 10.5 | 9.06 | 11.51 |
| Rb | 1 | 312.6 | 1.479 | 0.025 | 9.5 | 10.26 | 12.77 |
| Cs | 1 | 301.6 | 1.84 | 0.026 | 9.0 | 11.11 | 13.60 |
| Mg | 2 | 922 | 1.59 | 0.031 | 10.9 | 8.81 | 11.18 |
| Ca | — | 1113 | 1.36 | 0.04 | 11.1 | 11.03 | 12.87 |
| Sr | — | 1042 | 2.48 | 0.04 | 11.1 | 12.10 | 14.13 |
| Ba | — | 1002 | 3.31 | 0.008 | 10.8 | 14.04 | 14.90 |
| Cu | 1 | 1358 | 8.00 | 0.045 | 11.3 | 10.09 | 12.55 |
| Ag | 1 | 1235 | 9.35 | 0.050 | 11.3 | 10.94 | 13.58 |
| Au | 1 | 1338 | 17.36 | 0.052 | 10.9 | 11.77 | 14.58 |
| Zn | 2 | 692.7 | 6.58 | 0.044 | 10.5 | 9.04 | 11.81 |
| Cd | 2 | 594.2 | 8.02 | 0.045 | 10.3 | 9.76 | 12.73 |
| Hg | 2 | 234.3 | 13.69 | 0.036 | 10.0 | 8.31 | 12.25 |
| Al | 3 | 933.5 | 2.385 | 0.070 | 11.5 | 8.58 | 11.05 |
| In | 3 | 429.8 | 7.02 | 0.020 | 11.6 | 9.11 | 12.43 |
| Tl | 3 | 577 | 11.22 | 0.032 | 11.6 | 10.93 | 13.85 |
| Pb | 4 | 600.6 | 10.63 | 0.036 | 10.9 | 11.13 | 13.99 |
| Ar | — | 83.81 | 1.415 | 0.146 | — | 6.38 | 8.94 |
| Kr | — | 115.76 | 2.442 | 0.147 | — | 8.11 | 10.73 |
| Xe | — | 161.39 | 2.963 | 0.148 | — | 9.51 | 12.16 |
| Ti | — | 1945 | 4.14 | 0.024 | 10.9 | 11.83 | 13.04 |
| Zr | — | 2128 | (6.0) | (0.04) | 10.6 | 13.39 | 14.42 |
| V | — | 2202 | 5.49 | 0.036 | 11.0 | (12.12) | 13.10 |
| Nb | — | 2744 | 7.76 | 0.030 | — | 13.24 | 14.58 |
| Ta | — | 3293 | 14.8 | 0.034 | — | 14.75 | 15.88 |
| Cr | — | 2133 | (6.28) | (0.064) | 11.2 | 11.69 | 12.97 |
| Mo | — | 2896 | 9.3 | 0.028 | — | (13.26) | 14.56 |
| W | — | 3695 | 17.2 | 0.044 | — | (14.52) | 15.94 |
| Fe | — | 1811 | 7.02 | 0.034 | 10.6 | 12.01 | 12.79 |
| Ni | — | 1728 | 7.89 | 0.048 | 11.6 | 11.54 | 12.72 |
| Pd | — | 1827 | 10.5 | 0.064 | 10.9 | (12.20) | 14.01 |
| Pt | — | 2045 | 19.1 | 0.056 | 11.1 | 13.09 | 15.10 |
| Th | — | 2031 | 10.5 | — | — | — | 16.12 |

Table 21.1 (Cont.)

| Element | z | $\frac{T_m}{(K)}$ | $\frac{\rho_{lm}}{(g/cm^3)}$ | $\eta$ | $n_1$ | $S_{expt}$ | $S_1$ |
|---|---|---|---|---|---|---|---|
| Ga | 3 | 302.9 | 6.09 | –0.031 | 10.4 | 7.18 | 10.80 |
| Si | 4 | 1687 | 2.51 | –0.090 | 6.4 | 11.05 | 11.99 |
| Ge | 4 | 1211 | 5.60 | –0.065 | 6.8 | 11.72 | 13.07 |
| Sn | 4 | 505.1 | 7.00 | 0.026 | 10.9 | 9.66 | 12.76 |
| Sb | (5) | 904 | 6.48 | –0.009 | 8.7 | 11.74 | 13.77 |
| Bi | (5) | 544.5 | 10.07 | –0.033 | 8.8 | 11.28 | 13.92 |

The classical partition function for indistinguishable particles is

$$Z = \frac{1}{h^{3N} N!} \int \cdots \int e^{-\beta \mathcal{H}} d\mathbf{r}_1 d\mathbf{p}_1 \cdots d\mathbf{r}_N d\mathbf{p}_N \quad . \tag{21.2}$$

The probability density that phase point $x = \{\mathbf{r}_K, \mathbf{p}_K\}$ is occupied is

$$f^{(N)} = \frac{e^{-\beta \mathcal{H}(x)}}{h^{3N} Z} \quad . \tag{21.3}$$

$f^{(N)}$ is normalized to $N!$, and can be factored to

$$f^{(N)} = f^{(1)}(\mathbf{p}_1) \cdots f^{(1)}(\mathbf{p}_N) g^{(N)}(\mathbf{r}_1, \cdots, \mathbf{r}_N) \quad . \tag{21.4}$$

Here $f^{(1)}(\mathbf{p}) = f(\mathbf{p})$ is the equilibrium Boltzmann distribution,

$$f(\mathbf{p}) = \rho_A \left( \frac{\beta}{2\pi M} \right)^{3/2} \exp \left( -\frac{\beta \mathbf{p}^2}{2M} \right) \quad , \tag{21.5}$$

where $\rho_A = N/V$ is the particle density, and the normalization is

$$\int f(\mathbf{p}) d\mathbf{p} = \rho_A \quad . \tag{21.6}$$

The equilibrium $N$-particle correlation function $g^{(N)}$ is defined by Eq. (21.4), and has the normalization

$$N! = \rho_A^N \int \cdots \int g^{(N)}(\mathbf{r}_1, \cdots, \mathbf{r}_N) d\mathbf{r}_1 \cdots d\mathbf{r}_N \quad . \tag{21.7}$$

Finally, the $n$-particle correlation functions for $n = 1, \cdots, N$ are defined by

$$\rho_A^n g^{(n)}(\mathbf{r}_1, \cdots, \mathbf{r}_n) = \frac{\rho_A^N}{(N-n)!} \int \cdots \int g^{(N)}(\mathbf{r}_1, \cdots, \mathbf{r}_N) d\mathbf{r}_{n+1} \cdots d\mathbf{r}_N \quad . \tag{21.8}$$

Accordingly, $g^{(1)}(\mathbf{r}) = 1$.

The correlation functions are relevant for equilibrium statistical mechanics, since $g^{(n)}$ can be used to express the average of an $n$-particle spatial function. By far the most important correlation function for monatomic liquids is the pair correlation function $g^{(2)}(\mathbf{r}_1, \mathbf{r}_2)$. Given there is a particle at $\mathbf{r}_1, \rho_A g^{(2)}(\mathbf{r}_1, \mathbf{r}_2) d\mathbf{r}_2$ is the probability there is a particle in the infinitesimal $d\mathbf{r}_2$ at $\mathbf{r}_2$. Since an equilibrium liquid is homogeneous, $g^{(2)}(\mathbf{r}_1, \mathbf{r}_2)$ can only depend on $|\mathbf{r}_1 - \mathbf{r}_2|$, hence the pair correlation function can always be written $g^{(2)}(r)$, or simply $g(r)$. For a sum of pair potentials $\phi(|\mathbf{r}_K - \mathbf{r}_L|)$, the statistical average potential per particle is (see problem 21.2)

$$\left\langle \frac{1}{2N} \sum_{KL} \phi(|\mathbf{r}_K - \mathbf{r}_L|) \right\rangle = \frac{1}{2} \rho_A \int_0^\infty \phi(r) g(r) 4\pi r^2 dr \quad . \tag{21.9}$$

Temperature dependence of the pair correlation function at constant density is illustrated in Fig. 21.1. For a monatomic liquid we define the mean nearest-neighbor distance $R_1$ as the location of the first maximum of $g(r)$. Then $g(x)$, where $x = r/R_1$, is a qualitatively universal function for normal melting monatomic liquids at $T_m$. The character of $g(x)$ at $T_m$ is shown in the bottom panel of Fig. 21.1, and is summarized as follows: $g(x) = 0$ out to $x \approx 0.75$; the number $n_1$ of particles in the nearest-neighbor shell, say out to the first minimum in $g(x)$, is around 9–11; shell structure beyond the first peak is pretty well fixed by the geometry of random close packing; and $g(x)$ goes to a constant value of $1 + O(N^{-1})$ at large $x$. Values of $n_1$ at temperatures near melting, from Table 3-1 of Waseda (1980), are listed in Table 21.1.

Upon increasing temperature at fixed density, the monatomic liquid progresses toward a gas, as illustrated in the upper two panels of Fig. 21.1. In the ideal gas limit, $g(r) = 1 + O(N^{-1})$. At the highest temperature shown, $T = 38.2\ T_m$, the system is a dense gas, with short-range repulsion still obviously significant. At some very high temperature, our calculation no longer represents real aluminum, since thermal ionization is not included (see Sec. 25).

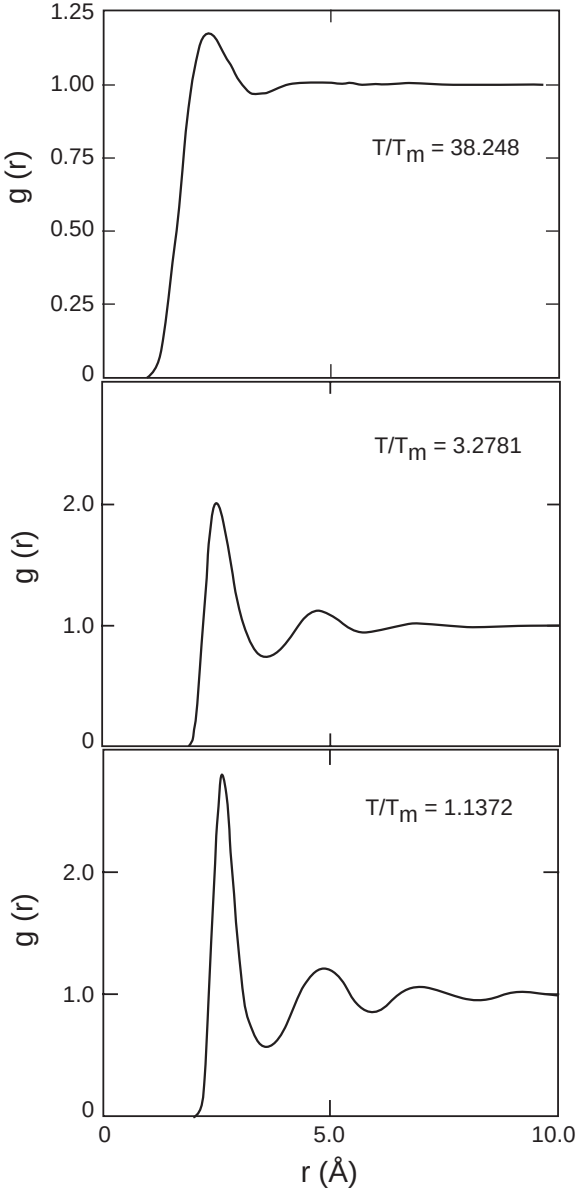


Figure 21.1. Pair correlation function for pseudopotential Al at fixed density and at several temperatures.

***Correlation Entropy***

From the canonical partition function (21.2), the entropy is (see problem 21.3)

$$S = -\frac{k}{N!}\int\cdots\int f^{(N)}\ln(h^{3N}f^{(N)})d\mathbf{r}_1 d\mathbf{p}_1\cdots d\mathbf{r}_N d\mathbf{p}_N \quad . \tag{21.10}$$

Notice this equation is the classical analog of the quantum state summation in Eq. (7.9), $S = -k\Sigma_n f_n \ln f_n$. With the factorization (21.4) of $f^{(N)}$, it follows

$$\begin{aligned} S &= -\frac{Nk}{\rho_A}\int f(p)\ln[h^3 f(p)]d\mathbf{p} \\ &\quad -\frac{k\rho_A^N}{N!}\int\cdots\int g^{(N)}\ln g^{(N)} d\mathbf{r}_1\cdots d\mathbf{r}_N \quad . \end{aligned} \tag{21.11}$$

The first term is the momentum-space contribution, or one-particle contribution, denoted $S_1$, where

$$\frac{S_1}{Nk} = \frac{3}{2} - \ln\left(\rho_A\Lambda^3\right) \quad , \quad \Lambda = \sqrt{\frac{2\pi\hbar^2}{MkT}} \quad . \tag{21.12}$$

$\Lambda$ is the thermal deBroglie wavelength, previously encountered in Eq. (9.33), where we observed that exchange effects are negligible when $\Lambda^2 << R_1^2$, or say $\rho_A\Lambda^3 << 1$. From Eq. (21.12), $\rho_A\Lambda^3 = \exp(\frac{3}{2} - S_1/Nk)$, and for the elemental liquids in Table 21.1, $\rho_A\Lambda^3$ is $e^{-7}$ to $e^{-15}$ at $T_m$.

The second term in Eq. (21.11) is the $N$-particle correlation entropy. To analyze the integrand, let us refer to the correlation which is present in an $n$-particle cluster, and not present in any smaller cluster, as the *irreducible part* of the $n$-particle correlation. Accordingly, the irreducible part of $g^{(2)}$ is $g^{(2)}$. The irreducible part of $g^{(3)}$ is $\delta g^{(3)}$, defined by

$$g^{(3)}(1,2,3) = g^{(2)}(1,2)g^{(2)}(2,3)g^{(2)}(3,1)\delta g^{(3)}(1,2,3) \quad . \tag{21.13}$$

The idea is to extend this factorization to $g^{(N)}$, and so express $\ln g^{(N)}$ as a sum of terms in $\ln g^{(2)}$, plus a sum of terms in $\ln \delta g^{(3)}$, and so on. But a problem arises. With the grand canonical distribution, where density fluctuations are present, $g^{(2)}(r) - 1$ and $\ln g^{(2)}(r)$ are local functions, i.e. they vanish for $r > l_c$, where $l_c$ is an appropriate correlation length (see Feenberg, 1969, Chap. 1). But with the canonical distribution, as with any

distribution having fixed $N$, $g^{(2)}(r)$ has a nonphysical long range correlation, because, given a particle at $\mathbf{r} = 0$, the number of remaining particles is exactly $N - 1$. Hence at $r > l_c$, $g^{(2)}(r) - 1$ and $\ln g^{(2)}(r)$ have the nonzero value $-\alpha/N$, where $\alpha$ is the measure of density fluctuations (see Eq. (7.28)),

$$\alpha = \frac{\langle \delta \mathcal{N}^2 \rangle_{GC}}{\langle \mathcal{N} \rangle} = \frac{\rho_A kT}{B_T} \quad . \tag{21.14}$$

Hence with the canonical distribution, the integral of $\rho_A \ln g^{(2)}(r)$ over the system volume acquires the contribution $-\alpha$ from the space $r > l_c$, and this is not a physically correct contribution to the system entropy.

The spurious contribution is removed by limiting the integration to the correlation region $r < l_c$, denoted by $\int_c d\mathbf{r}$. Then the total liquid entropy is expressed in the multiparticle correlation expansion,

$$S = S_1 + S_2 + S_3 + \cdots \quad , \tag{21.15}$$

where the two-particle term is

$$\frac{S_2}{Nk} = -\frac{1}{2}\rho_A \int_c g(r) \ln g(r) dr \quad . \tag{21.16}$$

Since the volume of the integral is of order $V/N$, and since $g(r)$ is the same in every distribution to $O(N^{-1})$, then $S_2$ is the same in every distribution to $RO(N^{-1})$. Derivation of the above results is discussed in more detail in Wallace (1989, 1994). For the elemental liquids in Table 21.1, at temperatures up to several times $T_m$, $\alpha$ ranges from 0.005 to 0.073 (see Table 2 of Wallace, 1991b).

A multiparticle correlation expansion was presented by H. S. Green (1952, Chap. III, Sec. 5), but the crucial one-particle term was undefined because it contained the log of a dimensioned quantity. Nettleton and M. S. Green (1958) made an entirely different expansion, in powers of the density, where the leading term is not $S_1$, but is the ideal gas entropy $S_1 + Nk$ (see problem 21.4). The number of expansions proliferated, along with the degree of confusion, as noted in Wallace (1994). The series (21.15) is the logical expansion for the liquid state, and has excellent convergence properties for elemental liquids, as we shall see next.

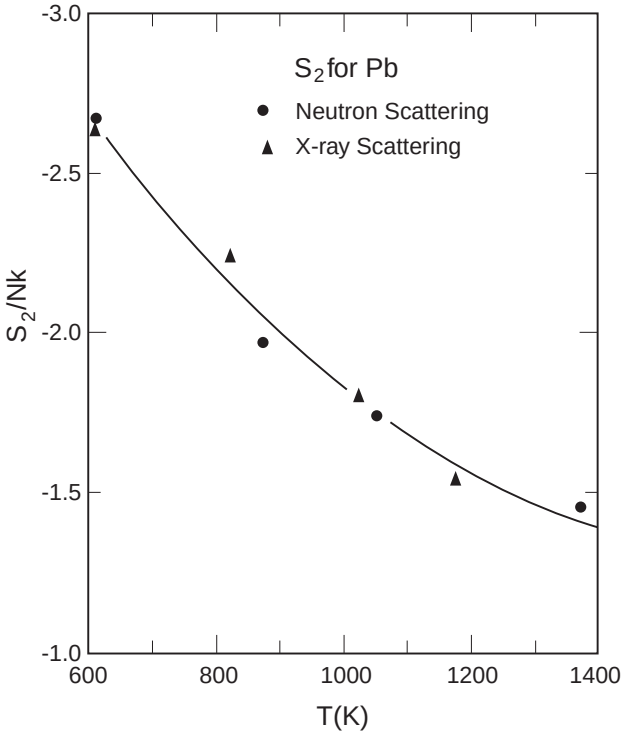


Figure 21.2. Pair correlation entropy as function of $T$ for Pb, where the points derive from experimental $g(r)$ data, and the line is a smooth fit to the points.

### *Pair Correlation Entropy*

We have analyzed the entropy for all elemental liquids for which sufficient data are available (Wallace, 1991b). Our data requirements are (a) experimental entropy accurate to around 1%, and (b) an evaluation of $S_{el}$ to an accuracy of at least 1% of $S$. These conditions limit us to the 22 nearly-free-electron metals indicated in Table 21.1. For these liquids, we calculated the pair correlation entropy from Eq. (21.16) at every temperature for which an experimental $g(r)$ was available. Results for Pb at temperatures from $T_m$ to 2.3 $T_m$, based on $g(r)$ from both neutron scattering and x-ray scattering experiments, are shown in Fig. 21.2. The figure demonstrates agreement between the two types of scattering experiments, and further shows that $S_2/Nk$ can be determined to the very good accuracy of $\pm 0.05$ when good $g(r)$ data are available.

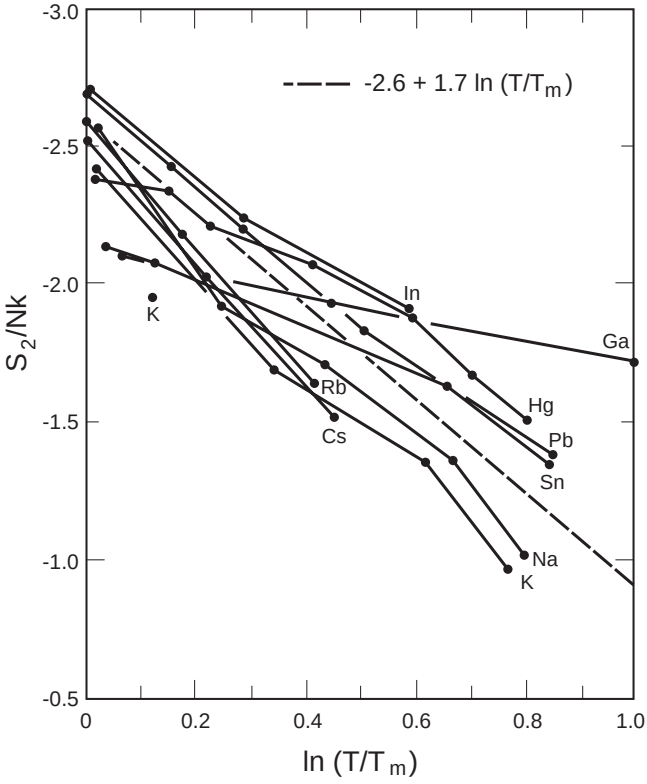


Figure 21.3. Pair correlation entropy as function of $\ln(T/T_m)$ for 9 liquid metals. The isolated point for $K$ is apparently in error.

Examination of the results for $S_2/Nk$ at $T \approx T_m$ led us to the discovery of two classes of elements. For the 16 "normal" elements, $S_2/Nk$ at $T_m$ lies in the narrow range $-2.4$ to $-2.8$, with a mean of $-2.6$. For the 6 "anomalous" elements, $S_2/Nk$ is always outside this range, and smaller in magnitude, being $-2.2$ for Sn and Ga, around $-1.8$ for Sb and Bi, and $-1.2$ for Si and Ge. It turns out that the normal elements have no significant change in electronic structure upon melting, while the anomalous elements do have. The situation will be clarified in detail when we study the melting process, in Sec. 22.

We have enough data to evaluate the temperature dependence of the pair correlation entropy for 9 liquid metals, 7 normal ones and Sn and Ga. The results in Fig. 21.3 show a remarkable similarity of all the curves. Data

for the 7 normal metals are well approximated by the line

$$\frac{S_2}{Nk} = -2.6 + 1.7 \ln\left(\frac{T}{T_m}\right) \quad . \tag{21.17}$$

This empirical finding brings much order into the concept of pair correlation entropy in monatomic liquids. It is not clear why the curves for Sn and Ga have smaller slopes than curves for the normal metals.

The physical origin of the sign and temperature dependence of the pair correlation entropy is easy to see. The leading entropy contribution is the momentum-space term $S_1$. Next, in configuration space, the particle-particle correlation strongly limits the motion, hence reduces the entropy, so that $S_2$ is always negative. Finally, as temperature increases, the increasing thermal energy allows the motion to overcome the restrictive pair correlations, so that the magnitude of $S_2$ decreases with temperature. The data for $S_2(T)$ show no exception to this behavior.

### *Higher-Order Correlation Entropy*

We are not able to calculate the correlation entropy terms $S_n$ for $n \geq 3$, because the correlation functions $g^{(n)}$ are not available. However, we can still learn something about higher-order correlation by using the experimental entropy. We shall argue in Sec. 25 that the entropy arising from interaction between nuclear motion and electronic excitation remains negligible for metals to several times $T_m$. Therefore, let us write

$$S_{expt} = S_1 + S_2 + S_x + S_{el} \quad , \tag{21.18}$$

where this equation defines $S_x = S_3 + S_4 + \cdots$. For our 22 liquid metals, $S_{el}$ was calculated from the free electron model, with the value of $z$ listed in Table 21.1. $S_{el}/Nk$ is small but not negligible in this analysis, and lies in the range 0.03–0.22 at $T_m$.

The first striking result is that $S_x/Nk = 0$ within combined errors of the analysis, for most of the elemental liquids at all temperatures studied. These errors are around $\pm 0.1$, or around 1% of the total entropy, for Li, Na, K, Rb, Cs, Al, Mg, and Si, and up to $\pm 0.4$ at most, or around 4% of the total entropy, for Cu, Ag, Au, Cd, Zn, Tl, and Ge. The larger errors here are due to inaccuracies in the experimental $g(r)$, and hence in the computed $S_2$.

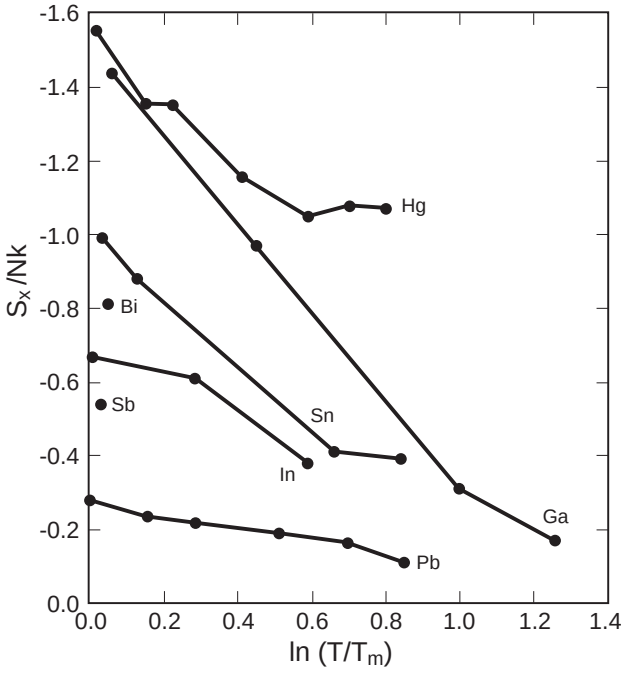


Figure 21.4. Higher-order correlation entropy for those 7 elements where it is significant.

When $S_x$ is significant, i.e. when it is not zero within errors, then $S_x(T)$ displays the same universal behavior as $S_2(T)$: $S_x$ is negative, and its magnitude decreases as temperature increases. Figure 21.4 shows the higher-order correlation entropy for those liquids where it is significant. Extensive details may be found in Wallace (1991b). In Table 2 of that reference, $S_{expt}$ and $S_x$ for Sn should both be increased by $0.85Nk$; the curve of $S_x(T)$ for Sn in Fig. 21.4 is correct. An analysis for Ar at a point on the saturation curve is given in Wallace (1988).

The behavior of $S_x$ has presumably the same physical explanation as does the similar behavior of $S_2$. When $S_x$ is significant, an irreducible n-particle correlation for $n \geq 3$ is present, and after the pair correlation is accounted for, this irreducible n-particle correlation further limits the motion, and further reduces the entropy. And again, thermal energy allows the motion to overcome the correlations, so that the magnitude of $S_x$ decreases as temperature increases. Ultimately, the multiparticle correlations arise

from the multiparticle potential energy $\Phi(\{\mathbf{r}_K\})$. We suspect that the appearance of a significant $S_x$ implies the presence of an irreducible n-particle potential for some particular value of $n$, say $n = 4$, or $n = 6$, depending on the element. This is an interesting proposition, but not proven.

What we want in liquid dynamics is a physical theory of the nuclear motion, expressed in a tractable Hamiltonian. The correlation expansion of entropy does not provide such a theory, since it only relates one statistical property (entropy) to another statistical property (multiparticle correlation functions). But the entropy expansion is intrinsically interesting, and it will help us to understand the melting process in Sec. 22, and that understanding will help us to develop a theory of the nuclear motion in Sec. 23.

*Problems*

*21.1.* In what property in Table 21.1 are Si and Ge strongly different from the other elements? Why is it that, in correlations of experimental data at $T_m$, for crystal or liquid phase, Li is a little out of line with the other alkali metals, and Ne is a little out of line with the heavier rare gases? Examine the distribution of $\eta$ for each of five groups of elements: metals which melt from fcc, from bcc, and from hcp; the rare gases; and the anomalous melting elements. For which group is the distribution far from normal? Of the other groups, which is strongly different?

*21.2.* Derive Eq. (21.9) for the statistical average of a pair function in terms of $g(r)$. Is this equation valid for a crystal? For a gas?

*21.3.* Derive Eq. (21.10) for the total entropy.

*21.4.* For the ideal gas, where $\Phi(\{\mathbf{r}_K\}) = 0$, show $g^{(N)} = N!/N^N$, and show $S = S_1 + Nk$. Hence the correlation entropy in units of $k$ per atom is $+1$, compared to around $-2.6$ for a normal liquid at melt.

## 22 MELTING OF ELEMENTS

### *Experimental Entropy of Fusion*

Motivated to gain information about the physical nature of the liquid state, we made an extensive analysis of experimental data related to melting of the elements (Wallace, 1991c). This analysis leads to the following important conclusions: (a) the elements exhibit two types of melting process, normal and anomalous, and (b) the constant-density entropy of fusion contains a

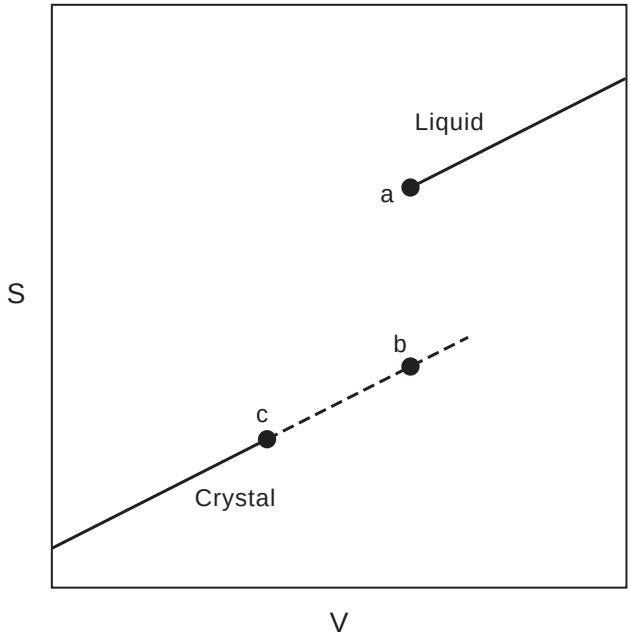


Figure 22.1. In melting at constant pressure, $\Delta S = S_a - S_c$ contains the contribution $S_a - S_b$ due to the disordering from crystal to liquid phase.

universal constant contribution. The study, slightly updated for improved accuracy, is summarized here.

For a material in crystal and liquid states at the same volume and temperature, the liquid has the larger entropy, because it moves over a larger portion of the configuration space. We want to evaluate this constant-volume entropy difference, the disordering entropy, for the elements. Experimental entropy of fusion is measured at constant pressure and temperature, and this measure needs to be corrected for the change in volume upon melting, as shown in Fig. 22.1, since the entropy change corresponding to the volume change is merely a thermal expansion effect, for either phase separately. We consider melting at $P = 0$, where the crystal and liquid densities are respectively $\rho_{cm}$ and $\rho_{lm}$, and the relative density decrease (volume increase) upon melting is $\eta$,

$$\eta = \frac{\rho_{cm}}{\rho_{lm}} - 1 \quad . \tag{22.1}$$

Table 22.1. Entropy of melting at constant density for 34 elements. Melting is normal in columns one and three, and anomalous in column two. Entropy units are $k$ per atom.

| Element | $\Delta S^*$ | Element | $\Delta S^*$ | Element | $\Delta S^*$ |
|---|---|---|---|---|---|
| Li | 0.75 | Sn | 1.48 | Ti | 0.70 |
| Na | 0.73 | Ga | 2.37 | Zr | 0.93 |
| K | 0.73 | Sb | 2.68 | V | 0.90 |
| Rb | 0.73 | Bi | 2.62 | Nb | 0.97 |
| Cs | 0.73 | Si | 3.76 | Ta | 1.09 |
| Mg | 0.96 | Ge | 3.85 | Cr | (0.7) |
| Ba | 0.90 | | | Mo | (1.2) |
| Cu | 0.86 | | | W | (1.1) |
| Ag | 0.73 | | | Pd | 0.74 |
| Au | 0.64 | | | Pt | 0.79 |
| Zn | 0.97 | | | | |
| Cd | 0.93 | | | | |
| Hg | 0.90 | | | | |
| Al | 0.88 | | | | |
| In | 0.76 | | | | |
| Pb | 0.68 | | | | |
| Fe | 0.68 | | | | |
| Ni | 0.88 | | | | |

The entropy of fusion is $\Delta S = S^l - S^c$, where superscript $l$ or $c$ indicates liquid or crystal, respectively. The disordering entropy is $\Delta S^* = \Delta S$ at constant $\rho$. The disordering entropy at the density of the liquid at melt, *i.e.* $S_a - S_b$ in Fig. 22.1, can be evaluated from (see problem 22.1)

$$\begin{aligned} \Delta S^* &= \Delta S(\rho_{lm}) \\ &= \Delta S(P=0) - \eta\gamma C_V + \cdots \quad , \end{aligned} \tag{22.2}$$

where $\gamma$ and $C_V$ are evaluated for the crystal at melt, and where $+\cdots$ represents terms of higher order in $\eta$ which are usually negligible, but not always so. Values of $\gamma^*$ for the crystal structure from which melting occurs, Table 19.1, provide accurate data for $\gamma$ in Eq. (22.2).

Values of $\Delta S^*/Nk$ for all the elements for which we are currently able to make a reliable estimate are listed in Table 22.1. Of the elements in Table 21.1, we cannot evaluate $\Delta S^*$ for Ca, Sr, and Tl, because we do not have $\gamma^*$ for the melting crystal structure. Note the evaluation for Tl in Wallace (1991c) was done with $\gamma^*$ for the low-temperature crystal structure,

an unreliable procedure, since $\gamma^*$ has a noticeable dependence on crystal structure (see problem 19.5). Also, we cannot evaluate $\Delta S^*$ for Ar, Kr, and Xe at 1 bar, because $\eta$ is so large that higher-order terms in Eq. (22.2) are not negligible. However, compressed Ar shows normal behavior, as we shall see in Chap. 6.

### *Normal and Anomalous Melting*

In Table 22.1, the entropy data and volume corrections are highly accurate in the first two columns, with errors in $\Delta S^*$ expected to be around $\pm$ 0.05, and a little larger for Si and Ge. We denote the elements in columns one and two respectively as normal and anomalous in their melting process. For the 18 normal elements, $\Delta S^*/Nk$ lies in the narrow range 0.64 – 0.97, and has mean and variance given by

$$\frac{\Delta S^*}{Nk} \text{ (normal)} \quad = 0.80 \pm 0.10 \; rms \quad . \tag{22.3}$$

In the normal group, there is a small dependence of $\Delta S^*$ on the crystal structure at melt, but this is not significant for our analysis. For the 6 anomalous elements, $\Delta S^*/Nk$ is 1.48 – 3.85, well outside the range for normal melting, and *much larger* than the normal value. Clearly something different is going on with anomalous melting.

In the normal melting process, there is no significant change in electronic structure: the elements in column one of Table 22.1 are metallic in both crystal and liquid phases at melt. The apparent universality of $\Delta S^*$ can be explained by the two-part hypothesis: (a) Since the electronic structure changes little on normal melting, the electronic excitation entropy is the same for crystal and liquid, within the experimental scatter of $\Delta S^*$, and $\Delta S^*$ is essentially a property of the nuclear motion. (b) Since the crystal has long range order, and the liquid does not, there exists a universal nuclear disordering entropy of the liquid, not present in the crystal, and of approximate value $0.80k$ per atom.

In anomalous melting, there *is* a significant change in the electronic structure, from crystal to liquid. This change is quite apparent for the two most anomalous elements, Si and Ge, which melt from covalent crystal to metallic liquid (Glazov *et al.*, 1969, Chap. 3). The change is also obvious for Sb and Bi, which melt from semimetal crystal to metal liquid (Faber, 1972, p. 81). The nature of the electronic structure change is not so obvious in the

two least-anomalous elements, Sn and Ga, but such a change is apparently present nonetheless. Also there is a correlation between anomalous melting and the sign of $\eta$, which tells whether the volume increases or decreases upon melting at constant pressure. For all the elements for which we have reliable values of $\eta$, the normal behavior is $\eta > 0$, while only Ga, Sb, Bi, Si, and Ge have $\eta < 0$, and $\eta$ is positive for Sn. The anomalous values of $\Delta S^*/Nk$, column two of Table 22.1, presumably result from two contributions, namely the universal nuclear disordering entropy of around 0.80, which must always be present in transforming from a crystal to a liquid, plus a large positive contribution due to the change in electronic structure. This picture will be clarified in the discussion of the anomalous melting process, at the end of the present section.

The first column of Table 22.1 includes two transition metals, Fe and Ni. Ten more transition metals have since been analyzed (Wallace, 1997a), and the results are listed in the third column of Table 22.1. Here the errors in $\Delta S^*/Nk$ are expected to be around $\pm 0.1$, and possibly larger still for those values in parentheses. Hence within expected errors, $\Delta S^*$ for these transition metals lies in the distribution of the first column, and therefore represents normal melting.

### *Historical Note on Melting Rules*

Over a century ago, Sutherland (1890) observed an empirical melting rule, that the product $bT_m M^{1/6}$ is nearly constant for metals, where $T_m$ is the melting temperature, $b$ is the "mean coefficient of expansion," and $M$ is the atomic mass. The following year he advanced a kinetic theory of solids (Sutherland 1891), in which he thought of atoms as hard spheres vibrating against one another, so that the mean distance between atom centers, say the crystal unit-cell edge, is the atomic diameter plus the vibration amplitude. Sutherland imagined melting would occur as a result of thermal expansion, when the space between atoms reaches a certain value relative to the atomic diameter, so that atoms are able to escape from imprisonment by their neighbors. To make this concept compatible with *measured* thermal expansions, Sutherland required the sphere diameter to decrease as temperature increases, reflecting that atoms are not hard spheres after all, but that their centers can come nearer as their kinetic energy increases. He actually carried out a hard-sphere simulation experiment, by shaking a box containing one layer of marbles, and noting by removing marbles one

at a time that the marbles become "mobile," hence a solid-liquid transition occurs, when a free volume of 25–33% is reached. Two points of particular interest contained in Sutherland's model are that the ratio of vibration amplitude to atomic spacing is the same for all elements at melting, and that the model actually perceives properties of both solid and liquid phases. Sutherland's observed inadequacy of the hard sphere model is examined quantitatively in Problem 22.2.

To demonstrate why the specific heat of a solid goes to zero as temperature goes to zero, Einstein (1907) approximated the thermal vibrational energy by means of a single-frequency model. Three years later, Lindemann (1910) searched for a way to estimate the Einstein frequency $\nu$. He accomplished this by combining the Sutherland picture, that the ratio of vibrational amplitude to atomic spacing is the same for all elements at $T_m$, with the Einstein formula for thermal energy evaluated at $T_m$, to obtain the formula

$$\nu = \text{const.} \sqrt{\frac{T_m}{M V_A^{2/3}}} \quad , \tag{22.4}$$

where $V_A$ is the volume per atom. This equation has become known as the Lindemann melting rule.

In Lindemann's rule, if $\nu$ is replaced by a characteristic temperature $\theta$, where $k\theta = h\nu$, the result is the form usually quoted today,

$$\frac{T_m}{M\theta^2 V_A^{2/3}} = \text{const.} \tag{22.5}$$

Through the years, many tests of this rule have been carried out, including an extensive test for the elements by Gschneidner (1964), where the validity of the rule was examined for several different "Debye temperatures" $\theta$. Similar tests continue to appear in the literature. The following properties are established.

1. The Lindemann rule is not well defined, because $\theta$ is not well defined in terms of any crystal property.

2. As a predictor of $T_m$ for a large group of elements, such as the metals, the Lindemann rule is accurate to no better than a factor of three.

From all we have learned about the entropy of crystal and liquid elements, and about the melting process, we can construct a melting rule which is not only well defined, but is much more accurate than Lindemann's.

***Normal Melting Rule***

Let us derive a theoretical expression for the entropy of melting at constant volume for an element. We shall treat the nuclear motion as classical, and will add a term for the electronic excitation. The crystal entropy is

$$S^c = 3Nk\left[\ln\left(\frac{T}{\theta_0^c}\right)+1\right] + S_{anh}^c + S_{el}^c \quad , \tag{22.6}$$

where the first term is the phonon contribution, from Eq. (17.6), and is dominant. With the multiparticle correlation expansion in the form of Eq. (21.18), the liquid entropy is

$$S^l = Nk\left[\frac{3}{2} - \ln(\rho_A\Lambda^3)\right] + S_2^l + S_x^l + S_{el}^l \quad , \tag{22.7}$$

where the dominant contribution $S_1^l$ has been written explicitly from Eq. (21.12). Now $\Delta S^*$ is $S^l - S^c$ evaluated at $T_m$ and $\rho_{lm}$, and this can be expressed from the preceding equations to find

$$\frac{3}{2}\ln L - \frac{3}{2} = \frac{1}{Nk}\left[\Delta S^* + \left(S_{anh}^c - S_2^l - S_x^l\right) + \left(S_{el}^c - S_{el}^l\right)\right] \quad , \tag{22.8}$$

where

$$L = \frac{Mk(\theta_0^c)^2}{2\pi\hbar^2(\rho_{lm})^{2/3}T_m} \quad . \tag{22.9}$$

$L$ has been called the "amended Lindemann function" (Wallace, 1991c), since it contains a well defined characteristic temperature, namely the phonon temperature $\theta_0^c(\rho_{lm})$.

Let us estimate the terms in Eq. (22.8), specifically for a normal melting element. From Eq. (22.3), we expect $\Delta S^*/Nk \approx 0.80$, and from our study of the pair correlation entropy, for example from Eq. (21.17), we expect $S_2^l/Nk \approx -2.6$. Since normal melting entails no change in electronic structure, we expect $S_{el}^c \approx S_{el}^l$, so the anticipated result for $\frac{3}{2}\ln L$ is

$$\frac{3}{2}\ln L + \frac{S_x^l}{Nk} - \frac{S_{anh}^c}{Nk} \approx 4.9 \quad . \tag{22.10}$$

In Table 15.1, experimental values of $\theta_0^c$ are listed for 36 elements. In order to make a first test of Eq.(22.10), we corrected all these $\theta_0^c$ to the density $\rho_{lm}$, ignoring any dependence of $\theta_0^c$ on the crystal structure. This approximation, plus the known scatter of $\pm 0.16$ in $\Delta S^*/Nk$, and of $\pm 0.2$

in $S_2^l/Nk$, leads us to expect scatter on the order of $\pm 0.3$ on the right side of Eq. (22.10). Note this compares to scatter on the order of $\pm 0.1$ in our accurate entropy analyses. For Ar, Kr, and Xe, in order to avoid the excessive volume correction of $\theta_0^c$ to density $\rho_{lm}$, we evaluated $L$ at the density where $\theta_0^c$ is measured. The corresponding melting temperatures are:

| Element | $\rho_{lm}(g/cm^3)$ | $T_m(K)$ |
|---|---|---|
| Ar | 1.7705 | 220 |
| Kr | 3.091 | 324 |
| Xe | 3.780 | (467) |

$L$ is calculated from Eq. (22.9), and results for $\frac{3}{2}\ln L$ are shown in the top panel of Fig. 22.2. On the left is a distribution of 28 elements, with $\frac{3}{2}\ln L$ in the range $4.6-5.3$, and having mean value 4.95. Comparison with Eq. (22.10) suggests that $S_x^l/Nk$ and $S_{anh}^c/Nk$ are contained in the scatter for these 28 elements. It is significant that the remaining elements all lie *above* the main distribution. One sees that these elements are all unusual in a specific property: they either have a large $|S_x^l|$, or a large $S_{anh}^c$, or else they exhibit anomalous melting. Let us correct the graph for these elements, and only these, in the following way: add $S_x^l/Nk$ for Hg and In (from Fig. 21.4), subtract $S_{anh}^c/Nk$ for Cr, Mo, and W (from Tables 19.2 and 19.3), and omit the anomalous melting elements Sn, Si, and Ge. The results are shown in the center panel of Fig. 22.2, where all 33 elements now lie in the range $4.6-5.3$, and have the mean value 4.94, so that when scatter is neglected,

$$\frac{3}{2}\ln L + \frac{S_x^l}{Nk} - \frac{S_{anh}^c}{Nk} = 4.94 \quad . \tag{22.11}$$

It seems we have found the major factors controlling $T_m$ for the normal melting elements. As a predictor of the normal melting temperature, Eq. (22.11) is accurate to around 25%.

To illustrate the quality of the Lindemann melting rule in its current standard form, the function $\frac{3}{2}\ln L_D$ is shown in the bottom panel of Fig. 22.2, for the same 36 elements at the same densities as are shown in the top panel, where $L_D$ is the function $L$ in Eq. (22.9) with $\theta_0^c$ replaced

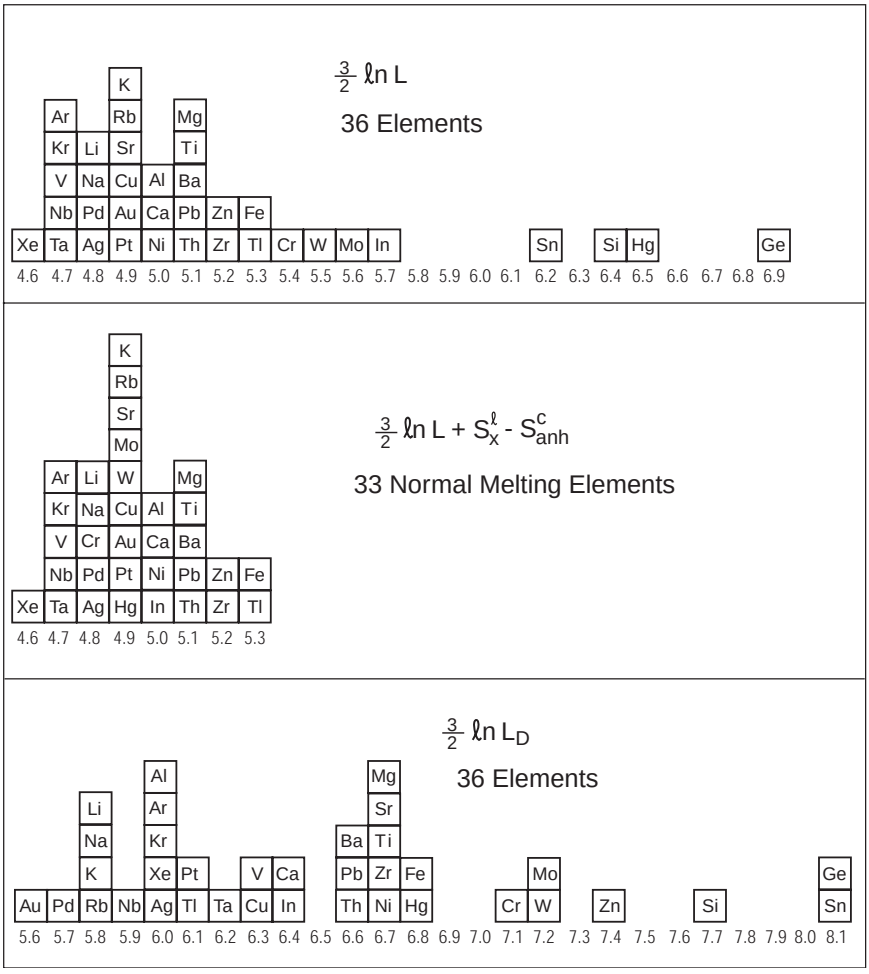


Figure 22.2. Top panel: Test of the constancy of $\frac{3}{2}\ln L$ for all 36 elements for which data are available. Center panel: Test of Eq. (22.10) for 33 normal melting elements. Bottom panel: Test of the constancy of $\frac{3}{2}\ln L_D$, the Lindemann melting rule.

by the Debye temperature $\Theta_D$. The poor quality of $\frac{3}{2}\ln L_D$ as a predictor of $T_m$ is due primarily to the fact that $\Theta_D$ is not related to the physics of the melting process.

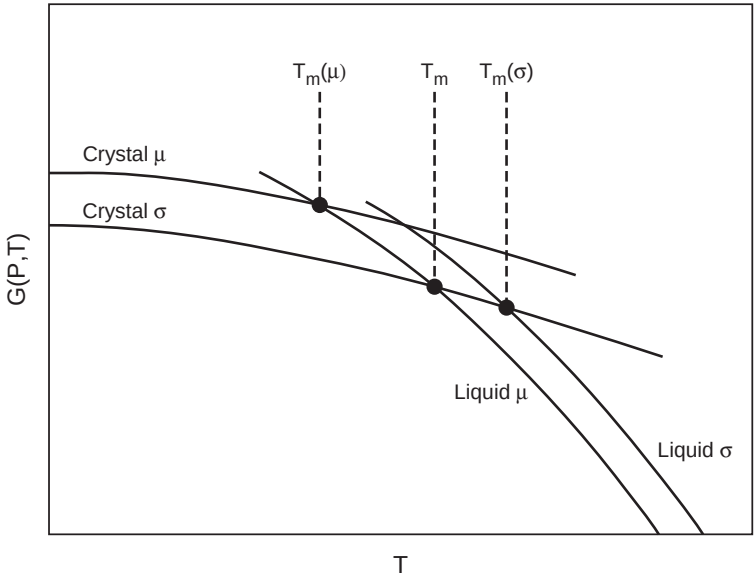


Figure 22.3. Schematic curves of the Gibbs free energy as function of temperature, at a constant pressure, illustrating melting accompanied by a change in the electronic structure, from crystal $\sigma$ to liquid $\mu$ at $T_m$.

### *Anomalous Melting Process*

Figure 22.3 shows schematic curves of the Gibbs free energy as functions of temperature, all curves for the same fixed pressure. Curves are drawn for crystal and liquid phases with electronic groundstate $\sigma$, for example a covalent semiconductor, and with electronic groundstate $\mu$, for example a metal. The stable crystal is $\sigma$, but the stable liquid is $\mu$. If only state $\sigma$ were present, normal melting would occur at temperature $T_m(\sigma)$, and likewise, if only state $\mu$ exists, normal melting would occur at temperature $T_m(\mu)$. The actual melting process is anomalous, and the actual melting temperature is $T_m$, where $T_m(\mu) < T_m < T_m(\sigma)$.

Let us enquire about the liquid pair correlation entropy $S_2$ of the anomalous element at the actual melting temperature $T_m$. Recall from Sec. 21 that $S_2$ for the normal liquids is around $-2.6$ at melt, and decreases in magnitude as temperature increases. Referring to Fig. 22.3, one can assume the pair correlation entropy is normal for liquid $\mu$ at $T_m(\mu)$, and that it decreases in magnitude along the liquid branch from $T_m(\mu)$ to $T_m$, so that the value at $T_m$ is of smaller magnitude than normal. This is why the pair

correlation entropy of an anomalous liquid at melt is smaller in magnitude than the normal value at melt. This also makes it clear, by example, that $T_m$ does not serve as a scaling temperature for the anomalous elements, as it does for the normal ones.

From the above observation, there must be a correlation between the constant-volume entropy of fusion, and the pair correlation entropy at melt. As shown in Fig. 22.4, this correlation is striking indeed.

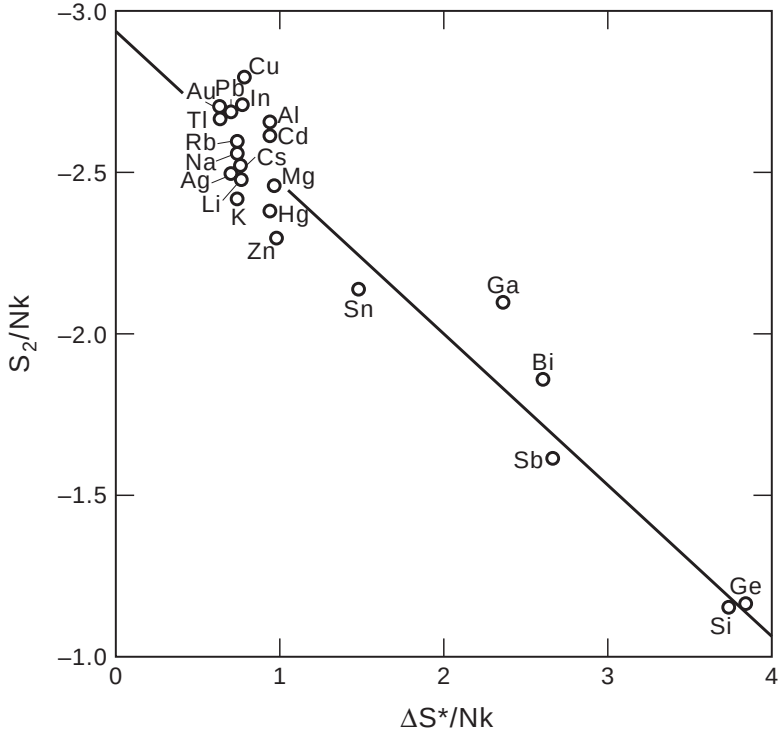


Figure 22.4. The correlation between $S_2$ in the liquid at $T \approx T_m$, and $\Delta S^*$. The points in the cluster are normal elements, for which $S_2$ and $\Delta S^*$ are nominally constants, and the six separated points are anomalous elements. The straight line is merely a guideline.

At a given pressure, the melting temperature is determined theoretically by the condition that the Gibbs free energies are equal for crystal and liquid phases. We used this condition to express $\Delta S^*$ for anomalous melting in terms of the universal $\Delta S^*$ for normal melting, and the main terms are (see

problem 26.6)

$$\frac{\Delta S^*}{Nk}(\text{anomalous}) \approx 0.80 + \frac{\Phi_0^c(\mu) - \Phi_0^c(\sigma)}{NkT_m} \quad . \tag{22.12}$$

For Si and Ge, $\Delta\Phi_0^c = \Phi_0^c(\mu) - \Phi_0^c(\sigma)$ was taken as the difference in crystal groundstate energies between the metallic $\beta$-Sn and the covalent diamond, at the density of the liquid at melt, from the graphs of Yin and Cohen (1982), and of Needs and Martin (1984). We found (Wallace 1991c):

| | Si | Ge |
|---|---|---|
| $\Delta\Phi_0^c/NkT_m$ | 2.9 | 3.3 |
| $\Delta S^*/Nk$ (Eq. (22.12)) | 3.7 | 4.1 |
| $\Delta S^*/Nk$ (experiment) | 3.76 | 3.85 |

It appears we are on the right track. One difficulty is that the $\beta$-Sn electronic structure might not be quite the right reference metal for the liquid state.

*Problems*

*22.1* Derive Eq. (22.2).

*22.2* Draw a curve of the mean interatomic distance from $T = 0$ to $T_m$ (a straight line will do). Make the increase compatible with experimental expansion data (problem 19.1). Thinking of the atoms as hard spheres in classical motion, reproduce Sutherland's argument that the atomic diameter must decrease with temperature, for melting to occur at $T_m$. How much does the atomic diameter decrease? Would the result be noticeably different if the thermal expansion were zero? How does quantum mechanics alter the picture? In view of this result, would you ever use a hard sphere model to represent the atomic dynamics of a solid or liquid?

## 23 LIQUID DYNAMICS THEORY

### *Interpretation of Specific Heat Data*

Let us work in the rigid ion description, and denote the ion motional free energy by $F_I$. At temperatures to several times $T_m$, the electronic excitation free energy reduces to $F_{el}$, the contribution from independent reference structure electrons (a discussion of electronic excitations at high temperatures can be found in Sec. 25). The total free energy is therefore

$$F = F_I + F_{el} \quad . \tag{23.1}$$

As the term is used here, liquid dynamics theory describes the motion of ions in a monatomic liquid. Over the years, we have developed a theory which is tractable in leading order, and is amenable to systematic treatment of effects beyond leading order. An important step in this development is an accurate analysis of $C_I$, the ion motional contribution to the specific heat $C_V$. Since $C_V = C_I + C_{el}$, from Eq. (23.1), we need accurate experimental data to correct $C_P$ to $C_V$, and we need an accurate evaluation of $C_{el}$. The latter requirement limits us to the rare-gas elements, where $C_{el} = 0$, and to the nearly-free-electron metals, where $C_{el}$ is obtained to sufficient accuracy from the free electron model. The analysis is currently possible for 19 elemental liquids at melt, and of these, the highly anomalous Si is omitted because of its nonscaling behavior at $T_m$ (for the Si data, see Table 1 of Wallace, 1997b). For the remaining elements, 17 nearly-free-electron metals and Ar, $C_I/Nk$ for both crystal and liquid at melt is shown in Fig. 23.1.

Figure 23.1 reveals the universal property $C_I \approx 3Nk$ for both crystal and liquid at melt. In general, $C_I = 3Nk$ is a property of $3N$ independent harmonic oscillators, and in particular, the ion motion in a crystal is resolved by lattice dynamics into $3N$ independent harmonic oscillators. We therefore assume the ion motion in an elemental liquid can also be resolved to good approximation into $3N$ independent harmonic oscillators. Consistent with this assumption, we picture the ions moving primarily within a number of nearly-harmonic many-particle valleys in the potential energy surface.

Estimated errors of the data in Fig. 23.1 are $\pm 0.05$ (except for compressed Ar, see below), hence some details of the figure are meaningful (Wallace, 1998a). For the alkali metals, $C_I$ is larger than $3Nk$, and in fact is around $3.4Nk$ for both crystal and liquid. This larger value is due to

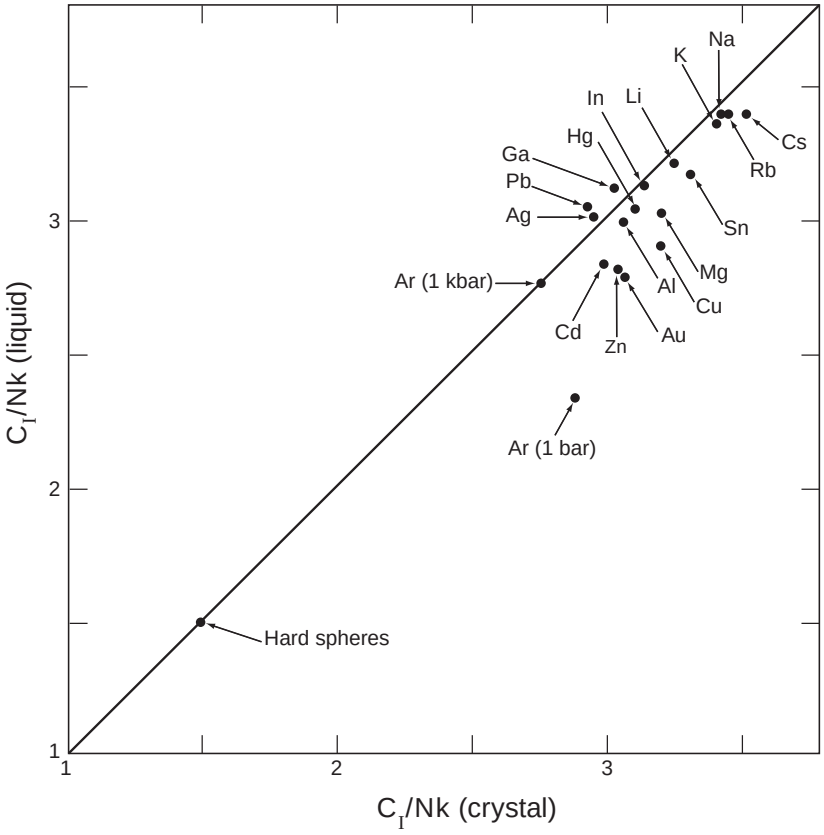


Figure 23.1. Ion motional specific heat for the liquid at melt, against the same quantity for the crystal at melt, for the elements. The line represents equality of liquid and crystal values.

anharmonicity in the crystal, and we believe it is due to the same kind of anharmonicity in the liquid as well. For Ar at 1bar, the crystal is nearly harmonic, but $C_I$ for the liquid is quite low, reflecting the fact that the liquid is rather gas like. Experimental data for $C_V/Nk$ at 1 kbar, with estimated errors of $\pm 0.1$, shows Ar behavior comparable to the liquid metals. Finally, $C_I$ for hard spheres demonstrates that this system does not provide a realistic model for the motion of ions in any real crystal or liquid.

For monatomic liquids, the general behavior of $C_I$ is to decrease as temperature increases at constant volume, and to decrease as volume increases at constant temperature. In either process, the system moves toward the

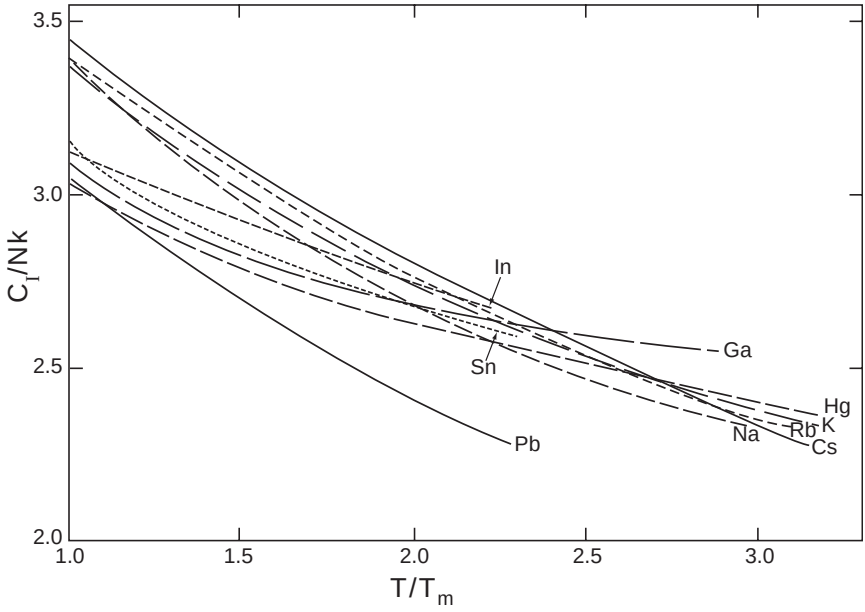


Figure 23.2. Ion motional specific heat for elemental liquids at high temperatures.

gas phase, and the ideal gas value is $C_I = \frac{3}{2}Nk$. Graphs of $C_I/Nk$ *vs* $T/T_m$ at 1 bar, for all elemental liquids for which this information can be determined, are shown in Fig. 23.2. The decrease of $C_I$ with $T$ is due both to the increase of temperature *and* to the increase of volume, the latter resulting from thermal expansion. $C_I \approx 3Nk$ is a crucial identifying property of the monatomic liquid state. Our estimate is that motion of ions among nearly harmonic valleys is an acceptable starting point for liquid dynamics theory as long as $C_I \gtrsim 2.2Nk$. We estimate this condition to hold for $T$ up to $5T_m$ at a given density. Hence our liquid dynamics theory is generally applicable to temperatures around $5T_m$. The curve of $C_I$ *vs* $T/T_m$ for Hg at a constant density is shown in Fig. 3 of Wallace (1998a).

### *Random, Symmetric, and Crystalline Valleys*

Our interpretation of the specific heat data, together with a few general arguments, leads us to a rather detailed description of the monatomic liquid,

as follows.

(a) The potential energy surface underlying the motion of the ions is composed of a large number of intersecting nearly-harmonic many-particle valleys.

(b) The large entropy of the liquid compared to the crystal is accounted for by the large number of valleys accessible to the liquid, compared to one accessible valley for the crystal.

(c) To account for the prevalent diffusive motion in the liquid, the system moves at a high rate among the valleys.

(d) Since the extensive intervalley motion does not significantly alter $C_I$ from its harmonic value, distortion of valley surfaces from harmonic at the valley intersections is small, or what is equivalent, the system spends only a small part of its time in the (necessarily anharmonic) motion between valleys.

It is important to recognize, in perspective, that the great majority of configuration space is inaccessible to the liquid state. This is evident from the pair correlation function, which shows that the ions remain rather uniformly distributed in space, and that they *never* approach one another closer than around 75% of the mean nearest neighbor distance (see Fig. 21.1). Hence above the network of intersecting valleys occupied by the liquid, potential energy peaks rise to great heights, and eventually narrow to the short-range two-ion repulsions responsible for collisions in the gas phase.

We can make a threefold classification of the potential energy valleys, based on their symmetry properties, which turns out to be essential in achieving a tractable liquid dynamics formulation. The valleys are labeled by the index $\gamma = 1, \cdots, w^N$, where $w$ is to be found. The stable equilibrium configuration at the bottom of a valley is called a *structure*. The system potential at structure $\gamma$ is $\Phi_0(\gamma)$, and the $3N$ normal modes of vibration about the structure $\gamma$ have frequencies given by the set $\{\omega_\lambda(\gamma)\}$, $\lambda = 1, \cdots, 3N$. For most elemental systems, at any density in the condensed phase, there are crystalline structures having long range order. One of the crystal structures normally has the lowest potential $\Phi_0$ of all the valleys, and this is the structure which is stable at low temperatures. Above the stable crystal structure are many structures without long range order, and generally called amorphous. From computer simulations, Stillinger and Weber (1982, 1983) and Weber and Stillinger (1984) found amorphous structures having a wide range of potentials $\Phi_0(\gamma)$, and this led to the notion of a highly complex

potential surface. Upon reflection, however, one sees it is necessary to further divide amorphous structures into two classes, as follows (Wallace, 1997b).

(a) There are structures having a remnant of crystal symmetry, at least among nearest neighbors, which we call *symmetric* structures. This class includes microcrystalline structures, apparent in displays of the early computer simulations, and also the amorphous carbon made experimentally by ion implantation (McKenzie, Muller, and Pailthorpe, 1991), where tetrahedral coordination is largely present but strongly distorted. Symmetric structures, though large in number, are still *relatively* few, because of the symmetry restriction. Further, the structural potential $\Phi_0(\gamma)$, and the set $\{\omega_\lambda(\gamma)\}$ of normal mode frequencies, are sensitive to near-neighbor symmetry, so these quantities have significant variations over the class of symmetric structures.

(b) There are structures with a wide distribution of nearest-neighbor arrangements, exemplified by the random close-packed hard-sphere model reviewed by Finney (1985). We call these *random* structures, and the random character leads to two important properties in the thermodynamic limit. First, because they suffer no symmetry restriction, they constitute the overwhelming majority of all structures, and hence dominate the statistical mechanics of the liquid state. Second, since the random structures have no order parameter, *i.e.* there is no macroscopic property to distinguish one of them from another, then the macroscopic structural properties are all the same in the thermodynamic limit. It follows that $\Phi_0(\gamma)$ and $\{\omega_\lambda(\gamma)\}$ are independent of $\gamma$ for random structures in the limit $N \to \infty$.

That the potential energy surface is indeed composed of valleys having the characteristics listed above has been verified by computer simulations, as we shall see in Sec. 24.

### *Ion Motion Hamiltonian*

Let us imagine the potential energy surface accessible to the liquid as composed entirely of intersecting many-particle valleys. A ridge is formed at the intersection of neighboring valleys, and a line along the ridge top constitutes the intervalley boundary. Configurations lying within valley $\gamma$ are said to be "in $\gamma$". The position of ion $K$ is $\mathbf{r}_K$, and the position of ion $K$ at the structure of valley $\gamma$ is $\mathbf{R}_K(\gamma)$. When the system is in $\gamma$, the

displacement of ion $K$ from equilibrium is $\mathbf{U}_K(\gamma)$, so that

$$\mathbf{r}_K = \mathbf{R}_K(\gamma) + \mathbf{U}_K(\gamma) \quad . \tag{23.2}$$

Again when the system is in $\gamma$, the adiabatic potential $\Phi(\{\mathbf{r}_K\})$ can be formally expanded in powers of the displacements,

$$\Phi(\gamma) = \Phi_0(\gamma) + \Phi_2(\gamma) + \Phi_{anh}(\gamma) \quad . \tag{23.3}$$

Here $\Phi_0(\gamma)$ is the structure potential,

$$\Phi_0(\gamma) = \Phi(\{\mathbf{R}_K(\gamma)\}) \quad . \tag{23.4}$$

Terms of second order in displacements are given by $\Phi_2(\gamma)$,

$$\Phi_2(\gamma) = \frac{1}{2} \sum_{\beta\beta'} \Phi_{\beta\beta'}(\gamma) U_\beta(\gamma) U_{\beta'}(\gamma) \quad , \tag{23.5}$$

where $\beta$ stands for the index pair $Ki$, $\beta = 1, \cdots, 3N$, and where the coefficients $\Phi_{\beta\beta'}(\gamma)$ are second derivatives of $\Phi(\{r_\beta\})$, evaluated at the structure $\gamma$. The rest of the system potential is contained in the anharmonic contribution $\Phi_{anh}(\gamma)$.

In leading approximation, $\Phi_{anh}$ is negligible, and motion of the ions in valley $\gamma$ is governed by a quasiharmonic Hamiltonian with potential $\Phi_2(\gamma)$. But restricting the motion to a finite valley presents a complicated boundary condition, and we can remove this condition by first extending $\Phi_2(\gamma)$ to infinity, and by then subtracting off the extension. For this purpose, we define the *phonon* potential $\Phi_{ph}(\gamma)$,

$$\Phi_{ph}(\gamma) = \frac{1}{2} \sum_{\beta\beta'} \Phi_{\beta\beta'}(\gamma) U_\beta U_{\beta'} \quad , \quad -\infty < U_\beta < \infty \quad . \tag{23.6}$$

The Hamiltonian for motion of ions in the extended harmonic valley is

$$\mathcal{H}_\gamma = \Phi_0(\gamma) + \mathcal{H}_{ph}(\gamma) \quad , \tag{23.7}$$

where

$$\mathcal{H}_{ph}(\gamma) = \sum_\beta \frac{p_\beta^2}{2M} + \Phi_{ph}(\gamma) \quad . \tag{23.8}$$

Notice $\mathcal{H}_\gamma$ applies to every potential energy valley, the crystalline, symmetric, and random alike, and the quasiharmonic lattice dynamics Hamiltonian is a particular one among the set of $\mathcal{H}_\gamma$.

The ion motion Hamiltonian will be $\Sigma_\gamma \mathcal{H}_\gamma$, plus two corrections which we now define. Let $P_\gamma$ be a set of projection operators, such that $P_\gamma = 1$ in $\gamma$, $P_\gamma = 0$ outside $\gamma$, and $\Sigma_\gamma P_\gamma = 1$. The potential $\Phi_{ph}(\gamma)$ which lies in $\gamma'$ is $\Phi_{ph}(\gamma)P_{\gamma'}$. Operators $\mathcal{H}_{\gamma\gamma'}$ are defined by

$$\begin{aligned} \mathcal{H}_{\gamma\gamma'} &= -\Phi_{ph}(\gamma)P_{\gamma'} \quad , \quad \gamma \neq \gamma' \quad ; \\ \mathcal{H}_{\gamma\gamma} &= 0 \quad . \end{aligned} \tag{23.9}$$

Subtraction of the harmonic potential extension for all valleys is accomplished by adding the *boundary* correction $\mathcal{H}_{bdy}$,

$$\mathcal{H}_{bdy} = \sum_{\gamma\gamma'} \mathcal{H}_{\gamma\gamma'} \quad . \tag{23.10}$$

This is called the boundary contribution because it expresses the presence of valley boundaries. The anharmonic potential for all valleys is $\mathcal{H}_{anh}$,

$$\mathcal{H}_{anh} = \sum_{\gamma} \Phi_{anh}(\gamma)P_\gamma \quad , \tag{23.11}$$

where $P_\gamma$ enforces that $\Phi_{anh}(\gamma)$ contributes only in $\gamma$. The total ion motion Hamiltonian $\mathcal{H}_I$ is

$$\mathcal{H}_I = \sum_{\gamma} \mathcal{H}_\gamma + \mathcal{H}_{anh} + \mathcal{H}_{bdy} \quad , \tag{23.12}$$

and is thus expressed in the form of a set of exactly solvable quasiharmonic phonon Hamiltonians, plus the terms $\mathcal{H}_{anh}$ and $\mathcal{H}_{bdy}$ which are supposed to represent small corrections. The complete set of solutions to $\Sigma_\gamma \mathcal{H}_\gamma$ is intended to comprise the set of solutions for each and every separate $\mathcal{H}_\gamma$.

It is useful to transform $\mathcal{H}_{ph}(\gamma)$ to normal modes, for any valley $\gamma$, and here we shall omit the index $\gamma$ for abbreviation. The elements $\Phi_{\beta\beta'}$ form a real symmetric matrix, which is diagonalized by a real orthogonal transformation whose matrix elements are $V_{\beta\lambda}$, with $\beta, \lambda = 1, \cdots, 3N$. The diagonalization equation is

$$\sum_{\beta} \tilde{V}_{\lambda\beta} \Phi_{\beta\beta'} V_{\beta'\lambda'} = M\omega_\lambda^2 \delta_{\lambda\lambda'} \quad , \tag{23.13}$$

showing that the eigenvalues are $M\omega_\lambda^2$, where $\omega_\lambda$ is the frequency of normal mode $\lambda$. Orthonormalization and completeness of the eigenvectors is

expressed in the equations

$$\sum_{\beta} \tilde{V}_{\lambda\beta} V_{\beta\lambda'} = \delta_{\lambda\lambda'} \quad , \quad \text{orthonormalization} \quad , \tag{23.14}$$

$$\sum_{\lambda} V_{\beta\lambda} \tilde{V}_{\lambda\beta'} = \delta_{\beta\beta'} \quad , \quad \text{completeness} \quad , \tag{23.15}$$

where $\tilde{V}_{\lambda\beta} = V_{\beta\lambda}$. The normal coordinates $q_\lambda$, and momenta $p_\lambda$, are defined by the transformation

$$U_\beta = \sum_{\lambda} V_{\beta\lambda} q_\lambda \quad , \tag{23.16}$$

$$p_\beta = M\dot{U}_\beta = \sum_{\lambda} V_{\beta\lambda} p_\lambda \quad , \tag{23.17}$$

and the transformed phonon Hamiltonian is

$$\mathcal{H}_{ph} = \sum_{\lambda} \left[ \frac{p_\lambda^2}{2M} + \frac{1}{2} M \omega_\lambda^2 q_\lambda^2 \right] \quad . \tag{23.18}$$

Hence $\mathcal{H}_{ph}$ is a sum of independent harmonic oscillators. Just as with the crystal phonons in Sec. 16, a further transformation yields

$$\mathcal{H}_{ph} = \sum_{\lambda} \hbar\omega_\lambda \left( A_\lambda^+ A_\lambda + \frac{1}{2} \right) \quad , \tag{23.19}$$

where $A_\lambda^+$ and $A_\lambda$ are respectively the phonon creation and annihilation operators (see problem 23.1).

### *Liquid Free Energy*

The canonical partition function for the ion motion is

$$Z_I = Tre^{-\beta\mathcal{H}_I} \quad . \tag{23.20}$$

We consider only the random valleys, since the relative error in omitting crystal and symmetric valleys vanishes as $N \to \infty$. The macroscopic uniformity of random valleys provides us with the great simplification

$$\left.\begin{array}{c} \Phi_0(\gamma) = \Phi_0^l \\ \{\omega_\lambda(\gamma)\} = \{\omega_\lambda\}^l \end{array}\right\} \text{for all random } \gamma \quad , \tag{23.21}$$

where the superscript $l$ refers to the liquid state. The partition function for a single extended harmonic random valley is $Z_1$,

$$Z_1 = Tr \exp\left[-\beta(\Phi_0^l + \mathcal{H}_{ph})\right] \quad . \tag{23.22}$$

The partition function for $w^N$ extended harmonic random valleys is $w^N Z_1$. The total anharmonic and boundary contributions are formally included in a factor $Z_{ab}$, defined by

$$Z_I = w^N Z_1 Z_{ab} \quad . \tag{23.23}$$

The total ion motion free energy is therefore (see *e.g.* Eq. (16.14))

$$F_I = \Phi_0^l - NkT \ln w + \sum_\lambda \left[\frac{1}{2}\hbar\omega_\lambda + kT \ln\left(1 - e^{-\beta\hbar\omega_\lambda}\right)\right] + F_{ab} \quad . \tag{23.24}$$

Here the set of phonon frequencies is that for a random valley. Because this equation is by definition exact, then $F_{ab}$ is the exact contribution from anharmonic and boundary effects, and is not limited to a perturbation expansion.

For most elemental liquids at $T \geq T_m$, the ion motion is quite accurately classical, hence it is useful to write the corresponding classical expressions for the thermodynamic functions. Let us define the liquid characteristic temperatures $\theta_n^l$, as moments of the phonon distribution for a random valley, just as the crystal characteristic temperatures are defined in Sec. 15. In particular,

$$\ln k\theta_0^l = \langle \ln \hbar\omega \rangle_R \quad , \tag{23.25}$$

where $\langle \cdots \rangle_R$ is an average over the random valley phonons. Then from Eq. (23.1), the liquid free energy for classical ion motion is $F_I^{cl} + F_{el}$, or

$$F = \Phi_0^l - NkT \ln w - 3NkT \ln(T/\theta_0^l) + F_{ab} + F_{el} \quad . \tag{23.26}$$

The corresponding internal energy $U$, and entropy $S$, are

$$U = \Phi_0^l + 3NkT + U_{ab} + U_{el} \quad , \tag{23.27}$$

$$S = Nk \ln w + 3Nk\left[\ln(T/\theta_0^l) + 1\right] + S_{ab} + S_{el} \quad . \tag{23.28}$$

The next step is to relate the number of random valleys in the liquid potential energy surface to the entropy of melting at constant volume. Superscripts $l$ and $c$ will refer to liquid and crystal respectively. The crystal entropy for classical ion motion is

$$S^c = 3Nk\,[\ln(T/\theta_0^c) + 1] + S_{anh}^c + S_{el}^c \quad . \tag{23.29}$$

Compared to $S^l$ in Eq. (23.28), the valley multiplicity $Nk \ln w$ is missing because the crystal moves in a single valley, and the crystal has an anharmonic contribution but no boundary contribution. The entropy of melting at constant volume is $\Delta S^* = S^l - S^c$, or

$$\Delta S^* = Nk \ln w + 3Nk \ln(\theta_0^c/\theta_0^l) + S_{ab}^l - S_{anh}^c + S_{el}^l - S_{el}^c \quad , \tag{23.30}$$

where all quantities are evaluated at the same volume. Now for normal melting elements, the experimental $\Delta S^*$ is approximately a universal constant, and specifically from Eq. (22.3),

$$\Delta S^* = 0.80Nk + \text{ small scatter} \quad . \tag{23.31}$$

The only quantity on the right of (23.30) which might reasonably be a universal constant is $w$, so we set

$$\ln w = 0.80 \quad . \tag{23.32}$$

Concerning the remaining terms on the right of (23.30), the anharmonic and boundary contributions are small at melt, and for normal melting elements, where crystal and liquid have qualitatively the same electronic structure, we expect $S_{el}^l \approx S_{el}^c$, and we further expect that the interionic forces are approximately the same, so that $\theta_0^c/\theta_0^l \approx 1$. These arguments, together with the above calibration of $\ln w$, reduce the theoretical Eq. (23.30) for $\Delta S^*$ to the experimental result in (23.31). In the process, we have found the number of random valleys in the potential energy landscape.

It is important to notice that the liquid dynamics theory developed here applies to all monatomic liquids, and is in no way restricted by the melting process. The same equations for liquid thermodynamic functions, with the same universal number of random valleys, are valid for normal and anomalous elements alike. But the melting *process* is not universal, and along with the change of electronic structure which accompanies anomalous melting, we expect significant changes in the phonon characteristic temperature $\theta_0$,

Table 23.1. Data for the high temperature entropy analysis. $\theta_0^c$ is for the crystal at density $\rho_{lm}$, and $S_{el}$ is the free electron model for the liquid at melt.

| Element | $\theta_0^c(K)$ | $S_{el}/Nk$ |
|---|---|---|
| Na | 102.2 | 0.053 |
| K | 61.9 | 0.080 |
| Rb | 37.7 | 0.089 |
| Hg | 56.4 | 0.029 |
| In | 74.4 | 0.065 |
| Pb | 52.1 | 0.089 |

and in the electronic entropy $S_{el}$. Hence from Eq. (23.30), the major contributions to the anomalous entropy of melting at constant volume are

$$\Delta S^* \ (anomalous) \ \approx 0.80Nk + 3Nk\ln(\theta_0^c/\theta_0^l) + S_{el}^l - S_{el}^c \quad . \qquad (23.33)$$

***Theory and Experiment for the Entropy***

We wish to compare theory and experiment for thermodynamic properties of monatomic liquids at elevated temperatures. The thermodynamic functions, all being derived from the free energy, contain only one independent function of temperature. We shall analyze the entropy, and will include only elements in both of the following categories.

(a) Normal melting elements, so we can approximate $\theta_0^l$ by $\theta_0^c$. Values of $\theta_0^c$ at the density of the liquid at melt are listed in Table 23.1.

(b) Elements for which data exist to find entropy at constant volume up to temperatures sufficiently high to reveal a meaningful temperature dependence, say up to $T \gtrsim 2T_m$.

The sum total of elements satisfying these conditions is six nearly-free-electron metals. For these, the free electron model is sufficiently accurate, and values of $S_{el}$ for the liquid at melt are listed in Table 23.1. The need for the entropy volume correction is as follows. We take accurate experimental values of $\theta_0^c$ at the density $\rho_{meas}$ from Table 15.1, and correct these to the density $\rho_{lm}$ by means of Eq. (19.15), where the Grüneisen parameter $\gamma^*$ is from Table 19.1. Now the liquid at melt is quite expanded from $\rho_{meas}$, and values of $\theta_0^c(\rho_{lm})/\theta_0^c(\rho_{meas})$ are in the range 0.81 – 0.90, which is as far as we can safely apply the formula (19.15). But the liquid continues to expand as $T$ increases above $T_m$, and since we cannot estimate $\theta_0^c$ at these lower densities, we correct the measured entropy back to the density $\rho_{lm}$.

If $\rho_a$ is the density at atmospheric pressure, the entropy at density $\rho_{lm}$ is obtained from

$$S(\rho_{lm}) = S(\rho_a) - \left(\frac{\rho_{lm}}{\rho_a} - 1\right) V\alpha B_T \quad . \tag{23.34}$$

From Eq. (23.28), when $\theta_0^l$ is replaced by $\theta_0^c$, and $S_{ab}$ is neglected, we have the leading theoretical approximation, denoted $S_{theory}$, for the liquid entropy for normal melting elements,

$$S_{theory} = Nk \ln w + 3Nk[\ln(T/\theta_0^c) + 1] + S_{el} \quad . \tag{23.35}$$

This equation has no adjustable parameters. The comparison with experiment is shown in Fig. 23.3 for mercury at temperatures to $3.2T_m$, and is quite striking. Figure 23.4 shows the difference $S_{expt} - S_{theory}$ for all the high temperature entropy data we are currently able to analyze. The error in $S_{theory}$, due to the volume correction of $\theta_0^c$ and use of the free electron model, is likely to be around $\pm 0.1Nk$. Combined errors in the experimental entropy and its volume correction range from around $0.02Nk$ at $T_m$, to around $0.1Nk$ at $3T_m$. Hence the values of $S_{expt} - S_{theory}$ in Fig. 23.4 are hardly beyond expected errors of the analysis. Our conclusion, for temperatures to $3T_m$, is that $S_{theory}$ has an error not larger than $\pm 0.2Nk$, which is at most 2% of the total entropy.

The next challenge is to work out the theory for anharmonic and boundary corrections to the entropy. As a step in this direction, we have suggested that the observed decrease of $C_I$ with temperature for Hg, shown in Fig. 23.2, is due mainly to the boundary effect, and have made a simple model which reproduces the experimental trend (Wallace, 1998a).

### *Nature of the Transit Process*

In Sec. 6, we invoked the image of a many-atom system moving classically in a box with uniform and time-invariant boundary conditions. Though the system may be in macroscopic equilibrium, it constantly undergoes microscopic fluctuations, and with each drift away from mechanical equilibrium of a small group of atoms, a restoring force develops to drive the group back toward equilibrium. These are the same restoring forces which operate to drive the system irreversibly toward equilibrium, if it is started out in a macroscopically nonequilibrium state. The same description applies to a system in gas, liquid, or solid phase, and to quantum as well as classical

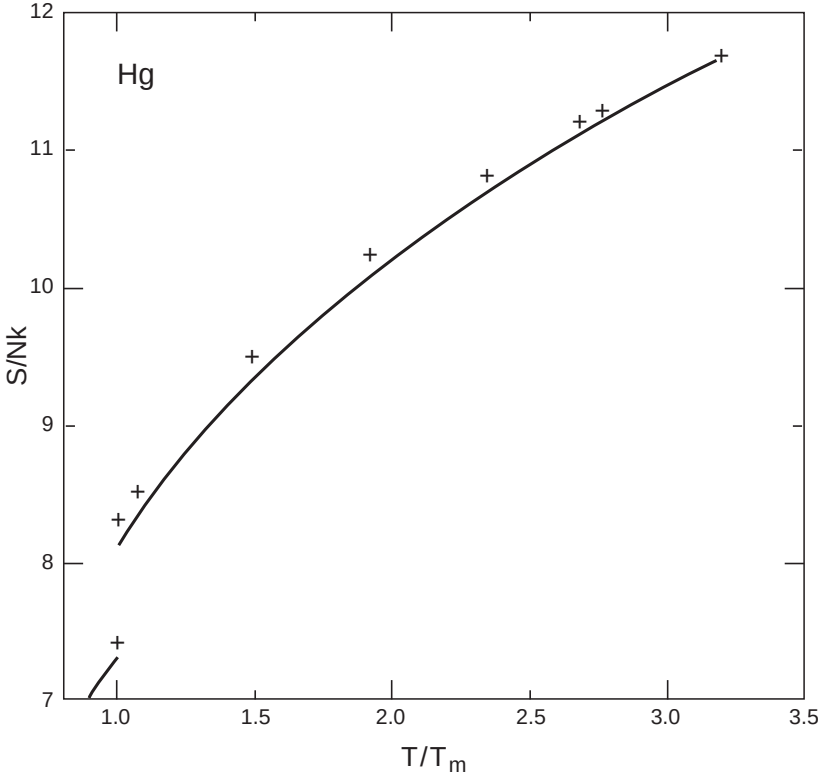


Figure 23.3. Theory for the entropy of crystal and liquid mercury (solid line), compared with experimental entropy (crosses), at the fixed volume of the liquid at melt.

motion. The important point is, for any normal many-atom system, which means to exclude macroscopically correlated states such as superfluids, the irreversible driving force is local. This property has a significant implication for liquid dynamics theory, as follows.

When the liquid system moves across a boundary, from one many-particle valley to another, we call the motion a *transit*. Transits are responsible for self diffusion in liquids, hence transits occur in the microscopic fluctuations of the equilibrium liquid state. Because the irreversible driving forces are local, the equilibrium fluctuations are local, and transits must also be local. That is, when the $N$-atom system transits from the valley whose structure is $\{\mathbf{R}_K(\gamma)\}$ to the valley whose structure is $\{\mathbf{R}_K(\gamma')\}$,

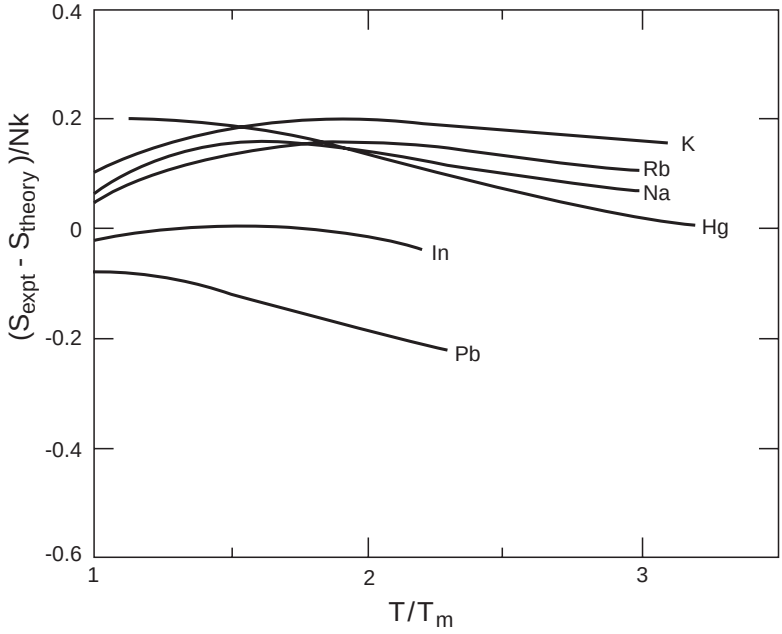


Figure 23.4. Difference between experimental and theoretical entropies for elemental liquids at high temperatures, at the fixed volume of the liquid at melt.

the equilibrium positions $\mathbf{R}_K$ change for only a *small local group* of atoms, a group of say five or ten atoms. Hence local transits are going on at a high rate, throughout the volume of an equilibrium liquid. And in keeping with our four-point description of the monatomic liquid state, specifically point $(d)$, early in the present section, transits are supposed to be nearly instantaneous.

As a matter of principle, the Hamiltonian term $\mathcal{H}_{\gamma\gamma'}$, defined in Eq. (23.9), induces transits from valley $\gamma'$ to $\gamma$, and the transit rate can be calculated from the golden rule. This means there is a connection between the mean transit rate and self diffusion on the one hand, and the boundary contribution to specific heat on the other, since both are determined by the set of operators $\mathcal{H}_{\gamma\gamma'}$. From a simple "independent atom" model for self diffusion in a monatomic liquid, we have estimated that each atom transits approximately once in a mean vibrational period (Wallace, 1998b). Further discussion of these points may be found in Chisolm and Wallace (2001).

*Problem*

*23.1* Use the standard communtators among particle positions and momenta, and the transformation (23.16) and (23.17), to show $[q_\lambda, q_{\lambda'}] = [p_\lambda, p_{\lambda'}] = 0$ and $[q_\lambda, p_{\lambda'}] = i\hbar\delta_{\lambda\lambda'}$. Define the transformation to operators $A_\lambda$ and $A_\lambda^+$, such that $[A_\lambda, A_{\lambda'}] = [A_\lambda^+, A_{\lambda'}^+] = 0$ and $[A_\lambda, A_{\lambda'}^+] = \delta_{\lambda\lambda'}$. Then derive the second quantized form (23.19) for $\mathcal{H}_{ph}$.

## 24 VERIFICATION FROM COMPUTER SIMULATIONS

### *Molecular Dynamics Equilibrium States*

The liquid dynamics theory of Sec. 23 is based on a detailed picture, suggested by experimental thermodynamic data, of the many-particle potential surface, and the motion of ions on that surface. A complete verification of this picture has been achieved for the example of pseudopotential sodium, by means of extensive computer simulations (Wallace and Clements, 1999; Clements and Wallace, 1999). A similar verification, but less complete, was also achieved for Lennard-Jones argon. Our central procedure was to start with a molecular dynamics system in equilibrium in a liquid state, to choose configurations at random times, and for each configuration to move the system part way down the potential surface by a series of quenches, and then to resume the molecular dynamics run and let the system come to equilibrium again. We studied these equilibrium states, called simply "states," and by further quenching to very low temperatures we were able to study the individual valleys among which the system moves in a given state. Each of the valleys we found was unambiguously distinguished as crystalline, symmetric, or random, with properties described below for each class.

Liquid sodium at 1 bar has $T_m = 371K$, and corresponding volume $V_A = 278a_0^3$. We studied pseudopotential sodium at this volume, and we note that our model has melting properties close to those measured for real sodium. The adiabatic potential is expressed in Eq. (5.54), and since $V$ is constant, $\Omega(V)$ is constant, and we can set $\Omega = 0$, leaving for the adiabatic potential

$$\Phi = \frac{1}{2}{\sum_{KL}}' \phi(|\mathbf{r}_K - \mathbf{r}_L|) \quad . \tag{24.1}$$

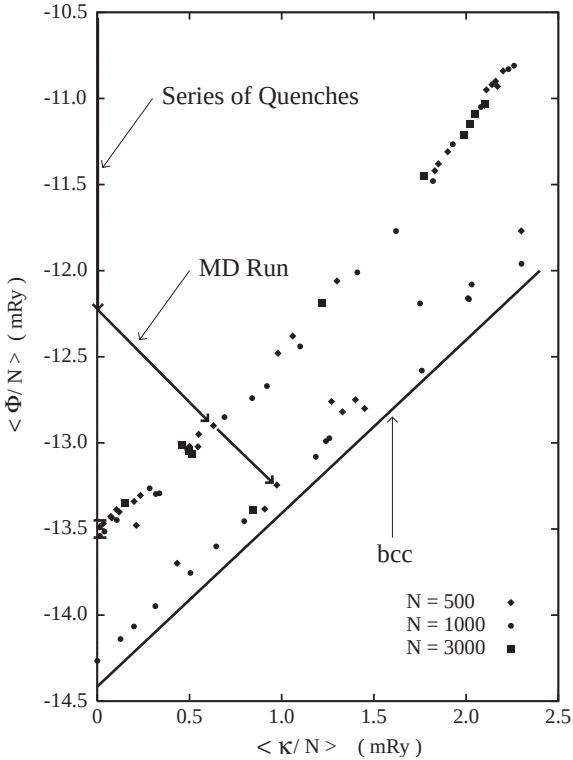


Figure 24.1. $\langle \Phi/N \rangle$ *vs* $\langle \mathcal{K}/N \rangle$ for equilibrium states, showing the states naturally fall into three groups, random, symmetric, and crystal.

For states at $T \lesssim \frac{1}{2} T_m$, the mean potential energy $\langle \Phi/N \rangle$ *vs* mean kinetic energy $\langle \mathcal{K}/N \rangle$ is shown in Fig. 24.1. The arrows show the path of a system during a series of quenches followed by a molecular dynamics run. The system always came to equilibrium in a state in the upper group. For temperatures above say 30K, after some time in the upper state, the system would spontaneously decay to a lower state and remain there, while for temperatures below 30K, the system remained in the upper state. Except

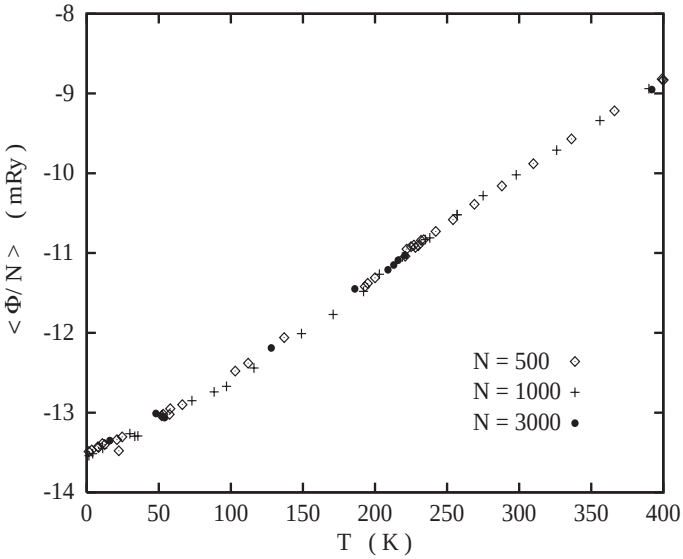


Figure 24.2. $\langle \Phi/N \rangle$ *vs* $T$ for random and liquid states, showing they lie on a single line.

once for a very small $N(N = 168)$, our system never spontaneously crystallized. Therefore the bcc states were generated separately, by warming a bcc crystal. For states in the upper group, the mean potential energy *vs* temperature is shown in Fig. 24.2. At $T \gtrsim 200$K, the upper states do not decay to lower states, and at $T \gtrsim 371$K, the upper states are genuine liquid states.

Here are some important things we learned about the valleys among which the system moves in the states shown in Figs. 24.1 and 24.2.

(a) In the upper states, the system moves entirely among random valleys, hence these states are called "random states." For $T \lesssim 30$K, the system moves within a single random valley, while for $T \gtrsim 30$K the system transits among random valleys, with the transit rate increasing as $T$ increases.

(b) In each of the lower states, the system moves within a single symmetric valley. The lower states in Fig. 24.1 occupy a number of different symmetric valleys, but the states at the lowest temperatures were obtained by cooling down within a single valley.

***Properties of the Random Valleys***

(a) The random valleys dominate the statistical mechanics of the liquid phase. We know this because quenching the equilibrium liquid always brings the system into a random valley, and also, as shown in Fig. 24.2, the branch of random states becomes the liquid states at $T \geq T_m$. Hence we infer that practically all the valleys in the potential energy landscape are random valleys.

(b) The random valleys are macroscopically uniform, in that they all have the same structure potential and the same set of phonon frequencies. In our calculations for $N = 500$ and 1000, the variation over random valleys is shown by the following mean and variance data.

$$\begin{aligned} \Phi_0 &= -13.52 \pm 0.02 mRy/atom \ , \\ \theta_2 &= 154.0 \pm 0.1K \ , \\ \theta_0 &= 98.7 \pm 0.1K \ , \\ \theta_{-2} &= 114 \pm 4K \ . \end{aligned} \tag{24.2}$$

The variance of $\theta_{-2}$ is large because $\theta_{-2}$ depends strongly on the few lowest frequencies. We expect all such variances to go to zero as $N \to \infty$. A graph of the phonon eigenvalues $M\omega_\lambda^2$ *vs* $\lambda$ for five different random valleys at $N = 500$ is shown in Fig. 24.3, where the agreement among the sets is striking indeed.

(c) The random valleys are approximately harmonic. The primary indication is that the slope of $\langle \Phi/N \rangle$ *vs* $kT$ is approximately $\frac{3}{2}$ for random states (Figs. 24.1 and 24.2). In the low temperature (nondiffusing) regime, a more accurate demonstration of purely harmonic motion is provided by the temperature dependence of the mean square displacement (Fig. 12 of Wallace and Clements, 1999), and a more complete demonstration of purely harmonic motion is provided by the time dependence of the velocity autocorrelation function (Fig. 2 of Chisolm, Clements, and Wallace, 2001).

(d) Though anharmonicity is small, it is not insignificant, and we found two manifestations of anharmonicity in the random valleys. First, the slope of $\langle \Phi/N \rangle$ *vs* $kT$ in Fig. 24.2 departs from $\frac{3}{2}$. There is a rise in the curve at 200–250K, the cause being as yet undetermined. Also, the slope is 1.8 at 371K, so the theoretical ion motion specific heat is $3.3Nk$ for the liquid at melt, in essential agreement with the experimental value of $3.4Nk$ (Fig. 23.1). Second, for low lying configurations within a random valley,

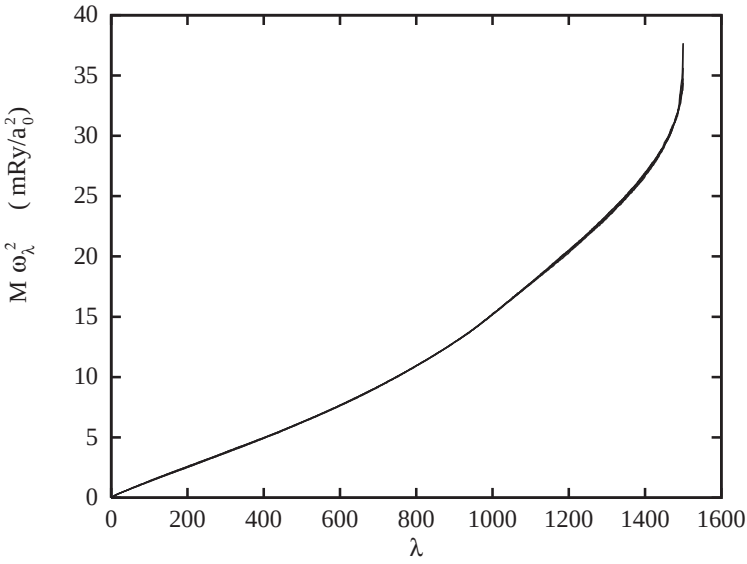


Figure 24.3. Eigenvalues $M\omega_\lambda^2$ as function of $\lambda$ for five different random valleys, showing the accurate uniformity of the set $\{\omega_\lambda\}$ for random valleys.

but not at the bottom of the valley, the potential energy curvature tensor, *i.e.* the matrix $[\Phi_{\beta\beta'}]$, possesses a small number of negative eigenvalues. This means the surface has negative curvature in a few of its $3N$ directions. We attribute this to the presence of irregular small bumps on the basic harmonic surface, a form of anharmonicity presumably arising from random near-neighbor configurations. Hence these negative eigenvalues are not associated with intervalley ridges.

(e) For the configuration at the bottom of valley $\gamma$, *i.e.* for the structure $\gamma$, the pair correlation function is denoted $G_\gamma(r)$. This function is shown in Fig. 24.4 for random valleys with different numbers of particles. The fluctuations gradually disappear as $N$ increases, and a universal $G_\gamma(r)$ emerges for random valleys. This random $G(r)$ exhibits two unique characteristics, namely very broad peaks, and a split second peak whose first subpeak is the higher. This characteristic split second peak has been observed in experimentally prepared amorphous metals.

(f) Though it is not a property of an individual random valley, but rather of the random states, the pair correlation function evolves continuously with increasing temperature, from the random $G(r)$ to the liquid $g(r)$. This

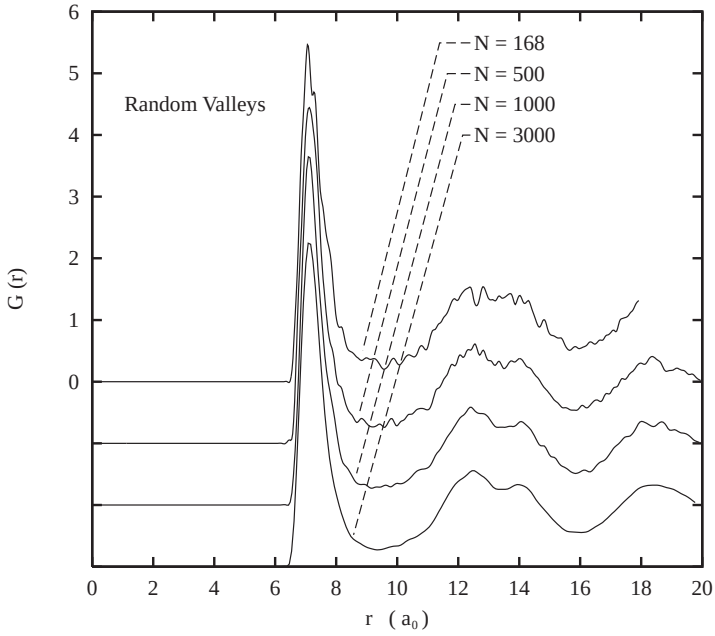


Figure 24.4. Random structural pair correlation functions $G_\gamma(r)$, showing the emergence of a universal random $G(r)$ as $N$ increases.

evolution is shown in Fig. 24.5.

### *Crystal and Symmetric Valleys*

For pseudopotential sodium at $V_A = 278a_0^3$, the bcc states are stable up to temperatures around 350K. In all such states, the system moves within a single potential energy valley. The bcc structural potential and phonon characteristic temperatures are as follows.

$$\begin{aligned} \Phi_0 &= -14.415 mRy/atom \ , \\ \theta_2 &= 151.4K \ , \\ \theta_0 &= 99.65K \ , \\ \theta_{-2} &= 121.4K \ . \end{aligned} \tag{24.3}$$

Comparison with the data for random valleys in Eq. (24.2) shows $\theta_0^l$ and $\theta_0^c$ differ by 1.0%, an accurate confirmation of the prediction of liquid dynamics theory for normal melting elements, in Sec. 23, that $\theta_0$ is approximately the

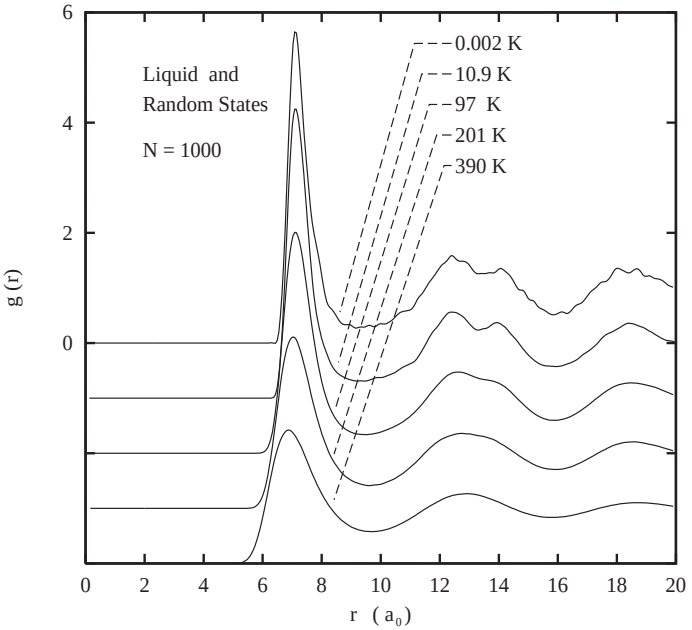


Figure 24.5. Continuous evolution of the pair correlation function for random states, from the random $G(r)$ at $T = 0$ to the liquid $g(r)$ at $390K$.

same for crystal and liquid at the same density.

The bcc valley is also nearly harmonic, and has the same small anharmonic effects as random valleys, namely that the ion motion specific heat is slightly larger than $3Nk$, and that away from the valley bottom, the potential energy curvature tensor has a few negative eigenvalues. With increasing temperature, negative eigenvalues first appear for a system at 52K in the bcc valley, far below the temperature where bcc states become unstable.

Pair correlation functions for bcc states at several temperatures are shown in Fig. 24.6. Characteristic of molecular dynamics calculations, *i.e.* of classical motion, the peaks continue to sharpen as temperature is lowered, so that the structural pair correlation function $G_{bcc}(r)$ is in principle a set of $\delta$-functions. On the other hand, with increasing temperature, the peaks broaden because of the increasing ion vibrational amplitude. It is interesting that the bcc vibrational broadening at 143K, Fig. 24.6, is about the same as the random-valley structural broadening at $T = 0$, Fig. 24.4.

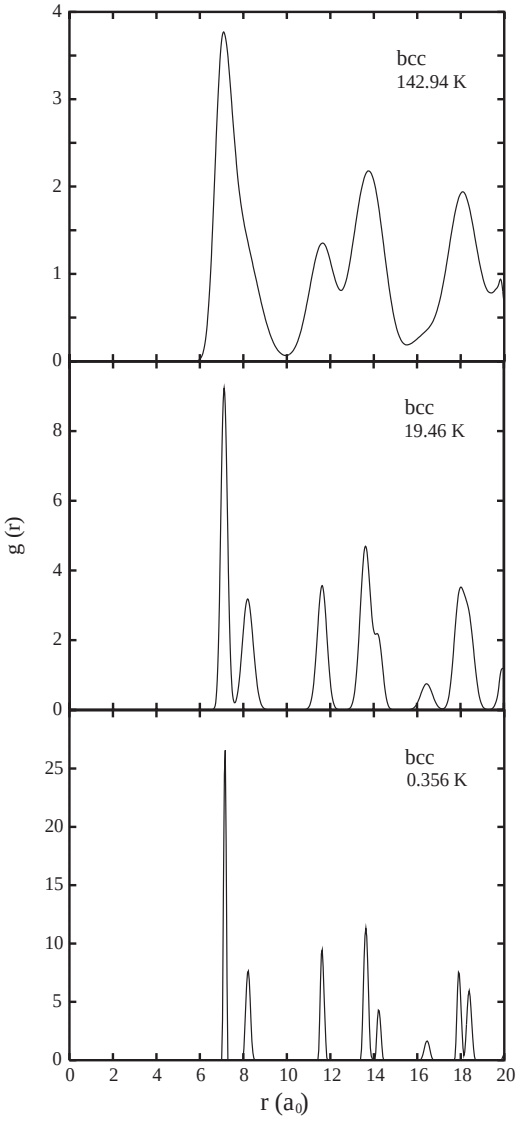


Figure 24.6. Bcc pair correlation functions, showing thermal broadening with increasing temperature. Notice in the split second peak at $143K$, the first subpeak is the lower.

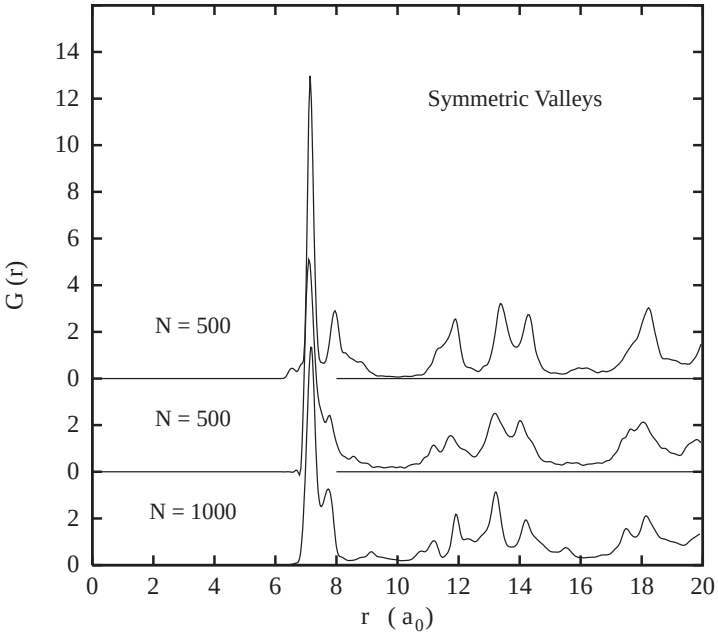


Figure 24.7. $G_\gamma(r)$ for three different symmetric valleys, showing nonuniversal ordering among symmetric structures.

Our investigation of symmetric valleys is not exhaustive, but the following properties are established for pseudopotential sodium. First, the symmetric valleys are stable, since they have $\omega_\lambda^2 > 0$ at the structure, for all $\lambda$ except the three zero-frequency translational modes. Second, different symmetric valleys exhibit nominal differences in their values of $\Phi_0$ and $\theta_n$, for $n = -2, 0, 2$. These differences are in sharp contrast to the accurate macroscopic uniformity of the random valleys. Third, symmetric valleys are also nearly harmonic, with anharmonicity contributing qualitatively the same small effects as in random valleys. And finally, the $G_\gamma(r)$ for symmetric valleys exhibit their own identifying characteristics, as shown for three different valleys in Fig. 24.7. The symmetric $G_\gamma(r)$ remain broadened compared to the $\delta$-functions of a crystal, but they have more and narrower peaks than the random $G(r)$.

An extensive study of the configurational order of various structures was carried out by Clements and Wallace (1999). The observation made there, also apparent from the figures shown here, is that one can say from

the graph of $G_\gamma(r)$ whether the structure is random, symmetric, or crystal. One can also say from the distribution of Voronoi coordination numbers, or from the distribution of angles between Voronoi neighbors, whether a structure is random, symmetric, or crystal.

### *Observation of Single Transits*

The most complete way to study the motion of a molecular dynamics system is to watch the particle coordinates as functions of time. We did this, *i.e.* the computer did this, for every particle in 500-particle systems, moving in equilibrium in a random state, at a temperature sufficiently low that a transit occurs only once in say $10^5$ timesteps (Wallace, Chisohm, and Clements, 2001). Here is what we saw. The graph of each coordinate of each particle is a fluctuating signal with constant mean for some period of time, then a shift appears in the mean coordinates of several particles, then the graph of each coordinate of each particle continues as a fluctuating signal with constant mean. Representative graphs of transiting particles are shown in Figs. 24.8 and 24.9. These figures constitute an unambiguous observation that the system moves for a time within a single potential valley, then transits to a new valley, then continues to move within the new valley. Our results are further characterized as follows. First, throughout each equilibrium run, those with transits and those without, the mean potential and kinetic energies showed no perceptible change, hence every transit observed is between two random valleys. Second, the mean coordinates of every particle were constant throughout each equilibrium run, except for transits. In other words, no motion other than vibrations and transits occurred.

Transits were observed in Lennard-Jones argon at 17.1K, and in pseudopotential sodium at 30.0K. The transiting groups consisted of 2–11 particles in loosely packed clusters, with the equilibrium positions shifting in various directions in a given transit. The magnitude of the particle equilibrium shift was around $0.4R_1$ in argon, and $0.25R_1$ in sodium, where $R_1$ is the mean nearest neighbor distance. The mean transit duration for the entire transiting group was around one mean vibrational period $\tau$, where $\tau = 2\pi/\omega$, and $\omega$ is the rms phonon frequency for a random valley. However, for most of the transiting particles the transit was effectively instantaneous, since there was usually some overlap of position fluctuations in the initial and final valleys.

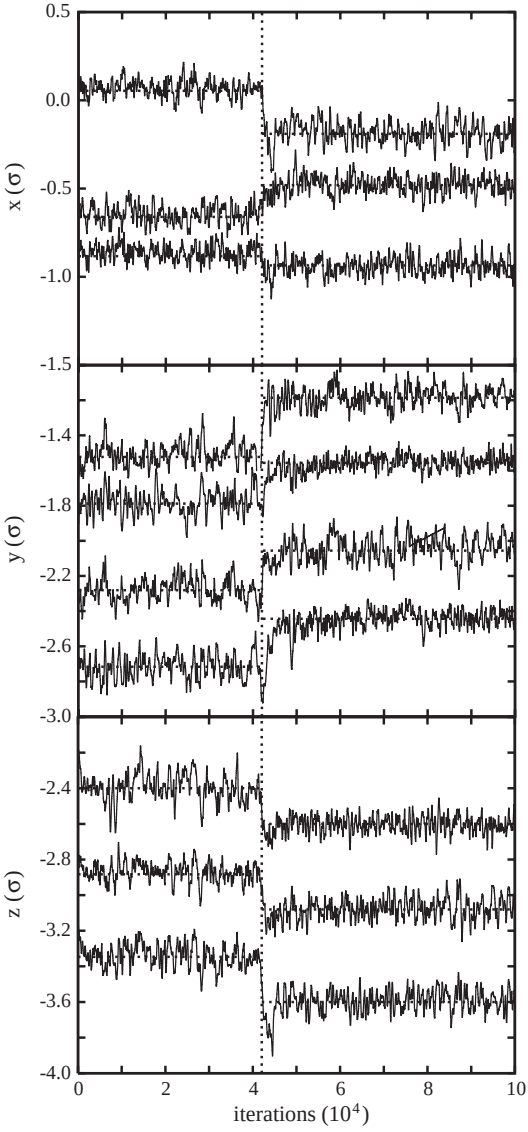


Figure 24.8. Cartesian coordinates of particles involved in an 8-particle transit in argon. Horizontal dotted lines are mean values, and the vertical dotted line is the transit time.

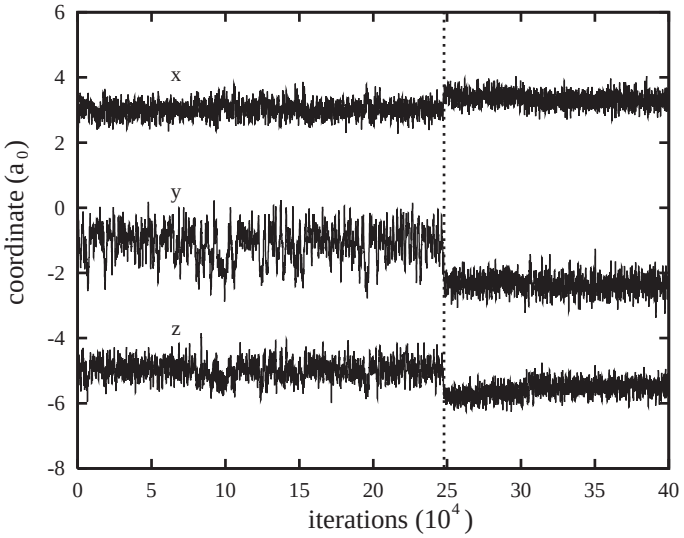


Figure 24.9. Cartesian coordinates of one particle involved in an 11-particle transit in sodium. Changes in vibrational amplitude across the transit are representative of a distribution of such amplitudes.

Liquid dynamics theory pictures the motion as consisting of nearly harmonic vibrations within individual many-particle valleys, and nearly instantaneous local transits between those valleys. The findings from our initial study of transits support this picture of liquid dynamics.

## 25 LIQUID EQUATION OF STATE

### *Ions and Electrons at High Temperatures*

Consider the phase diagram in Fig. 1.2. When the liquid is heated at 1 bar, thermal expansion carries it to the liquid-vapor coexistence curve, and when additional thermal energy is supplied at 1 bar, vaporization proceeds as the system crosses the two-phase region. Presumably, an elemental liquid metal in equilibrium with its vapor at 1 bar is properly described by condensed matter theory. But if the liquid is heated along the saturation curve, pressure increases, vaporization is prevented, and the system approaches its critical point. The continued volume expansion will lead to significant changes in the electronic structure, and to theoretical situations

beyond our present scope. An interesting discussion of expanded liquid metals is given by Hensel (1980).

Let us examine the motion of ions as temperature increases in a system at constant volume. The potential energy landscape consists of a vast array of intersecting, virtually identical random valleys. The ions move rapidly among these valleys, transiting over the ridges at their intersections. As temperature increases, the ions can pass over ever higher ridges, and hence they move ever more freely among the valleys. The motion becomes more gas like. Since the motion is classical, the mean kinetic energy increases as $\frac{3}{2}kT$ per ion, but the mean potential energy increases ever more slowly toward a constant value at high temperatures. Correspondingly, the specific heat decreases from $3k$ per ion in the liquid, toward $\frac{3}{2}k$ per ion in the ideal gas. All of this behavior can be found in the ion motion Hamiltonian $\mathcal{H}_I$, which is based on the ion motion potential $\Phi(\{\mathbf{r}_K\})$ evaluated in the electronic groundstate.

As temperature increases, while the ion motion becomes more gas like, the electrons are also becoming thermally excited. At sufficiently high temperatures, and over a broad temperature range, the outer shell of core electrons will become excited into valence electronic states, leaving smaller ion cores and altering the ion motional dynamics. The process of removing electrons from the core is called *ionization*, and the process just described is *thermal ionization*. Its presence does not mean that we have to introduce a temperature-dependent potential for the ion motion. Instead, we can use the groundstate potential $\Phi(\{\mathbf{r}_K\})$ for the ion cores which *do* remain rigid at all temperatures of interest. Then $\mathcal{H}_I$ is well defined, and thermal ionization becomes part of the ordinary processes of electronic excitation, and includes the interaction of electronic excitations with ion motion. As temperature increases, thermal ionization will eventually become the dominant part of the system free energy.

A related process appears with compression, when the ion cores begin to overlap and the core electron energies split into bands. This process is *compression ionization* and is always included in our formulation of the electronic groundstate. In addition, *any* level of ionization is formally included when we work with the groundstate potential for the motion of bare nuclei (see Problem 25.1).

Formulation of the electronic excitation free energy in the liquid is similar to that in the crystal. Liquid dynamics theory tells us that the appropriate reference structure is any one of the equivalent random structures.

Though density functional calculations have yet to be done for a random structure, nothing in principle stands in the way. Thermodynamic functions arising from the excitation of reference structure electrons can be calculated from the electronic density of states, according to Eqs. (7.49) – (7.52). Considering the free energy due to the interaction between electronic excitation and ion motion, since the ion motion is classical, only the adiabatic part $F_{ad}$ survives. That part is given by Eq. (9.41),

$$F_{ad} = \sum_{\lambda} (\bar{f}_\lambda - g_\lambda) \langle \delta E_\lambda \rangle \quad , \tag{25.1}$$

where $\delta E_\lambda = E_\lambda(\{\mathbf{r}_K\}) - E_\lambda(\{\mathbf{R}_K\})$, and the average $\langle \delta E_\lambda \rangle$ is over the ion motion. While $F_{ad}$ goes as $T^3$ at high $T$ for a crystal, the temperature dependence softens to something between $T^2$ and $T^3$ for a liquid. In Sec. 18, we estimated $S_{ad} << S_{el}$ for a crystal at temperatures to melt, and it is very likely that $S_{ad}$ remains negligible compared to $S_{el}$ for the liquid as well, say at temperatures to $5T_m$. Of course, $S_{ad}$ can be calculated if it is needed, from Eq. (25.1) in leading order perturbation theory, or else from the Zwanzig equation (9.37).

### *Classical Nuclear Motion from Computer Simulations*

For the liquid, as for the crystal, statistical averages over the classical ion motion can be calculated by molecular dynamics or Monte Carlo techniques. However, compared to the crystal, calculations for the liquid require a more extensive knowledge of the potential $\Phi(\{\mathbf{r}_K\})$. While the crystal ions move in a single highly-ordered potential valley, the liquid ions move on a landscape of many disordered valleys. We have calculated the ion motional contribution to thermodynamic properties for pseudopotential sodium at temperatures where experimental data are available, namely from $T_m$ to $3T_m$, and find agreement between theory and experiment to within the following limits (Straub, Schiferl, and Wallace, 1983): $C_P$ to 7%, $C_V$ to 4%, $B_T$ to 20%, and $\gamma$ to 7%. This level of accuracy is excellent for liquid theory, but is less than what we can expect for crystals.

To calculate liquid entropy, it is necessary to determine the entropy constant. This can be done by calculating the internal energy $U(T)$ for a molecular dynamics system at constant volume, up to the very high temperature $T_c$, where the cluster expansion converges rapidly. $S(T_c)$ is then calculated from the cluster expansion, and the liquid entropy is determined

by integrating $dS_V = T^{-1}dU_V$ down from $T_c$. To find the liquid entropy at different volumes, one can calculate $P(V)$ at constant temperature, and then integrate $dF_T = -PdV_T$. The procedure is capable of evaluating the theoretical liquid entropy with an error small compared to the experimental error present in measured liquid entropies. Additional details may be found in Wallace *et al.* (1982).

Having determined the entropy for pseudopotential sodium, we calculated the melting temperature by equating the theoretical Gibbs free energies of crystal and liquid (Holian *et al.*, 1983). At pressures from 0 to 16 kbar, the theoretical $T_m$ lies below experiment by 12 to 7%. The detailed comparison of theory and experiment for melting at zero pressure, Table 25.1, is excellent.

Table 25.1. Zero-pressure melting data from molecular dynamics calculations for pseudopotential sodium, compared with experiment.

| | $T_m$ $(K)$ | $V_{lm}$ $(cm^3/mole)$ | $\Delta H_m$ $(cal/mole)$ | $\Delta S_m$ $(Nk/mole)$ | $\frac{V_{lm}-V_{cm}}{V_{lm}}$ | $dT_m/dP$ $(K/kbar)$ |
|---|---|---|---|---|---|---|
| Theory | 327 | 24.9 | 548 | 0.84 | 0.024 | 8.6 |
| Expt. | 371 | 24.8 | 621 | 0.84 | 0.025 | 8.5 – 11.7 |

We undertook still another calculation, to test our ability to achieve an *ab initio* determination of thermodynamic properties of condensed matter (Straub *et al.*, 1994). This study was done for aluminum, and began with density functional calculations of the static fcc potential $\Phi_0$, and of four zone-boundary phonon frequencies, at several volumes. The density functional results were used to calibrate a pseudopotential model of the adiabatic potential, and this in turn was used in molecular dynamics calculations of crystal and liquid phases. Theory and experiment for $T_m$ at zero pressure are respectively 955K and 933.45K. Entropy at classical temperatures is shown in Fig. 25.1, where the theoretical entropy is evaluated at the experimental volume, and is lower than experiment by around 1% in the crystal and 2% in the liquid. If instead the theoretical entropy is evaluated at the volume where the theoretical pressure is zero, it is lower than experiment by 5% in the crystal and 7% in the liquid.

Our conclusion is that one can rely on computer simulations of the ion motional statistical mechanics of real monatomic liquids, to an accuracy limited mainly by the accuracy of the adiabatic potential $\Phi(\{\mathbf{r}_K\})$.

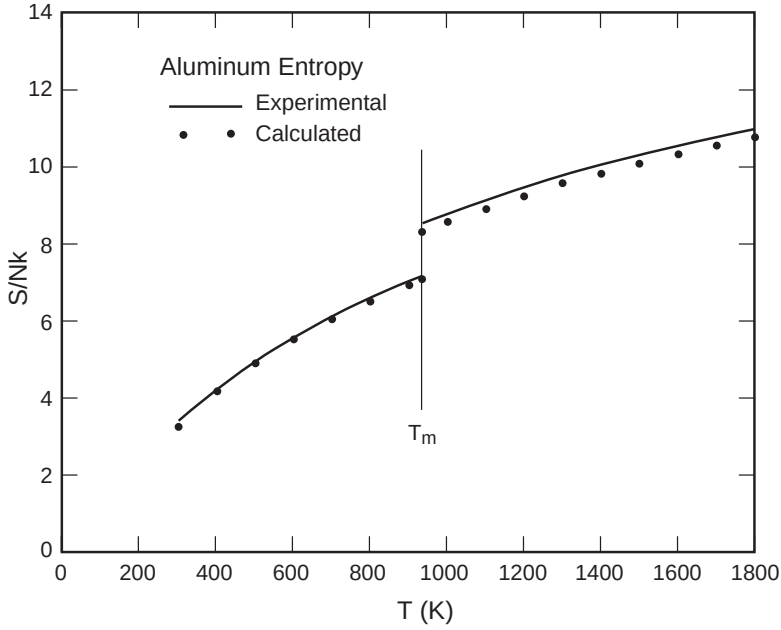


Figure 25.1. Theoretical entropy (points) and experimental entropy (lines) for aluminum at zero pressure. The discrepancy at $300K$ is due to quantum effects in the ion motion (note $\theta_2 \approx 400K$).

### *Role of Liquid Dynamics Theory*

Liquid dynamics theory can in principle provide the physical basis for highly accurate equations of state for liquids, just as lattice dynamics theory does for crystals. But liquid dynamics theory is still in the research state, and much study will be needed to bring us to the level of understanding that has been achieved in lattice dynamics theory. Let us consider the research situation, what we know and what we must learn, to be able to construct highly accurate equations of state. The thermodynamic functions are derived in Sec. 23, as

$$F = \Phi_0 - NkT \ln w + F_{ph} + F_{ab} + F_{el} \quad , \tag{25.2}$$

$$U = \Phi_0 + U_{ph} + U_{ab} + U_{el} \quad , \tag{25.3}$$

$$S = NkT \ln w + S_{ph} + S_{ab} + S_{el} \quad . \tag{25.4}$$

Entropy due to the multiplicity of random valleys is calibrated to give $\ln w = 0.80$. The electronic excitation contribution, $F_{el}$ in the free energy, is rather well understood for the liquid, as discussed at the beginning of this section. The remaining contributions will be discussed in turn.

$\Phi_0(V)$ is the static structure potential for the liquid state, the potential at the bottom of a random valley. This can be calculated from density functional theory, at any volume, and in principle will be as reliable as the corresponding results obtained for crystals. $d\Phi_0/dV$ can also be calibrated from experimental data, e.g. the experimental volume and bulk modulus at zero pressure, but here the thermal contribution to pressure is not so easily neglected as it is for crystals at low temperatures.

The phonon contribution to a thermodynamic function arises from vibrations within one extended harmonic random valley, and for the entropy it is

$$S_{ph} = 3Nk\,[\ln(T/\theta_0) + 1 + \cdots] \quad . \tag{25.5}$$

The characteristic temperature $\theta_0(V)$ can be calculated from density functional theory, at any volume, in principle again to the same accuracy as it can be calculated for a crystal. As for experimental data, we can hope someday to measure the phonon distribution $g(\omega)$ for a random valley, from neutron scattering experiments on a properly prepared amorphous solid. In the meantime we have only the estimate that $\theta_0$ is approximately the same for crystal and liquid at the same volume, when melting is normal, as discussed in Sec. 23. The leading quantum correction (in $+\cdots$) in Eq. (25.5) is of the same form as in Eq. (17.6) for a crystal, and is analyzed in problem 17.1.

The thermodynamic contribution we know least about is the combined anharmonic and boundary contribution, $F_{ab}$ in the free energy. This contribution is magnified in $C_I$, the ion motional contribution to $C_V$, since in classical motion,

$$C_I = 3Nk + C_{ab} \quad . \tag{25.6}$$

Practically all the experimental information we have is in Fig. 23.2, nine curves of $C_I/Nk$ *vs* $T/T_m$ at 1 bar, where the decrease of $C_I$ with $T$ results

from both the $V$ and $T$ dependences of $C_{ab}$. An attractive possibility for studying the anharmonic plus boundary contribution is with computer simulations, where $U_{ab}$ at constant volume is easily determined (see problem 25.2). There might be a way to separate $U_{ab}$ into its anharmonic and boundary components, and one could hope to find more or less universal behavior of the boundary contribution.

Even though liquid dynamics theory is unfinished in detail, the overall picture is clear. The form of the free energy given in Eq. (25.2), and the detailed temperature and volume dependences of its terms, express the physical nature of monatomic liquids, and this form alone carries much information about the liquid equation of state. For a given set of input data, calibrating Eq. (25.2) will in principle produce the best possible equation of state. We estimate the following contributions to the total entropy at $5T_m$, for normal melting elements at normal densities (entropy units are $k$ per atom).

$$\begin{aligned} S_{ph} + \ln w &\approx 13 - 18 \ , \\ S_{el} &\approx 0.2 - 1.0 \text{ for NFE metals} \ , \\ S_{el} &\approx 3 - 5 \text{ for transition metals} \ , \\ S_{ab} &\approx -0.4 \text{ to } 0.0 \ . \end{aligned} \tag{25.7}$$

Any magnetic contribution is still to be added.

*Problems*

*25.1* In the picture of rigid ions plus valence electrons, it is intuitively obvious what happens in thermal ionization and compression ionization. Describe the same processes in the picture of bare nuclei plus all electrons.

*25.2.* In connection with Fig. 24.2, show that

$$U_{ab}(V,T) = \langle \Phi(V) \rangle - \Phi_0(V) - \frac{3}{2} NkT \ .$$

*This page intentionally left blank*

# Chapter 6

# Phase Transitions and Nonequilibrium Processes

## 26 THEORETICAL ANALYSIS OF PHASE TRANSITIONS

### *Phase Boundary and Two-Phase Region*

Experiments are usually done at fixed pressure and temperature. At a given $P$ and $T$, phase stability is determined by the Gibbs free energy $G(P,T)$: the phase with lowest $G$ is absolutely stable, and any other phase, if present, is metastable. Here we consider only first-order phase transitions. Two phases $\alpha$ and $\beta$ are in equilibrium when $G^\alpha(P,T) = G^\beta(P,T)$, and this equation determines the phase boundary. These properties are illustrated in Fig. 26.1a. Since $G = F + PV$, derivatives with respect to the independent variables are (see problem 26.1)

$$\frac{\partial G}{\partial P}\Big)_T = V \quad , \frac{\partial G}{\partial T}\Big)_P = -S \quad . \tag{26.1}$$

We have previously encountered the Gibbs free energy in the statistics of quantum particles, Sec. 7, and in the crossing of $G$ curves in anomalous melting, Fig. 22.3.

In theoretical work, it is most convenient to choose volume and temperature as independent variables. Then the phase boundary is located by the Helmholtz construction, shown in Fig. 26.1b. At a given temperature, $F(V,T)$ is drawn for each phase, and the common tangent locates the equilibrium condition $G^\alpha(P,T) = G^\beta(P,T)$, since $P = -(\partial F/\partial V)_T$. In the actual process, as volume decreases, the system is $\alpha$ phase at $V \geq V^\alpha$, then the system moves along the line at constant pressure, where it is a mixture of $\alpha$ at $V^\alpha$ and $\beta$ at $V^\beta$, until it is entirely $\beta$ phase at $V \leq V^\beta$.

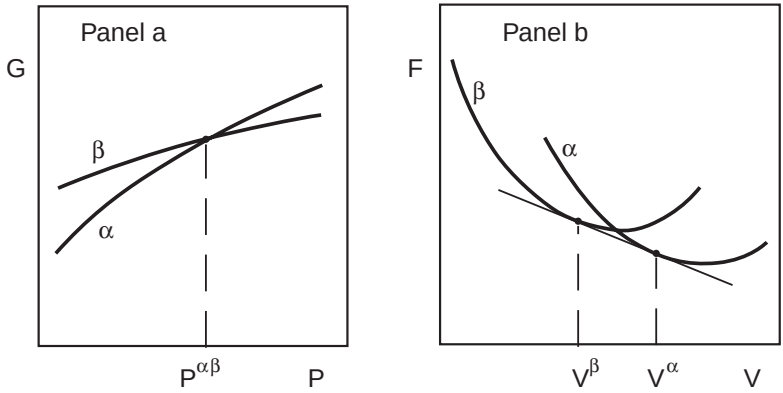


Figure 26.1. Graphs at constant $T$ of $G$ *vs* $P$ (panel a), and of $F$ *vs* $V$ (panel b). Panel a shows that $\alpha$ is stable at $P < P^{\alpha\beta}$ , $\beta$ is stable at $P > P^{\alpha\beta}$, and the phases are in equilibrium at $P^{\alpha\beta}$. Panel b shows the Helmholtz construction for the same point on the phase boundary, where the slope of the tangent line is $-P^{\alpha\beta}$.

The two-phase region is concealed at the point $G^\alpha = G^\beta$ in Fig. 26.1a, but is revealed in Fig. 26.1b. The two-phase region is shown in $V-T$ space in Fig. 26.2. If the transformation takes place at temperature $T_2$, the system crosses the two-phase region between $V^\alpha$ and $V^\beta$, just as in Fig. 26.1. If the transformation takes place at volume $V^\beta$, the system crosses the two phase region between $T_1$ and $T_2$. Even though experiments are not usually done at constant volume, relations between two phases are equally well defined across the two-phase region at constant $T$ *or* at constant $V$. By way of example, the regions comprising gas + liquid, and liquid + crystal, are shown on the phase diagram of Fig. 1.2.

A theoretical extension of thermodynamics is to define an equilibrium property for both phases at the same $V$ *and* $T$, for example along one boundary of the two-phase region in Fig. 26.2. This procedure is motivated by physical interpretation. Indeed, an important point of our analysis of the entropy of melting is that $\Delta S^*$, which is $S^l - S^c$ at a fixed $V$ and $T$, has a direct physical interpretation, while $\Delta S$ at a fixed $P$ and $T$ has no such interpretation. The method for finding $\Delta S^*$ is shown in Fig. 22.1, and is written in Eq. (22.2). While the procedure is sensible as an extrapolation of equilibrium states, justification through statistical mechanics of metastable states is presented in Sec. 27.

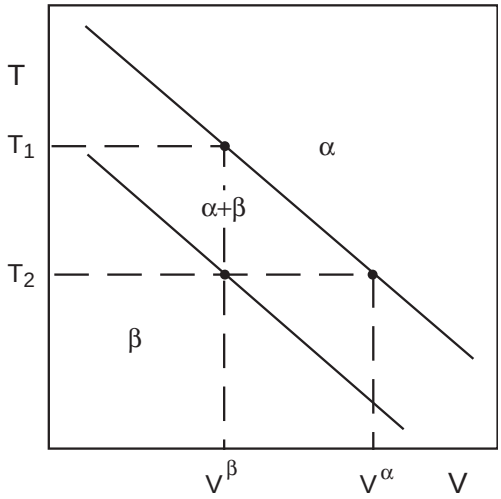


Figure 26.2. Phase diagram in $V - T$ space, showing stability regions for $\alpha$, $\beta$, and $\alpha + \beta$.

***Relations Across the Transition***

We are interested in the difference in volume $\Delta V$, and the difference in entropy $\Delta S$, between two phases in equilibrium at a given $P$ and $T$. Since $V = (\partial G/\partial P)_T$, from Eq. (26.1), it follows from Fig. 26.1a that $V^\beta < V^\alpha$ when the two phases are in equilibrium. Hence, when a phase boundary is crossed by increasing $P$ at constant $T$, $\Delta V < 0$. Similarly, when a phase boundary is crossed by increasing $T$ at constant $P$, $\Delta S > 0$ (see problem 26.2). This information on the signs of $\Delta V$ and $\Delta S$ is illustrated in Fig. 26.3.

For a first-order phase transition, the slope of the phase boundary, by which we mean specifically the derivative $dT/dP$, is given by the Clapeyron equation,

$$\frac{dT}{dP} = \frac{\Delta V}{\Delta S} \quad . \tag{26.2}$$

Notice this equation is consistent with the signs of $\Delta V$ and $\Delta S$ in Fig. 26.3, for either positive or negative slope. Phase diagrams also have points where the sign of $dT/dP$ is not defined. The characteristics shown in Fig. 26.3 have to be extended to cover these points, and the Clapeyron equation tells us how to do this. When $dT/dP = 0$, we have $\Delta V = 0$, so that both phases

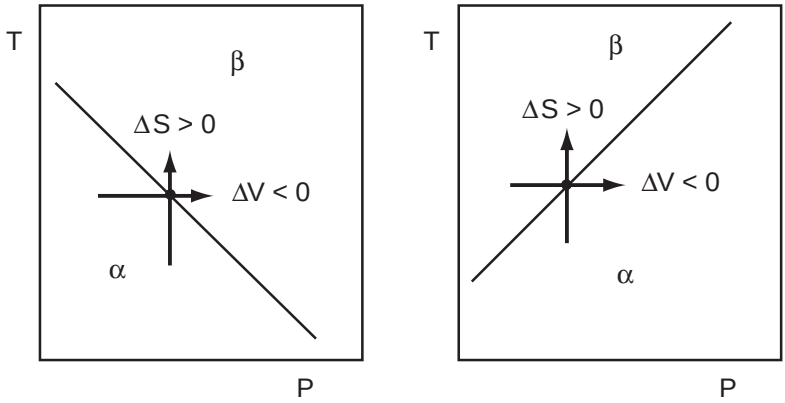


Figure 26.3. The system moves along the path of an arrow, and in crossing the phase boundary the system undergoes the changes $\Delta S$ and $\Delta V$, whose signs are shown.

have the same volume (density), while the higher temperature phase still has the higher entropy. When $dT/dP = \infty$, we have $\Delta S = 0$, while the higher pressure phase still has the smaller volume. Since $S \to 0$ as $T \to 0$ for all phases, then $\Delta S$ must vanish at $T = 0$, hence phase boundaries have infinite slope at $T = 0$. In most crystalline materials, phase boundaries are still "very steep" at room temperature.

The relative volume change in a phase transition is usually small, and can often serve as an expansion parameter for theoretical work. At a point on the phase boundary, phase $\alpha$ has volume $V^\alpha$, phase $\beta$ has volume $V^\beta$, and $\eta$ is defined by (see problem 26.3)

$$\eta = \frac{V^\alpha - V^\beta}{V^\beta} \quad . \tag{26.3}$$

The equilibrium condition $G^\alpha = G^\beta$ can be expressed in terms of $F^\alpha$ and $F^\beta$, and $F^\beta$ can be expanded about $V^\beta$ to find (see problem 26.4)

$$F^\alpha(V^\alpha, T) - F^\beta(V^\alpha, T) = -\frac{1}{2}\eta^2 V^\beta B_T^\beta(V^\beta, T) + \cdots \quad , \tag{26.4}$$

where $B_T^\beta$ is the isothermal bulk modulus of phase $\beta$, and $+\cdots$ represents terms of higher order in $\eta$. Notice the term linear in $\eta$ vanishes in Eq. (26.4). Often but not always in condensed matter systems, the right side converges rapidly.

Let us apply Eq. (26.4) to normal melting, and set $\alpha = l$ for liquid, and $\beta = c$ for crystal. We write $\Delta F = \Delta U - T\Delta S$, express $\Delta U$ from the crystal theory of Chap. 4 and the liquid theory of Sec. 23, for the case of classical nuclear motion, to find (see problem 26.5).

$$\Delta\Phi_0(V_{lm}) = T_m \Delta S^*(V_{lm}, T_m) + \text{ several small terms } . \tag{26.5}$$

Here $\Delta\Phi_0 = \Phi_0^l - \Phi_0^c$, and the small terms consist of the $\eta^2$ term in (26.4), and contributions to $\Delta U$ from anharmonic, boundary, and electronic excitation terms. When the small terms are neglected, one has for normal melting

$$\Delta\Phi_0(V_{lm}) \approx NkT_m \ln w \quad . \tag{26.6}$$

This expresses a fundamental balance in the melting of elements, between the lower structural potential of the crystal, and the higher liquid entropy due to the multiplicity of random valleys. Equation (26.4) can also be applied to anomalous melting (see problem 26.6).

### *Note on Thermodynamic Stability*

Let us consider the nature of thermodynamic stability. In the thermodynamic space $P$, $V$, $T$, and so on, an equilibrium state is specified by two variables, so that the equilibrium surface is two dimensional in a space of higher dimension. Suppose a system is moved away from equilibrium, into a nonequilibrium state, say by giving $S$ an increment $\delta S$ at constant $U$ and $V$, from its equilibrium value $S(U, V)$. This can be done by a fluctuation which transfers energy or volume between parts of the system (Callen, 1985, Sec. 8-1). It can also be done more generally by modifying the phase space distribution $f_n$ from its equilibrium value (see Eqs. (7.4) – (7.6)). In any case, a restoring force develops, which operates to drive the system toward equilibrium. The restoring force expresses the property that entropy is locally maximum on the equilibrium surface. This stability property is present over the entire equilibrium surface, for single-phase and two-phase regions alike.

Wherever a single phase is present, the stability conditions are those expressed in Eqs. (7.18). The same conditions hold on the equilibrium surface where a single phase is metastable. Hence in Fig. 26.1b, the stability conditions hold for the $\alpha$ phase where it is metastable at $V < V^\alpha$, and for the $\beta$ phase where it is metastable at $V > V^\beta$.

In a two phase region, $P$ and $T$ are not independent variables, and this changes the algebra, but not the property of thermodynamic stability. In the two phase region at constant $P$ and $T$, shown in Fig. 26.1b, the system is a mixture of $\alpha$ at $V^\alpha$ and $\beta$ at $V^\beta$, and the system free energy is

$$F(V,T) = \left(\frac{V - V^\beta}{V^\alpha - V^\beta}\right) F^\alpha(V^\alpha, T) + \left(\frac{V - V^\alpha}{V^\beta - V^\alpha}\right) F^\beta(V^\beta, T) \quad . \quad (26.7)$$

Hence anywhere in the two phase region, as illustrated in Fig. 26.2, the system state is completely specified by the variables $V$ and $T$. The two phase region is a two-dimensional surface. Thermodynamic stability in the two phase region is examined in problems 26.7 and 26.8.

It is widely stated that a phase transition is the consequence of thermodynamic instability (e.g. Callen, 1985, p. 203). This view is based on the fact that a smooth curve connecting $F^\alpha$ and $F^\beta$, within the interval $V^\beta < V < V^\alpha$ in Fig. 26.1b, exhibits a thermodynamically unstable segment at a finite distance above the two-phase free energy (Callen, 1985, Fig. 8.2). The view is incorrect for a first order phase transition, because in the transition process the system moves on a surface of stable equilibrium states, where the system fluctuations see only positive restoring forces, and the presence of a thermodynamic instability some distance away is irrelevant.

### *Theory and Experiment for Crystal-Crystal Transitions*

Density functional theory is currently able to reproduce experimental observations of crystal-crystal transitions as function of pressure at low-temperatures. Theory is done in the potential approximation, where $F(V,T)$ is replaced by the static lattice potential $\Phi_0(V)$, and experiments are usually at room temperature. Curves of $\Phi_0(V)$ are calculated for a number of crystal structures, and phase transitions are located from Helmholtz constructions (Fig. 26.1b). The level of agreement between theory and experiment is illustrated by the calculations in local density approximation of Yin and Cohen (1982), for the pressure-induced transition from dia to bct in Si and Ge (see Table 26.1). A further transition of Si from bct to simple hexagonal was observed at 130–160 kbar, and calculations of Needs and Martin (1984) verify this transition at 143 kbar. Additional comparisons of theory and experiment are mentioned in the tabulation of phase diagrams by Young (1991). The small theoretical contributions from nuclear vibrations can

also be included when needed (Sec. 16).

Table 26.1. Theory and experiment for the dia–bct transition in Si and Ge (from Yin and Cohen, 1982). Volumes are normalized to zero-pressure volumes, and the most recent experimental transition pressures are given.

| | | $V^{dia}$ | $V^{bct}$ | P(kbar) |
|---|---|---|---|---|
| Si | calculation | 0.928 | 0.718 | 99 |
| | experiment | 0.918 | 0.710 | 120 |
| Ge | calculation | 0.895 | 0.728 | 96 |
| | experiment | 0.875 | 0.694 | 108 |

The equilibrium condition $\Delta G = 0$ is resolved into

$$\Delta U - T\Delta S + P\Delta V = 0 \quad . \tag{26.8}$$

The presence of three terms makes the general analysis quite complicated. When the phase boundary is steep, i.e. $|dT/dP|$ is large, then $T\Delta S$ tends to be unimportant, and the transition pressure is given by $\Delta U + P\Delta V \approx 0$. This is the case discussed above for Si and Ge. When $P \approx 0$, and also when the phase boundary has small slope, so that $\Delta V \approx 0$, the transition temperature is determined by $\Delta U - T\Delta S \approx 0$. Let us consider in more detail the case $P = 0$. The equilibrium condition is $\Delta F = 0$, where $\Delta F$ is the sum of five theoretical contributions,

$$\Delta F = \Delta\Phi_0 + \Delta F_{ph} + \Delta F_{anh} + \Delta F_{el} + \Delta F_{ep} \quad . \tag{26.9}$$

Unlike the theory for $F$, we cannot neglect any term in $\Delta F$ without estimating them all, since their sum is zero. While $\Phi_0$ dominates $F$, and $F_{ph}$ dominates the thermal part of $F$, the terms $\Delta\Phi_0$ and $\Delta F_{ph}$ do not necessarily dominate $\Delta F$. If the transition occurs at a temperature where the nuclear motion is classical, $\Delta F_{ep}$ is very likely negligible. Each contribution $\Delta F_a$ is $\Delta U_a - T\Delta S_a$, and when $\Delta F_a$ is important, then usually $\Delta U_a$ and $T\Delta S_a$ are both important. The smaller is $\Delta S$, the more difficult is the theory. For a transition with negligible change in electronic structure, such as metal to metal, $\Delta S$ is apt to be small compared to $Nk$. For a transition with significant change in electronic structure, such as covalent to metal, $\Delta S$ can be on the order of $Nk$.

Upon increasing temperature at zero pressure, tin transforms at $286K$

from $\alpha$ phase (covalent bonding, dia structure) to $\beta$ phase (metallic bonding, bct structure). This is the same physical transition as the pressure-induced transition in Si and Ge, discussed in connection with Table 26.1. Because of the significant change in electronic structure, $\Delta S$ is large, the experimental value being $0.83Nk$. The electronic entropy is zero for $\alpha$-Sn, and with the free electron model for $\beta$-Sn, we find $\Delta S_{el} = 0.05Nk$. Though the effect of anharmonicity is unknown, we expect it to be small in both phases. Pavone, Baroni, and Gironcoli (1998) used density functional theory to calculate the static lattice potential and phonon dispersion curves, and hence the Helmholtz free energy in the harmonic approximation, for Sn in dia and bct structures at fixed lattice parameters. The phonon dispersion curves are in good agreement with inelastic neutron scattering data, and the $\alpha-\beta$ transition occurs at $311K$, in good agreement with the experimental transition at zero pressure. Including the free electron evaluation of the electronic free energy would reduce the theoretical transition temperature by around $10K$.

Upon increasing temperature at zero pressure, metals in close packed structures often transform to bcc before melting. This occurs at low temperatures for Li and Na, and at higher temperatures for Be, Ca, Sr, and Tl, for several transition metals, and for most lanthanides and actinides. This transformation occurs because bcc has a low lying phonon branch, namely the $T_1$ branch along $[0, 1, 1]$, which gives rise to a large phonon entropy in bcc. This mechanism was suggested by Zener (1947). The hcp–bcc transition in Ti and Zr has $\Delta S_{expt} = 0.43Nk$, and this is qualitatively understood through our analysis in Eq. (19.26), and in Fig. 19.5. In some metals we have studied, e.g. Li, Na, Tl, and Fe, $\Delta S$ for this transition is extremely small at around $0.1Nk$.

### *Soft Phonons*

Consider an $N$-particle system having two stable crystal valleys, say fcc and bcc, and suppose each valley is perfectly harmonic. Then each valley is prescribed by a set of $3N - 3$ parabolas in real space, each parabola having positive curvature $M\omega_\kappa^2$, and the two valleys intersect along ridges where the system can pass from one valley to the other. Suppose fcc lies lowest, and bcc has lower frequencies on average. Then the fcc phase is stable at low temperatures, bcc is stable at high temperatures, and a phase transition occurs at some intermediate temperature.

The transition is driven by supplying thermal energy. In the process the system moves from the fcc valley to bcc, where the bcc valley is *much larger* than fcc in the $3N$-dimensional system space. In fact, after the transition, the system presumably moves within *both* valleys, but it spends virtually all its time in bcc, because bcc is so much larger. In this way, the system in bcc is *thermodynamically stable*, and the stabilizing factor is the larger bcc phase space, i.e. the larger bcc entropy.

Notice in the situation described, mechanical stability of the bcc valley is not required. Certainly $M\omega_\kappa^2$ must be positive for most of the bcc phonons, so that bcc symmetry is present, but some negative values of $M\omega_\kappa^2$ are allowed. Indeed this appears to be the actual case in the high temperature bcc phase of Ti, Zr, and Hf, which is reached by a transition from the low temperature hcp phase. Calculations in local density approximation by the Ames group, summarized by Ho and Harmon (1990), for hcp and bcc Zr, show that hcp has the lower potential $\Phi_0$, and the bcc N-point $T_1$ phonon has $\omega^2 < 0$. Note this phonon is part of the bcc $\rightarrow$ hcp path. We can presume that *all* hcp phonons are stable, while a *group* of bcc phonons are unstable. Then hcp is mechanically stable, and is thermodynamically stable at low temperatures, while bcc is mechanically unstable, but is thermodynamically stable at high temperatures.

Notice the bcc crystal still possesses a kind of mechanical stability, since it is mechanically trapped within a certain region of configuration space. Ultimately this kind of mechanical stabilization, in the presence of a quasiharmonic instability, is an anharmonic effect.

An unusually strong decrease in the frequencies of some phonons, in response to a change in laboratory conditions, is called *phonon softening*. Temperature dependent phonon softening is observed in inelastic neutron scattering experiments on hcp and bcc phases of Ti and Zr. The temperature dependence is contained in the renormalized phonon entropy $\hat{S}(V,T)$, as calculated from the neutron scattering data, and partly recorded in Table 19.3. From $\hat{S}(V,T)$, we extracted the renormalized characteristic temperature $\Theta_0(V,T)$, defined by

$$\ln(k\Theta_0) = \langle \ln \hbar\Omega_\kappa \rangle_{BZ} \quad , \tag{26.10}$$

where $\Omega_\kappa(V,T)$ are the measured phonon frequencies (see Eq. (16.22)). The graphs of $\Theta_0$ *vs* $T$ for Ti and Zr, Fig. 26.4, show softening as the transition is approached from below, and also from above. The lines drawn for hcp

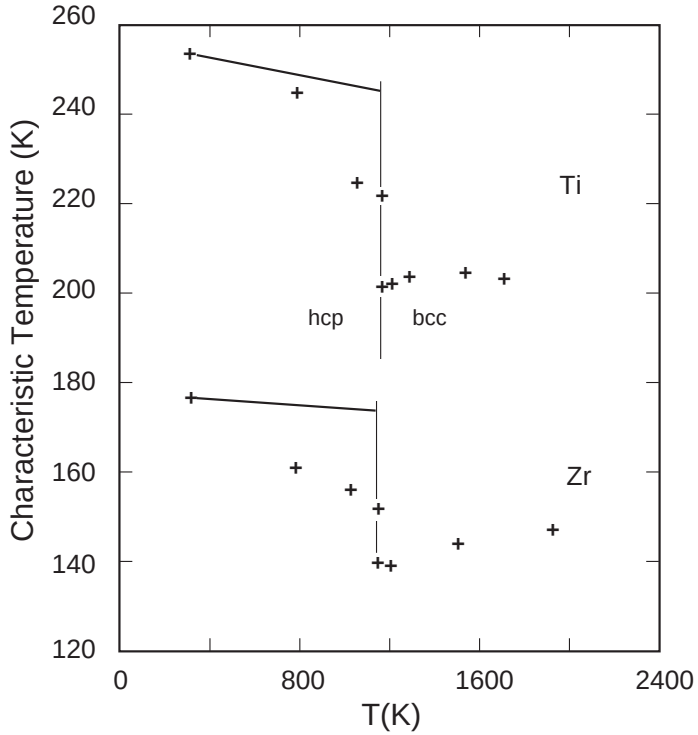


Figure 26.4. Points are the experimental $\Theta_0$ *vs* $T$ in hcp and bcc Ti and Zr. Solid lines in hcp show the variation in $\Theta_0$ in quasiharmonic theory, due to thermal expansion. $\Theta_0$ shows significant softening in both phases.

show the variation of $\Theta_0$ due to thermal expansion, i.e. the quasiharmonic contribution to the temperature dependence. A similar weak decrease with temperature is caused by thermal expansion in the bcc phase. Hence the softening of $\Theta_0$ in Ti and Zr is not a quasiharmonic effect.

Our presumption is that the phonon softening in Ti and Zr is due to the mechanical instability of some of the bcc phonons. Because of this instability, fluctuations between the two valleys occur more often than usual, especially in the vicinity of the transition temperature. Our experience suggests that phonon softening is a negligible effect in *most* crystal-crystal transitions, and in melting as well. When phonon softening is indeed small, the indication is that the many-particle potential valleys remain nearly harmonic up to their intersections.

### *Compression Dependence of the Melting of Elements*

The primary characteristic of melting of elements at zero pressure, which we learned from our study of experimental data in Sec. 22, is that the melting process always falls into one of two classes: (a) in normal melting there is no significant change in electronic structure, and within small scatter, $\Delta S^*$ is a universal constant with value $0.80Nk$, and (b) in anomalous melting there is a significant change in electronic structure, and $\Delta S^*$ is much larger than the normal value. From a study of experimental melting data for all elements for which accurate data are available, we have verified that the same properties hold for elements under compression (Wallace, 1992a).

Here is some lore on thermodynamic properties of normal melting elements. The quantities $B_T$ or $B_S$, $C_V$ or $C_P$, $\alpha$, and $\gamma$, are each pretty much the same for crystal and liquid at a point on the melt curve. For crystal and liquid alike, in the vicinity of the melt curve, the bulk modulus increases strongly with compression, but the quantity $\alpha B_T = (\partial S/\partial V)_T$ is only weakly dependent on compression, and so are $C_V$ and $\gamma$. The relative change in volume on melting at constant pressure decreases strongly with compression. The melting temperature $T_m$ can be considered a function of $\rho_{lm}$, and by differentiating the normal melting rule one finds (see problem 26.9)

$$\frac{d\ln T_m(\rho_{lm})}{d\ln \rho_{lm}} \approx 2\frac{d\ln \theta_0^c(\rho_{lm})}{d\ln \rho_{lm}} - \frac{2}{3} \quad . \tag{26.11}$$

From this approximation, together with $\theta_2 \approx e^{1/3}\theta_0$, we find $\theta_2/T_m$ decreases with compression, hence the temperature range where nuclear motion is classical becomes a larger fraction of $T_m$, as a crystal is compressed.

The Clapeyron equation applies to both normal and anomalous melting, and since it relates $dT_m/dP$, $\Delta V$, and $\Delta S$, one of these quantities can be determined from the other two (see problem 26.10). Of the three quantities mentioned, $\Delta S$ is usually the most accurately measured at zero pressure.

Of the elements whose melting under compression was studied, four have complete data to the high compression of around 30%. For Na and K, $\Delta S^*$ is in the normal range, and is remarkably constant up to the highest compression we could study. For Ar, we are unable to evaluate $\Delta S^*$ at low pressures, since $\eta$ is very large, and the terms of higher order in Eq. (22.2) are not negligible. However, $\eta$ decreases under compression, so that $\Delta S^*$ can be evaluated, and the result reveals normal melting behavior for com-

pressed Ar (see Table 3 of Wallace, 1992a). The fourth element studied to high compression is Cs, discussed next.

While the melting curve has positive slope for normal melting, $dT_m/dP$ is negative for anomalous melting (except for Sn, where the slope is positive but small). In all cases of negative slope, and indeed for Sn as well, a triple point appears on the melting curve at modest compression, beyond which $dT_m/dP$ is positive. An interesting case is Cs, for which $\Delta S^*$ is graphed in Fig. 26.5, along with the phase diagram. Cs is normal at 1 bar, and $\Delta S^*$ remains constant to around 15 kbar, then $\Delta S^*$ increases rapidly and moves out of the normal range. Just as $\Delta S^*$ moves out of the normal range, $dT_m/dP$ passes through a maximum, so that Cs above say 20 kbar shows anomalous melting, in both the negative slope of the melting curve and the large value of $\Delta S^*$. Beyond the first triple point, Cs is briefly normal, then is strongly anomalous up to the next triple point.

The physical process going on in compressed Cs was discussed by Jayaraman *et al.* (1967), by Yamashita and Asano (1971), and by McWhan *et al.* (1974). Compression of Cs drives the empty 5d band down with respect to 6s, hence causes a 6s to 5d electronic structure change. The change can proceed more or less continuously in the liquid, but it is hindered in the solid by crystal symmetry, and can only proceed in steps, by means of crystal-crystal transitions. In this way the electronic structure of crystal and liquid can differ, giving rise to anomalous melting, especially in the vicinity of a triple point.

*Problems*

*26.1* Derive equations (26.1).

*26.2* Draw the curves of $G^\alpha(T)$ and $G^\beta(T)$ at a constant $P$, where there is a phase transition at $T^{\alpha\beta}$, and the stable phase is $\alpha$ at $T < T^{\alpha\beta}$. Show $S^\beta > S^\alpha$ at $T^{\alpha\beta}$.

*26.3* In detailed work, the transition *direction* must be specified in quantities such as $\Delta V$ and $\Delta S$. Let $\eta^{\alpha\beta}$ measure the change in the transition $\beta \to \alpha$, where $\eta^{\alpha\beta} = (V^\alpha - V^\beta)/V^\beta$. Find the relation between $\eta^{\alpha\beta}$ and $\eta^{\beta\alpha}$.

*26.4* Derive the expansion (26.4).

*26.5* Derive equation (26.5), identifying the small terms.

*26.6* With approximations similar to those used in finding Eq. (26.6), show that the major contributions to anomalous melting are given by

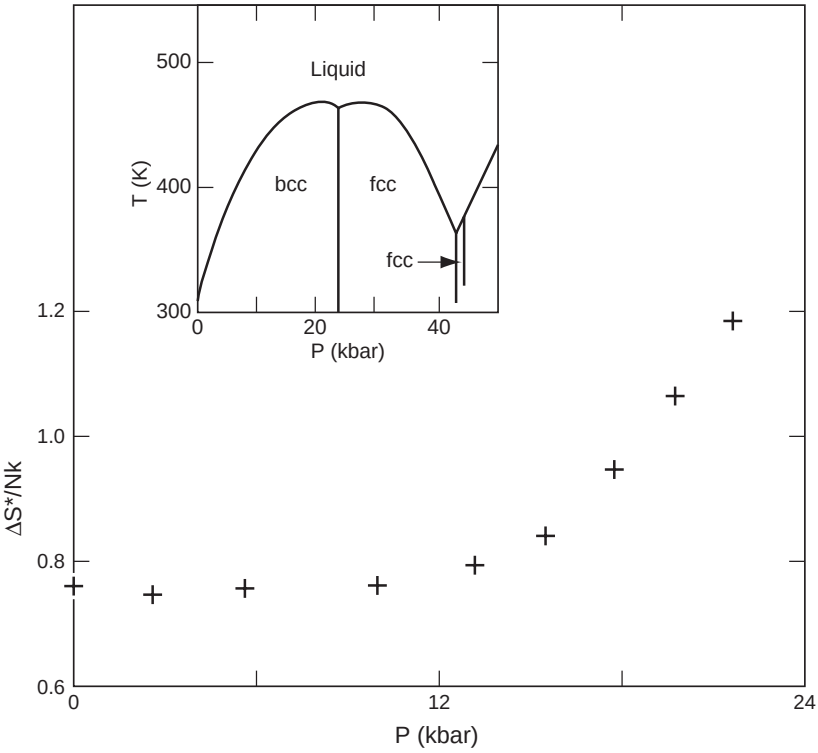


Figure 26.5. Constant-density entropy of melting $\Delta S^*$ *vs* $P$ for Cs, and the phase diagram, showing $\Delta S^*$ becomes anomalous as $dT_m/dP$ becomes negative.

Eq. (22.12).

*26.7* Show $B_T = 0$ and $C_P = \infty$ in the two phase region. Show the thermodynamic stability conditions reduce to $C_V > 0$ and $B_S > 0$.

*26.8* From Eq. (26.7), show $G(P,T) = G^\alpha(P,T) = G^\beta(P,T)$ in the two phase region. Also show the stability conditions in problem 26.7 are satisfied, where you may use that $C_V^\alpha(V^\alpha,T)$ and $C_V^\beta(V^\beta,T)$ are positive.

*26.9* Use the normal melting rule in the form $\frac{3}{2}\ln L \approx$ constant to write an approximation for $T_m(\rho_{lm})$, in terms of $\theta_0^c(\rho_{lm})$, and hence derive Eq. (26.11).

*26.10* Use the Clapeyron equation, and data for $\Delta S$ and $\Delta V$ from Tables 19.2, 19.3, and 21.1, to calculate $dT_m/dP$ at zero pressure. Compare with measurements of $dT_m/dP$, e.g. from Table 1 of Wallace (1992a). This will give you an idea of the level of errors present in the experimental results.

## 27 NONEQUILIBRIUM PROCESSES

### *Information Content of the Partition Function*

In consideration of an ordinary element, one which is crystalline at low temperatures, and whose entropy is zero at zero temperature, my colleague once asked, "What is the entropy of the liquid at $T = 0$?" That question is a driving force behind the theoretical development of this section. At the outset, it is not difficult to conclude that equilibrium statistical mechanics does not answer the question. But then, what is it that equilibrium statistical mechanics does answer?

In equilibrium statistical mechanics, we consider a theoretical mechanical system as representative of the experimental laboratory system, and we evaluate average properties of the mechanical system by averaging, with a distribution, over all its states of motion. The procedure is encapsulated in the partition function, which is a generating functional for all the equilibrium average properties of the mechanical system. In quantum mechanics, the system energy levels are $E_n(V)$, and the canonical partition function is $Z = \Sigma_n \exp(-\beta E_n)$, so that $Z$ is a *unique function* of $V$ and $T$. The free energy and all its derivatives are unique functions of $V$ and $T$, they are the equilibrium properties of the system, and no other properties are defined by the partition function. In particular, $F^\alpha(V,T)$ and $F^\beta(V,T)$ for phases $\alpha$ and $\beta$ are not defined.

Let us consider the mechanical system of a very large number $N$ of atoms in a volume $V$, interacting through the potential $\Phi(\mathbf{r}_1, \cdots, \mathbf{r}_N)$, and let us consider the motion classical, since this helps in visualization. In the partition function, the momentum integrals can be done, leaving the configuration integral $Q$, where one has to integrate $\exp(-\beta\Phi)$ over all possible configurations of the atoms. The potential energy surface contains a vast number of many-particle valleys, crystalline valleys at the bottom, then symmetric valleys and a host of random valleys, and at higher energies still and comprising the great majority of the many-particle space are the gas configurations. Now with $N$ and $V$ fixed, the potential function $\Phi(\mathbf{r}_1, \cdots, \mathbf{r}_N)$ is fixed, and for every temperature we have to integrate $\exp(-\beta\Phi)$ over exactly the same potential energy surface. But at any temperature, virtually the *entire contribution* to $Q$ arises from the phase which is absolutely stable at that temperature: it is the crystal at low temperatures, the liquid at intermediate temperatures, and the gas at high tem-

peratures. At a temperature where say fcc crystal is absolutely stable, the integral over *all the remaining* many-particle space, i.e. over states belonging to the gas, the liquid, and to the amorphous solid and all other crystals, adds up to virtually zero relative to the fcc contribution. Even in a two phase region, for example the crystal plus liquid region, the entire contribution to $Q$ arises from just the correct percentage contributions from crystal configurations and liquid configurations, while the integral over all the remaining many-particle surface is negligible.

In this way, the partition function provides the equilibrium average properties of the system, nothing more and nothing less. At every $V$ and $T$, the partition function represents the absolutely stable phase, and contains no information about any metastable phase. Yet the partition function does not tell us what the stable phase is. To find the stable phase, it would be necessary to examine the contributions to the partition function, and to find the configurations which dominate $Q(V, T)$.

### *Extension to Metastable States*

In practice, we never calculate the global partition function of statistical mechanics. We always limit the quantum states which are summed over, or the classical configurations which are integrated over, because we know which states are the important ones for the problem at hand. The first example of such a limitation is the statistical mechanics of a monatomic gas, where Maxwell and Boltzmann considered a collection of particles having only kinetic energy. In the opposite extreme of statistical mechanics of crystals, Born considered only the collective harmonic-oscillator levels of a system of atoms in a single crystalline potential valley. And the essential point of our liquid statistical mechanics theory, Sec. 23, is that one can start with the collective harmonic-oscillator levels of atoms in each separate random valley, and one can correct from there. In each of these theories, gas, crystal, and liquid, we apply the global technique of equilibrium statistical mechanics to an individual phase, and we interpret the result as expressing equilibrium properties of that phase only. Further, we do this without asking whether or not that phase is absolutely stable. This procedure is so useful in practice, it is worthwhile to set down some intuitive notions about it.

In principle, under conditions where a given phase is absolutely stable, those quantum states which contribute significantly to the partition

function constitute the states of that phase. In practice, this situation does not help us to find those states. Instead, we use our imagination to construct states which ought to belong to a given phase, and then we compare statistical averages with thermodynamic experiments, to see how good our construction is. Let us identify the best currently available construction of the states belonging to a phase $\alpha$, and denote their energy levels $E_n^\alpha, n = 1, 2, \cdots$, and let use define the canonical partition function of phase $\alpha$ by

$$Z^\alpha = \sum_n \exp\left(-\beta E_n^\alpha\right) \quad . \tag{27.1}$$

The states have to satisfy mechanical stability conditions, and the statistical averages have to satisfy the thermodynamic stability conditions (7.18). Then $\alpha$ phase is at least metastable, and we can interpret $Z^\alpha(V,T)$ as the generating function for all the equilibrium properties of the $\alpha$ phase. The interpretation is the same whether or not the $\alpha$ phase exists in nature. With this interpretation applied to two separate phases, $\alpha$ and $\beta$, we can draw free energy curves for each phase, as in Fig. 26.1, and we can find which phase is relatively stable, and where the equilibrium phase transition occurs.

This theory is still an equilibrium statistical mechanics theory, and therefore cannot provide any information about a nonequilibrium process. Consider for example a nonequilibrium phase transition. Referring again to Fig. 26.1a, suppose a laboratory system is brought to the metastable state of being in phase $\alpha$ at $P > P^{\alpha\beta}$. Our equilibrium theory for the $\alpha$ phase can be expected to correctly describe the macroscopic properties of this metastable state. But now the laboratory system will spontaneously transform to the $\beta$ phase, by means of a dynamical process depending on the microscopic initial condition, and controlled by the Hamiltonian and the microscopic boundary conditions. The laboratory system moves along a nonequilibrium path, where even its macroscopic properties cannot be described by any equilibrium statistical mechanics theory.

### *Application to Supercooled Liquids*

Here we are interested only in the ion motional degrees of freedom, and in the simplest description which will exhibit metastability and eventual nonequilibrium motion. When a liquid is cooled below its melting temper-

ature, and when it does not crystallize, the system is metastable, and is called a supercooled liquid. For a monatomic system, the potential surface accessible at liquid temperatures is composed entirely of intersecting many-particle valleys, hence nothing but the same surface is accessible at lower temperatures. The stable liquid and the metastable liquid are therefore governed by the same Hamiltonian. We shall omit crystal and symmetric valleys, and shall neglect anharmonic and boundary corrections, and follow Eq. (23.24) to write the free energy as $F = U - TS$, where

$$U = \Phi_0^l + \sum_\lambda \hbar\omega_\lambda \left(\bar{n}_\lambda + \frac{1}{2}\right) \quad , \tag{27.2}$$

$$S = Nk \ln w + k \sum_\lambda \left[(\bar{n}_\lambda + 1)\ln(\bar{n}_\lambda + 1) - \bar{n}_\lambda \ln \bar{n}_\lambda\right] \quad , \tag{27.3}$$

and where $\bar{n}_\lambda$ is the thermal average boson occupation number,

$$\bar{n}_\lambda = \frac{1}{e^{\hbar\omega_\lambda/kT} - 1} \quad . \tag{27.4}$$

The structural potential $\Phi_0^l$ and the frequencies $\{\omega_\lambda\}$ correspond to a random valley, and the internal energy arises from vibrations within one or more random valleys, with no energy contribution from transits. The entropy has two contributions, the first arising from the multiplicity of random valleys, and the second from vibrations within a single random valley.

When the liquid is cooled through its melting temperature, the above thermodynamic functions show no discontinuity, in agreement with supercooling experiments. In fact, those functions are continuous at all temperatures, they satisfy $dU_V = TdS_V$, and the value of $S$ at $T = 0$ is $Nk \ln w$. But this is the equilibrium result, and it assumes the system moves rapidly among the random valleys, even at $T = 0$. In reality, as temperature is lowered in the supercooled liquid, the transit rate decreases strongly, until the system can no longer maintain equilibrium among the random valleys. At that temperature and below, equilibrium statistical mechanics fails, and one has to use nonequilibrium statistical mechanics to describe the system behavior.

The concepts just used, of "moving rapidly among valleys," and of "maintaining equilibrium among valleys," are not defined, at least not yet, but rest instead upon our intuition. The failure of equilibrium statistical mechanics is something we *know* will happen. We know, for example, that

the supercooled liquid will freeze into a single random valley at a sufficiently low temperature, and will become an amorphous solid, for which the entropy contribution $Nk \ln w$ is completely inappropriate. Better still, experiments can always tell us when a laboratory system passes out of equilibrium, through the appearance of *relaxation processes*. Ultimately, then, it is our responsibility to find out when equilibrium statistical mechanics fails, and to extend our theory accordingly. Notice that nonequilibrium statistical mechanics is always valid in principle, and will correctly reproduce equilibrium statistical mechanics results whenever a system moves sufficiently close to equilibrium. In other words, equilibrium statistical mechanics is merely a limiting case of nonequilibrium statistical mechanics.

Let us now outline the physically realistic nonequilibrium theory for a supercooled monatomic liquid. We shall continue to express the vibrational motion within each random valley in the quasiharmonic approximation, and will assume that phonon-phonon interactions are sufficient to keep this motion in statistical equilibrium. Hence the total energy is still given by equilibrium statistical mechanics, Eq. (27.2), and temperature is defined through the average occupation numbers (27.4). The vibrational entropy is also given by equilibrium statistical mechanics, in the second term on the right of (27.3). But when the transit motion slows down, and equilibrium among the random valleys is not maintained on the *timescale of an experiment*, then the entropy contribution $Nk \ln w$ is invalid, and indeed the entropy due to the multiplicity of valleys cannot be defined. Instead, one has to introduce a kinetic equation for the transit rate, and this equation couples into the equilibrium vibrational motion to produce a nonequilibrium statistical mechanics theory.

### *Glass Transition*

We have developed an independent atom model, which yields simple expressions for the velocity autocorrelation function and the self-diffusion coefficient (Wallace, 1998b). An atom oscillates classically with frequency $\omega$ in a three-dimensional well, and at each turning point it moves forward into a new well with probability $\mu$, and moves back in the same well with probability $1 - \mu$. The self-diffusion coefficient $D$ is given by

$$D = \frac{4kT}{\pi M \omega} \left( \frac{\xi}{2 - \xi} \right) \quad , \tag{27.5}$$

where $M$ is the atomic mass, and $\xi = [1 + \langle \cos\theta' \rangle]\mu$. The trajectory of an atom changes by angle $\theta'$ at a transit, and $\langle \cos\theta' \rangle$ is the average over transits. We can set $\xi = \frac{3}{2}\mu$ as a first approximation. Molecular dynamics calculations of $D(T)$ for pseuedopotential sodium can be fitted with Eq. (27.5) by using a Vogel-Tamann-Fulcher (VTF) function for $\xi(T)$,

$$\xi(T) = \exp\left(\frac{-T_0}{T - T_0}\right) \quad , \tag{27.6}$$

with $T_0 = 121K$. The fit is shown in Fig. 27.1. Hence the strong temperature dependence of $D(T)$ implies the strong temperature dependence (27.6) of $\xi(T)$, and also of $\mu(T)$. In this model, $T_0$ is the glass transition temperature.

The independent atom model can be extended to represent a binary system by letting each atom oscillate in two intersecting wells of slightly different depth. Let us say the bottom of well 2 is at energy zero, the bottom of well 1 is at energy $\Delta > 0$, and each well has frequency $\omega$. Our system has $N$ atoms, with $N_1(t)$ in well 1, $N_2(t)$ in well 2, and the occupation numbers are defined by $n_1 = N_1/N$ and $n_2 = N_2/N$. At a turning point, an atom in well 1 has probability $\mu_1$ of transiting to well 2, and an atom in well 2 has probability $\mu_2$ of transiting to well 1. Since the time between turning points is $\pi/\omega$, the rate per atom of transiting out of well 1 is $R_1 = (\omega/\pi)\mu_1$, and the rate per atom of transiting out of well 2 is $R_2 = (\omega/\pi)\mu_2$. The time rates of change of the occupation numbers are

$$\begin{aligned} \dot{n}_1 &= -n_1 R_1 + n_2 R_2 \quad , \\ \dot{n}_2 &= n_1 R_1 - n_2 R_2 \quad , \end{aligned} \tag{27.7}$$

or, eliminating $n_2$,

$$\dot{n}_1 = R_2 - n_1(R_1 + R_2) \quad . \tag{27.8}$$

Following Eq. (27.6), let us model $\mu_1$ and $\mu_2$ with VTF functions, each containing a single parameter in the form of a critical temperature,

$$\begin{aligned} R_1 &= \frac{\omega}{\pi} \exp\left(\frac{-T_1}{T - T_1}\right) \text{ for } T \geq T_1 \quad , \\ R_1 &= 0 \text{ for } T \leq T_1 \quad ; \\ R_2 &= \frac{\omega}{\pi} \exp\left(\frac{-T_2}{T - T_2}\right) \text{ for } T \geq T_2 \quad , \\ R_2 &= 0 \text{ for } T \leq T_2 \quad . \end{aligned} \tag{27.9}$$

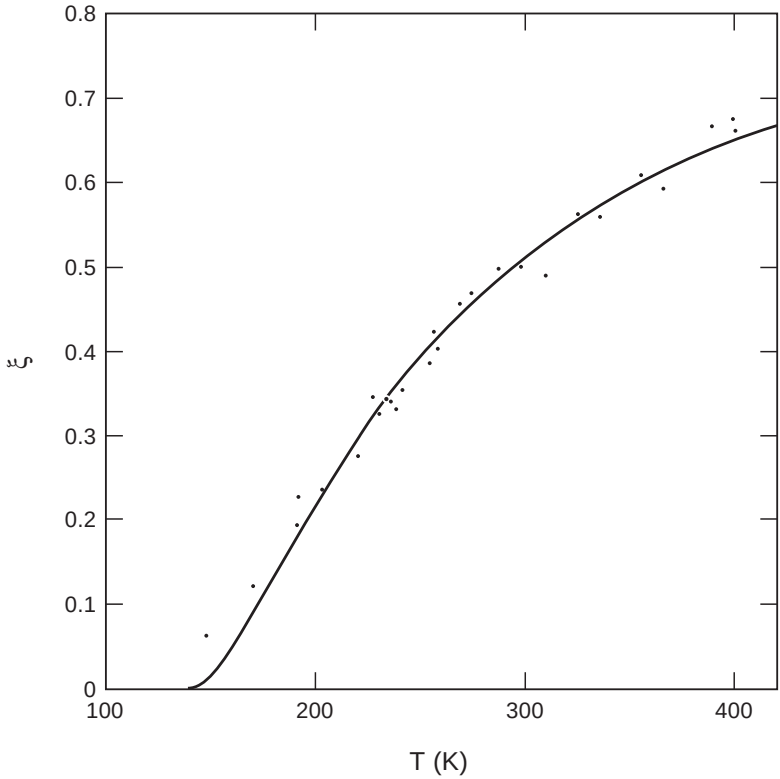


Figure 27.1. Points are values of $\xi$ from molecular dynamics calculations of $D$ for supercooled liquid sodium (Wallace and Clements, 1999), and the line is the VTF function with $T_0 = 121K$.

Since well 1 lies at potential above well 2, we expect $T_1 < T_2$. But $T_1$ should be near $T_2$, so that $R_1$ and $R_2$ slow down together, to achieve glass-transition behavior.

The equilibrium condition is $\dot{n}_1 = 0$, and from Eq. (27.8) this gives

$$n_1(eq) = \frac{R_2}{R_1 + R_2} \quad . \tag{27.10}$$

This tells us that $n_1(eq) \to \frac{1}{2}$ as $T \to \infty$, and $n_1(eq) \to 0$ as $T$ decreases to $T_2$. Let us calculate $n_1(T)$ under the condition that the system is placed in equilibrium at a high temperature, and is then cooled at a constant rate

$\gamma$, defined by

$$\dot{T}/T_2 = -\gamma \quad . \tag{27.11}$$

$n_1(T)$ is obtained by simultaneous integration of Eqs. (27.11) and (27.8). In the process, the system remains near equilibrium, and $n_1(T)$ follows just above the equilibrium curve, down to a glass transition temperature $T_g$, then the system passes out of equilibrium and freezes into a state with nonzero $n_1$. Representative curves are shown in Fig. 27.2, for a range of cooling rates as expressed by the dimensionless variable $\gamma\tau$, where $\tau = 2\pi/\omega$. These curves exhibit rate dependence of $T_g$, rate dependence of the frozen-in value of $n_1$, and sharpening of the glass transition as the cooling rate is decreased. In all these properties, the present model shows the same behavior as do large-scale computer simulations of binary Lennard-Jones systems.

Relaxation of the system toward equilibrium can also be calculated, and both exponential and nonexponential relaxation processes are exhibited. The independent atom model of the glass transition is presented in detail, and is compared with computer simulations, in Wallace (1999).

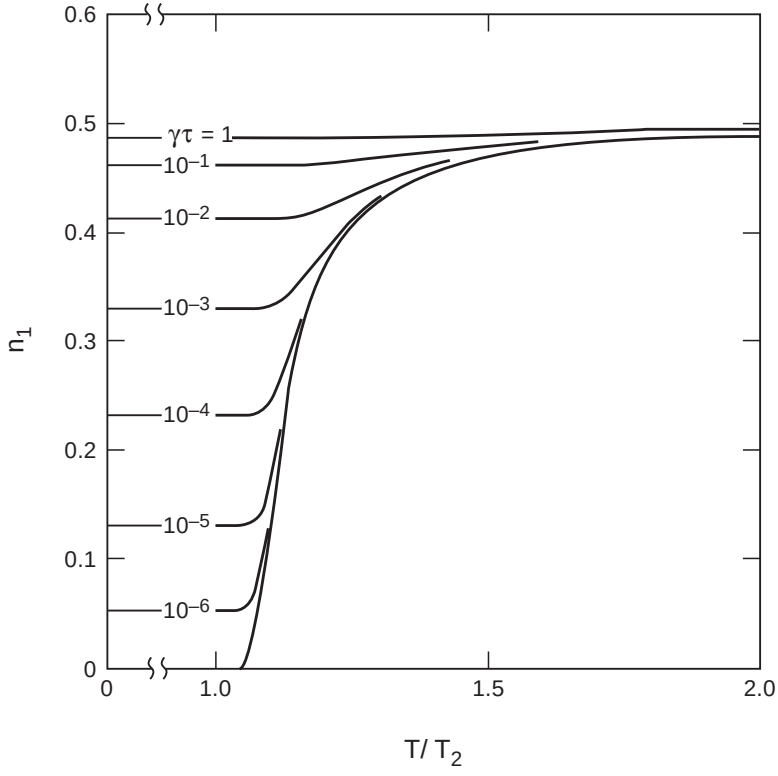


Figure 27.2. Curves of $n_1$ *vs* $T/T_2$ for cooling from equilibrium at the constant rates labeled by values of $\gamma\tau$. $T_1/T_2$ is 0.98, and the lower envelope curve is $n_1(\text{eq})$.

# Bibliography


Allen M.P. and Tildesley D.J. (1990) *Computer Simulation of Liquids* (Oxford University Press).

Allen P.B. (1987) *Phys. Rev.* **B36**, 2920.

Allen P.B. and Hui J.C.K. (1980) *Z. Physik* **B37**, 33.

Ambegaokar V., Conway J.M., and Baym G. (1965) in *Lattice Dynamics* ed. Wallis R.F (Pergamon, Oxford) p. 261.

Ashcroft N.W. (1963) *Phil. Mag.* **8**, 2055.

Ashcroft N.W. (1990) *Nuovo Cimento* **D12**, 597.

Ashcroft N.W. and Langreth D.C. (1967) *Phys. Rev.* **155**, 682.

Bailyn M. (1994) *A Survey of Thermodynamics* (AIP, New York).

Barron T.H.K. (1965) in *Lattice Dynamics* ed. Wallis R.F. (Pergamon, Oxford) p. 247.

Barron T.H.K., Berg W.T., and Morrison J.A. (1957) *Proc. R. Soc. Lond.* **A242**, 478.

Barron T.H.K., Collins J.G., and White G.K. (1980) *Adv. Phys.* **29**, 609.

Barron T.H.K. and White G.K. (1999) *Heat Capacity and Thermal Expansion at Low Temperatures* (Kluwer Academic/Plenum, New York).

Bilz H. and Kress W. (1979) *Phonon Dispersion Relations in Insulators* (Springer, Berlin).

Birch F. (1947) *Phys. Rev.* **71**, 809.

Blackman M. (1935) *Proc. R. Soc. Lond.* **A148**, 365, 384.

Blackman M. (1937) *Proc. R. Soc. Lond.* **A159**, 416.

Boettger J.C. and Wallace D.C. (1997) *Phys. Rev.* **B55**, 2840.

Born M. and Huang K. (1954) *Dynamical Theory of Crystal Lattices* (Clarendon, Oxford).

Born M. and von Karman Th. (1912) *Phys. Zeit.* **13**, 297.

Brockhouse B.N. and Stewart A.T. (1955) *Phys. Rev.* **100**, 756.

Brockhouse B.N. and Stewart A.T. (1958) *Rev. Mod. Phys.* **30**, 236.

Brugger K. (1965) *J. Appl. Phys.* **36**, 768.

Callen H.B. (1985) *Thermodynamics and an Introduction to Thermostatics* 2nd. Ed. (Wiley, New York).
Campbell C.E. (1978) in *Progress in Liquid Physics* ed. Croxton C.A. (Wiley, New York) p. 213.
Chase M.W. Jr., Davies C.A., Downey J. R. Jr., Frurip D.J., McDonald R.A., and Syverud A.N. (1985) *J. Phys. Chem. Ref. Data* **14**, Suppl. 1.
Chisolm E.D., Clements B.E., and Wallace D.C. (2001) *Phys. Rev.* **E63**, 031204.
Chisolm E.D. and Wallace D.C. (2001) *J. Phys.: Condens. Matter* **13**, R739.
Clements B.E. and Wallace D.C. (1999) *Phys. Rev.* **E59**, 2955.
Coffey D. and Pethick C.J. (1988) *Phys. Rev.* **B37**, 442.
Debye P. (1912) *Ann. Phys.* **39**, 789.
de Koning M., Antonelli A., and Yip S. (1999) *Phys. Rev. Lett.* **83**, 3973.
Dirac P.A.M. (1947) *Quantum Mechanics* 3rd. Ed. (Clarendon, Oxford).
Dreizler R.M. and Gross E.K.U. (1990) *Density Functional Theory* (Springer, Berlin).
Einstein A. (1907) *Ann. Phys.* **22**, 180.
Eriksson O., Wills J.M., and Wallace D.C. (1992) *Phys. Rev.* **B46**, 5221.
Faber T.E (1972) *Theory of Liquid Metals* (Cambridge University Press).
Fast L., Wills J.M., Johansson B., and Ericksson O. (1995) *Phys. Rev.* **B51**, 17431.
Favot F. and DalCorso A. (1999) *Phys. Rev.* **B60**, 11427.
Feenberg E. (1969) *Theory of Quantum Liquids* (Academic, New York).
Finney J.L. (1985) in *Amorphous Solids and the Liquid State* ed. March N.H, Street R.A., and Tosi M. (Plenum, New York) p. 31.
Fritz J.N. and Olinger B. (1984) *J. Chem. Phys.* **80**, 2864.
Giannozzi P., de Gironcoli S., Pavone P., and Baroni S. (1991) *Phys. Rev.* **B43**, 7231.
Glazov V.M., Chizhevskaya S.N., and Glagoleva N.N. (1969) *Liquid Semiconductors* (Plenum, New York).
Glyde H.R. (1994) *Excitations in Liquid and Solid Helium* (Clarendon, Oxford).
Glyde H.R., Hansen J.P., and Klein M.L. (1977) *Phys. Rev.* **B16**, 3476.
Görling A. (1999) *Phys. Rev.* **A59**, 3359.
Götze W. (1967) *Phys. Rev.* **156**, 951.
Greeff C.W. and Moriarty J.A. (1999) *Phys. Rev.* **B59**, 3427.
Green A.E. (1962) *Proc. R. Soc. Lond.* **A266**, 1.
Green H.S. (1952) *The Molecular Theory of Fluids* (North-Holland, Amsterdam).
Grimvall G. (1976) *Physica Scripta* **14**, 63.
Grimvall G., Häglund J., and Guillermet A.F. (1993) *Phys. Rev.* **B47**, 15338.
Gschneidner K.A. Jr. (1964) in *Solid State Physics* ed. Seitz F. and Turnbull D. (Academic, New York) Vol. 16, p. 275.
Güthoff F., Petry W., Stassis C., Heiming A., Hennion B., Herzig C., and Trampenau J. (1993) *Phys. Rev.* **B47**, 2563.
Guyer R.A. (1969) in *Solid State Physics* ed. Seitz F., Turnbull D., and Ehrenreich H. (Academic, New York) Vol. 23, p. 413.

Hansen J.P. and McDonald S.R. (1986) *Theory of Simple Liquids* 2nd. Ed. (Academic, New York).
Harrison W.A. (1989) *Electronic Structure and the Properties of Solids* (Dover, New York).
Hearmon R.F.S. (1969) in *Landolt-Börnstein* New Series, ed. Hellwege K.-H. (Springer, Berlin) Vol. 2, p. 1.
Heid R., Bohnen K.-P., and Ho K.M. (1998) *Phys. Rev.* **B57**, 7407.
Heiming A., Petry W., Trampenau J., Alba M., Herzig C., Schober H.R., and Vogl G. (1991) *Phys. Rev.* **B43**, 10948.
Hensel F. (1980) *Angew. Chem. Intl. Ed. Engl.* **19**, 593.
Hirschfelder J.O., Curtiss C.F., and Bird R.B. (1954) *Theory of Gases and Liquids* (Wiley, New York).
Ho K.M. and Harmon B.N. (1990) *Materials Science and Engineering* **A127**, 155.
Hohenberg P. and Kohn W. (1964) *Phys. Rev.* **136**, B864.
Holian B.L., Straub G.K., Swanson R.E., and Wallace D.C. (1983) *Phys. Rev.* **B27**, 2873.
Huang K. (1950) *Proc. R. Soc. Lond.* **A203**, 178.
Hubbard J. (1958) *Proc. R. Soc. Lond.* **A243**, 336.
Hultgren R., Desai P.D., Hawkins D.T., Gleiser M., Kelley K.K., and Wagman D.D. (1973) *Selected Values of the Thermodynamic Properties of the Elements* (ASM, Metals Park, Ohio).
Irving J.H. and Kirkwood J.G. (1950) *J. Chem. Phys.* **18**, 817.
Jayaraman A., Newton R.C., and McDonough J.M. (1967) *Phys. Rev.* **159**, 527.
Johansson B., Ahuja R., Ericksson O., and Wills J.M. (1995) *Phys. Rev. Lett.* **75**, 280.
Kellermann E.W. (1940) *Phil. Trans. R. Soc.* **A238**, 513.
Kellermann E.W. (1941) *Proc. R. Soc. Lond.* **A178**, 17.
Kirkwood J.G. (1933) *Phys. Rev.* **44**, 31.
Kittel C. (1963) *Quantum Theory of Solids* (Wiley, New York).
Klotz S., Besson J.M., Braden M., Karch K., Pavone P., Strauch D., and Marshall W.G. (1997) *Phys. Rev. Lett.* **79**, 1313.
Kohn W. and Sham L.J. (1965) *Phys. Rev.* **140**, A1133.
Landau L. and Lifshitz E. (1938) *Statistical Physics* (Oxford University Press).
Landau L. and Lifshitz E. (1980) *Statistical Physics* 3rd Ed., Part 1 (Pergamon, New York).
Landheer D., Jackson H.E., McLaren R.A., and Stoicheff B.P. (1976) *Phys. Rev.* **B13**, 888.
Lebowitz J.L., Percus J.K., and Verlet L. (1967) *Phys. Rev.* **153**, 250.
Leighton R.B. (1948) *Rev. Mod. Phys.* **20**, 165.
Levy M. (1979) *Proc. Natl. Acad. Sci. USA* **76**, 6062.
Levy M. and Nagy A. (1999) *Phys. Rev. Lett.* **83**, 4361.
Lieb E.H. (1982) in *Physics as Natural Philosophy* ed. Shimony A. and Feshbach H. (MIT Press, Cambridge, Mass.).
Lindemann F.A. (1910) *Phys. Zeit.* **11**, 609.

Lovesey S.W. (1984) *Theory of Neutron Scattering from Condensed Matter* (Clarendon, Oxford) Vol. 1.
Mahan G.D. (1981) *Many-Particle Physics* (Plenum, New York).
McKenzie D.R., Muller D., and Pailthorpe B.A. (1991) *Phys. Rev. Lett.* **67**, 773.
McQuarrie D.A. (1976) *Statistical Mechanics* (Harper & Row, New York).
McWhan D.B., Parisot G., and Bloch D. (1974) *J. Phys.* **F4**, L69.
Mermin N.D. (1965) *Phys. Rev.* **137**, A1441.
Milonni P.W. (1994) *The Quantum Vacuum* (Academic, Boston).
Mizuki J. and Stassis C. (1985) *Phys. Rev.* **B32**, 8372.
Murnaghan F.D. (1951) *Finite Deformation of an Elastic Solid* (Wiley, New York).
Nardone M., Ricci F.P., Filabozzi A., and Pastorino P. (1996) *Phys. Rev.* **E54**, 6381.
Needs R.J. and Martin R.M. (1984) *Phys. Rev.* **B30**, 5390.
Nettleton R.E. and Green M.S. (1958) *J. Chem. Phys.* **29**, 1365.
Parr R.G. and Yang W. (1989) *Density-Functional Theory of Atoms and Molecules* (Oxford University Press).
Pavone P., Baroni S., and de Gironcoli S. (1998) *Phys. Rev.* **B57**, 10421.
Petry W., Heiming A., Trampenau J., Alba M., Herzig C., Schober H.R., and Vogl G. (1991) *Phys. Rev.* **B43**, 10933.
Petry W., Trampenau J., and Herzig C. (1993) *Phys. Rev.* **B48**, 881.
Pollack L., Perdew J.P., He J., Marques M., Nogueira F., and Fiolhais C. (1997) *Phys. Rev.* **B55**, 15544.
Puff R.D. and Gillis N.S. (1968) *Annals of Physics* **46**, 364.
Quong A.A. (1994) *Phys. Rev.* **B49**, 3226.
Ray J.R. and Zhang H. (1999) *Phys. Rev.* **E59**, 4781.
Reif F. (1965) *Fundamentals of Statistical and Thermal Physics* (McGraw-Hill, New York).
Sanborn B.A., Allen P.B., and Papaconstantopolous D.A. (1989) *Phys. Rev.* **B40**, 6037.
Schiferl S.K. and Wallace D.C. (1985) *Phys. Rev.* **B31**, 7662.
Schober H. and Dederichs P.H. (1981) in *Landolt-Bornstein* New Series, Ed. Hellwege K.-H. (Springer, Berlin) Vol. 13a.
Simmons G. and Wang H. (1971) *Single Crystal Elastic Constants and Calculated Aggregate Properties* 2nd. Ed. (MIT Press, Cambridge, Mass.).
Singwi K.S. and Tosi M.P. (1981) in *Solid State Physics* ed. Ehrenreich H., Seitz F., and Turnbull D. (Academic, New York) Vol. 36, p. 177.
Slater J.C. (1974) *The Self-Consistent Field for Molecules and Solids* (McGraw-Hill, New York).
Söderlind P., Ahuja R., Eriksson O., Wills J.M., and Johansson B. (1994) *Phys. Rev.* **B50**, 5918.
Söderlind P., Eriksson O., Johansson B., and Wills J.M. (1995) *Phys. Rev.* **B52**, 13169.
Söderlind P., Eriksson O., Wills J.M., and Boring A.M. (1993) *Phys. Rev.* **B48**,

5844.
Spruch L. (1986) *Phys. Today* Nov., p. 37.
Squire D.R., Holt A.C., and Hoover W.G. (1969) *Physica* **42**, 388.
Stassis C., Arch D., Harmon B.N., and Wakabayashi N. (1979) *Phys. Rev.* **B19**, 181.
Stassis C., Smith G.S., Harmon B.N., Ho K.-M., and Chen Y. (1985) *Phys. Rev.* **B31**, 6298.
Stassis C., Zarestky J., Arch D., McMasters O.D., and Harmon B.N. (1978) *Phys. Rev.* **B18**, 2632.
Stillinger F.H. and Weber T.A. (1982) *Phys. Rev.* **A25**, 978.
Stillinger F.H. and Weber T.A. (1983) *Phys. Rev.* **A28**, 2408.
Straub G.K., Aidun J.B., Wills J.M., Sanchez-Castro C.R., and Wallace D.C. (1994) *Phys. Rev.* **B50**, 5055.
Straub G.K., Schiferl S.K., and Wallace D.C. (1983) *Phys. Rev.* **B28**, 312.
Sudarshan E.C.G. and Mukunda N. (1974) *Classical Dynamics: A Modern Perspective* (Wiley, New York).
Suni I.I. (1997) *Thin Solid Films* **306**, 62.
Sutherland W. (1890) *Phil. Mag.* **30**, 318.
Sutherland W. (1891) *Phil. Mag.* **32**, 31, 215, 524.
Swanson R.E., Straub G.K., Holian B.L., and Wallace D.C. (1982) *Phys. Rev.* **B25**, 7807.
Theophilou A.K. (1979) *J. Phys.* **C12**, 5419.
Thurston R.N. and Brugger K. (1964) *Phys. Rev.* **133**, A1604.
Toupin R.A. and Bernstein B. (1961) *J. Acoust. Soc. Am.* **33**, 216.
Trampenau J., Heiming A., Petry W., Alba M., Herzig C., Miekeley W., and Schober H.R. (1991) *Phys. Rev.* **B43**, 10963.
Trampenau J., Petry W., and Herzig C. (1993) *Phys. Rev.* **B47**, 3132.
Wallace D.C. (1964) *Phys. Rev.* **133**, A153.
Wallace D.C. (1965) *Rev. Mod. Phys.* **37**, 57.
Wallace D.C. (1967) *Phys. Rev.* **162**, 776.
Wallace D.C. (1968) *Phys. Rev.* **176**, 832.
Wallace D.C. (1969a) *Phys. Rev.* **182**, 778.
Wallace D.C. (1969b) *Phys. Rev.* **187**, 991.
Wallace D.C. (1970) in *Solid State Physics* ed. Ehrenreich H., Seitz F., and Turnbull D. (Academic, New York) Vol. 25, p. 301.
Wallace D.C. (1972) *Thermodynamics of Crystals* (Wiley, New York); (1998) Republication (Dover, New York).
Wallace D.C. (1980) *Phys. Rev.* **B22**, 1477, 1487, 1495.
Wallace D.C. (1981) *Phys. Rev.* **B24**, 5597, 5607.
Wallace D.C. (1982) *Phys. Rev.* **A25**, 3290.
Wallace D.C. (1985) *Thermoelastic-Plastic Flow in Solids* (LA-10119, Los Alamos National Laboratory, Los Alamos, NM).
Wallace D.C. (1988) *Phys. Rev.* **A38**, 469.
Wallace D.C. (1989) *Phys. Rev.* **A39**, 4843.

Wallace D.C. (1991a) *Structure of Shocks in Solids and Liquids: Six Reprints with an Introduction* (LA-12020, Los Alamos National Laboratory, Los Alamos, NM).
Wallace D.C. (1991b) *Proc. R. Soc. Lond.* **A433**, 615.
Wallace D.C. (1991c) *Proc. R. Soc. Lond.* **A433**, 631.
Wallace D.C. (1992a) *Proc. R. Soc. Lond.* **A439**, 177.
Wallace D.C. (1992b) *Phys. Rev.* **B46**, 5242.
Wallace D.C. (1994) *Intl. J. Quant. Chem.* **52**, 425.
Wallace D.C. (1997a) *Phys. Rev.* **E56**, 1981.
Wallace D.C. (1997b) *Phys. Rev.* **E56**, 4179.
Wallace D.C. (1998a) *Phys. Rev.* **E57**, 1717.
Wallace D.C. (1998b) *Phys. Rev.* **E58**, 538.
Wallace D.C. (1999) *Phys. Rev.* **E60**, 7049.
Wallace D.C. (2000) *Phys. Rev.* **E62**, 3077.
Wallace D.C., Chisolm E.D., and Clements B.E. (2001) *Phys. Rev.* **E64**, 011205.
Wallace D.C. and Clements B.E. (1999) *Phys. Rev.* **E59**, 2942.
Wallace D.C., Holian B.L., Johnson J.D., and Straub G.K. (1982) *Phys. Rev.* **A26**, 2882.
Wallace D.C., Schiferl S.K., and Straub G.K. (1984) *Phys. Rev.* **A30**, 616.
Wallace D.C. and Straub G.K. (1983) *Phys. Rev.* **A27**, 2201.
Wang J., Yip S., Phillpot S.R., and Wolf D. (1993) *Phys. Rev. Lett.* **71**, 4182.
Waseda Y. (1980) *The Structure of Non-Crystalline Materials.* (McGraw-Hill, New York).
Weber T.A. and Stillinger F.H. (1984) *J. Chem. Phys.* **80**, 2742.
Wilson A.H. (1954) *The Theory of Metals* 2nd. Ed. (Cambridge University Press).
Yamashita J. and Asano S. (1970) *J. Phys. Soc. Japan* **29**, 264.
Ye Y.Y., Chan C.T., Ho K.M., and Harmon B.N. (1990) *Intl. J. Supercomputer Appl.* **4**, 111.
Yin M.T. and Cohen M.L. (1982) *Phys. Rev.* **B26** 5668.
Young D.A. (1991) *Phase Diagrams of the Elements* (University of California Press, Berkeley).
Zener C. (1947) *Phys. Rev.* **71**, 846.
Zwanzig R.W. (1957) *Phys. Rev.* **106**, 13.

# Index